



**HAL**  
open science

# Reliability assessment of tower crane structural members

Simon Bucas

► **To cite this version:**

Simon Bucas. Reliability assessment of tower crane structural members. Human health and pathology. Université Blaise Pascal - Clermont-Ferrand II, 2015. English. NNT : 2015CLF22539 . tel-01155510

**HAL Id: tel-01155510**

**<https://theses.hal.science/tel-01155510v1>**

Submitted on 26 May 2015

**HAL** is a multi-disciplinary open access archive for the deposit and dissemination of scientific research documents, whether they are published or not. The documents may come from teaching and research institutions in France or abroad, or from public or private research centers.

L'archive ouverte pluridisciplinaire **HAL**, est destinée au dépôt et à la diffusion de documents scientifiques de niveau recherche, publiés ou non, émanant des établissements d'enseignement et de recherche français ou étrangers, des laboratoires publics ou privés.

N° d'ordre : D.U. : 2539  
EDSPIC : 685

Université BLAISE PASCAL - Clermont II  
École Doctorale  
Sciences pour l'Ingénieur de Clermont-Ferrand

# Thèse

présentée par

**Simon BUCAS**  
Ingénieur IFMA

en vue d'obtenir le grade de :

**Docteur d'Université**  
Spécialité : Génie Mécanique

## Évaluation de la fiabilité des éléments de charpente de grues à tour

Soutenue publiquement le 9 Janvier 2015 devant le jury :

|                       |                                    |                    |
|-----------------------|------------------------------------|--------------------|
| Pr. Jean-Louis ROBERT | IUT d'Allier, Montluçon            | Président du jury  |
| Dr. André BIGNONNET   | AB Consulting, Beaulieu-sur-Layon  | Examinateur        |
| Pr. Christian BES     | Université Paul Sabatier, Toulouse | Rapporteur         |
| Pr. Franck SCHOEFS    | Université de Nantes, Nantes       | Rapporteur         |
| Pr. Alaa CHATEAUNEUF  | Polytech', Clermont-Ferrand        | Directeur de thèse |
| Dr. Nicolas GAYTON    | IFMA, Clermont-Ferrand             | Co-encadrant       |
| M. Arnaud MITON       | Manitowoc Cranes, Dardilly         | Invité             |
| M. Emmanuel KIRCHNER  | Manitowoc Cranes, Dardilly         | Invité             |

**Institut Pascal - Axe Mécanique Matériaux et Structures**  
**Université Blaise Pascal et Institut Français de Mécanique Avancée**



# Reliability assessment of tower crane structural members

by

**Simon BUCAS**

*A thesis submitted in partial fulfillment  
of the requirements for the degree of  
Doctor of Philosophy  
(Mechanical Engineering)*

**Blaise Pascal University - Clermont II**

Clermont-Ferrand, France

Defended publicly on 9th January 2015 before the following jury :

|                       |                                    |                       |
|-----------------------|------------------------------------|-----------------------|
| Pr. Jean-Louis ROBERT | IUT d'Allier, Montluçon            | President of the jury |
| Dr. André BIGNONNET   | AB Consulting, Beaulieu-sur-Layon  | Examiner              |
| Pr. Christian BES     | Université Paul Sabatier, Toulouse | Reviewer              |
| Pr. Franck SCHOEFS    | Université de Nantes, Nantes       | Reviewer              |
| Pr. Alaa CHATEAUNEUF  | Polytech', Clermont-Ferrand        | Supervisor            |
| Dr. Nicolas GAYTON    | IFMA, Clermont-Ferrand             | Co-supervisor         |
| M. Arnaud MITON       | Manitowoc Cranes, Dardilly         | Guest member          |
| M. Emmanuel KIRCHNER  | Manitowoc Cranes, Dardilly         | Guest member          |



---

*A Pierre, Valérie, Antoine et Joseph.*

---

---

# Remerciements

Je tiens en premier lieu à remercier mes rapporteurs de thèse, Christian BES et Franck SCHOEFS, d'avoir accepté ce travail de relecture minutieuse. Je remercie également André BIGNONNET, d'avoir endossé le rôle d'examineur et Jean-Louis Robert, d'avoir présidé ce jury de thèse et assisté à mes divers comités de thèse. Je tiens également à leur exprimer ma reconnaissance pour la pertinence de leurs remarques et pour les précieux conseils prodigués lors de ma soutenance.

Je remercie aussi Alaa CHATEAUNEUF, pour m'avoir fait l'honneur d'être mon directeur de thèse et Nicolas GAYTON, pour m'avoir co-encadré pendant ces trois années. Votre rigueur, votre expérience et vos nombreux encouragements m'ont permis de guider pertinemment mon travail tout au long ce projet de thèse.

De plus, j'aimerais remercier mes collègues thésards ou enseignants et les amis que j'ai pu cotoyer régulièrement lors de mes venues à Clermont-Ferrand. Je remercie notamment Saâd, Sylvain, Marie, Paul, Benjamin, Julien, Cécile, Pierre, Antoine, William, Richard, Nathalie, Georges, Sami, Bastien et Aurélie. Vous avez tous, chacun à votre manière, contribué à égayer mes divers séjours Clermontois.

Je remercie également Arnaud MITON et Emmanuel KIRCHNER, de m'avoir accueilli dans le service calcul de structures de Manitowoc et de m'avoir donné les moyens matériels pour mener à bien mon projet. Je voudrais aussi témoigner ma reconnaissance à mes collègues de Manitowoc : Véronique, Christophe, Brice, Philippe B., Adrien, Aymen, Antoine, Philippe H., Régis, Michël, Tania, Jean-Christophe, Sylvain, Gabriel, Arnaud et tous les autres... Votre soutien et votre bonne humeur m'ont permis de passer trois années très agréables en votre présence.

Toute ma gratitude va à Pierre RUMELHART, grâce à qui ce projet de thèse n'aurait jamais vu le jour. Pierre, tu n'as malheureusement pas pu assister à la finalisation de ce formidable projet mais, où que tu sois, j'aime à penser que tu liras ces quelques lignes. La confiance que tu m'as témoignée, les innombrables conseils que tu m'as prodigués et la grande bienveillance dont tu as fait preuve pendant tout ce temps ont été des facteurs



---

déterminants qui ont contribué à la réussite de cette thèse. Tu as assuré mon encadrement semaine après semaine avec brio en me poussant toujours plus dans mes retranchements, ce qui a eu pour effet de tirer le meilleur de moi-même, et pour cela, je te remercie infiniment. Ces quelques années passées à travailler avec toi ont laissé sur moi une trace indélébile puisque tu m'as permis de grandir tant du point de vue personnel que professionnel. Je terminerais seulement pas citer une petite phrase d'un livre que tu m'as offert un jour, phrase que tu aimais beaucoup prononcer quand il s'agissait de me remotiver : *Les possibilités sont prodigieuses!*

Un grand merci également à Claude RUMELHART et Christine DESFOSSEZ pour leur présence lors de ma soutenance et pour les échanges qui ont suivis. Grâce à vous, j'ai entrevu une facette de Pierre que je ne connaissais pas et je comprends maintenant d'où il tenait toute sa détermination et sa pugnacité.

Enfin, je tiens à remercier chaleureusement mes parents, Isabelle et Jean-Philippe, qui m'ont permis d'arriver jusque-là. J'ai également une pensée pour mes deux frères, François et Antoine, et ma petite soeur Armelle. Enfin, je suis infiniment reconnaissant envers ma femme Asenet pour l'immense soutien dont elle a fait preuve tout au long de cette aventure. ¡Muchisimas gracias Ase!

---

# Résumé

Les grues à tour sont des engins de levage utilisés de manière cyclique sur les chantiers de construction. De ce fait, la prise en compte du phénomène de fatigue dans le dimensionnement des charpentes de grue est primordiale. La fatigue est usuellement considérée dans les normes au moyen de règles déterministes ayant pour but de garantir l'intégrité de la structure sous diverses conditions d'utilisation. Bien que cette approche fournisse des résultats satisfaisants dans la plupart des cas, celle-ci ne permet pas d'évaluer le niveau de fiabilité des éléments de charpente en fonction de leur durée d'exploitation. De ce point de vue, les approches probabilistes permettent de pallier cette difficulté en proposant des outils pertinents servant à caractériser et à propager les incertitudes liées à la fatigue au travers d'un modèle mécanique.

Une approche probabiliste originale permettant la prise en compte des incertitudes liées à la fatigue dans le dimensionnement des charpentes de grues à tour est proposée dans ce manuscrit. La méthode proposée est basée sur la définition de deux densités de probabilité représentant respectivement les variabilités liées à la résistance des joints soudés d'une part, et les nombreuses dispersions associées à la sollicitation des éléments de charpente d'autre part. La définition de la densité de probabilité de résistance repose sur la capitalisation d'un grand nombre de résultats d'essais d'endurance sur structures soudées, tandis que la définition de la distribution de sollicitation est basée sur une modélisation à deux niveaux tenant compte de divers jeux de données collectés sur chantier. Les résultats de l'analyse de fiabilité présentée dans ce manuscrit démontrent la pertinence des approches probabilistes dans le cadre du dimensionnement en fatigue des éléments de charpente de grue à tour.

**Mots-clés :** grues à tour, fatigue des joints soudés, analyse de fiabilité, modélisation du chargement en fatigue, analyse de sensibilités stochastiques

---

---

# Abstract

Tower cranes are lifting appliances which are cyclically used on construction sites. Thus, the consideration of the fatigue phenomenon in the design of crane structural members is essential. This phenomenon is usually taken into account in standards by means of deterministic rules enabling to ensure structural safety under various operating conditions. Although it provides satisfactory results in most cases, the deterministic approach do not enable to evaluate the reliability of crane structural members according to their operating time. From this point of view, probabilistic approaches allow to overcome this difficulty by proposing relevant tools enabling to characterize and propagate uncertainties related to fatigue through a mechanical model.

An original probabilistic approach enabling the consideration of the uncertainties related to crane members fatigue design is proposed in this manuscript. It relies on the definition of two probability density functions related respectively to the strength variability of crane welded joints on one hand, and the dispersion of operating conditions (stress) on this other hand. The definition of the strength distribution stems from the capitalization of various welded joint fatigue test results, while the characterization of the stress distribution relies on the analysis of various data sets coming from crane monitoring performed on different construction sites. The results coming from the reliability analysis presented in this manuscript show the relevance of probabilistic approaches in the frame of tower crane structural members fatigue design.

**Keywords :** tower cranes, fatigue of welded joints, reliability analysis, fatigue load modeling, stochastic sensitivity analysis



---

# Résumé étendu

## Contexte

Les grues à tour sont des engins de levage capables de lever une grande variété d'outils et de matériaux de construction sur les chantiers. La charpente d'une grue à tour est principalement constituée d'éléments structuraux en acier (plaques ou poutres) assemblés par soudage. Le travail effectué sur chantier étant intrinsèquement cyclique, les grues à tour sont soumises au phénomène de fatigue au cours de leur utilisation. La prise en compte de ce phénomène est donc primordiale lors du dimensionnement des structures. La fatigue est affectée par un grand nombre d'incertitudes provenant de la dispersion intrinsèque du comportement en fatigue des matériaux d'une part, et du caractère aléatoire du chargement d'autre part. Le dimensionnement en fatigue de structures industrielles telles que les grues s'effectue usuellement au moyen de méthodes déterministes basées sur les normes ou sur le retour d'expérience.

Les normes de dimensionnement en fatigue spécifient généralement des règles déterministes ayant pour but de garantir l'intégrité de la structure sous diverses conditions d'utilisation. Les incertitudes liées à la fatigue sont alors prises en compte implicitement au travers de ces règles. Bien que l'approche normative fournisse des résultats satisfaisants, elle n'apporte pas de renseignement qualitatif quand au niveau de fiabilité qui en résulte et par voie de conséquence, sur le niveau optimal de dimensionnement. Cela constitue la principale limite des approches déterministes dans un contexte mondial de plus en plus concurrentiel où l'optimisation des coûts est devenu un enjeu majeur. Ainsi, le dimensionnement de structures fonctionnelles et robustes nécessite l'acquisition de plus de connaissances permettant de gérer les incertitudes liées au phénomène de fatigue. De ce point de vue, les approches probabilistes représentent des outils pertinents permettant de caractériser et de propager au travers d'un modèle mécanique les incertitudes liées à la fatigue afin d'approcher le dimensionnement optimal vis-à-vis d'un objectif de fiabilité.

Les approches probabilistes restent à l'heure actuelle rarement utilisées dans l'industrie, principalement à cause du clivage culturel qu'elles peuvent engendrer. Néanmoins, deux projets français ayant pour objectif de promouvoir ce type d'approches dans un contexte industriel ont vu le jour respectivement en 2005 et 2008. Le premier projet nommé DEFFI

---

(**DE**marche **Fi**abiliste de conception en **F**atigue pour l'**I**ndustrie) avait pour but de développer l'approche "contrainte-résistance" pour le dimensionnement en fatigue de structures provenant de divers secteurs industriels (aéronautique, aérospatial, ferroviaire, etc) [1–3]. Le projet APPRoFi (**AP**proche mécano-**PR**obabiliste pour la conception robuste en **F**atigue) [4] a été lancé quelques années plus tard pour démontrer les intérêts et bénéfices engendrés par l'utilisation d'approches probabilistes pour le dimensionnement en fatigue. De nombreux partenaires académiques et industriels ont collaboré à la réalisation de ce projet. Ces deux projets démontrent l'intérêt grandissant que les entreprises manifestent à l'égard des approches probabilistes. C'est pourquoi le présent travail de recherche vise à développer une démarche fiabiliste globale permettant d'évaluer le niveau de fiabilité des éléments de charpente de grues à tour en fonction de leur durée d'exploitation.

## Objectifs

Les axes de travail suivants ont été investigués afin d'atteindre l'objectif principal de cette étude :

- **Analyse des règles déterministes de dimensionnement en fatigue des grues à tour.** Une étude préliminaire de la norme EN 13001 permet de souligner les concepts de base et les hypothèses principales utilisés dans le processus de validation en fatigue des éléments de charpente de grue à tour.
- **Modélisation stochastique de la résistance en fatigue des joints soudés.** Ce point consiste à développer une méthode de capitalisation de résultats d'essais d'endurance afin de modéliser les incertitudes liées à la résistance en fatigue des éléments soudés de charpente de grue à tour.
- **Modélisation stochastique de l'utilisation des grues.** L'utilisation réelle des grues sur chantier étant à ce jour mal connue, ce point représente un enjeu majeur de ce travail puisqu'il consiste à identifier, caractériser et modéliser les incertitudes et variations liées au chargement des charpentes de grue à tour.
- **Analyse de sensibilité des paramètres du modèle d'utilisation de grue.** Etant donné que la dispersion de l'utilisation des grues influence fortement les résultats du calcul de fiabilité en fonction du temps, une analyse de sensibilité est menée afin d'identifier les paramètres influents intervenant dans le modèle stochastique d'utilisation des éléments de charpente.
- **Evaluation de la fiabilité des éléments de charpente de grue.** Une méthode probabiliste globale est mise en place à partir des modèles de résistance et d'utilisation développés dans les points précédents. Celle-ci a pour objectif d'évaluer le

---

niveau de fiabilité des divers éléments structuraux de grue en fonction de leur durée d'exploitation.

## Les grues à tour et leur dimensionnement en fatigue

Cette partie introduit le vocabulaire associé aux grues à tour, souligne les règles déterministes utilisées pour leur dimensionnement en fatigue et présente les opportunités offertes par l'utilisation des approches probabilistes pour ce type de problème. Les grues à tour de chantier sont des engins permettant de transporter des charges. Deux grandes familles de grues à tour de chantier existent : les grues à montage automatisé et les grues à montage par éléments, dont la charpente est composée de différents ensembles structuraux. Cette deuxième famille se subdivise en deux sous-groupes comprenant respectivement les grues à flèche relevable ainsi que les grues à flèche distributrice. Cette thèse porte exclusivement sur les grues à montage par éléments à flèche distributrice. Comme le montre la figure 1, la partie tournante est constituée de la flèche, de la contre-flèche et de lests de contre-flèche, la mâture est composée de nombreux éléments de mâât et la base permet la liaison au sol et le maintien des lests de stabilité. De plus, les différents mouvements effectués par une grue à montage par éléments sont respectivement le levage (mouvement vertical du crochet), la distribution (déplacement du chariot le long de la flèche), l'orientation (rotation de la partie tournante autour de l'axe d'orient) et la translation quand la grue est montée sur bogies. L'étude présentée dans cette thèse est restreinte aux trois premiers mouvements, *i.e.* le mouvement de translation n'est pas considéré.

La durée de vie en fatigue des éléments de charpente de grue à tour est usuellement exprimée en nombre de cycles de levage. Un cycle commence lorsque la grue lève une charge et se termine lorsque la grue est prête à lever une autre charge. Cela suppose qu'il puisse être décomposé en plusieurs étapes : levage de la charge depuis une position initiale, déplacement de la charge (distribution et orientation) jusqu'à une nouvelle position, dépose de la charge, puis mouvements à vide. Le dimensionnement des éléments de charpente de grue est basé sur cette définition. Leur chargement en fatigue est généralement spécifié par les normes au travers de spectres de charge ou de contrainte.

Le processus normatif de vérification à la fatigue des éléments de grue s'effectue en deux étapes. Chaque élément de charpente est d'abord classé dans une "classe de chargement" en fonction de la sévérité des charges auquel celui-ci est supposé être soumis. Les éléments de charpente de grue à tour appartiennent chacun à l'une des classes S1, S2 ou S3 de l'EN 13001 [5]. Ensuite, les joints soudés de charpente sont classés en fonction de leur géométrie dans des classes de détail. Chaque classe stipule une valeur d'étendue de contrainte caractéristique à  $2 \cdot 10^6$  cycles avec une probabilité de survie égale à 97.7%. Cette valeur caractéristique est ensuite convertie en une valeur d'étendue de contrainte limite  $\Delta\sigma_{R_d}$  tenant compte de la sévérité du chargement, *i.e.* de la classe de chargement auquel



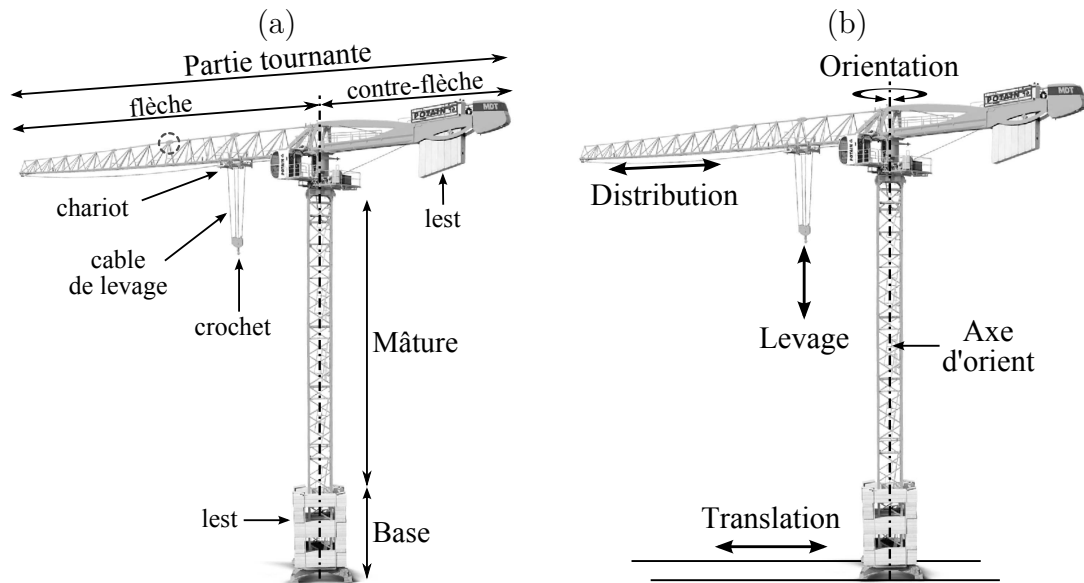


FIGURE 1 – Vocabulaire relatif (a) aux principaux ensembles structuraux d’une grue à montage par éléments et (b) à ses mouvements.

l’élément appartient. Enfin la méthode normative consiste à effectuer un calcul nominal permettant de trouver l’étendue de contrainte maximale  $\Delta\sigma_{S_d}$  à comparer avec l’étendue de contrainte limite  $\Delta\sigma_{R_d}$ . L’élément de charpente considéré est validé du point de vue de la fatigue si  $\Delta\sigma_{S_d}$  est inférieur à  $\Delta\sigma_{R_d}$ .

Le processus de validation présenté précédemment tient compte d’un chargement déterministe au travers des classes de chargement S1, S2 ou S3 et des classes de détails soudés. Cependant, de nombreuses incertitudes inhérentes au phénomène de fatigue existent. Le chargement en fatigue des grues présente notamment un caractère aléatoire, et ce, pour plusieurs raisons :

- La **configuration de la grue** est variable d’un chantier à l’autre, puisque la longueur de flèche ou la hauteur de la mât sont adaptées en fonction de la topographie des bâtiments à construire.
- Etant donné que chaque chantier est unique, la **topographie des chantiers** (position des bâtiments à construire, zones de chargement/déchargement, zones de stockage, etc.) est intrinsèquement variable.
- Les **matériaux de construction et outils** déplacés à l’aide de la grue peuvent être de nature très différente en fonction des chantiers à réaliser.
- Les **durées de chantier et durées de non utilisation** entre deux chantiers représentent des paramètres importants qui influent sur la répartition du travail de la grue dans le temps.

- 
- Le **nombre d'équipes** présentes sur le chantier et leur **efficience** sont inhérentes aux entreprises de construction et constituent des données variables impactant l'utilisation de la grue.

Toutes les sources d'incertitudes listées précédemment contribuent à montrer que l'utilisation des grues présente un caractère aléatoire. Celles-ci sont prises en compte implicitement dans les normes par l'intermédiaire des classes de chargement (S1, S2 ou S3). De même, les incertitudes liées à la résistance en fatigue des éléments de grue sont considérées au travers de classes de détails soudés. Bien que l'approche normative fournisse des solutions satisfaisantes dans la majorité des cas, celle-ci ne permet pas d'optimiser les charpentes de grue à tour vis-à-vis de la fatigue. De plus, les normes telles que l'EN 13001 ne donnent aucune information permettant de faire le lien entre le nombre de cycles de chargement et la durée d'exploitation de la grue. Dès lors, il est difficile, voire impossible, de planifier de manière pertinente la maintenance des éléments de charpente de grue à tour en fonction de leur durée d'utilisation. L'obtention de ce type d'information et l'optimisation des structures nécessitent par conséquent une meilleure connaissance des incertitudes liées à la fatigue. De ce point de vue, les approches probabilistes représentent des outils pertinents permettant d'atteindre ce double objectif, étant donné qu'elles visent à caractériser les incertitudes liées au phénomène de fatigue et à les propager dans tout le processus de dimensionnement.

## Acquisition et traitement de données d'utilisation de grue

Des données d'utilisation de grue sont récoltées et traitées dans le but d'identifier et de caractériser les nombreuses incertitudes inhérentes au chargement en fatigue des éléments de charpente de grue à tour. Les données récoltées proviennent de plusieurs sources : enregistrements effectués sur chantier en conditions réelles, base de données de durées de chantier fournie par une agence de location de grues, et base de données de plans de chantier pourvue par une entreprise de construction.

### Enregistrements sur chantier en conditions réelles

Des dispositifs expérimentaux d'enregistrement ont été développés lors de cette thèse, puis placés sur des grues travaillant sur chantier en conditions réelles. Ces dispositifs permettent la récolte de nombreuses données temporelles d'utilisation de grues telles que la charge levée, la portée (position du chariot le long de la flèche), l'angle d'orientation de la flèche, les vitesses des différents moto-variateurs, etc. Les données récoltées sont traitées numériquement afin d'identifier de manière automatique des cycles de grue et de les différencier en fonction de la nature du travail effectué sur chantier. L'examen du signal temporel de charge tracé sur la figure 2 illustre les trois types de cycle caractéristiques qui ont pu être identifiés sur le chantier. Premièrement, les cycles de **coulage** sont composés

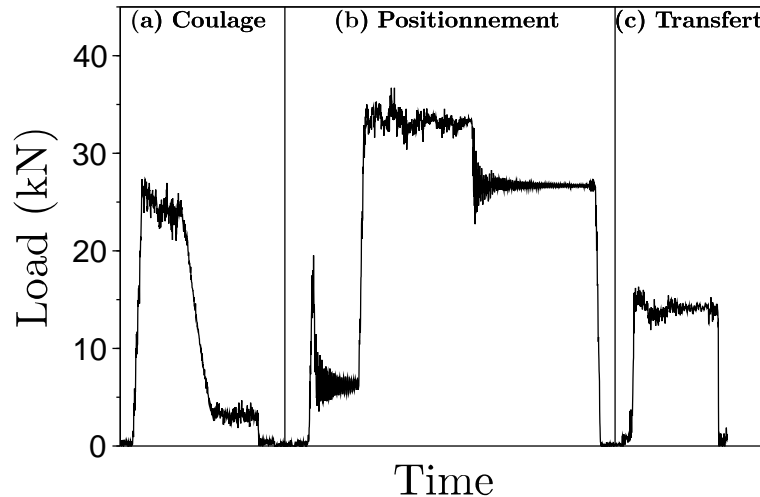


FIGURE 2 – Illustration des trois types de cycle de grue qu’il est possible d’identifier à partir du signal temporel de charge : (a) coulage, (b) positionnement et (c) transfert.

de deux paliers de charge correspondant respectivement aux situations dites “benne à béton chargée” et “benne à béton vide”. Deuxièmement, les cycles de **positionnement** correspondent aux levage d’éléments lourds (banches, escaliers préfabriqués, etc) devant être mis en position avec précaution. Cela explique les nombreux paliers de charge sur la figure 2. Enfin, les cycles dits de **transfert** sont constitués d’un unique palier de charge, ce qui correspond au déplacement d’une charge sans précaution particulière d’un endroit du chantier à l’autre.

Une fois les cycles de grue identifiés en fonction de leur nature, il est possible de présenter les résultats de différentes manières. Il est possible par exemple de tracer les couples de points d’utilisation  $\{\text{portée, charge}\}$  vis-à-vis de la courbe de charge (charge maximale pouvant être levée en fonction de la portée). Cette représentation permet notamment de tracer le spectre de charge auquel la grue est soumise. Le deuxième type de représentation consiste à tracer les coordonnées cartésiennes dans l’espace du chantier des points de début et fin de cycles en fonction de l’aire de travail de la grue, ce qui permet de se faire une idée de la topographie du chantier (position des bâtiments, emplacement des zones de stockage). Enfin, les données peuvent être aussi représentées séparément à l’aide de divers histogrammes relatifs aux portées de départ et d’arrivée, à l’angle d’orientation en début et fin de cycle et à la charge maximale levée pendant le cycle. Ce dernier type de représentation est utilisé dans le chapitre 4 de cette thèse afin de créer un modèle de sollicitation des éléments de grue tenant compte de la topographie des chantiers.

### Données provenant d’une agence de location de grues

Une entreprise spécialisée dans la location d’appareils de manutention et de levage a fourni lors de ce travail de thèse de nombreuses données inhérentes aux durées de location et de

---

non location des grues. Des histogrammes de durées d'utilisation et de non utilisation des grues sont caractérisés à l'aide de ces données en fonction de la capacité des grues concernées (très petite, petite et moyenne). Ces histogrammes sont ensuite utilisés afin que le modèle de sollicitation des éléments de grue développé dans le chapitre 4 tienne compte de la répartition de l'utilisation de la grue dans le temps, *i.e.* de sa durée effective d'exploitation.

### **Données recueillies à partir de plans de chantier**

Une entreprise de construction a fourni dans le cadre de cette thèse plusieurs dizaines de plans de chantiers. Ces plans constituent une source d'information disponible permettant de caractériser plusieurs incertitudes inhérentes à l'utilisation des grues. Tout d'abord, ces plans permettent de connaître la topographie du chantier en termes de position des bâtiments à construire, de localisation des zones de chargement/déchargement ou des camions-benne. Ensuite, ils permettent de connaître la configuration de la grue (longueur de flèche ou hauteur) utilisée en fonction de chaque chantier. Enfin, les volumes prévisionnels de béton à couler sur le chantier peuvent être estimés à partir des plans et comparés à posteriori aux volumes de béton réellement coulés une fois le chantier terminé. De la même manière que les autres types de données décrites précédemment, les données récoltées à partir des plans permettent d'enrichir le modèle de sollicitation des éléments de grue développé dans le chapitre 4.

## **Evaluation de la fiabilité des éléments de charpente de grue**

Le développement d'une méthode "contrainte-résistance" [6] dépendante du temps est présenté dans le chapitre 4. La méthode proposée nécessite la modélisation stochastique de deux densités de probabilité tenant compte des incertitudes inhérentes à la résistance en fatigue des joints soudés d'une part, et à la sollicitation des éléments de charpente de grue à tour d'autre part. Ces deux distributions, nommées respectivement  $N_R$  et  $N_S(t)$  sur la figure 3, sont exprimées en nombre de cycles à capacité nominale de l'élément de charpente considéré.

### **Modélisation stochastique de la résistance**

La modélisation stochastique de la résistance des joints soudés de grue est effectuée en deux temps. La première étape consiste à calibrer plusieurs facteurs (contrainte moyenne, épaisseur des tôles, indice de flexion) intervenant dans la formule de calcul de durée de vie en fatigue des assemblages soudés à partir de résultats d'essais de la littérature. La seconde étape vise à confronter, au travers d'un nuage de points unique, des résultats expérimentaux avec les durées de vie calculées à partir d'un modèle par éléments finis et de la formule calibrée précédemment. Le nuage de points ainsi obtenu permet d'évaluer la

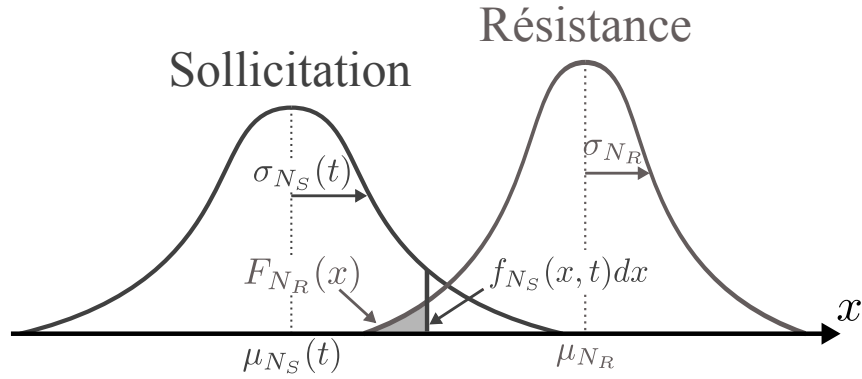


FIGURE 3 – Méthode de fiabilité dite “contrainte-résistance”.

dispersion globale des durées de vie en fatigue des assemblages soudés couramment utilisés dans les chapentes de grue à tour. Connaissant cette dernière, la densité de probabilité liée à la résistance d’un détail soudé particulier est facilement obtenue en effectuant un unique calcul par éléments finis permettant de prédire sa durée de vie médiane.

### Modélisation stochastique de la sollicitation

La modélisation stochastique de la sollicitation des éléments de charpente s’appuie sur l’ensemble des données présentées dans le chapitre 3. La procédure proposée est basée sur la définition de diverses densités de probabilité paramétriques tenant compte à la fois des paramètres dits “intra-chantier” (topographie) et “inter-chantier” (durée de chantier, configuration de grue, etc). Des cycles de grue sont ensuite générés artificiellement en tirant successivement des réalisations des paramètres intra-chantier dans leurs distributions respectives (portée de départ et d’arrivée, angle de départ et d’arrivée et charge levée). Cela suppose que les paramètres de ces distributions soient fixés pour le chantier considéré. La deuxième phase consiste alors à renouveler l’étape précédente sur de nombreux chantiers en tirant des réalisations dans les distributions des paramètres inter-chantier (temps de chantier et d’inter-chantier, longueur de flèche, paramètres des distributions intra-chantier, etc). Les cycles générés sont ensuite convertis à chaque itération en un effort dans l’élément de charpente considéré. De ce signal temporel sont extraites des étendues d’effort à l’aide de la méthode de comptage rainflow [7–9]. Enfin, ces cycles de fatigue sont transformés en un nombre de cycles équivalents à capacité nominale de l’élément par l’intermédiaire de la loi d’endommagement de Palmgren-Miner [10, 11]. La méthode décrite précédemment est réitérée un grand nombre de fois via la méthode de simulation de Monte Carlo [12, 13] afin d’évaluer la distribution de nombre de cycles de sollicitations en fonction de la durée d’exploitation de la grue (1 an, 5 ans, 10 ans, etc).

### Etude de sensibilités du modèle de sollicitation

Sachant que la dispersion des distributions de la résistance et de la sollicitation a un

---

fort impact sur le niveau de fiabilité évalué par la méthode “contrainte-résistance”, et étant donné que le modèle de sollicitation développé précédemment repose sur un certain nombre d’hypothèses, une analyse de sensibilité est mise en place. Celle-ci repose sur le calcul des indices globaux de Sobol’ et a pour objectif d’identifier les paramètres dont la variance a un impact significatif sur la variance de la distribution de la sollicitation, *i.e.* la distribution du nombre de cycles de chargement équivalents à capacité nominale de l’élément de charpente considéré.

### **Etude fiabiliste des éléments de charpente de grue à tour**

L’étude fiabiliste présentée dans cette thèse est basée sur la méthode “contrainte-résistance” [6, 14–17] et a pour particularité de dépendre de la durée d’exploitation des grues. Comme le montre la figure 4, les densités de probabilité de la résistance et de la sollicitation sont définies séparément. Le modèle de résistance des joints soudés permet, à l’aide d’un calcul par éléments finis de l’élément de charpente considéré, de caractériser la distribution de la résistance  $N_R$ . Dans le même temps, les données provenant du monitoring de grue et des bases de données de durées et de plans de chantier conduisent à la création d’un modèle de sollicitation permettant d’obtenir la distribution de sollicitation  $N_S(t)$ . Une fois ces deux densités de probabilité caractérisées, il est possible d’évaluer la fiabilité  $\mathcal{R}$  des éléments de charpente de grue à tour en fonction de leur durée d’exploitation  $t$  :

$$\mathcal{R}(t) = 1 - P_f(t) = 1 - \int_{-\infty}^{\infty} f_{N_S}(x, t) F_{N_R}(x) dx \quad (1)$$

où  $P_f$  est la probabilité de défaillance instantanée,  $f_{N_S}$  est la fonction de densité de probabilité liée à la sollicitation et  $F_{N_R}$  est la fonction de répartition de la résistance. Il convient régulièrement d’utiliser dans les études probabilistes une mesure de fiabilité adimensionnée nommée *indice de fiabilité*  $\beta(t)$ , qui peut être calculé de la façon suivante :

$$\beta(t) = -\Phi^{-1}(1 - \mathcal{R}(t)) \quad (2)$$

La procédure présentée en figure 4 permet ainsi d’évaluer le niveau de fiabilité en fatigue de tous les éléments de charpente de grue en fonction de leur durée d’exploitation.

## **Applications et résultats**

Une application de la méthode présentée précédemment est effectuée à la fin du chapitre 4. Celle-ci concerne l’élément d’éclissage de membrure supérieure de flèche, cerclé en pointillé sur la figure 1 (a). Ayant vérifié que ce type d’élément de charpente est exclusivement sollicité par les mouvements de distribution et de levage et que son endommagement par fatigue est gouverné par les cycles de coulage (plus de 70% de l’endommagement total), la modélisation stochastique des paramètres dits “intra-chantier” est réduite aux seules distributions

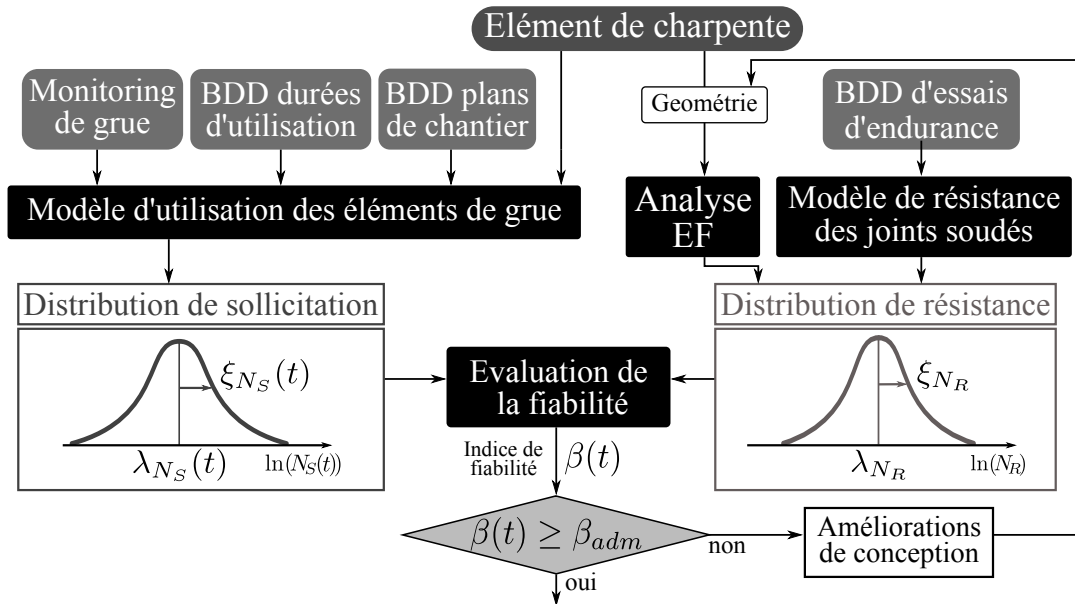


FIGURE 4 – Procédure d’évaluation de l’indice de fiabilité des éléments de charpente de grues à tour.

de portée et de charge associées uniquement au coulage. C’est pourquoi les distributions de portée de départ et de charge levée sont respectivement modélisées par des densités de probabilité normales tandis que la distribution de portée d’arrivée est caractérisée à l’aide d’une densité triangulaire. Les paramètres “inter-chantier” sont quant à eux modélisés de la même façon quel que soit l’élément de charpente considéré. La distribution de la sollicitation de l’éclissage de membrure supérieure de flèche est ensuite obtenue en utilisant la méthode itérative décrite précédemment. Dans le même temps, un calcul par éléments finis permet d’évaluer la résistance médiane, et donc la distribution de la résistance totale, de cet élément de charpente, étant donné que sa dispersion est connue à l’avance. Une fois ces densités de probabilité caractérisées, la méthode “contrainte-résistance” développée durant cette étude permet d’évaluer l’indice de fiabilité de cet élément de grue en fonction de sa durée d’exploitation. Il s’avère que même après 40 années en service, l’indice de fiabilité de cet élément de charpente reste élevé (supérieur à 6 après 40 ans). De plus, l’analyse de sensibilité liée au modèle de sollicitation révèle que les paramètres les plus influents sur la dispersion de la distribution de sollicitation sont le poids de la benne à béton, la position des camions-benne, le nombre de mètres cubes de béton coulé par mois et par équipe, et le nombre de quarts effectués par jour de chantier.

## Conclusions et perspectives

Une méthode fiabiliste permettant d’évaluer le niveau de fiabilité d’éléments de charpente de grue à tour a été développée au cours de ce travail de recherche. Basée sur l’utilisation

---

d'une méthode "contrainte-résistance" dépendante du temps, la méthode proposée consiste à considérer séparément, au travers de deux distributions de probabilité, les incertitudes liées à la résistance en fatigue des joints soudés de grue et à la variabilité du chargement dans le temps des éléments de charpente de grue. La capitalisation d'un grand nombre de résultats d'essais d'endurance au travers d'un nuage de points unique permet de prédire la distribution de la résistance en fatigue de n'importe quel joint soudé, même pour une géométrie complexe. D'autre part, la modélisation stochastique du chargement des éléments de charpente tient compte à la fois de la variabilité dite "intra-chantier" (topographie des chantiers) ainsi que des incertitudes liées au passage d'un chantier à l'autre (paramètres dits "inter-chantier"). De plus, une analyse de sensibilité globale visant à évaluer l'impact de la variance de chaque variable aléatoire sur la dispersion de la distribution de sollicitation permet de guider a posteriori les investigations à réaliser dans le futur concernant certaines hypothèses de modélisation.

Ce travail de recherche ouvre diverses perspectives. Tout d'abord, l'application de la méthode fiabiliste proposée dans cette thèse peut être menée sur d'autres éléments de charpente de grue dont le chargement provient aussi du mouvement d'orientation de la flèche. Cela suppose de prendre en compte dans le modèle de sollicitation les variations d'angle d'orientation. Bien que la forme des distributions de charge et de portée soit sensiblement identique d'un chantier à l'autre, ce n'est pas le cas des distributions d'angle, ce qui implique d'investiguer la manière de les considérer dans le modèle de sollicitation.

La méthode "contrainte-résistance" proposée dans cette thèse permet de cartographier le niveau de fiabilité de tous les éléments de charpente de grue à tour, ce qui représente la première étape du dimensionnement fiabiliste. La seconde étape consiste à définir des objectifs de fiabilité pour chaque élément de charpente vis-à-vis de divers critères. Ceux-ci pourraient par exemple considérer la capacité de l'élément à résister à une fissure (redundance), la gravité des conséquences en cas de rupture de l'élément, la capacité à détecter une fissure (accessibilité en cas d'inspection) ou bien le nombre d'éléments de charpente identiques en exploitation. Il faut noter que ces objectifs de fiabilité devront être en accord avec le retour d'expérience provenant de bases de données de retours clients ou de garanties à long terme.

L'analyse de sensibilité développée dans ce travail de recherche traite de l'évaluation d'indices de Sobol' qui permettent de quantifier l'impact de la variance de paramètres d'entrée sur la dispersion des résultats d'un modèle mathématique ou mécanique. Néanmoins, ces indices ne permettent pas de juger de l'impact de la valeur moyenne des variables aléatoires sur la valeur moyenne de la sortie du modèle, or cette information peut s'avérer utile au même titre que les indices de Sobol'. C'est pourquoi l'évaluation d'autres mesures de sensibilités telles que les indices de Borgonovo [18] pourrait être mise en place dans le but de compléter l'analyse de sensibilité réalisée dans cette thèse.



---

---

# Contents

|                                                                               |           |
|-------------------------------------------------------------------------------|-----------|
| <b>List of notations</b>                                                      | <b>1</b>  |
| <b>Introduction</b>                                                           | <b>5</b>  |
| <b>1 General aspects and motivations for tower crane probabilistic design</b> | <b>9</b>  |
| 1.1 Introduction . . . . .                                                    | 10        |
| 1.2 Tower cranes and structural members . . . . .                             | 10        |
| 1.3 Crane structural members deterministic design . . . . .                   | 13        |
| 1.4 Construction site variabilities . . . . .                                 | 16        |
| 1.5 Probabilistic approaches opportunities . . . . .                          | 19        |
| 1.6 Conclusion . . . . .                                                      | 21        |
| Chapter summary . . . . .                                                     | 22        |
| <b>2 Fatigue design and reliability assessment under operating loads</b>      | <b>23</b> |
| 2.1 Introduction . . . . .                                                    | 24        |
| 2.2 Fatigue phenomenon . . . . .                                              | 25        |
| 2.2.1 Fatigue of welded details . . . . .                                     | 25        |
| 2.2.2 Influence factors on fatigue of welded joints . . . . .                 | 26        |
| 2.2.3 Equivalent stress representing fatigue behavior . . . . .               | 28        |
| 2.2.4 Probabilistic S-N curves . . . . .                                      | 29        |
| 2.2.5 Cumulative damage assessment . . . . .                                  | 33        |
| 2.3 Fatigue loading assessment and modeling . . . . .                         | 35        |
| 2.3.1 Rainflow cycle counting method . . . . .                                | 35        |
| 2.3.2 Random processes models for fatigue loading . . . . .                   | 38        |
| 2.3.3 Elementary loads mix strategy . . . . .                                 | 45        |
| 2.3.4 Mixture models of loading spectra . . . . .                             | 46        |
| 2.4 General reliability methods . . . . .                                     | 50        |
| 2.4.1 Time-dependent reliability . . . . .                                    | 51        |
| 2.4.2 Stress-strength interference methods . . . . .                          | 52        |
| 2.4.3 Reliability index . . . . .                                             | 53        |
| 2.4.4 Monte Carlo simulations . . . . .                                       | 55        |

|          |                                                                                  |           |
|----------|----------------------------------------------------------------------------------|-----------|
| 2.4.5    | Stochastic sensitivity analysis . . . . .                                        | 57        |
| 2.5      | Conclusion . . . . .                                                             | 60        |
|          | Chapter summary . . . . .                                                        | 61        |
| <b>3</b> | <b>Crane work data analysis</b>                                                  | <b>63</b> |
| 3.1      | Introduction . . . . .                                                           | 64        |
| 3.2      | Construction site data processing . . . . .                                      | 64        |
| 3.2.1    | Construction site data recording . . . . .                                       | 64        |
| 3.2.2    | Crane cycle identification . . . . .                                             | 66        |
| 3.2.3    | Crane cycle per type of work . . . . .                                           | 67        |
| 3.3      | Construction sites characteristics . . . . .                                     | 71        |
| 3.4      | Intra-construction site data post-processing . . . . .                           | 72        |
| 3.4.1    | Data versus load chart . . . . .                                                 | 73        |
| 3.4.2    | Data versus construction site working area . . . . .                             | 75        |
| 3.4.3    | Data depicted by using histograms . . . . .                                      | 75        |
| 3.5      | Intra-construction site loading severity assessment . . . . .                    | 80        |
| 3.5.1    | Severity calculation procedure . . . . .                                         | 84        |
| 3.5.2    | Severity assessment of a jib top member connection . . . . .                     | 85        |
| 3.6      | Inter-construction site variability quantification . . . . .                     | 87        |
| 3.6.1    | Inter-construction site durations from crane rental agency data . . . . .        | 87        |
| 3.6.2    | Inter-construction site configuration parameters from drawings . . . . .         | 89        |
| 3.7      | Conclusion . . . . .                                                             | 94        |
|          | Chapter summary . . . . .                                                        | 95        |
| <b>4</b> | <b>Reliability assessment of crane members using a time-dependent SSI method</b> | <b>97</b> |
| 4.1      | Introduction . . . . .                                                           | 98        |
| 4.2      | Crane member strength stochastic modeling . . . . .                              | 98        |
| 4.2.1    | Welded details FE modeling . . . . .                                             | 98        |
| 4.2.2    | Fatigue lifespan prediction using shell elements with MPC equations . . . . .    | 101       |
| 4.2.3    | Strength distribution of crane welded details . . . . .                          | 105       |
| 4.3      | Crane use stochastic modeling . . . . .                                          | 111       |
| 4.3.1    | Crane use distribution . . . . .                                                 | 111       |
| 4.3.2    | Application to a jib top member connection . . . . .                             | 116       |
| 4.4      | Sensitivity analysis of jib member use distribution . . . . .                    | 125       |
| 4.5      | Reliability assessment of crane welded details . . . . .                         | 128       |
| 4.5.1    | General synoptic of the proposed SSI method in the design stage . . . . .        | 128       |
| 4.5.2    | Application on jib top member connections . . . . .                              | 130       |
| 4.6      | Conclusion . . . . .                                                             | 131       |
|          | Chapter summary . . . . .                                                        | 133       |

|                                                               |            |
|---------------------------------------------------------------|------------|
| <b>Conclusion and future works</b>                            | <b>135</b> |
| <b>Bibliography</b>                                           | <b>137</b> |
| <b>A Construction site drawing processing</b>                 | <b>149</b> |
| A.1 Data collection from construction site drawings . . . . . | 149        |
| A.2 Processing of the collected data . . . . .                | 152        |



---

# List of notations

## Values related to crane use

---

|                                     |                                                                        |
|-------------------------------------|------------------------------------------------------------------------|
| $C$                                 | Crane capacity                                                         |
| $R_{\text{jib}}$                    | Jib length                                                             |
| $R_{\text{jib}}/R_{\text{jib,max}}$ | Jib length ratio                                                       |
| $M, L, R, \alpha$                   | Moment, force, radius and slewing angle                                |
| $R_1$                               | Initial radius of a crane cycle                                        |
| $R_2$                               | Final radius of a crane cycle                                          |
| $\alpha_1$                          | Initial slewing angle of a crane cycle                                 |
| $\alpha_2$                          | Final slewing angle of a crane cycle                                   |
| $L_{\text{max}}$                    | Maximum load that can be hoisted during a crane cycle                  |
| $R_{\text{max}}$                    | Maximum radius that can be reached during a crane cycle                |
| $T_{\text{on-site}}$                | Construction site duration                                             |
| $T_{\text{stored}}$                 | Time between two construction sites                                    |
| $N_{\text{shifts}}$                 | Number of shifts on the construction site                              |
| $C_{\text{bucket}}$                 | Concrete bucket capacity                                               |
| $V_{\text{concrete}}$               | Volume of concrete poured per month and per shift                      |
| $d_{CG}/R_{\text{jib}}$             | Normalized location of the center of gravity of loading/unloading area |

---

## Values related to fatigue analysis

---

|                                       |                                                                                 |
|---------------------------------------|---------------------------------------------------------------------------------|
| $(A), (B)$                            | Extreme load cases reached during a crane cycle                                 |
| $N$                                   | Number of cycles                                                                |
| $N_{\text{cal}}, N_{\text{exp}}$      | Predicted and experimental median number of cycles                              |
| $N_i$                                 | Total number of cycles before failure at constant stress range $\Delta\sigma_i$ |
| $N_{eq}, N_{eq}^{res}$                | Equivalent number of cycles at nominal capacity                                 |
| $F_{\text{min}}, \sigma_{\text{min}}$ | Force or stress minimum                                                         |
| $F_{\text{max}}, \sigma_{\text{max}}$ | Force or stress maximum                                                         |
| $F_a, \sigma_a$                       | Force or stress amplitude                                                       |

---

|                                         |                                                                                 |
|-----------------------------------------|---------------------------------------------------------------------------------|
| $F_m, \sigma_m$                         | Force or stress mean                                                            |
| $\Delta F, \Delta \sigma$               | Force or stress range                                                           |
| $s_c$                                   | Stress history parameter                                                        |
| $\Delta \sigma_c$                       | Characteristic fatigue strength at $2 \cdot 10^6$ cycles with 97.7% of survival |
| $\Delta \sigma_{R_d}$                   | Limit design stress range                                                       |
| $\Delta \sigma_{S_d}$                   | Maximum nominal stress range                                                    |
| $\bar{\sigma}$                          | Stress tensor                                                                   |
| $\sigma_D$                              | Endurance limit                                                                 |
| $\tau_a$                                | Shear stress amplitude                                                          |
| $P$                                     | Hydrostatic pressure                                                            |
| $r, r_0$                                | Bending index                                                                   |
| $e$                                     | Plate thickness                                                                 |
| $\kappa$                                | Stress or force ratio ( $\sigma_{\min}/\sigma_{\max}$ or $F_{\min}/F_{\max}$ )  |
| $\tau_{0,i}$                            | Local equivalent shear stress amplitude related to $N_i$                        |
| $\tau_0$                                | Local equivalent shear stress amplitude                                         |
| $\tau_{\text{ref}}, e_{\text{ref}}$     | Reference values of shear stress and plate thickness                            |
| $\Delta F_{\text{ref}}, N_{\text{ref}}$ | Reference values of force and number of cycles                                  |
| $\epsilon$                              | Predictive model error                                                          |
| $E$                                     | Damage indicator function (Dang Van criterion)                                  |
| $q, p$                                  | Percentages of survival and failure ( $q = 1 - p$ )                             |
| $D_i, D$                                | Partial and total damage                                                        |

---

## Random values

### Scalar and statistical values

---

|                                  |                                                                              |
|----------------------------------|------------------------------------------------------------------------------|
| $X$ or $X(\omega)$               | Random variable                                                              |
| $f_X(\cdot)$                     | Probability density function (PDF) of the random variable $X$                |
| $F_X(\cdot)$                     | Cumulative distribution function (CDF) of the random variable $X$            |
| $\mathcal{N}(\mu_X, \sigma_X)$   | Gaussian probability law of mean $\mu_X$ and standard deviation $\sigma_X$   |
| $\mathcal{LN}(\lambda_X, \xi_X)$ | Lognormal probability law of mean $\lambda_X$ and standard deviation $\xi_X$ |
| $\mathcal{U}(a_X, b_X)$          | Uniform probability law of lower bound $a_X$ and upper bound $b_X$           |
| $\mathbf{x}$                     | Vector of realizations of the random variable $X$                            |
| $T$                              | Isoprobabilistic transformation                                              |
| $R$                              | Strength (supply)                                                            |
| $S$                              | Stress (demand)                                                              |
| $N_R$                            | Strength number of cycles at nominal capacity                                |
| $N_S$                            | Stress number of cycles at nominal capacity                                  |
| $G$                              | Performance function                                                         |

---

---

|                    |                                                      |
|--------------------|------------------------------------------------------|
| $\mathcal{R}$      | Reliability                                          |
| $P_f$              | Failure probability                                  |
| $P_{f,i}, P_{f,c}$ | Instantaneous and cumulative failure probability     |
| $\beta$            | Reliability index                                    |
| $\beta_c$          | Cornell reliability index                            |
| $\beta_{HL}$       | Hasofer-Lind reliability index                       |
| $\beta_{adm}$      | Admissible reliability index                         |
| $D_f$              | Failure domain                                       |
| $I_{D_f}$          | Indicator function                                   |
| $\phi_n$           | Joint standard Gaussian probability density function |

---

## Random processes

---

|                             |                                                               |
|-----------------------------|---------------------------------------------------------------|
| $t$                         | Time                                                          |
| $\omega$                    | Randomness                                                    |
| $(\Omega, \mathcal{F}, P)$  | Probability space                                             |
| $\mathcal{T}$               | Metric space                                                  |
| $E$                         | State space                                                   |
| $X(\omega, t)$              | Random process                                                |
| $m_X(t)$                    | Mean of the random process $X(\omega, t)$                     |
| $\text{Var}_X(t)$           | Variance of the random process $X(\omega, t)$                 |
| $\text{Cov}_X(t_1, t_2)$    | Autocovariance function of the random process $X(\omega, t)$  |
| $\Gamma_X(t_1, t_2)$        | Autocorrelation function of the random process $X(\omega, t)$ |
| $\phi_1, \dots, \phi_p$     | Real coefficients of AR models                                |
| $\theta_1, \dots, \theta_p$ | Real coefficients of MA models                                |
| $X_t(\omega)$               | Discrete-time random process                                  |
| $X_n$                       | Discrete-time Markov chain                                    |
| $P$                         | Transition matrix of the markov chain $X_n$                   |

---

## Elementary load mix strategy

---

|                 |                                                                               |
|-----------------|-------------------------------------------------------------------------------|
| $p, q$          | Probabilities                                                                 |
| $A_i$           | $i$ th situation related to quantity $A$                                      |
| $B_j$           | $j$ th situation related to quantity $B$                                      |
| $L_{i,j}^{(k)}$ | $k$ th elementary load related to the $i$ th and $j$ th elementary situations |
| $\mathbb{L}$    | Mixed loading                                                                 |

---



## Mixture models

---

|                     |                                                             |
|---------------------|-------------------------------------------------------------|
| $f(\Delta\sigma)$   | Multi-modal rainflow ranges PDF                             |
| $F(\Delta\sigma)$   | Multi-modal rainflow ranges CDF                             |
| $f_l(\Delta\sigma)$ | $l$ th component PDF                                        |
| $w_l$               | $l$ th weighting factor related to the $l$ th component PDF |
| $H(\Delta\sigma)$   | Loading spectrum                                            |
| $H_0$               | Total number of load cycles                                 |

---

## Monte Carlo simulations

---

|                       |                                                  |
|-----------------------|--------------------------------------------------|
| $N_{MC}$              | Number of Monte Carlo simulations                |
| $t_{1-\alpha/2}(\nu)$ | Student variable of parameter $\nu = N_{MC} - 1$ |
| $\alpha$              | Percentage of confidence of the estimation       |

---

## Sensitivity analysis

---

|                    |                                                                        |
|--------------------|------------------------------------------------------------------------|
| $f$                | Integrable function on the $p$ -dimensional interval $I^p$             |
| $X$                | Random variables involved in $f$                                       |
| $V$                | Variance of the response $Y = f(X)$                                    |
| $V_i$              | Variance related to the $i$ th random variable                         |
| $\hat{V}_{\sim i}$ | Variance resulting from the variation of all parameters excepted $X_i$ |
| $V_{ij}$           | Variance related to the $i$ th and $j$ th random variables             |
| $S_i$              | First-order Sobol' index related to $X_i$                              |
| $S_{ij}$           | Second-order Sobol' index related to $X_i$ and $X_j$                   |
| $S_{T_i}$          | Total Sobol' index related to $X_i$                                    |
| $N$                | Number of realizations used to estimate the Sobol' indices             |

---

---

# Introduction

## Context

Tower cranes are equipments that enable to hoist a wide variety of building materials (concrete, steel grids, heavy tools, etc.) on construction sites. They are made of structural members (steel plates or beams) connected by welding. Due to the cyclic nature of the work performed on the sites, tower cranes may undergo fatigue failure after a given operating period. As a result, the consideration of this phenomenon in structural design is essential. Nonetheless, a substantial number of uncertainties inherent to fatigue may complicate this task. Various experimental studies showed for instance, that the fatigue behavior of materials is intrinsically scattered. Moreover, crane users face increasing pressure to shorten drastically the time required to complete a job, which leads to an intensive crane use. Therefore, the operating conditions (loading levels applied to structures) may vary significantly depending on customer uses. Industrial structures such as crane structural members are generally designed for fatigue by means of deterministic procedures provided by standards and are sometimes completed by additional knowledge acquired through experience feedback. These methods usually consider deterministic rules that are supposed to ensure structural safety. Therefore, the uncertainties inherent to fatigue are implicitly taken into account through these rules. Even though deterministic approaches provide appropriate results in most cases, they do not give any information concerning the reliability level of the structure according to the operating period, which represents their main limit. Thus, the design of optimized structures that remain functional and safe requires a better understanding and management of the uncertainties influencing the structural behavior. From this perspective, reliability approaches represent helpful methods allowing engineers to fulfill this objective. They enable to acquire a better knowledge of the uncertainties related to fatigue and to propagate them into the mechanical response of structures.

Probabilistic approaches are still rarely used in industry due to the cultural breakaway that they represent. Nonetheless, two French projects involving reliability approaches in an industrial context was launched respectively in 2005 and 2008. The first project named DEFFI (**DE**marche **Fi**abiliste de conception en **F**atigue pour l'**I**ndustrie) was started by CETIM in 2005. This project aimed at developing the probabilistic stress-strength

interference approach for mechanical fatigue design of industrial structures from different fields (aeronautics, aerospace, railway, etc) [1–3]. A few years later, the APPRoFi project (**AP**proche mécano-**PR**obabiliste pour la conception robuste en **F**atigue) [4] was launched in order to promote the potential benefits of reliability approaches in fatigue design. This project involved academic partners (LaMI-IFMA, LMT-ENS Cachan, Laboratoire Roberval-UTC) in collaboration with companies (Modartt, Phimeca, CETIM, SNECMA). The DEFFI and APPRoFi projects demonstrate the growing interest that companies manifest concerning probabilistic approaches. In a similar way, the present work aims at developing a comprehensive probabilistic procedure enabling to assess the reliability level of tower crane structural members depending on their operating time.

### Thesis objectives

The following points are investigated in this work in order to fulfill the main scientific objective mentioned above:

- **Analysis of fatigue design rules provided by standards.** EN 13001 standard is studied in order to underline the basic principles and main assumptions involved in the fatigue design validation process of crane structural members.
- **Stochastic modeling of crane member strength.** This point aims at developing a procedure enabling the capitalization of fatigue test results and the modeling of the uncertainties inherent to the strength of crane structural welded details.
- **Stochastic modeling of crane member use.** Based on crane monitoring data, a two-level modeling procedure is proposed to identify and characterize the uncertainties related to crane member operating loads according to their operating time. This point constitutes the first key issue of this research work.
- **Sensitivity analysis of the crane member use model.** Given that the scatter of crane member use may have a large influence on reliability results, a sensitivity analysis must be performed in order to identify the most influencing parameters involved in the crane member use model.
- **Reliability assessment of crane structural members.** A general probabilistic approach is proposed to assess the reliability level of crane structural members according to their operating time. This point constitutes the second key issue of this research work.

### Contents

This thesis is divided into four chapters. Chapter 1 is devoted to the presentation of the opportunities that represent probabilistic approaches for fatigue design of tower cranes.

The vocabulary related to tower crane structural members and movements is first introduced, and the deterministic procedure provided by standards to validate crane structural members is detailed. Following this, the different sources of variability that influence tower crane use on the construction sites are listed, and several opportunities offered by probabilistic approaches are examined.

Chapter 2 is concerned with the fatigue design and reliability assessment under operating loads. Efficient tools commonly used to assess the fatigue strength of welded details are first detailed. Three methods enabling the stochastic modeling of fatigue operating loads are then discussed, and the general principles related to the assessment of the reliability according to operating time are finally detailed.

Chapter 3 focuses on the characterization of the work performed by the crane on construction sites. After explaining the methods implemented to handle data coming from crane monitoring, the results of intra-construction site post-processing are illustrated on three construction sites. Then, the loading severity assessment procedure is presented and applied on a given crane structural member. Lastly, data from crane rental agencies and construction companies are processed in order to characterize the variability induced by the change of construction site.

Chapter 4 describes the comprehensive probabilistic method proposed in this work to assess the reliability of crane structural members according to their operating time. The stochastic modeling of fatigue strength of crane welded details is first detailed. Following this, a two-level procedure enabling to model the crane member use is proposed, and the impact of the variability of each input parameter on the scatter of crane use model is quantified by means of sensitivity analysis. Finally, the global reliability assessment procedure of crane structural members is detailed and applied to a given crane member.



---

# Chapter 1

## General aspects and motivations for tower crane probabilistic design

### Contents

---

|     |                                                         |    |
|-----|---------------------------------------------------------|----|
| 1.1 | Introduction . . . . .                                  | 10 |
| 1.2 | Tower cranes and structural members . . . . .           | 10 |
| 1.3 | Crane structural members deterministic design . . . . . | 13 |
| 1.4 | Construction site variabilities . . . . .               | 16 |
| 1.5 | Probabilistic approaches opportunities . . . . .        | 19 |
| 1.6 | Conclusion . . . . .                                    | 21 |
|     | Chapter summary . . . . .                               | 22 |

---

## 1.1 Introduction

Cranes are machines enabling the transportation of heavy loads beyond the normal capability of a human. Although first cranes were invented by Greeks in the late 6th century before Christ, the first cranes using internal combustion, hydraulic or electric engines were designed during the 20th century. Cranes have become more and more efficient thanks to the great technological inventions and progresses appeared during the last century. That explains why they are today essential tools for many types of work. For instance, harbor cranes are used to load or unload container ships, overhead cranes are usually used to hoist heavy weights from one place to another in a factory, tower cranes are used in construction sites, etc. Only tower cranes are studied in the framework of this thesis.

Tower crane structures are principally made of steel plates and beams connected by welding. The use of tower cranes on construction sites is essential for construction companies in order to shorten the amount of time needed to complete a work by maximizing the efficiency of teams. Tower cranes are therefore used in an intensive manner on successive construction sites during its operating lifespan. Each construction site being unique in terms of topography and duration, the work performed by the crane can be substantially different from one construction site to another. Thus, tower crane structures are subjected to cyclic loading of variable amplitudes, which may lead to fatigue issues after a given operating period. This explains why the fatigue strength of crane structural members is a fundamental aspect that must be considered by designers.

Probabilistic approaches are helpful to consider the variability of the crane welded details strength, which is intrinsically unpredictable, and the uncertainties coming from various crane uses. They provide engineers with efficient tools enabling to handle these uncertainties in order to design functional structures that remain safe. This chapter, which is devoted to the introduction of tower cranes and the presentation of the opportunities offered by probabilistic approaches, is organized as follows. Section 1.2 briefly describes the different types of tower cranes, enumerates the main structural joints that constitute a tower crane and shows the movements that can be performed by the tower crane. Section 1.3 introduces the deterministic rules specified by European standards dealing with the design of tower cranes and section 1.4 presents how construction sites are organized. Finally, the numerous advantages that probabilistic approaches can bring to the fatigue design of tower cranes are pointed out in section 1.5.

## 1.2 Tower cranes and structural members

This section aims at presenting the different tower crane ranges, the main assemblies constituting a saddle jib tower crane and all the movements that can be performed by a tower crane.

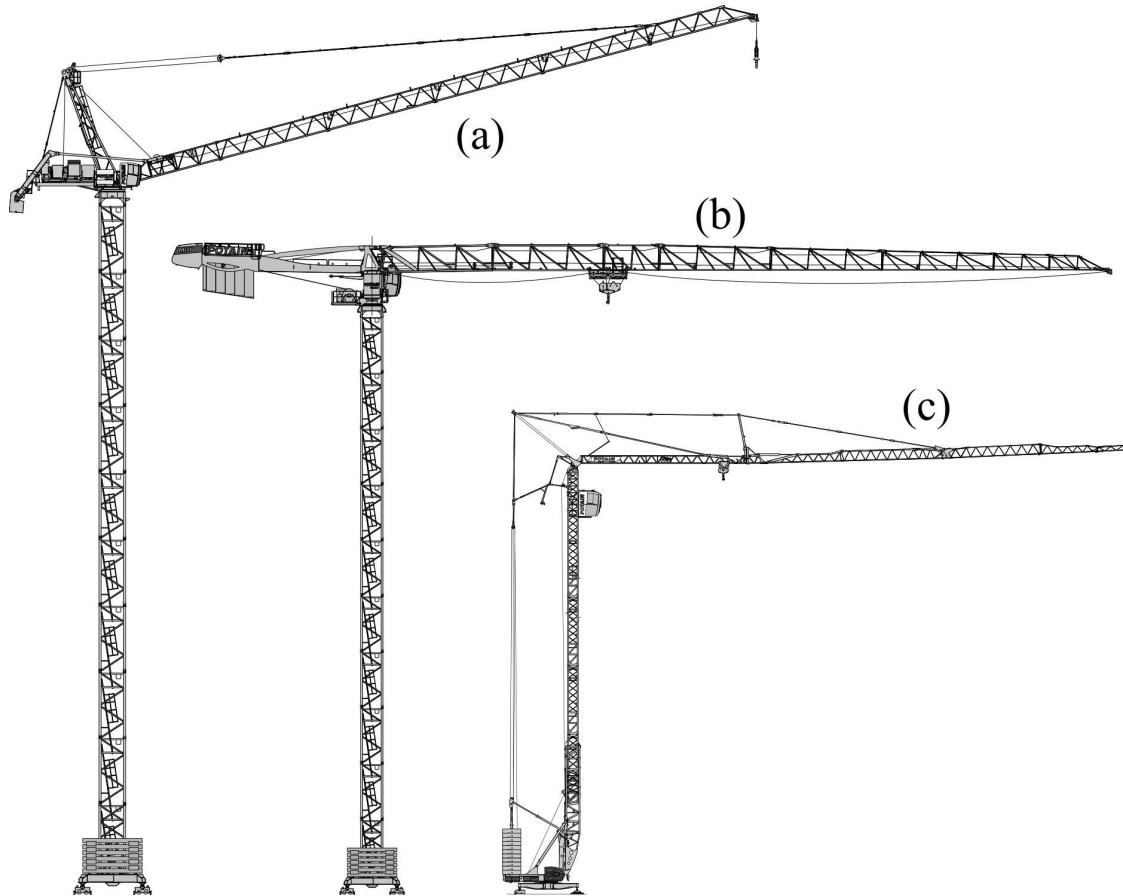


Figure 1.1 – Tower crane ranges: (a) luffing jib tower crane, (b) saddle jib tower crane and (c) self-erecting tower crane.

### Tower crane ranges

The first tower crane family includes luffing jib tower cranes and saddle jib tower cranes denoted respectively by (a) and (b) in figure 1.1. Because their jib have the ability to tilt, luffing jib tower cranes are useful when the work area is very limited. This is the case for instance of very tall buildings constructed in big cities where loads cannot be hoisted above the streets for safety reasons. Saddle jib tower cranes is the most commonly used for medium-to-big sized construction sites. The main advantage of these cranes is the possibility to use very different configurations in terms of horizontal or vertical dimensions. This makes them extremely adjustable in order to fit well the dimensions of the building to be built. Then, the second tower crane family denoted by (c) in figure 1.1 corresponds to self-erecting cranes, which are mainly used for small-to-medium sized construction sites. As their name implies, these cranes have the ability to be assembled without outside help in a short time-period (a few hours). Although the procedure presented in this thesis is applicable to any type of tower crane, for the sake of clarity, the following developments focus exclusively on saddle jib tower cranes.



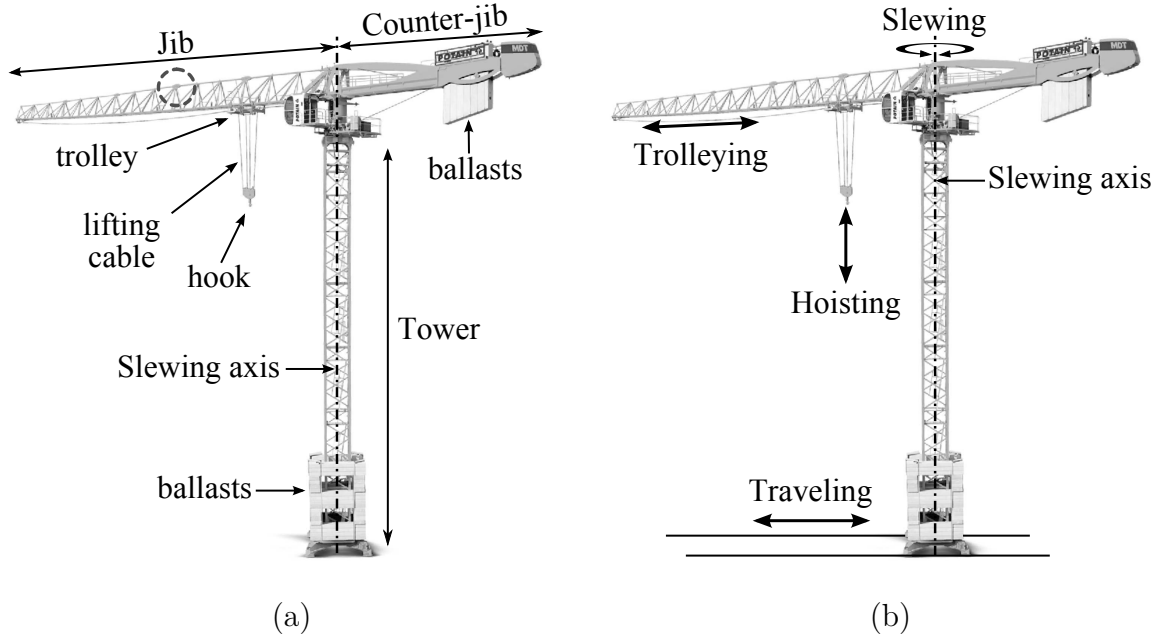


Figure 1.2 – Saddle jib tower crane vocabulary for (a) crane structural assemblies (a jib chord member is surrounded by a dotted circle) and (b) crane movements.

### **Tower crane main assemblies**

As presented in figure 1.2 (a), a saddle jib tower crane consists of three main structural assemblies, namely the jib, the counter-jib and the tower. The jib is on the left side of the slewing axis (neutral axis of the tower) and the counter-jib on the right side. The function of the counter-jib is to support ballasts, generally made of reinforced concrete, while the jib allows the trolley to move from one radius to another. The tower, which consists of a series of similar elements and is ballasted at its base, supports the total weight of the slewing assembly made of the jib and the counter-jib plus the hoisted load. Finally, the lifting wire rope enables the vertical displacement of the hook in order to hoist or lower a load. Note that all the results deriving from the application of the global procedure presented in this thesis are fully detailed on a jib chord member connection (see figure 1.2(a)) only, for the sake of clarity.

### **Tower crane movements**

As illustrated in figure 1.2 (b), the first of the four movements performed by the crane is the *hoisting* of a load by means of the hook. The second movement, named *trolleying*, corresponds to the horizontal displacement of the trolley along the jib. The third movement is the *slewing* of the jib around the vertical slewing axis. Sometimes, tower cranes are also used on bogeys in order to travel on rails, which corresponds to a new crane movement, namely the *traveling*. In the frame of this thesis, the traveling movement is not considered.

## 1.3 Crane structural members deterministic design

This section presents the basic concepts and the design process used in standards dealing with the fatigue design of tower cranes.

### Crane design European standards

Steel structures are usually designed by following the rules provided by standards such as Eurocodes [19] or DNV recommended practices [20] for instance. Note that only the standards dealing specifically with the design of lifting appliances, including those used in Manitowoc's engineering services, are presented in the frame of this thesis.

France and Germany have actively contributed since the 1960's to the elaboration of European standards dealing with the design of tower cranes. These standards are all based on similar basic principles, and the differences that exist lie in the definition of slightly shifted safety factors. The French national organization for standardization published in 1975 a standard dedicated to the design of tower cranes, namely the NF E 52081 [21]. In addition to this standard, the European Federation of Material Handling published a manual of recommendations for the design of lifting devices, namely the FEM 1.001 [22]. This manual aims at providing solid foundations enabling the design of any kind of lifting device by ranking them in use classes. In all these standards or recommendations, cranes must be validated according to several criteria such as static and fatigue strength, buckling and rigid body (tipping) stability.

A process emerged in the recent years (about the middle of the 2000's) in order to homogenize the standards at European level. This process started in 2004 is currently ongoing and consists in creating the EN 13001 [5]. Although EN 13001 is still experimental and starts to be referenced in product standards, this new European standard aims at replacing in a couple of years the standards and recommendations previously quoted. All the notions and concepts presented in the following are based on the European standards and recommendations presented previously, and are focused on fatigue strength validation only.

### Crane lifespan

Although the lifespan of a component is sometimes expressed in terms of operating duration, it is more relevant for tower crane structural members to specify the conventional lifespan in terms of the number of cycles  $N$ .

### Crane cycle definition

A crane hoisting cycle conventionally starts when the crane hoists a load and ends when the crane is ready to hoist another load. It consists of several stages: load hoisting, trolley in movement with the hoisted load, slewing of the jib around the slewing axis, load drop off, trolleying and slewing with no load. As depicted in figure 1.3, a simple way to represent

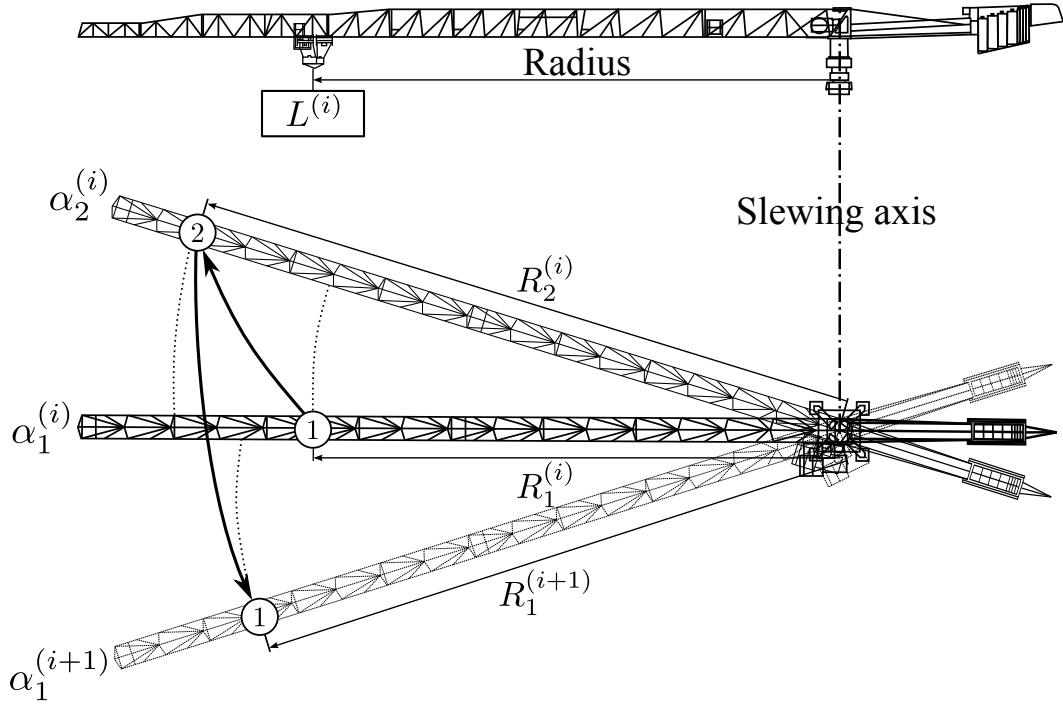


Figure 1.3 – Illustration of a crane cycle.

a crane cycle is to consider the set of variables  $\{R_1^{(i)}, R_2^{(i)}, \alpha_1^{(i)}, \alpha_2^{(i)}, L^{(i)}, R_1^{(i+1)}, \alpha_1^{(i+1)}\}$  where numbers 1 and 2 refer respectively to initial and final positions. The first part of the crane cycle is performed from  $\{R_1^{(i)}, \alpha_1^{(i)}\}$  to  $\{R_2^{(i)}, \alpha_2^{(i)}\}$  in order to move a load  $L^{(i)}$  from one place to another. The second part of the cycle is done from  $\{R_2^{(i)}, \alpha_2^{(i)}\}$  to  $\{R_1^{(i+1)}, \alpha_1^{(i+1)}\}$  without load in order to go to the location of another load to be hoisted.

### Load chart concept

To understand tower crane loading, the concept of load chart has to be introduced. The load chart example depicted in figure 1.4 shows the maximum load it is possible to hoist according to the position of the trolley along the jib, i.e. the radius  $R$ . For a given value of radius  $R^{(i)}$  during crane cycle, the load  $L^{(i)}$  that can be hoisted by the crane is necessarily below the load chart, i.e. below  $L_{\max}^{(i)} = f(R_1^{(i)})$  (see figure 1.4). As depicted in figure 1.4, the crane cycle loading sequence viewed from the load chart point of view is reduced to four stages: (1) load hoisting, (2) trolley in movement with the hoisted load, (3) load drop off, (4) trolleying with no load.

### Loading and stress spectra

Most of the time, operating loads of complex structures consist of series of events which cannot be fully defined by a Constant Amplitude (CA) loading with known characteristics (*e.g.* minimum and maximum). Therefore, Variable Amplitude (VA) loadings determined

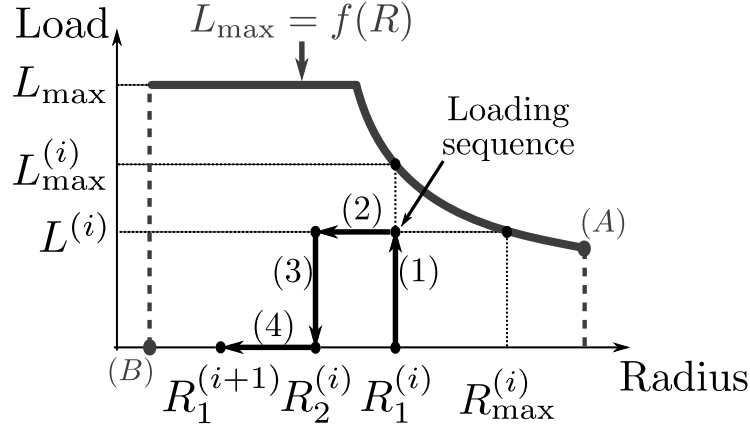


Figure 1.4 – Definition of the load chart.

by using a counting method such as the Rainflow method presented in 2.3.1 can be studied by using a convenient representation named *loading spectrum*. As depicted in figure 1.5, a loading spectrum is a curve characterizing all the VA loads counted during the lifespan of the structure and ordered by decreasing normalized load ranges  $\Delta L_i / \Delta L_{\max}$  depending on their occurrence  $i$ . If the VA loads derive directly from strain gauges signals (*i.e.* measured stress), a *stress spectrum* can be defined in the same manner by using normalized stress ranges  $\Delta \sigma_i / \Delta \sigma_{\max}$ . Note that a log-normal scale is sometimes used for the occurrences  $i$  in order to facilitate the understanding of the assessed spectra.

The stress history parameter  $s_c$  is a value reflecting the severity of the loading on a structural component. Based on the linear Palmgren-Miner damage accumulation rule presented in section 2.2.5, this parameter is assessed by using a stress spectrum as presented before and depends on the S-N curve slope  $c$  (see Basquin’s model in section 2.2.4):

$$s_c = \frac{1}{N_t} \sum_i \left[ \frac{\Delta \sigma_i}{\Delta \sigma_{\max}} \right]^c \quad (1.1)$$

where  $N_t$  is the total number of occurrences  $i$  of stress ranges  $\Delta \sigma_i$  during the design life of the crane and  $\Delta \sigma_{\max}$  is the maximum stress range. Note that in case of linear analysis of a structural component, *i.e.* linear relation between internal stress  $\sigma$  and applied force  $F$ , equation (1.1) can be rewritten by replacing  $\Delta \sigma_i$  and  $\Delta \sigma_{\max}$  respectively by  $\Delta F_i$  and  $\Delta F_{\max}$ .

### Fatigue design validation process according to standards

As depicted in figure 1.6, the fatigue strength validation process of a crane structural member consists of several steps. On one hand, the use of the crane member is determined, which enables to find the corresponding loading class depending on the value of the stress history parameter  $s_c$ . Tower crane structural members usually belong to S1, S2 or S3 classes in EN 13001 [5] (or E2, E3 or E4 in FEM 1.001 [22]). At the same time, the

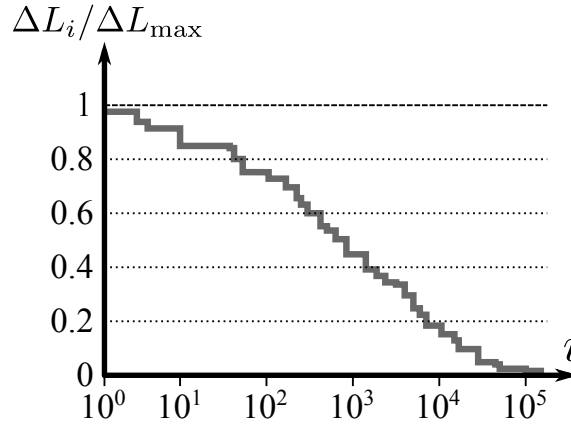


Figure 1.5 – Loading spectrum example.

structural member is classified into a notch class depending on its geometry. This leads to find the characteristic fatigue strength  $\Delta\sigma_c$ , corresponding to the fatigue strength at  $2 \cdot 10^6$  cycles under constant stress range loading, with a probability of survival of 97.7%. Note that stresses considered here are nominal stresses and that stress concentration factors are considered through the notch classification process. When both classes are determined, the limit design stress range  $\Delta\sigma_{R_d}$  is assessed. On the other hand, knowing the geometry of the crane member, the nominal maximum stress range induced by its most damaging loading cycle ( $\Delta\sigma_{S_d} = \max \sigma - \min \sigma$ ) is assessed. Finally, the maximum stress range is compared to the limit design stress range. If  $\Delta\sigma_{S_d}$  is greater than  $\Delta\sigma_{R_d}$ , design improvements must be performed, if not, the crane structural member is validated according to the fatigue criterion.

## 1.4 Construction site variabilities

This section introduces the vocabulary related to construction sites and highlights the different sources of variability related to tower crane use. Figure 1.7 depicts a construction site drawing illustration where two saddle jib tower cranes are used. As seen in the figure, four types of area are usually depicted on a construction site drawing:

- The **building location** is an essential information that indicates where the buildings are constructed on the site.
- The **loading/unloading area** designates the location on the site where trucks transporting raw materials must be parked.
- The **storage area** is reserved to store the raw materials before use.
- The **truck mixer location** indicates where the truck mixers are parked before being emptied.

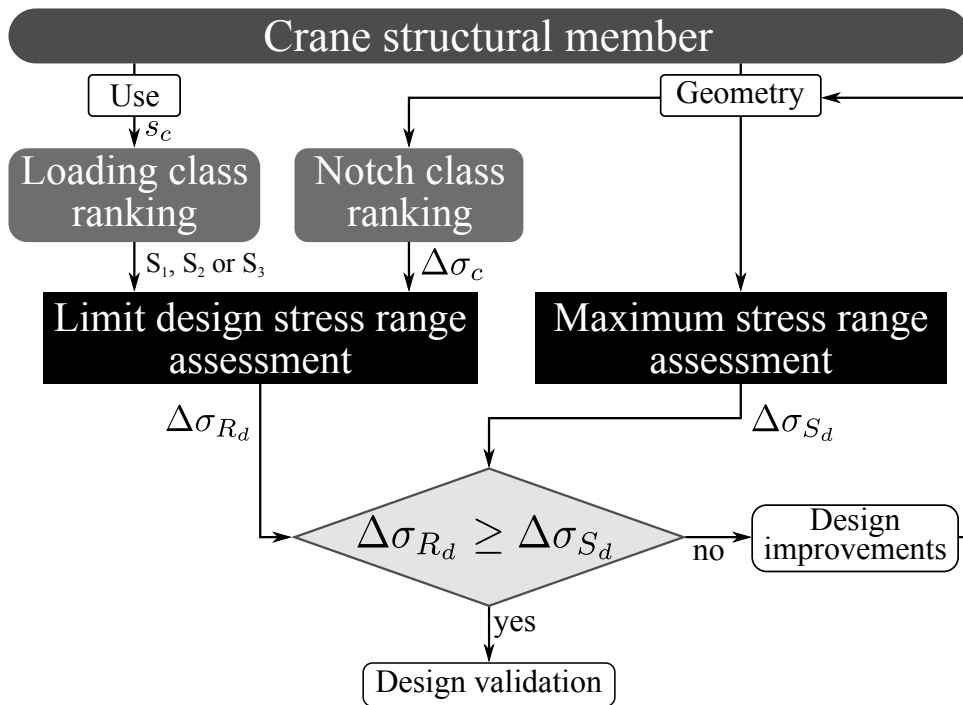


Figure 1.6 – Crane structural member validation process according to standards.

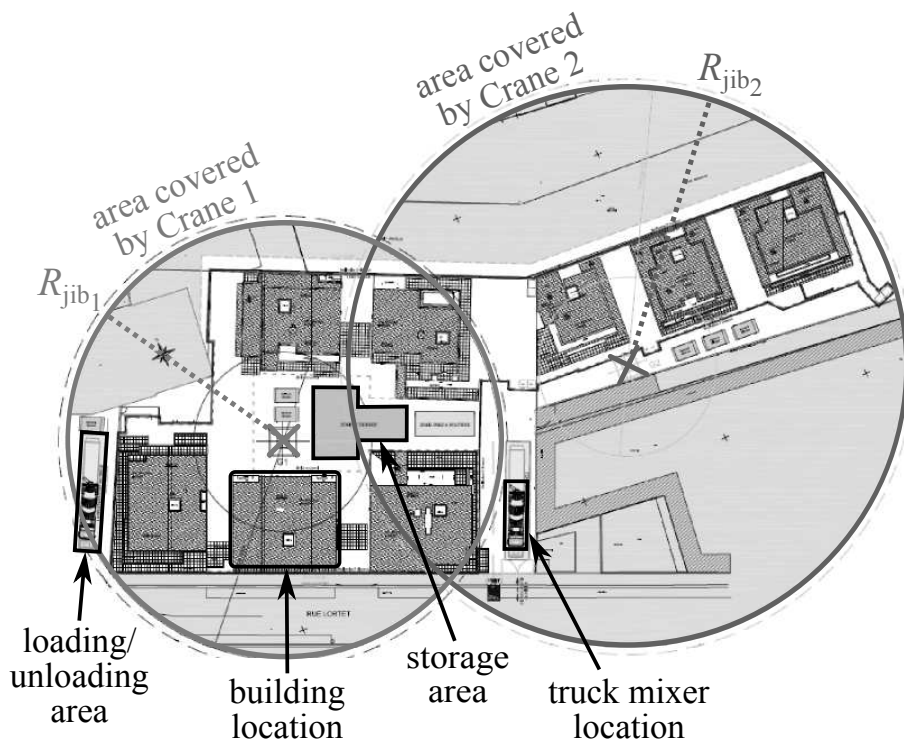


Figure 1.7 – Construction site vocabulary.

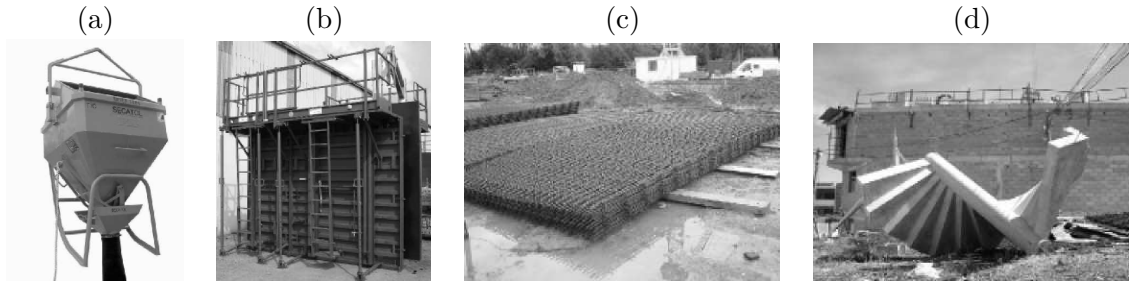


Figure 1.8 – Examples of loads hoisted by the crane on the construction site: (a) Concrete bucket, (b) Forms, (c) Steel frameworks and (d) Prefab stairs.

Thus, the work performed by the crane consists in moving materials and tools from one of the areas previously mentioned to another. The following paragraphs outline the different sources of variability inherent to crane uses.

### **Tower crane configuration**

As depicted in figure 1.7, the working areas related to cranes 1 and 2 are not the same, which is due to the use of different jib lengths ( $R_{jib_1} < R_{jib_2}$ ). As outlined in section 1.2, the main advantage of saddle jib tower cranes is the ability to be used in variable configurations depending on the construction site's topography. Almost ten different jib lengths exist for a given crane model, and a large number of tower elements can be assembled to reach high altitudes. Given that the maximum hoisted load that can be hoisted by the crane depends on these two parameters, the crane use is highly influenced by the broad range of available crane configurations.

### **Construction site topography**

The second source of crane use variability comes from the construction site configuration. The organization of each construction site is unique due to several criteria. First, the location of the buildings is fixed by architects from the beginning and is different for each construction site. Second, the loading/unloading area or truck mixer location highly depends on the construction site accessibility. Third, even though a unique storage area is theoretically defined on the construction site, every place that is not built or that is not reserved for truck parking is generally used to store raw materials. All these reasons show that the location of the different areas listed previously is unique for each construction site and contributes to the randomness of crane use.

### **Hoisted materials and tools**

Figure 1.8 depicts a few types of materials and tools likely to be hoisted on a construction site. A wide range of loads having different weights can be hoisted by the crane on the site, including concrete buckets, forms, walkways, prefab walls, prefab stairs, steel frameworks,

junk dumpsters, etc. Therefore, a great variety of hoisting situations may occur on the construction site. For instance, the full concrete bucket or the forms are moved frequently over the construction site duration while some other loads such as junk dumpsters or prefab stairs are rarely hoisted, which contributes to influence the crane use dispersion.

### **Construction site duration**

A crane is used on numerous sites during its lifespan and is stored between two jobs. Actually, two cranes sold at the same time to two different customers will not be used on the same construction sites, leading to different uses after an identical operating period. Thus, the construction site duration and the storage period between two consecutive sites represent other parameters contributing significantly to the variability of crane uses.

### **Workers**

Lastly, another factor that contributes to the crane use dispersion is the human factor. This factor depends on various parameters such as the efficiency of the teams that work on the site, the crane operator skills and the scheduled number of shifts (*i.e.* number of teams per day). For instance, a construction site performed in three shifts, with an experimented crane operator and with very efficient workers will be logically finished in a short period of time. However, this leads at the same time to use the crane very intensively.

All the previous sources of variability on crane use can be organized into two main groups: the construction site topography and the possible hoisted loads constitute **intra-construction site parameters** while the crane configuration, the construction site duration and the workers efficiency belongs to the **inter-construction site parameters** category. Chapter 3 is devoted to present the processing of data recorded on three construction sites, the handling of data originated from a rental agency, and the processing of drawings construction firms.

## **1.5 Probabilistic approaches opportunities**

A substantial number of industrial structures such as cranes may experience fatigue issues after a given operating period. This progressive deterioration process is caused by the weakening of a material subjected to repeated loads, which may lead to an irregular functioning of the structure. Therefore, the consideration of this phenomenon in structural design is a priority for engineers. However, the fatigue behavior of materials is known to be intrinsically scattered. Concerning tower crane structures, the non-even fabrication process (welding) leads to material and geometry differences in the structure that affect the fatigue strength of welded details. In addition, the loading levels applied to structures may vary considerably due to variable customer uses. This is particularly the case of tower cranes which are intensively used on various construction sites by numerous customers.



Thus, the fatigue phenomenon deals with several uncertainties. Standards usually provide the designers with deterministic rules enabling to account for these uncertainties in the structural design. These rules are supposed to ensure structural integrity by considering implicitly the previous uncertainties. Even though these deterministic rules give satisfactory solutions in most cases, they often lead to over-designed structures. Moreover, current standards commonly specify the fatigue lifespan of crane structures in terms of number of cycles, regardless of the theoretical crane operating period, which may complicate the planning of preventive maintenance tasks. Lastly, complex structural modeling requires simplification assumptions that may result in modeling uncertainties, depending on the considered analysis techniques. All these reasons explain why the fatigue design of tower cranes, regarded from a deterministic point of view, leads to non-optimized structures, and indicates a lack of knowledge concerning the evolution of fatigue damage according to operating time. Thus, the design of optimized structures that remain functional and safe requires a better understanding and management of the uncertainties outlined previously. From this perspective, probabilistic approaches represent convenient tools enabling the designers to fulfill this double objective.

Several studies have been performed concerning the development of reliability approaches for fatigue design in industrial applications, such as in the DEFFI (Reliability Approach in Fatigue Design for Industry) [1] and APPRoFi (Probabilistic Approach to Robust Fatigue Design) [4] projects. Other reliability approaches have been performed in various fields (aerospace, aeronautics, automotive industry, railway). For instance, Lorang *et al.* [23] assessed the probability of failure of train wheels subjected to different loading situations (straight and curved railways or switching points), Szerszen *et al.* [24] determined the reliability of steel girder bridges stressed by the passage of vehicles (cars or trucks) and other authors contributed to the dissemination of probabilistic approaches in the automotive industry [25, 26]. The previous methods, which are presented in chapter 2, are usually named SSI (Stress-Strength Interference) methods [27] because they share the same basic principle which consists in separating the stochastic modeling of the Stress  $S$  (demand) on one hand and the strength  $R$  (supply) on the other hand. Note that  $S$  and  $R$  are commonly expressed by means of a quantity reflecting the structural fatigue behavior such as a force, a stress or a number of cycles. A structural member is thus supposed to be reliable if at any time, the applied stress remains below the strength of the component.

Beside the fact that reliability based-design methods are applicable to any industrial field, they present advantages for several reasons. First, they provide efficient tools enabling the management of stress and strength uncertainties. Second, the collection of statistical data needed to perform the reliability analysis allows a thorough understanding of the strength and loading characterization which is very useful for the improvement or development of predictive models. Third, probabilistic analyses provide sensitivity factors which measure the importance of each input variable on the failure probability of the

structure. This turns out to be particularly helpful to guide future researches and developments. Fourth, making the link between reliability and operating time is a crucial aspect enabling to manage inspection strategies of structural assemblies. As done in the studies previously quoted, the aim of the work presented in this thesis is to take advantage of the opportunities offered by reliability approaches in order to assess the failure probability of crane structural members according to their operating period.

## 1.6 Conclusion

In this chapter, the vocabulary related to main crane structural assemblies and crane movements has been defined, and the different crane ranges have been presented. Additionally, the deterministic rules provided by European standards dealing with fatigue design of tower cranes have been reminded. The prescriptive approach specifies that the crane lifespan is expressed in terms of the number of crane cycles and is thus founded on the concept of stress or loading spectrum. Following this, the validation process of crane structural members has been discussed by means of a general synoptic. Thereafter, the multiple sources of variability inherent to crane use have been highlighted through the description of the work performed on a construction site. These uncertainties can be classified into two groups, namely the intra- and inter-construction site parameters. Lastly, the probabilistic approaches have been presented as convenient tools that enable engineers to characterize the uncertainties inherent to fatigue design in order to manage the reliability of crane members according to their operating period. The following chapter aims to introduce the concepts regularly used in fatigue strength analysis, discusses three methods enabling the stochastic modeling of fatigue operating loads, and defines the basic principles involved in probabilistic approaches.

### Chapter summary

Tower cranes are classified into three main groups, namely the luffing jib tower cranes, the saddle jib tower cranes and the self erecting tower cranes. The movements that can be performed by the crane are called respectively trolleying (movement of the trolley along the jib), slewing, hoisting and traveling (movement of the crane along rails).

Tower crane structural members are usually classified according to European standards into element groups, e.g. namely S1, S2 and S3 in EN 13001 [5], corresponding to related deterministic groups of design number of cycles depending on a typical crane application (e.g. crane used for building). Hence, each crane member belonging to a group is validated in a deterministic manner by comparing the maximal nominal stress range  $\Delta\sigma_{S_d}$  induced by its most damaging loading cycle to an admissible stress range  $\Delta\sigma_{R_d}$ .

The randomness of construction sites' topography and duration leads to uncertainties concerning crane use after several years of work. These uncertainties are implicitly taken into account by standards through the use of deterministic rules. Therefore, fatigue design of tower cranes, regarded from a deterministic point of view, leads to undetermined and inhomogeneous reliability level according to the crane operating period.

The probabilistic approaches are efficient tools enabling engineers to assess the failure probability (or reliability index) of structures by managing the uncertainties inherent to the structural strength on one hand, and the randomness of operating loads on the other hand. The global procedure developed in this research work aims to assess and manage the reliability of crane structural members subjected to fatigue according their operating period.

---

## Chapter 2

# Fatigue design and reliability assessment under operating loads

### Contents

---

|            |                                                 |           |
|------------|-------------------------------------------------|-----------|
| <b>2.1</b> | <b>Introduction</b>                             | <b>24</b> |
| <b>2.2</b> | <b>Fatigue phenomenon</b>                       | <b>25</b> |
| 2.2.1      | Fatigue of welded details                       | 25        |
| 2.2.2      | Influence factors on fatigue of welded joints   | 26        |
| 2.2.3      | Equivalent stress representing fatigue behavior | 28        |
| 2.2.4      | Probabilistic S-N curves                        | 29        |
| 2.2.5      | Cumulative damage assessment                    | 33        |
| <b>2.3</b> | <b>Fatigue loading assessment and modeling</b>  | <b>35</b> |
| 2.3.1      | Rainflow cycle counting method                  | 35        |
| 2.3.2      | Random processes models for fatigue loading     | 38        |
| 2.3.3      | Elementary loads mix strategy                   | 45        |
| 2.3.4      | Mixture models of loading spectra               | 46        |
| <b>2.4</b> | <b>General reliability methods</b>              | <b>50</b> |
| 2.4.1      | Time-dependent reliability                      | 51        |
| 2.4.2      | Stress-strength interference methods            | 52        |
| 2.4.3      | Reliability index                               | 53        |
| 2.4.4      | Monte Carlo simulations                         | 55        |
| 2.4.5      | Stochastic sensitivity analysis                 | 57        |
| <b>2.5</b> | <b>Conclusion</b>                               | <b>60</b> |
|            | <b>Chapter summary</b>                          | <b>61</b> |

---

## 2.1 Introduction

Crane structural members, which are mainly made of steel plates and beams connected by welding, are subjected to repeated operating loads. Intensive crane use usually stems from the need to minimize the amount of time required to complete a construction by maximizing the efficiency of equipments and teams. Therefore, the fatigue design of tower cranes must be accounted for. As highlighted in chapter 1, the probabilistic approaches represent promising methods enabling to quantify and manage the reliability of crane structural members. These methods require the characterization of the uncertainties related to the fatigue phenomenon of welded joints and fatigue operating loads. Thus, this chapter aims to introduce the concepts commonly used for modeling fatigue strength and operating loads on one hand, and to define the basic principles used in reliability analyses, on the other hand.

This chapter is organized as follows. Starting from a general description of fatigue phenomenon, section 2.2 lists the major factors influencing fatigue lifespan of welded connections. Afterward, the section presents a local fatigue criterion enabling the prediction of crack initiation, namely the Dang Van criterion, and introduces the probabilistic S-N curves. These curves are obtained by repeating fatigue tests at different load levels in identical conditions, and then plotting the number of cycles to failure versus the applied stress for each test. This section also describes the linear cumulative damage rule originally proposed by Palmgren and Miner.

Section 2.3 introduces the rainflow cycle counting method enabling to count fatigue cycles from any time-dependent loading and presents three different loading models suitable for fatigue analysis. First, the mathematical definitions are given for random processes with application to fatigue. Second, a method consisting in mixing elementary loads (*e.g.* rainflow matrices) coming from on-site recording is detailed. Third, the REBMIX method initiated by Nagode and Fajdiga is shown as a practical procedure enabling the probabilistic characterization and extrapolation of loading spectra (or rainflow matrices).

Lastly, section 2.4 deals with the notions related to reliability approaches in general. After introducing the definitions of the time-dependent reliability, the Stress-Strength Interference (SSI) method is outlined. This section also describes the relationship between the failure probability and the reliability index, and presents the simplest method allowing to assess them, namely the Monte Carlo simulations. Finally, this section discusses a global sensitivity analysis procedure. Considering a given mathematical model, the Sobol's method aims at quantifying the sensitivity indices reflecting the impact of the variability of each input parameters on the mechanical response.

## 2.2 Fatigue phenomenon

After introducing the fatigue phenomenon, this section outlines the main factors influencing the fatigue lifespan of welded details and provides the notions needed to predict crack initiation and to analyze fatigue test results. Then, the Palmgren-Miner rule is presented as a simple tool enabling to assess the cumulative damage induced by fatigue loading.

### 2.2.1 Fatigue of welded details

Fatigue is a localized damage occurring when a structural component is subjected to cyclic loading and, as outlined in section 1.5, large uncertainties affect this phenomenon. In fact, the scatter usually observed from fatigue results can be explained by three physical reasons:

- Test bench or operating loading conditions can lead to additional unforeseen thermal or mechanical loads.
- Inhomogeneities and microscopic defects (inclusions, dislocations) create intrinsic material discontinuities.
- Manufacturing processes cause geometric variations, surface roughness differences and residual stresses.

These defects induce plastic deformations at a microscopic scale. Although this seems negligible for one cycle, the succession of stress cycles generates an accumulation of microplasticity leading to the appearance of micro-cracks. The propagation of these cracks leads to the creation of a macroscopic crack (visible with naked eye). Two steps are usually distinguished concerning the fatigue degradation process:

- **Initiation** of a macroscopic crack. Fatigue test results dealing with crack initiation are generally represented by means of *S-N curves*, as described in section 2.2.4. In the framework of this thesis, crack initiation is considered as the failure criterion for crane structural members.
- **Propagation** of a macroscopic crack which may lead to a sudden fracture at a critical crack size. Studies dealing with crack propagation belong to the field of fatigue analyses named *fracture mechanics*.

As depicted in figure 2.1, crack initiation of welded joints may occur at two different locations where stress concentration is high, namely the weld toe or the weld root. The crack type (from toe or root) is governed by several factors such as the misalignment of plates, the ratio between weld throat and plate thickness, the weld shape, the loading mode, the welding residual stresses, etc. Both crack types are detected depending on their features because toe cracks initiate in the weld toe line, while root cracks appear on the weld surface after penetrating the weld throat. Weld toe cracks are usually considered

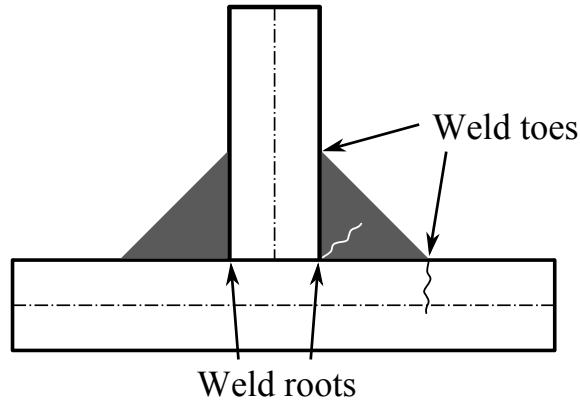


Figure 2.1 – Illustration of crack initiation areas on welded details.

to be less dangerous than weld root cracks because they can be observed by a simple visual inspection. By contrast, weld root cracks cannot be detected before they entirely propagate into the weld throat and reach the weld surface. Therefore, fatigue strength of welded structures has to be accounted for by avoiding unexpected fatigue failures in order to ensure an appropriate reliability level. Although the principles apply to both cases, note that only the initiation of macroscopic weld toe cracks is considered in the frame of this work.

### 2.2.2 Influence factors on fatigue of welded joints

This section aims at giving a brief review of the main factors influencing the fatigue lifespan of metal components. A detailed overview of these factors is given in [28].

#### Material strength

As outlined in the book of Maddox [29], although fatigue lifespan of un-welded details generally increases with the material tensile strength, the latter does not influence significantly crack initiation of welded joints. Nevertheless, due to the appearance of new weldable structural steels of very high yield strength (greater than 1000 MPa) during the past decade, the previous statement may be reconsidered for these materials.

#### Mean stress

The mean stress effect has been widely studied during the recent decades. Various authors [30–34] emphasized the mean stress effect by performing fatigue tests at different stress ratios  $\kappa = \sigma_{\min}/\sigma_{\max}$ . They have shown that, due to high residual stresses induced by the welding process, crack initiation of as-welded details is not significantly influenced by the mean stress. In fact, Krebs and Kassner [33] insisted on the fact that the notch effect induced by the local geometry of the weld is extremely significant compared to the mean stress effect. Nonetheless, as shown in the next paragraph, the mean stress may have an

impact on fatigue lives of welded details in case of stress relieved specimens.

### **Residual stress relieving**

The welding process induces residual stresses in the components due to the local heating and cooling of the parts being joined. Sometimes stress relieving is performed in order to reduce or remove the residual stresses in welded assemblies. As shown by several authors [32, 35], the presence of residual stresses influences fatigue lifespan of welded details in some cases. They demonstrated from test results that stress relieving improves significantly the fatigue strength of welded joints in compression ( $\kappa = \sigma_{\min}/\sigma_{\max} = -1$ ) while it does not have any influence in case of tensile loading ( $\kappa = 0$ ). In any case, recommendations published by the International Institute of Welding [34] suggest to account for the effect of stress ratio (*i.e.* mean stress) in fatigue design exclusively when reliable data are available concerning stress relieving.

### **Plate thickness**

The plate thickness effect on fatigue lifespan of welded details has been widely studied during the last decades [36–38]. The greater the thickness of assembled plates, the lower the fatigue lifespan for identical surface stress. The plate thickness effect being well-documented, a conventional approach consists in multiplying the predicted fatigue stress by a correction factor of the form  $(e/e_{\text{ref}})^\gamma$ , where  $e$  and  $e_{\text{ref}}$  are respectively the actual and reference thicknesses and  $\gamma$  is a constant parameter. For instance, IIW recommendations [34] set  $e_{\text{ref}}$  as equal to 25 mm and specify  $\gamma$  between -0.1 and -0.3 depending on the type of welded joint.

### **Stress gradient**

The stress gradient is a measure reflecting the local evolution of the stress according to the geometry of a component. Several authors such as Papadopoulos [39] or Weber [40] highlighted its beneficial effect on fatigue lifespan and proposed multi-axial fatigue criteria accounting for this parameter. The presence of a stress gradient has two opposite effects. On one hand, a high gradient leads to an increase of the local stress level in the material. On the other hand, the volume of material highly stressed is reduced, which tends to lower the possibilities of micro-crack appearance starting from material defects.

### **Loading mode**

Literature dealing with the influence of the loading mode (tension, bending, etc.) on fatigue lifespan is scarce. Nevertheless, a few authors [41, 42] emphasized the loading mode effect by showing from test results that the fatigue lifespan of welded details subjected to bending is greater than the life of those loaded in tension. Note that the loading mode reflects the stress gradient only in one direction, *i.e.* in the plate thickness.



### **Weld post-treatment**

As seen before, fatigue cracks appear in high stress concentration areas due to sharp geometry changes between plates and welding. As a result, surface finishing can play an important role in fatigue lifespan prediction. This explains why weld post-treatment is widely studied in fatigue lifespan improvement. All the techniques such as toe grinding, shot or hammer peening, water-jet eroding, aim at extending fatigue lifespan. For more information concerning this topic, an extensive review of existing methods is proposed by Kirkhope *et al* [43].

### **Environmental effects**

Structures working in extreme conditions are subjected to environmental effects that must be accounted for in fatigue analysis. This is the case of temperature (in polar regions or in desert) or corrosion (in marine environment) for instance.

The major factors influencing the fatigue lifespan of metal components were listed above. Note that only the effects of the mean stress, the plate thickness and the loading mode are taken into account explicitly in chapter 4. The other factors contribute intrinsically to the scatter observed in fatigue strength.

### **2.2.3 Equivalent stress representing fatigue behavior**

A great number of fatigue criteria has been proposed during the last century. These criteria, which aim at predicting as well as possible crack initiation of materials, can be classified into three groups:

- **Empirical criteria**, whose first models were defined at the beginning of the 30s, enable the accurate modeling of experimental results obtained under specific multi-axial loading (bending or tension generally combined with torsion). Their major drawback derives from their lack of generality. In fact, these criteria remain valid solely when similar loading conditions are duplicated.
- **Critical plane criteria** assume that fatigue damage behavior is governed by a critical plane which depends on the multi-axial stress state of the structure according to the time. The main differences between various criteria in this category arise from the definition of the critical plane and from the scale of interest (microscopic or macroscopic).
- **Global criteria**, which include microscopic, macroscopic and energy criteria, provide more general formulations of the fatigue damage of materials. For instance, when many critical planes may be equivalently damaged, global criteria may give better predictions than critical plane methods. However, these criteria may become difficult to use in some situations because of their complicated formulation.

Note that only one critical plane criterion is presented in this thesis, namely the Dang Van criterion. Nonetheless, if the reader wants more information concerning fatigue criteria, an exhaustive presentation of these methods is given in [40].

Dang Van criterion, which was formulated for the first time in 1972, postulates that crack initiation is sensitive to both the amplitude of shear stress  $\tau_a$  and the hydrostatic pressure  $P$  along the loading time. Therefore, the method consists in finding the critical plane of normal vector  $\vec{h}$  where the damage indicator function  $E$  is maximal:

$$E = \max_{\vec{h}} \left[ \max_t \left( \frac{\tau_a(t) + \alpha P(t)}{\beta} \right) \right] \quad (2.1)$$

The coefficients  $\alpha$  and  $\beta$  are usually calibrated by means of two fully reversed tension and torsion fatigue tests.

The concept of *local equivalent stress* is sometimes used in practical applications. Starting from equation (2.1), Dang Van [44] defined a local equivalent stress  $\tau_{0,i}$ , related to a median number of cycles  $N_i$ , as a linear combination of the local shear stress  $\tau$  in the critical plane and the hydrostatic pressure  $P$ :

$$\tau_{0,i} = \tau + a_i P \quad (2.2)$$

Dang Van observed from test results that the parameter  $a_i$  was almost independent of  $N_i$  in case of high cycle fatigue ( $a_i \simeq a = \text{constant}$  for  $N_i > 5 \cdot 10^5$  cycles), leading to the following expression:

$$\tau_0 = \tau + a P \quad (2.3)$$

The previous expression of  $\tau_0$  is used in chapter 4 in order to correlate the responses of Finite Element modeling with experimental results.

#### 2.2.4 Probabilistic S-N curves

In fatigue analyses dealing with crack initiation, Wöhler curves constitute a convenient representation enabling to relate experimental fatigue lives to the applied loads. These curves, also named S-N curves, are assessed by submitting various specimens to a regular constant amplitude load until crack initiation. Then, the applied stress (derived from the applied load and the cross section) and the number of cycles to failure  $N$  are plotted in a S-N diagram. Wöhler curves, which are usually obtained for a given stress ratio  $\kappa$ , consist generally of three domains (see figure 2.2):

1. **Low cycle fatigue:** this domain is related to high load ranges leading to significant plastic deformations of the material, and therefore to a low number of cycles to failure ( $N \leq 10^4 - 10^5$  cycles).
2. **Limited endurance:** this corresponds to the high cycle fatigue domain with finite

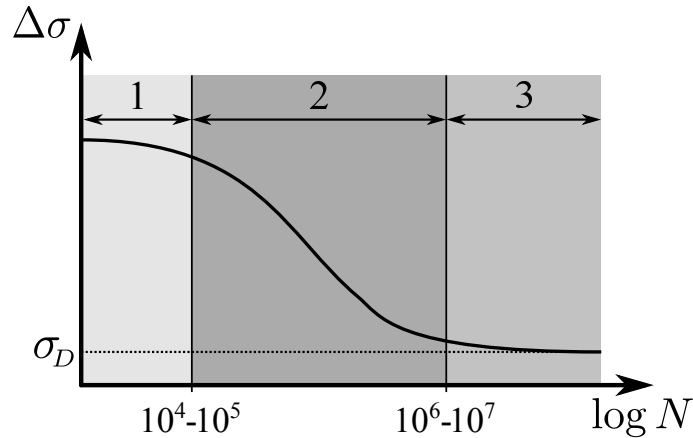


Figure 2.2 – Illustration of S-N curve domains: 1 low cycle fatigue, 2 limited endurance and 3 unlimited endurance.

life where the applied load ranges are lower than those used in the low cycle fatigue domain. The number of cycles-to-failure in this domain varies between  $10^4 - 10^5$  and  $10^6 - 10^7$  cycles.

3. **Unlimited endurance:** in this domain ( $N \geq 10^6 - 10^7$  cycles), fatigue lifespan is considered to be infinite because Wöhler curve slope changes significantly and sometimes tends towards an asymptotic horizontal limit, also named fatigue limit  $\sigma_D$ .

As seen in section 2.2.1, several parameters (manufacturing defects, loading conditions, etc) contribute to the large scatter usually observed on fatigue test results. As a consequence, the fatigue phenomenon deals with large uncertainties that must be accounted for. Therefore, probabilistic S-N curves can be fully defined by determining the median trend corresponding to 50% of survivals for the tested specimens, on one hand, and the fatigue resistance scatter, on the other hand.

### Median trend modeling

Various deterministic models  $\mathcal{D}$  exist in literature to make the link between the number of cycles-to-failure  $N$  and the applied stress range  $\Delta\sigma$ . These relations usually take the form  $N = \mathcal{D}(\Delta\sigma)$  or equivalently  $\Delta\sigma = \mathcal{D}^{-1}(N)$ :

- Wöhler (1870) [45]:  $N = b \exp(-c\Delta\sigma)$
- Basquin (1910) [46]:  $N = b(\Delta\sigma)^{-c}$
- Stromeier (1924) [47]:  $N = b(\Delta\sigma - \sigma_D)^{-c}$
- Bastenaire (1960) [48]:  $N = b \exp[-c(\Delta\sigma - \sigma_D)] / (\Delta\sigma - \sigma_D) - d$

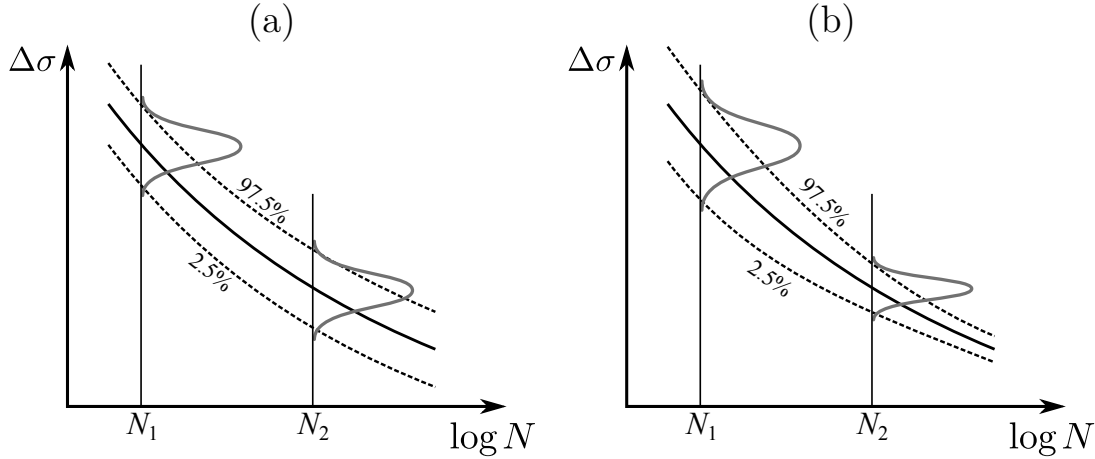


Figure 2.3 – Illustration of Gaussian probabilistic models of  $\Delta\sigma$  with (a) constant standard deviation of  $\Delta\sigma$  at a given  $N$  and (b) constant coefficient of variation of  $\Delta\sigma$  at a given  $N$ . The solid line represents the median curve (50% probability of survival) obtained from Basquin’s model while the dashed lines are the isoprobabilistic curves related to the percentage of failure.

where  $b$ ,  $c$  and  $d$  are constant parameters inferred from fatigue tests.

Note that the Bastenaire’s formula enables to account for both low and high cycle fatigue. The median trend of the S-N curve can be characterized by using one of the previous deterministic models. The study presented in this thesis being reduced to high cycle fatigue with finite life (*i.e.* limited endurance domain), only the Basquin’s model is used in the following. This leads to express  $N_{50\%}$  for a given stress range or  $\Delta\sigma_{50\%}$  for a given number of cycles to failure as follows:

$$N_{50\%}(\Delta\sigma) = b(\Delta\sigma)^{-c} \quad (2.4)$$

$$\Delta\sigma_{50\%}(N) = (N/b)^{-1/c} \quad (2.5)$$

### Scatter probabilistic modeling

Once the median trend is characterized, a probabilistic distribution has to be chosen in order to model the fatigue strength scatter. As noted in the book of Lalanne [49], the number of cycles to failure  $N$  at a given stress range is generally modeled by a lognormal distribution, while the stress range  $\Delta\sigma$  at a given number of cycles to failure is usually defined by a Gaussian distribution. Note that the dispersion of the distributions of  $N$  or  $\Delta\sigma$  can be characterized by either a constant standard deviation or a constant coefficient of variation.

Considering a median trend modeled by Basquin’s relation, figures 2.3 and 2.4 depict two couples of probabilistic S-N curve models. Figure 2.3 illustrates the modeling of  $\Delta\sigma(N)$  as a Gaussian distribution with (a) a constant standard deviation  $s_{\Delta\sigma}$  and (b) a constant

coefficient of variation  $\delta_{\Delta\sigma}$ , respectively. Note that this type of scatter modeling indicates a lack of consistency compared to the fatigue testing procedure. Specimens are usually tested under a constant stress range level and the number of cycles-to-failure is the result of the fatigue test. Thus, the fatigue strength dispersion is intrinsically related to the number of cycles to failure. As a result, it does not appear logical to model the scatter of the stress range.

As depicted in figure 2.4, another type of scatter modeling enable to overcome this contradiction. Figure 2.4 considers the modeling of a lognormal distribution for  $N(\Delta\sigma)$  with (a) a constant standard deviation  $s_{\ln N}$  and (b) a constant coefficient of variation  $\delta_{\ln N}$ , respectively. The choice between a constant standard deviation or a constant coefficient of variation influences the assessment of the isoprobabilistic curves presented in the following. In the frame of this work, the distribution of number of cycles-to-failure is assumed to be lognormal with a constant standard deviation of  $\ln(N)$  at any stress range level (see figure 2.4 (a)). Note that a constant standard deviation of  $\ln(N)$  stems from a constant coefficient of variation of  $N$  ( $\delta_N$ ).

### Isoprobabilistic curves

Standards dealing with fatigue usually provide probabilistic S-N curves accounting for a high percentage of survival  $q$  for the studied specimens (*e.g.* 95% or 97.7%). These curves, also named isoprobabilistic curves, are assessed by shifting the median curve until a percentage of failure  $p$ , or equivalently a percentage of survival  $q = 1 - p$ , is reached. As detailed in the work of Perrin [50], let  $F(N)$  be the function characterizing the probability  $p$  that a specimen fails before  $N$  cycles under the stress range level  $\Delta\sigma$ . At a given  $\Delta\sigma$ , this function is assumed to vary with  $N$  as the CDF of a lognormal random variable with mean  $m_N(\Delta\sigma)$  and coefficient of variation  $\delta_N(\Delta\sigma)$ . The mean corresponds to the Basquin's model ( $m_N(\Delta\sigma) = N_{50\%}(\Delta\sigma)$ ) chosen before and the coefficient of variation  $\delta_N(\Delta\sigma)$  is supposed to be constant for any  $\Delta\sigma$ , *i.e.*  $\delta_N(\Delta\sigma) = \delta_N$ .  $N(\Delta\sigma)$  being log-normally distributed, the random variable  $\ln N(\Delta\sigma)$  is normally distributed. As a result,  $F(N)$  reads:

$$F(N) = \Phi\left(\frac{\ln(N) - m_{\ln N}(\Delta\sigma)}{s_{\ln N}(\Delta\sigma)}\right) \quad (2.6)$$

where  $\Phi$  is the standard Gaussian CDF and:

$$m_{\ln N}(\Delta\sigma) = \ln\left(\frac{m_N(\Delta\sigma)}{\sqrt{1 + \delta_N^2}}\right) \quad (2.7)$$

$$s_{\ln N}(\Delta\sigma) = \sqrt{\ln(1 + \delta_N^2)} \quad (2.8)$$

Note that from equation (2.8) a constant coefficient of variation  $\delta_N$  for the random variable  $N(\Delta\sigma)$  leads to a constant standard deviation  $s_{\ln N}(\Delta\sigma)$  for the random variable  $\ln N(\Delta\sigma)$ ,

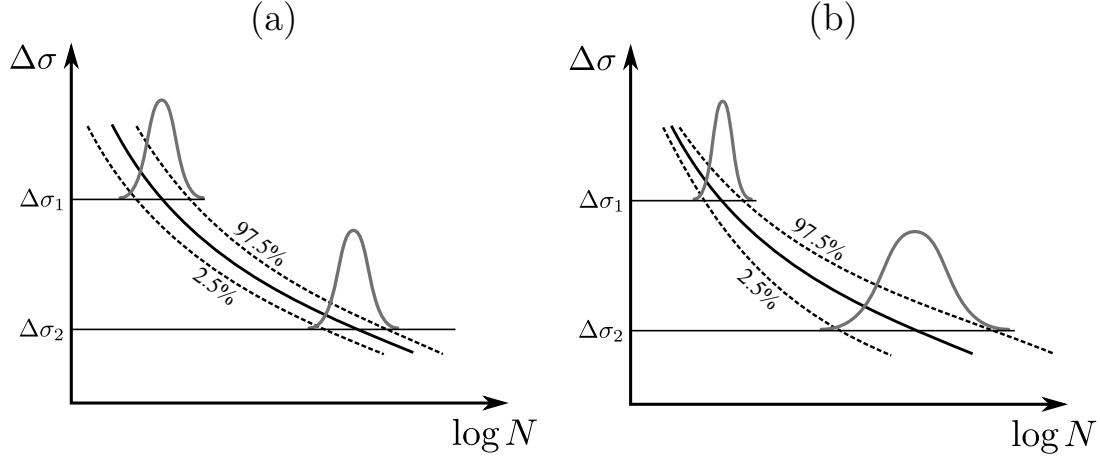


Figure 2.4 – Illustration of lognormal probabilistic models of  $N$  with (a) constant standard deviation of  $\ln(N)$  at a given  $\Delta\sigma$  and (b) constant coefficient of variation of  $\ln(N)$  at a given  $\Delta\sigma$ . The solid line represents the median curve (50% probability of survival) obtained from Basquin's model while the dashed lines are the isoprobabilistic curves related to the percentage of failure.

*i.e.*  $s_{\ln N}(\Delta\sigma) = s_{\ln N}$ , and vice versa. Thus, for a  $p$  probability of failure (realization of  $F(N)$ ), the isoprobabilistic curve  $N_{p\%}(\Delta\sigma)$  is obtained by inverting equation 2.6:

$$N_{p\%}(\Delta\sigma) = \exp \left[ \Phi^{-1}(p) s_{\ln N} + m_{\ln N}(\Delta\sigma) \right] \quad (2.9)$$

Assuming that the median trend is defined by the Basquin's model and considering a percentage of survival of 95% (*i.e.* a probability of failure of 5%), equation (2.9) becomes:

$$N_{95\%}(\Delta\sigma) = \exp \left[ \Phi^{-1}(0.05) \sqrt{\ln(1 + \delta_N^2)} + \ln \left( \frac{b(\Delta\sigma)^{-c}}{\sqrt{1 + \delta_N^2}} \right) \right] \quad (2.10)$$

The previous isoprobabilistic curves are used in chapter 4 in order to compare the approach proposed in this thesis with European standards dealing with fatigue of tower cranes.

### 2.2.5 Cumulative damage assessment

Cumulative damage assessment is a topic widely studied since Palmgren [10] introduced the concept of linear summation of the damage in 1924. Nevertheless, as pointed out by Fatemi *et al* [51], none of the existing approaches enable to account for major phenomenological factors as load dependence, interaction effects, overload effects, load sequence, mean stress, etc. This explains why the linear damage rule introduced by Palmgren and mathematically formulated by Miner [11] in 1945 is still mainly used in fatigue design.

The Palmgren-Miner linear damage rule considers the linear summation of partial

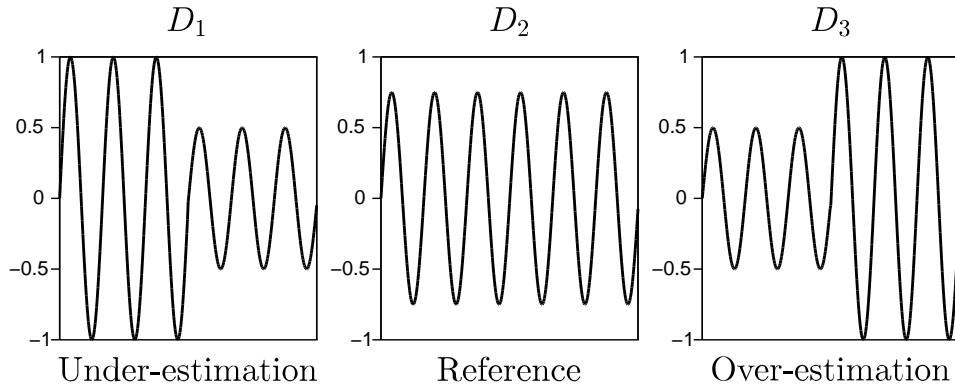


Figure 2.5 – Illustration of the sequential effect on the damage for two consecutive loading blocks.

damage  $D_i$  induced by the application of  $n_i$  cycles of stress range  $\Delta\sigma_i$ :

$$D_i = \frac{n_i}{N_i} \quad (2.11)$$

where  $N_i$  is the total number of cycles before failure at constant range  $\Delta\sigma_i$ . By considering that the whole loading of a structure consists of  $z$  loading blocks of different levels, the total damage  $D$  is expressed as follows:

$$D = \sum_{i=1}^z D_i = \sum_{i=1}^z \frac{n_i}{N_i} \quad (2.12)$$

Failure is deemed to occur when  $D$  reaches 1.

Due to its linear nature, the main drawbacks of this approach lies in the fact that the damage is independent of the loading level and does not account for the loading sequence [49]. However, experimental results showed that the total damage can be over-estimated in case of low-to-high loading sequence and under-estimated for high-to-low loading sequence. Figure 2.5 depicts three histories leading to identical damage according to Miner's definition. Nonetheless,  $D_1$  and  $D_3$  are respectively under- and over-estimated in comparison to damage  $D_2$  corresponding the reference one-block case. This explains why many authors intended during the last decades to develop non-linear models (Marco-Starkey, Henry, Corten-Dolan, etc.) in order to avoid these drawbacks. For further details, the reader can refer to [51] in order to have a good overview of existing cumulative damage approaches. For sufficiently random loading with moderate ranges, the Palmgren-Miner linear damage accumulation rule remains valid, which is the case in this thesis.

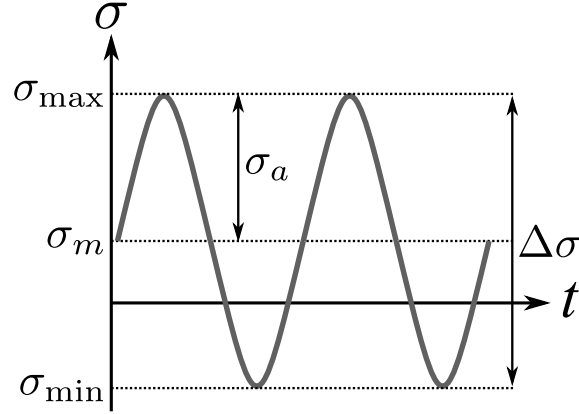


Figure 2.6 – Illustration of a constant amplitude stress history.

## 2.3 Fatigue loading assessment and modeling

In the frame of this thesis, crane operating loads need to be characterized and simulated in order to reconstruct virtual lives related to various crane structural members. For this reason, this section is devoted to the assessment and modeling of operating loads related to fatigue. The rainflow counting procedure is first described as a useful method enabling to assess fatigue loading cycles. Then, three different methods are presented as convenient tools enabling the modeling of fatigue operating loads. These methods are respectively based on the random process theory, the elementary loads mix strategy and the mixture models of loading spectra.

### 2.3.1 Rainflow cycle counting method

As seen in chapter 1, fatigue damage appears when a component is cyclically stressed. Figure 2.6 illustrates an example of Constant Amplitude (CA) stress history. Note that  $\sigma$  may be replaced in the figure by other time-variant quantities reflecting fatigue loading (force, strain, etc). As seen in the figure, a stress cycle can be described by the “minimum-maximum” paired value  $\{\sigma_{\min}, \sigma_{\max}\}$ , the “amplitude-mean” paired value  $\{\sigma_a, \sigma_m\}$  or the “range-mean” paired value  $\{\Delta\sigma, \sigma_m\}$  with:

$$\sigma_m = (\sigma_{\max} + \sigma_{\min})/2 \quad (2.13)$$

$$\Delta\sigma = \sigma_{\max} - \sigma_{\min} \quad (2.14)$$

$$\sigma_a = \Delta\sigma/2 \quad (2.15)$$

Most of the time, laboratory specimens are tested under CA loading. Nonetheless, in operating conditions structural loading is characterized by complex time-histories leading to the question: how to identify fatigue loading cycles from complex variable amplitude signals?



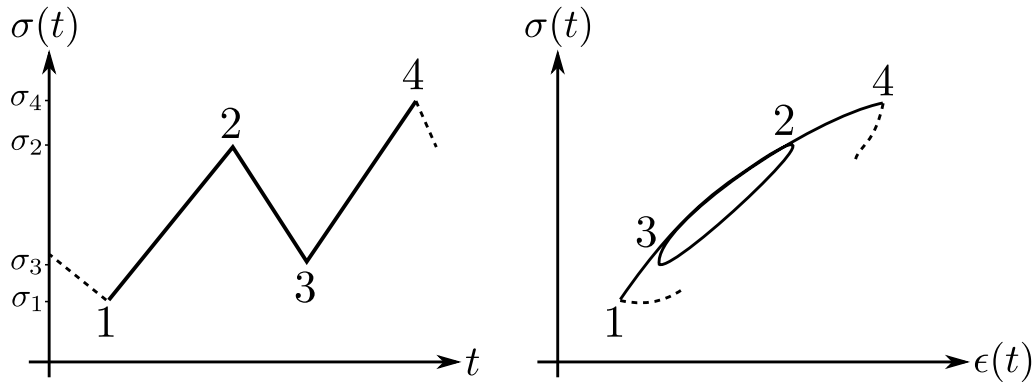


Figure 2.7 – Rainflow cycle meaning in terms of fatigue.

Various cycle counting methods such as peak count method, range count method, level-crossing count method, mean-crossing peak count method, range-pair cycle counting or rainflow counting method have been developed and implemented during the past decades. However, Dowling [52] highlighted that excepting the range-pair [53] and the rainflow [7, 8] methods, all the other counting methods may lead to unrealistic fatigue results in some situations. In addition, he showed that the range-pair and rainflow methods are nearly identical. Starting from this observation, this section focuses exclusively on the description of the widely-used rainflow counting method.

The rainflow method has been proposed in Japan by Endo [7] in 1967 and translated into English by Matsuishi and Endo [8] in 1969. The method consists in counting reversals (half-cycles) or pairs of reversals (cycles) from a stress or load history. The popularity of this method is due to the fact that rainflow method has a physical meaning in the field of fatigue lifespan prediction. In fact, as seen in figure 2.7, the counted cycles represent hysteresis loops in the stress-strain plane which are directly related to the fatigue degradation process.

A problem arises in the original method developed by Endo [7] when one wants to find an analytical expression of the algorithm. A simpler formulation have been given by Downing and Socie [54] and the procedure was standardized by Amzallag et al. [9]. This algorithm, namely the "four-point" algorithm, proceeds by following the steps described in table 2.1, and stops when less than four local extrema remain or if the condition in step 2 is no more satisfied.

One limit of the rainflow procedure lies in the fact that once cycles are counted, the loading sequence (*i.e.* order in which cycles appear) is lost. This can be a problem if one is interested in crack propagation issues or nonlinear fatigue damage. Anthes [55] solved this problem by proposing a modified rainflow algorithm enabling to keep the loading sequence. Moreover, shortcomings of the rainflow counting method are pointed out by Hong [56] when unclosed hysteresis loops are encountered into the stress-strain path. This explains why he proposed a modified algorithm consisting in rearranging the residual history in order

1. **Convert** the stress history in a sequence of local extrema (series of peaks and valleys).
2. **Consider** four consecutive local extrema  $\{1, 2, 3, 4\}$  (see figure 2.7).
3. **Calculate** the ranges  $\Delta\sigma_{12}$ ,  $\Delta\sigma_{23}$  and  $\Delta\sigma_{34}$ .
4. *If*  $\Delta\sigma_{12} > \Delta\sigma_{23}$  and  $\Delta\sigma_{23} < \Delta\sigma_{34}$ :
  - **Add** range  $\Delta\sigma_{23}$  and its corresponding mean to the rainflow matrix.
  - **Delete** local extrema 2 and 3 from the remanent history (also called residual).

*Else*

  - **Re-start** from step 2 by considering the four consecutive local extrema  $\{2, 3, 4, 5\}$  instead of  $\{1, 2, 3, 4\}$ .
5. **Duplicate** the residual.
6. **Re-start** from step 2.

Table 2.1 – Four-point algorithm enabling to extract rainflow ranges from a temporal signal.

to always start or end with the maximum peak or minimum valley. Finally, an alternative definition of the rainflow counting method was given by Rychlik [57], namely the toplevel-up cycle (TUC) counting method. Rychlik demonstrated that his method, which considers the crossing of a stress level during the time interval  $[-T, T]$ , is equivalent to the rainflow counting method and can be convenient if one needs to study the extreme properties of random processes (*e.g.* for dynamic loads).

In this section, a relevant counting method enabling the assessment of fatigue loading cycles from a time series has been presented. The following section deals with the theory of random processes in the frame of the modeling of fatigue operating loads.

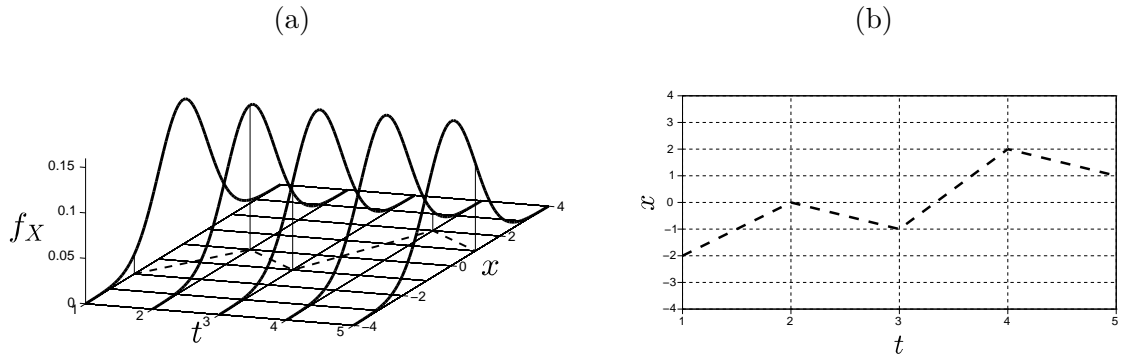


Figure 2.8 – Gaussian random process: (a) 3D view of the random process joint density function, (b) Example of one trajectory  $X(\omega_0, t)$ .

### 2.3.2 Random processes models for fatigue loading

This section gives the general characteristics related to random processes, and introduces a few random process models that can be used in the field of fatigue load modeling.

#### Random process characteristics

Let  $(\Omega, \mathcal{F}, P)$  be a probability space,  $\mathcal{T}$  a metric space and  $E$  a state space.  $X$  is called a *random process* defined on  $(\Omega, \mathcal{F}, P)$ , indexed by  $\mathcal{T}$  and taking values in  $E$ , if  $X$  is a measurable application of  $\Omega$  in  $E^{\mathcal{T}}$ :

$$\begin{aligned} X : \Omega &\rightarrow E^{\mathcal{T}} \\ \omega &\rightarrow X(\omega) : \mathcal{T} \rightarrow E \\ t &\rightarrow X(\omega, t) \end{aligned} \quad (2.16)$$

Figure 2.8 (a) presents a 3D view of the distribution of a Gaussian random process. For a given randomness  $\omega_0$ , the application whose  $t$  associates  $X(\omega_0, t)$  is a realization of the process  $X(\omega, t)$  and is called *trajectory* (or *path*) of the process. For instance, figure 2.8 (b) depicts one possible trajectory of a Gaussian random process.

The temporal law of a random process is known if, for all instants  $(t_1, t_2, \dots, t_n)$ , the joint probability law  $f(x, t)$  of the set of random variables  $X(\omega, t_1), X(\omega, t_2), \dots, X(\omega, t_n)$  is known. In practice, this joint probability law is difficult to assess. Moreover, the mean of a stochastic process  $X(\omega, t)$  is a deterministic function  $m_X(t)$  which, for each value of  $t$ , is equal to the mathematical expectation of the random variable  $X(\omega, t)$ :

$$m_X(t) = \mathbb{E}[X(\omega, t)] = \int_{-\infty}^{\infty} x f(x, t) dx \quad (2.17)$$

If  $m_X(t)$  equals zero for all values of  $t$ , the process is said to be *centered*. The variance of

a random process can be defined similarly:

$$\text{Var}_X(t) = \mathbb{E} \left[ \{X(\omega, t) - m_X(t)\}^2 \right] = \int_{-\infty}^{\infty} (x - m_X(t))^2 f(x, t) dx \quad (2.18)$$

Note that  $m_X(t)$  and  $\text{Var}_X(t)$  are functions of  $t$ , *i.e.* they change from one time point to another.

The definition of the autocovariance and autocorrelation functions should also be given in addition to the mean and standard deviation description. The autocovariance of a stochastic process  $X(\omega, t)$  is the non-random function  $\text{Cov}_X(t_1, t_2)$  which, for each couple  $(t_1, t_2) \in \mathcal{T} \times \mathcal{T}$ , is equal to the covariance of the random pair  $\{X(\omega, t_1), X(\omega, t_2)\}$ :

$$\text{Cov}_X(t_1, t_2) = \mathbb{E}[\{X(\omega, t_1) - m_X(t_1)\}\{X(\omega, t_2) - m_X(t_2)\}] \quad (2.19)$$

Furthermore, the autocorrelation of a stochastic process  $X(\omega, t)$  is the non-random function  $\Gamma_X(t_1, t_2)$ , which for each couple  $(t_1, t_2) \in \mathcal{T} \times \mathcal{T}$ , is equal to the second order moment of the random pair  $\{X(\omega, t_1), X(\omega, t_2)\}$ :

$$\Gamma_X(t_1, t_2) = \mathbb{E}[X(\omega, t_1)X(\omega, t_2)] \quad (2.20)$$

$\Gamma_X(t_1, t_2)$  represents the correlation coefficient between two pairs of values of  $X(\omega, t)$  separated by an interval of length  $t_2 - t_1$ . This is a measure of the stochastic dependency between the two values of the random process  $X(\omega, t_1)$  and  $X(\omega, t_2)$ . In practice, the autocovariance and autocorrelation functions estimated from observation data give useful information about which kind of model is the most representative to fit a measured random process.

Other important definitions concerning random processes are the *ergodicity* and the *stationarity*. On one hand, a random process is defined as a set of random variables indexed by a parameter  $t$  but it can also be seen as a set of functions of  $t$ , indexed by the parameter  $\omega$ . This means that the process is considered as a *union of trajectories*. Thus, a random process is said to be *ergodic* if all its temporal means exist and have the same value regardless the considered trajectory, excepted for a set of trajectories of zero probability. On the other hand, a random process is a *strictly stationary process of order  $N$*  if its characteristics are invariant for every change of time origin:

$$F(x_1, x_2, \dots, x_n; t_1, t_2, \dots, t_n) = F(x_1, x_2, \dots, x_n; t_1 + \tau, t_2 + \tau, \dots, t_n + \tau) \quad (2.21)$$

In practice, the *second order stationarity* assumption is generally sufficient. This assumption is valid if the two following conditions are verified for the studied process:

- $m_X(t) = m_X, \forall t$ ,
- $\Gamma_X(t_1, t_2) = \Gamma_X(t_2 - t_1) = \Gamma_X(\tau)$  (the autocorrelation function only depends on the

time interval  $\tau = t_2 - t_1$ ).

Stationary processes are generally used to describe signals such as radio signals, vibration, turbulence, price indices, etc while unstationary processes are useful to represent growth or decay processes.

### Random process families

A random process  $X(\omega, t)$  is said to be discrete-time if the metric space  $\mathcal{T}$  is countable (finite or infinite). In this case, the term *process* is sometimes replaced by *sequence* or *series* and  $X(\omega, t)$  is denoted  $X_t(\omega)$ . When  $\mathcal{T}$  is uncountable, the random process is called continuous-time process. The main difference between discrete-time and continuous-time processes lies in the fact that the integrals used in the previous definitions are replaced by algebraic sums. Moreover, if the random process  $X(\omega, t)$  takes values in a countable state space  $E$  the process is said to be discrete. Otherwise, the process is said to be continuous. Accounting for the previous definitions, every random process can be classified into one of these four families: discrete or continuous random sequence and discrete or continuous random process.

### Random process models

A wide range of random process models were defined during the last century. For sake of concision, only a few linear discrete-time random process models are presented in this manuscript. The reader can refer to the books of Priestley [58], Hamilton [59] and Box, Jenkins and Reinsel [60] for further information.

The *white noise*, denoted  $(e_t)_{t \in \mathbb{Z}}$ , is the most simple stationary random process model. This *purely random process* is a sequence of uncorrelated centered (*i.e.* with zero mean) real random variables of finite variance  $\sigma^2$ . Based on this definition, two other simple random process models can be described, namely the *autoregressive* and *moving average* random processes. The *AutoRegressive* (AR) model was first introduced by Yule [61] in 1927. A stationary process  $(X_t)_{t \in \mathbb{Z}}$  is a  $p$ -order autoregressive process denoted AR( $p$ ) if a process  $(e_t)_{t \in \mathbb{Z}}$  exists and  $p$  real numbers  $\phi_1, \dots, \phi_p, \phi_p \neq 0$  such as  $(X_t)_{t \in \mathbb{Z}}$  verifies the following recurrence equation:

$$X_t - \phi_1 X_{t-1} - \dots - \phi_p X_{t-p} = e_t \quad (2.22)$$

An illustration of this model is given in figure 2.9 (a). Furthermore, the *Moving Average* (MA) model was first introduced by Slutsky in 1927 and traduced in English in 1937 [62]. A process  $(X_t)_{t \in \mathbb{Z}}$  is a  $q$ -order moving average process denoted MA( $q$ ) if a process  $(e_t)_{t \in \mathbb{Z}}$  exists and  $q$  real numbers  $\theta_1, \dots, \theta_q, \theta_q \neq 0$  such as  $(X_t)_{t \in \mathbb{Z}}$  verifies the following equation:

$$X_t = e_t - \theta_1 e_{t-1} - \dots - \theta_q e_{t-q} \quad (2.23)$$

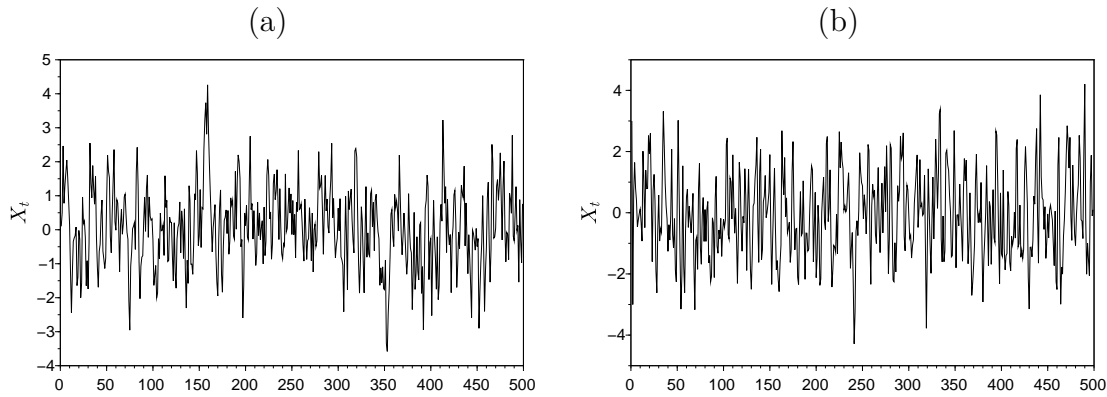


Figure 2.9 – 500 observations of a (a) AR(1) process of equation:  $X_t - 0.6X_{t-1} = e_t$  and (b) MA(1) process of equation:  $X_t = e_t + 1.1e_{t-1}$  [58].

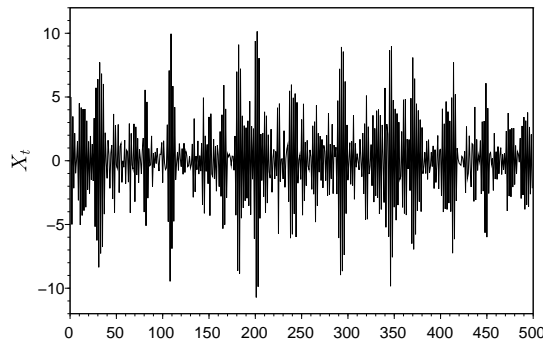


Figure 2.10 – 500 observations of a ARMA(2,2) process of equation:  $X_t + 1.4X_{t-1} + 0.5X_{t-2} = e_t - 0.2e_{t-1} - 0.1e_{t-2}$  [58].

An illustration of this model is given in figure 2.9 (b).

Following these definitions, the combination of an AR process and a MA process results in an *AutoRegressive Moving Average* (ARMA) model. A stationary process  $(X_t)_{t \in \mathbb{Z}}$  is  $p$ -order autoregressive process, a  $q$ -order moving average process denoted ARMA( $p, q$ ) if a process  $(e_t)_{t \in \mathbb{Z}}$  exists,  $p$  real numbers  $\phi_1, \dots, \phi_p$  and  $q$  real numbers  $\theta_1, \dots, \theta_q$  such as  $(X_t)_{t \in \mathbb{Z}}$  verifies the following equation:

$$X_t - \phi_1 X_{t-1} - \dots - \phi_p X_{t-p} = e_t - \theta_1 e_{t-1} - \dots - \theta_q e_{t-q} \quad (2.24)$$

with  $\phi_p \theta_q \neq 0$ . An illustration of this model is given in figure 2.10.

ARMA models have been found to be helpful for describing stationary nonseasonal (without trends) time series with a small number of parameters. The fitting of an ARMA( $p, q$ ) model to experimental data is usually performed by following three steps:

- **Model identification:** this step consists in selecting the orders of the random process, namely  $p$  and  $q$ . This can be performed by using the classical method which

aims to study the correlogram and partial correlogram diagrams (see the book of Box and Jenkins [60]). Even though these diagrams are helpful to determine separately the order of AR or MA models, they unfortunately do not provide information about the choice of  $p$  and  $q$  for an ARMA model. Other more objective methods enable to choose these parameters by minimizing an information criterion (*e.g.* Akaike Information Criterion (AIC), Bayesian Information Criterion (BIC), etc). In any case, the guiding principle to remember during the identification step is the parsimony, *i.e.* the model providing an accurate description of the data and that considers the smallest number of parameters is the most adequate.

- **Parameters estimation:** when  $p$  and  $q$  are chosen, the parameters of the process  $\{\phi_1, \dots, \phi_p, \theta_1, \dots, \theta_q\}$  can be estimated by using the Maximum-Likelihood Estimation (MLE) method. After specifying a distribution for the white noise  $(e_t)_{t \in \mathbb{Z}}$ , the log-likelihood function of the joint PDF  $f$  is computed in order to estimate the unknown parameters by means of an optimization procedure.
- **Diagnostic checking:** a model that has been identified and estimated is generally used to forecast future values. Nonetheless, due to the fact that the fitted model is just a simplification of the true model, forecasting may lead large errors. Thus, the last step consists in checking the accuracy of the proposed model by examining the correlogram of the residuals from the fitted model in order to see if these residuals represent a white noise.

ARMA models are widely used in the finance field in order to forecast the evolution of market indices for instance. These ARMA models are convenient for several reasons. Since various theories are well-developed in the fields of linear differences equations, Gaussian models and statistical inference, the fitting procedure of this type of model is quite easy to compute. Moreover, due to the fact that this class of models has gained in popularity in data analysis and forecasting, several numerical packages are now available for handling these models. Although ARMA models give satisfactory results in various cases, the main shortcoming of this type of model lies in the assumption of a constant variance. Thus, these models are not able to capture some data characteristics such as the volatility (*i.e.* changes of variance). Note also that ARMA models can be extended to VARMA (Vector Autoregressive Moving Average) models in the multivariate case. The following paragraph gives further details on a particular autoregressive model used for fatigue load modeling, namely the discrete-time Markov chain.

### Discrete-time Markov chains

Markovian processes is a particular family of autoregressive processes. A particular feature of this type of process, named *Markov property*, relies into the fact that they are memoryless, *i.e.* the next state depends solely on the current state and does not depend on

the past states. In the following, only the discrete-time Markov processes are presented. A first order discrete-time Markov chain is a sequence of random variables  $(X_n)_{n \in \mathbb{N}^*}$  taking values in a finite state space  $E$  in such a way that the conditional distribution of  $X_{n+1}$  knowing  $(X_m)_{m \leq n}$  equals the distribution of  $X_{n+1}$  knowing  $X_n$ :

$$P(X_{n+1} = e_{n+1} | X_n = e_n, X_{n-1} = e_{n-1}, \dots, X_1 = e_1) = P(X_{n+1} = e_{n+1} | X_n = e_n) \quad (2.25)$$

A Markov chain is said to be *time homogeneous*, if the conditional probabilities  $P(X_{n+1} = e_k | X_n = e_l)$  do not depend on  $n$ :

$$P(X_{n+1} = e_k | X_n = e_l) = P(X_2 = e_k | X_1 = e_l), (e_k, e_l) \in E \times E \quad (2.26)$$

A Markov chain is completely defined by its initial distribution  $P(X_1 = e_l)$  and its *transition matrix* or *stochastic matrix*, denoted  $\mathbf{P}$ :

$$\mathbf{P} = \begin{pmatrix} p_{1,1} & p_{1,2} & \cdots & p_{1,l} & \cdots & p_{1,K} \\ p_{2,1} & p_{2,2} & \cdots & p_{2,l} & \cdots & p_{2,K} \\ \vdots & \vdots & \cdots & \vdots & \cdots & \\ p_{k,1} & p_{k,2} & \cdots & p_{k,l} & \cdots & p_{k,K} \\ \vdots & \vdots & \cdots & \vdots & \cdots & \\ p_{K,1} & p_{K,2} & \cdots & p_{K,l} & \cdots & p_{K,K} \end{pmatrix} \quad (2.27)$$

where  $p_{k,l}$  is the conditional probability to change from one state  $e_k$  to another state  $e_l$  and  $K = \text{Card}(E)$ . Note that  $\mathbf{P}$  is a non-negative matrix whose rows sum to 1.

The conditional probabilities  $p_{k,l}$  can be inferred from observed trajectories of the process  $X$  by means of the MLE method. Let  $\{x_1, x_2, \dots, x_N\}$  be a set of  $N$  consecutive realizations of the Markov chain  $X$ . The likelihood function  $L(p_{k,l}, x_1, x_2, \dots, x_N)$  reads:

$$L(p_{k,l}, x_1, x_2, \dots, x_N) = \prod_{k,l} p_{k,l}^{n_{k,l}} \quad (2.28)$$

where  $n_{k,l}$  is the number of transitions observed between the states  $e_k$  and  $e_l$ . The estimates  $\hat{p}_{k,l}$  of the conditional probabilities  $p_{k,l}$  can be assessed by maximizing the logarithm of the likelihood function under the restrictions  $\sum_{l=1}^K p_{k,l} = 1$  and  $0 \leq p_{k,l} \leq 1$ :

$$\hat{p}_{k,l} = \frac{n_{k,l}}{\sum_{l=1}^K n_{k,l}} \quad (2.29)$$

The transition probabilities are computed by dividing the observed number of transition from  $e_k$  to  $e_l$  by the total number of transitions starting from the state  $e_k$ . More details can be found concerning the transition probability estimation in the article of Anderson [63]. A few applications of ARMA models and Markov chains to the modeling of fatigue



operating loads are presented in the following paragraph.

### **Applications of random processes to fatigue analysis**

Random processes are used in a wide range of application fields like econometrics [64], earthquake engineering [65], fluid mechanics [66], offshore structures and coastal engineering [67–69], material and fracture mechanics [70]. Concerning fatigue analysis, several authors focused their work on the modeling of sequence of peaks and valleys by means of random processes and studied the connection which exists between rainflow counting results and random processes. For instance, Rychlik *et al.* [71] proposed to model a sequence of peaks and valleys by means of a Markov chain and demonstrated the interest of their method on regular and irregular Gaussian stationary processes. Soon after that, Rychlik [72] dealt with the inverse problem consisting in reconstructing a Markov chain of local extrema from an average rainflow counting.

Johannesson [73] mainly contributed during his PhD to extend the works done by Rychlik by presenting algorithms for the calculation of expected rainflow matrices for random loads described by switching processes with Markov structure. More recently, Benasciutti *et al.* [74] estimated the statistical distribution of fatigue cycles of non-stationary random loadings. Castillo *et al.* [69] also extended the rainflow matrices assessment by means of first-order switching Markov chains to the case of switching second order Markov chains to model a sequence of sea states in order to improve the design of rumble mound breakwaters. Moreover, in a similar way as performed by Rychlik and Johannesson, Mattrand *et al.* [75] experimented the use of discrete-time Markov chains and hidden Markov chains to model sequences of max-min fatigue stress cycles. Rather than modeling the sequence of local extrema, *i.e.* from a min to a max or from a max to a min, Markov chains directly define the sequence of stress cycles (a cycle being defined as a sequence of a max and a min together). They have shown that this new Markov chain definition provides satisfactory results for the modeling of stress cycles of an in-flight aircraft.

A recent work done by Ling *et al.* [76] consists in testing three methods (rainflow counting, Markov chain, ARMA model) to characterize and reconstruct fatigue load spectra. The corresponding rainflow matrices, transition probability matrices and ARMA model parameters are assessed and updated in real time by means of data coming from helicopter combat maneuver. Then, artificial load-time histories are re-generated by using each method. The authors conclude, by means of a Bayes hypothesis testing, that the three models are comparably suitable to fit well the studied load-time history even though the ARMA model seems to be the most appropriate model according to the overall confidence value.

Although stationary Gaussian processes are not detailed in this manuscript, this class of random processes was found to be suitable for fatigue loads modeling in automotive and aerospace industry, especially concerning spectral analyses of fatigue loading. For instance,

Pitoiset [77] and Benasciutti [78] contributed to the development of spectral methods to perform fatigue analysis of components subjected to Gaussian or non-Gaussian random loadings.

As detailed before in the case of random processes, the following section presents another model that enable to consider the uncertainties related to fatigue loading.

### 2.3.3 Elementary loads mix strategy

The elementary load mix strategy considers that fatigue loading of structural components is a combination of elementary loads induced by a specific use of the component. This method, which was used in industrial applications [2, 3, 6], is suitable to model fatigue loading if two kinds of data are available: the field records of the considered fatigue loading and the proportion of time spent in each elementary situation.

Lefebvre et al. [2] consider for instance that the use profile of a space launcher component can be classified according to three quantities of interest: the space rocket velocity (three classes: Mach 1, Mach 2 or Mach 3), the incidence angle (three classes) and the yawing angle (three classes). Thus 27 elementary load situations are defined accounting for these parameters. In the same way, let us consider the simple example considering two quantities of interest  $A_i$  and  $B_j$  depicted in figure 2.11.  $A_i$  and  $B_j$  consist respectively of two-by-three classes with their related percentages of occurrence  $p_i$  and  $q_j$  ( $i = \{1, 2\}$  and  $j = \{1, 2, 3\}$ ). Therefore, the six possible situations are  $\{A_1B_1, A_1B_2, A_1B_3, A_2B_1, A_2B_2, A_2B_3\}$ . Several field records are performed in order to assess the elementary loads  $L_{i,j}^{(1)}$ ,  $L_{i,j}^{(2)}$ , ... for each elementary situation  $A_iB_j$ . Note that these field recordings are usually converted into loading spectra or Rainflow matrices normalized by a chosen reference case (e.g.  $A_1B_1$ ) in order to facilitate further mixing. The proportion of time spent in each elementary load situation  $(p_i, q_j)$  during the lifespan of the structure is considered as random, these being generally selected in uniform probability laws.

A mixed loading  $\mathbb{L}$  can be reconstructed by selecting a virtual life in the possible elementary situations:

$$\mathbb{L} = \sum_{i=1}^2 \sum_{j=1}^3 p_i q_j L_{i,j}^{(k)} \quad (2.30)$$

where  $k$  is the  $k$ th elementary load randomly selected for each situation. Considering the example of virtual life depicted in figure 2.11, equation 2.30 becomes:

$$\mathbb{L} = p_1 q_1 L_{1,1}^{(1)} + p_1 q_2 L_{1,2}^{(4)} + p_1 q_3 L_{1,3}^{(2)} + p_2 q_1 L_{2,1}^{(3)} + p_2 q_2 L_{2,2}^{(1)} + p_2 q_3 L_{2,3}^{(3)} \quad (2.31)$$

The elementary load mix strategy requires to select realizations of random variables related to the proportions  $p_i$  and  $q_j$  on one hand, and discrete probabilities enabling to choose an elementary load for each situation on the other hand. Note that  $p_i$  and  $q_j$  are fully correlated since their sum must equal 1. In the case of two possibilities of occurrence

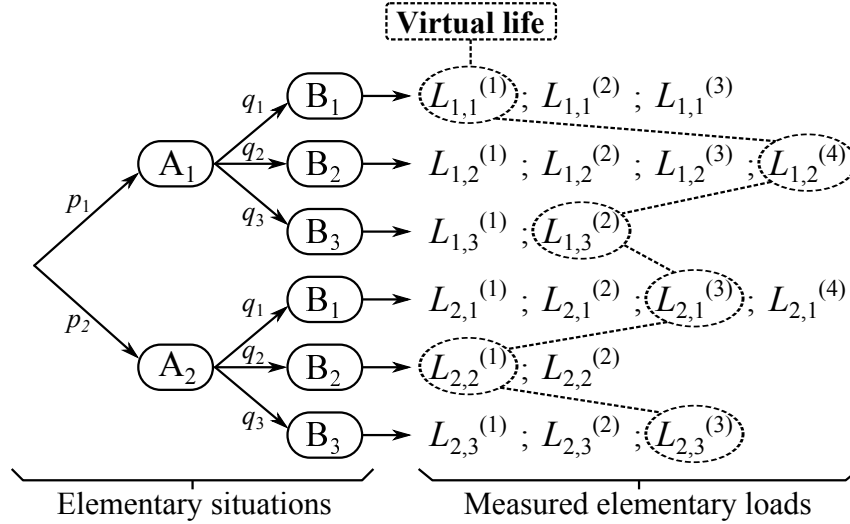


Figure 2.11 – Illustration of the load mix strategy in the case of two quantities of interest.

for an elementary situation as depicted in figure 2.11,  $p_2$  can be entirely inferred since  $p_1$  is known ( $p_2 = 1 - p_1$ ). Nevertheless, this becomes more complex when the number of classes exceeds 2. This is the case for instance of the elementary situation B that consists of three classes (see figure 2.11). Given that  $K$  is the number of recorded elementary loads per situation, the  $k$ th elementary load selected for a virtual life is chosen by using discrete probabilities that equal  $1/K$ . As seen in figure 2.11, three elementary loads ( $L_{1,1}^{(k)}$  with  $k = 1, 2, 3$ ) have been recorded for the situation  $A_1B_1$ . Therefore, the probability to select one of these loads is equal to  $1/3$ . Then, the probability to choose an elementary load related to the situation  $A_1B_2$  equals  $1/4$ , and so on.

Although the elementary load mix strategy is suitable for the modeling of operating loads, this procedure presents some limits. Actually, if a great number of elementary loads belongs to each class, the number of random variables to be handled becomes very high, which leads to increase drastically the computational time needed to perform the procedure.

In the following section, mixture models of loading spectra are presented as another convenient method allowing to account for the uncertainties related to fatigue loading.

### 2.3.4 Mixture models of loading spectra

As presented in the previous section, the elementary load mix strategy requires the monitoring of components over an extended operating period. Nonetheless, the monitoring of structures may be difficult due to the fact that equipments and devices (*e.g.* strain gauges) used to perform field recordings are sometimes expensive and difficult to install when the structure to monitor is relatively inaccessible. Moreover, if the monitoring period becomes very long, the amount of data is sometimes too large to be analyzed with ease. These rea-

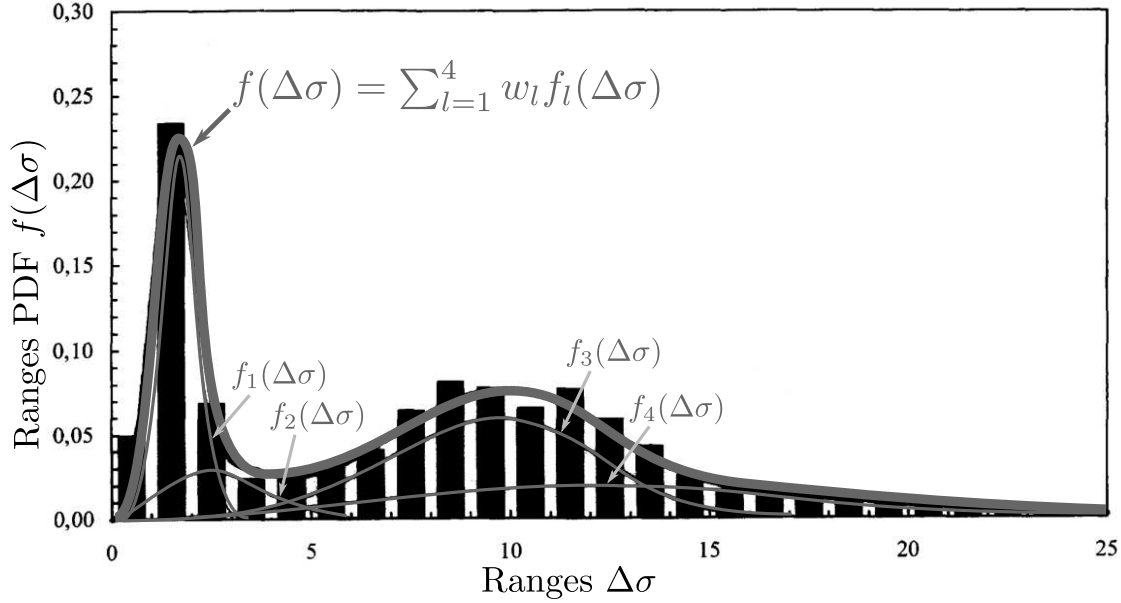


Figure 2.12 – Illustration of the mixture model proposed by Nagode and Fajdiga [79].

sons explain why field recordings are generally performed during short time-periods, which may cause some problems since collected data do not necessarily account for all the cycles applied to the structure during its service life. The problem of extrapolating with accuracy field measurements thus arises. One method to solve this problem consists in modeling the load ranges by means of a uni-modal probability density function. Although this method may be helpful in the case of stationary random processes, this becomes ineffective for non-stationary random loads. This explains why during the last decade, some authors [79–85] were interested in handling the problem of extrapolating the structural fatigue loading by means of mixture models of Rainflow matrices or loading spectra. Although the method presented in the following is suitable for the modeling of rainflow matrices, only the mixture models of loading spectra is presented in this section.

Multi-modal rainflow ranges distribution  $f(\Delta\sigma)$  is assumed to be modeled by a mixture of component PDFs as follows :

$$f(\Delta\sigma) = \sum_{l=1}^m w_l f_l(\Delta\sigma) \quad (2.32)$$

where  $\Delta\sigma$  are the counted ranges,  $w_l$  is the  $l$ th weighting factor with  $w_l \geq 0$  ( $l = 1, \dots, m$ ) and  $\sum_{l=1}^m w_l = 1$ . PDF examples which are listed in table 2.2 correspond to parametric component PDFs commonly used in mixture models (see Nagode [86]).

As pointed out by Bučar et al. [87], the most efficient methods to assess the number of component distributions  $l$ , the weighting factors  $w_l$  and the parameters of each component PDF are respectively the EM algorithm [87] and the REBMIX procedure [86]. For the sake

|           |                                                                                                                                                            |
|-----------|------------------------------------------------------------------------------------------------------------------------------------------------------------|
| Normal    | $\frac{1}{\sqrt{2\pi}\sigma_l} \exp\left\{-\frac{1}{2}\left(\frac{\Delta\sigma-\mu_l}{\sigma_l}\right)^2\right\}$                                          |
| Lognormal | $\frac{1}{\sqrt{2\pi}\xi_l\Delta\sigma} \exp\left\{-\frac{1}{2}\left(\frac{\ln(\Delta\sigma)-\lambda_l}{\xi_l}\right)^2\right\}$                           |
| Weibull   | $\frac{\beta_l}{\theta_l} \left(\frac{\Delta\sigma}{\theta_l}\right)^{\beta_l-1} \exp\left\{-\left(\frac{\Delta\sigma}{\theta_l}\right)^{\beta_l}\right\}$ |
| Gamma     | $\frac{1}{\Gamma[\beta_l]\Delta\sigma} \left(\frac{\Delta\sigma}{\theta_l}\right)^{\beta_l} \exp\left\{-\frac{\Delta\sigma}{\theta_l}\right\}$             |
| Binomial  | $\binom{\theta_l}{\Delta\sigma} p_l^{\Delta\sigma} (1-p_l)^{\theta_l-\Delta\sigma}$                                                                        |
| Poisson   | $\frac{e^{-\theta_l} \theta_l^{\Delta\sigma}}{\Delta\sigma!}$                                                                                              |
| Dirac     | $\begin{cases} 1 & \text{if } \Delta\sigma = \theta_l \\ 0 & \text{otherwise} \end{cases}$                                                                 |

Table 2.2 – Parametric component PDF families commonly used in mixture models [86].

of clarity, only the general principle and the advantages and drawbacks of these estimation methods are detailed in this thesis. On one hand, the EM (Expectation Maximization) algorithm is an iterative procedure consisting of two steps. First, the expectation of the maximum likelihood function is evaluated by considering a set of estimated parameters. Second, a new set of parameters is found by maximizing the expectation assessed at the previous step. Then, the new set of parameters is used as an input of the first step and the procedure is reiterated. The EM algorithm provides a good agreement between observed and assessed PDFs if the number of component PDFs is properly chosen. Nevertheless, the results and convergence of this method are highly dependent on the chosen initial conditions leading to a high computational time for a large number of component PDFs. On the other hand, the REBMIX method consists in identifying the global mode of the multivariate distribution which corresponds to the first component PDF. Then, the observations belonging to this PDF are automatically clustered and the maximum likelihood method is used to infer the corresponding PDF parameters. Subsequently, the mode corresponding to the second component PDF is identified and the procedure is repeated until a sufficient number of components allows the mixture model to fit well the observed distribution. Although more component PDFs are required in comparison with the EM algorithm in the mixture model assessment, the REBMIX procedure presents many advantages. Initial conditions (number of components or component parameter initial values) are not required. The procedure also features numerical stability and high speed convergence. The reader can refer to [86] and [87] for further details about the implementation of the REBMIX

algorithm.

One example of the REBMIX promoted by Nagode and Fajdiga [79] is detailed in the following. As depicted in figure 2.12, Nagode and Fajdiga originally proposed to use a mixture of two-parameters Weibull PDFs (see the third line of table 2.2) in order to model the distribution of rainflow ranges  $\Delta\sigma$ . The associated cumulative distribution function  $F(\Delta\sigma)$  reads:

$$F(\Delta\sigma) = 1 - \sum_{l=1}^m w_l \exp \left\{ - \left( \frac{\Delta\sigma}{\theta_l} \right)^{\beta_l} \right\} \quad (2.33)$$

where  $\beta_l$  and  $\theta_l$  are respectively the shape and scale parameters of the  $l$ th Weibull distribution. Therefore, the loading spectrum  $H(\Delta\sigma)$  is expressed as a function of  $F(\Delta\sigma)$ :

$$H(\Delta\sigma) = H_0(1 - F(\Delta\sigma)) \quad (2.34)$$

where  $H_0$  is the total number of load cycles. The loading spectra  $H_{ij}$  ( $j = \{1, 2, \dots, r\}$ ) and the resulting average spectrum  $H_i$  depicted in figure 2.13 were determined from  $r$  experimental data sets (measurements on a forklift in operation). Moreover, the loading spectra assessed by using the model presented above are given for  $m$  respectively equal to 1, 2, 3 and 4. As shown in figure 2.13, a good agreement between the mixture model and the experimental average loading spectrum is found when  $m$  reaches 4, *i.e.* when four component PDFs are used. Nagode and Fajdiga [79] showed the efficiency of their method on several loading spectrum examples having shapes noticeably different. Note that the proposed method also enables to extrapolate loading spectra outside of the measurement range.

Beside the fact that the loading sequence is lost in the mixture models proposed by Nagode and Fajdiga, Tovo [88] highlighted two other drawbacks. He emphasized that at least three or four component PDFs are needed to properly describe the range distributions and that there is no unique solution for the unknown parameters estimation because it strongly depends on the chosen shutoff criterion. By investigating the relationship between the multi-modal distribution and the damage caused on a structural element, Tovo proposed to simplify the previous multivariate model into a single Weibull distribution for the case of stationary load histories having one dominating mode in the damage calculations. The efficiency of the method is demonstrated by using experimental measurements coming from a motorcycle frame in off-road riding.

Although Nagode and Fajdiga improved their method [89, 90], another main drawback remains due to the subjectivity introduced by the user choice of the number of component PDFs of the mixture model. Klemenc and Fajdiga proposed alternative methods as a hierarchical clustering of load cycles [83, 91] or a modified EM algorithm [92] enabling to avoid this problem. Nagode and Fajdiga [93] also introduced a method where the number of component PDFs is no longer needed and they provided improvements consisting in

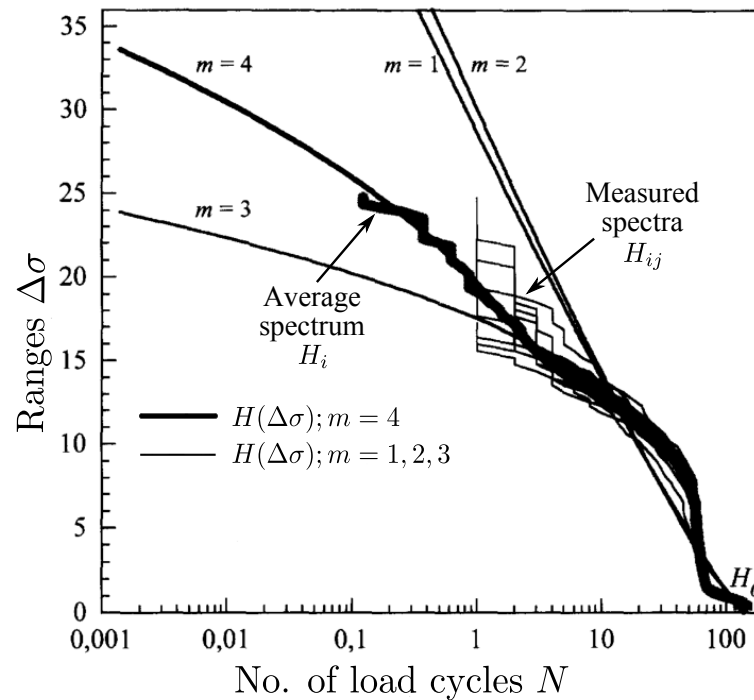


Figure 2.13 – Illustration of spectrum assessed by Nagode and Fajdiga [79] with the mixture model.

changing the shutoff criterion and treating the residual by using the Bayesian decision rule. Lastly, note that the unknown parameters and the weighting factors still depend on the choice of the binning of observations (*i.e.* class widths of the histogram of rainflow ranges).

Three different models enabling the modeling of operating loads related to fatigue were presented in the above sections. The choice of an appropriate method in the case of fatigue loading of crane members will be performed in chapter 4 after having studied carefully in chapter 3 the available data related to crane use. The following section is devoted to the description of the general probabilistic principles and reliability methods used in this research work.

## 2.4 General reliability methods

The main objective of this research work is to develop a comprehensive probabilistic procedure enabling to assess the reliability of crane members according to their operating time. For this purpose, the basic principles of reliability methods needed to achieve this essential task are discussed in this section. The time-dependent reliability is first introduced in section 2.4.1 and, section 2.4.2 presents the so-called stress-strength interference (SSI) methods. Following this, section 2.4.3 gives definitions related to the reliability index, and

section 2.4.4 describes the Monte Carlo simulations. Lastly, the Sobol sensitivity analysis method is outlined in section 2.4.5.

### 2.4.1 Time-dependent reliability

The design of a structure is considered as acceptable when it fulfills the predefined requirements (thermal or mechanical response, volume, etc). Standards usually distinguish several types of acceptance criteria, known as the limit states:

- The ultimate limit state (ULS) is generally related to the collapse of a structure due to a loss of capacity (stiffness or strength).
- The serviceability limit state (SLS) is stated in order to guarantee the good operation of the structure under normal use conditions.
- The fatigue limit state (FLS) is conventionally connected to the fatigue damage accumulation in structural details subjected to repeated loading.
- The accidental limit state (ALS) is associated to an excessive structural damage due to accidents (*e.g.* explosion, collision, earthquake).

Structural reliability consists in predicting the probability (*i.e.* numerical measure of occurrence) of exceeding a limit state at any moment, throughout its lifespan. The limit state is generally described by a rule (or a set of rules) corresponding to a failure scenario. As introduced in section 1.5, this can be mathematically expressed by means of a *performance function*  $G$  involving random variables  $\mathbf{X}(\omega, t)$ .  $\omega$  means that  $\mathbf{X}$  are random and  $t$  suggests that  $\mathbf{X}$  vary according to the time. As a consequence, the limit state coincides with  $G(t, \mathbf{X}(\omega, t)) = 0$  while  $G(t, \mathbf{X}(\omega, t)) > 0$  and  $G(t, \mathbf{X}(\omega, t)) < 0$  represent respectively the safety and failure domains.

Considering a reliability analysis involving random variables  $\mathbf{X}(\omega, t)$  related to a failure scenario and assuming that there is an instant  $\tau$ , belonging to the time interval  $[t_1, t_2]$ , for which the structure fails, the general form of the failure probability can be written as follows:

$$P_f(t_1, t_2) = \text{Prob}(\exists \tau \in [t_1, t_2], G(\tau, X(\tau, \omega)) \leq 0) \quad (2.35)$$

Assuming the regularity of the process, *i.e.* if the performance function is equal or lower than zero ( $G \leq 0$ ) only one time during the small time interval  $[\tau, \tau + \Delta\tau]$ , the previous formula becomes the exact expression of the *cumulative failure probability*  $P_{f,c}(t_1, t_2)$ . Moreover, the *instantaneous failure probability*  $P_{f,i}(t)$ , representing the failure probability of the structure at the time instant  $t$ , is expressed by means of the following relation:

$$P_{f,i}(t) = \text{Prob}(G(t, X(\omega, t)) \leq 0) \quad (2.36)$$



As shown by Céline Andrieu-Renaud during her PhD [94],  $P_{f,i}$  and  $P_{f,c}(t_1, t_2)$  are theoretically different, excepted if the performance function  $G$  decreases monotonically according to  $t$ . This may occur for instance for degradation processes such as corrosion and fatigue cracking. Once a crack appears, fatigue cracking leads to the degradation of material characteristics until a potential strengthening (re-welding, etc) of the structure. Therefore, in the case of a performance function strictly decreasing until a time  $t < \infty$ , the instantaneous failure probability is identical to the cumulative failure probability:

$$P_{f,i}(t) = P_{f,c}(0, t) \quad (2.37)$$

As described in section 2.2.1, only the initiation of macroscopic weld toe cracks is considered in this work, which leads to assume that the resistance of crane welded details is not supposed to evolve with time. Thus, given that the crane member fatigue damage induced by cyclic loading increases with operating time, the margin between the resistance and the stress of the structure decreases monotonically. Consequently, the probabilities calculated in the following correspond either to instantaneous or cumulative failure probabilities and are denoted  $P_f$ . Additionally, for the sake of clarity, the notation  $\omega$ , indicating the randomness inherent to the variables, is omitted in the following.

#### 2.4.2 Stress-strength interference methods

In industrial context, the most simple failure scenario consists in comparing two random variables related respectively to a stress  $S$  (demand) on one hand and a strength  $R$  (supply) on the other hand. In other words, a structure is safe in accordance with a failure criterion if, at any time, the applied stress remains below the strength of the component. Methods based on the separation of  $S$  and  $R$  are named **SSI (Stress-Strength Interference) methods**. As shown in section 2.4.1,  $S$  and  $R$  can be time-variant depending on the physical behavior of the studied structure. For instance,  $R = R(t)$  if the corrosion of a metallic component is considered or  $S = S(t)$  if a structure is subjected to random loading. By the way, the performance function  $G$  is regularly expressed as a combination of progressive degradation process  $R(t)$  and a random loading  $S(t)$ :  $G(t) = S(t) - R(t)$ . More details about SSI methods are given in [14, 15] and examples of industrial applications can be found in [6, 16, 17].

The failure criterion considered in this thesis concerns exclusively the initiation of a macroscopic crack at weld toe. Thus, the material characteristics decrease induced by crack propagation is not considered here. Furthermore, crane structural assemblies are painted in order to prevent corrosion problems. As a result, fatigue strength of crane welded assemblies is supposed to be time-independent. By contrast, as seen in section 1.4, the construction site duration and the time between two jobs imply uncertainties concerning crane use (*i.e.* structural loading) leading to the conclusion that crane member

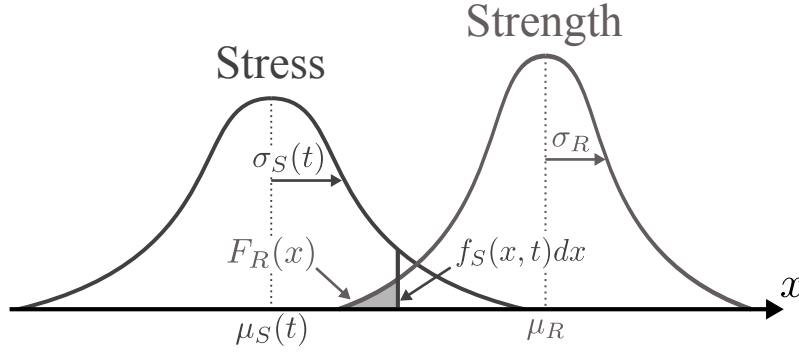


Figure 2.14 – Stress-strength interference method.

loading is highly time-dependent. Hence, the performance function  $G$  corresponding to the reliability method presented in this thesis is expressed as follows:

$$G(t) = R - S(t) \quad (2.38)$$

As depicted in figure 2.14 for the case of two Gaussian distributions, the reliability of a crane structural member can be assessed by characterizing two PDFs related respectively to the stress  $S(t)$  and the strength  $R$ . Assuming that these distributions can be determined and are independent, the failure probability  $P_f(t) = \text{Prob}(G(t) \leq 0)$  or equivalently the reliability  $\mathcal{R}(t)$ , depending on operating time  $t$ , is assessed as follows:

$$\mathcal{R}(t) = 1 - P_f(t) = 1 - \int_{-\infty}^{\infty} f_S(x, t) F_R(x) dx \quad (2.39)$$

where  $f_S$  and  $F_R$  are respectively the stress PDF and the strength CDF.

SSI methods assume that stress and strength distributions are statistically independent which is not the case in some situations. A second assumption highlighted by Echard et al. [95] lies in the fact that these distributions cannot be fully observed. Therefore, reliability results are very sensitive to the PDF models chosen to fit experimental data. Concerning tower cranes, the intrinsic fatigue strength of crane members is independent of loading history. The first assumption is therefore verified and, provided that the stress and strength PDFs can be fully determined, the stress-strength interference method can be used.

### 2.4.3 Reliability index

Rather than talking about failure probability, it is sometimes convenient to use a dimensionless measure which reflects the reliability of a structure, namely the *reliability index*. Cornell [96] proposed in 1970 to define the reliability index as the inverse of the coefficient

of variation of the margin  $Z = R - S$ :

$$\beta_C = \frac{\mu_Z}{\sigma_Z} \quad (2.40)$$

For instance, concerning the two independent Gaussian distributions presented in section 2.4.2, the previous formula becomes:

$$\beta_C(t) = \frac{\mu_R - \mu_S(t)}{\sqrt{\sigma_R^2 + \sigma_S(t)^2}} \quad (2.41)$$

Although the Cornell reliability index seems to be convenient in some simple situations (*e.g.* Gaussian distributions and linear limit state), this index is sometimes difficult to use because of its lack of generality. In fact, the most general form of the reliability index was given by Hasofer and Lind in 1974 [97]. They proposed to convert random variables from the physical space to a space of standardized independent Gaussian variables (having zero mean and unit variance) by introducing an isoprobabilistic transformation  $T$ . Thus, the method consists in converting independent physical random variables  $\mathbf{X}$  (of realizations  $\mathbf{x}$ ) into independent standard Gaussian variables  $\mathbf{U}$  (of realizations  $\mathbf{u}$ ) by writing the mathematical equality of CDFs:

$$\Phi(\mathbf{u}) = F_X(\mathbf{x}) \Rightarrow \mathbf{x} \xrightarrow{T} \mathbf{u} = \Phi^{-1}(F_X(\mathbf{x})) \quad (2.42)$$

where  $\Phi$  refers to the standard Gaussian CDF. Thereafter, as seen in figure 2.15, the performance function  $G$  is transformed into  $H$  in the standardized space, *i.e.*  $H(\mathbf{U}) \equiv G(T^{-1}(\mathbf{U}))$ . Hence, the Hasofer-Lind reliability index  $\beta$  corresponds to the minimum distance between the origin and the failure domain:

$$\beta = \beta_{HL} = \sqrt{\mathbf{u}^t \mathbf{u}} \text{ under the constraint } H(\mathbf{u}) \leq 0 \quad (2.43)$$

In the case of two independent Gaussian distributions and linear limit state as presented before, the Hasofer-Lind and Cornell reliability indexes are equivalent and derived from equation (2.41). Furthermore, when an analytical expression of  $\mathcal{R}$  exists,  $\beta$  derives directly from  $\mathcal{R}$ . Thus, remembering the time-dependent reliability  $\mathcal{R}(t)$  expression given in section 2.4.2, this leads to:

$$\beta(t) = -\Phi^{-1}(1 - \mathcal{R}(t)) \quad (2.44)$$

If no analytical expression exists for  $\mathcal{R}$ , the reliability index has to be quantified by means of a numerical method such as Monte Carlo simulations presented in the following section. More details concerning the reliability index can be found in the book of M. Lemaire [12]. Furthermore, the assessment of the stress  $S$  and strength  $R$  distributions is detailed in chapter 4 in this thesis.

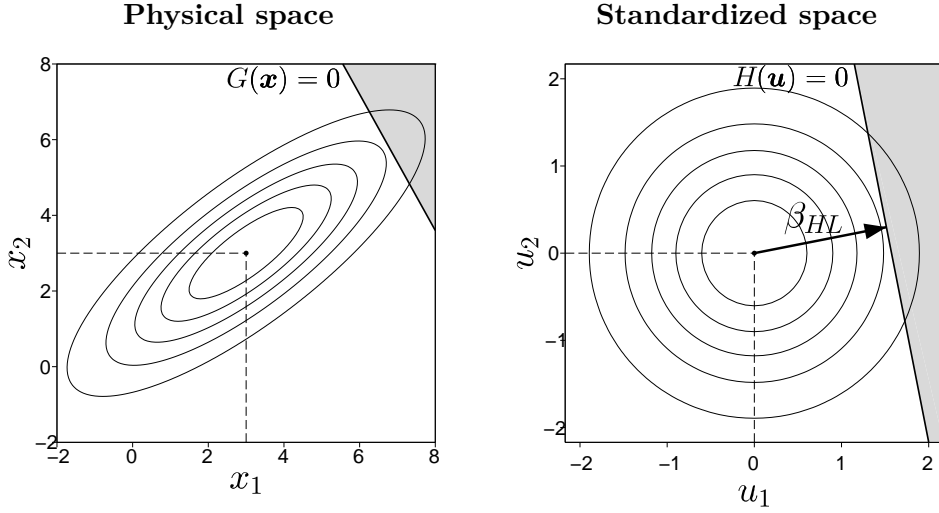


Figure 2.15 – Illustration of an isoprobabilistic transformation.

#### 2.4.4 Monte Carlo simulations

As shown in section 2.4.1, the failure probability reads:

$$P_f = \text{Prob}(G(X) \leq 0) \quad (2.45)$$

By introducing the joint probability density function  $f_X(\mathbf{x})$ , Monte Carlo simulations consist in performing random sampling of variables  $X$  in the whole physical space in order to evaluate the following integral:

$$P_f = \int_{D_f} f_X(\mathbf{x}) dx_1 dx_2 \dots dx_n \quad (2.46)$$

where  $D_f$  is the failure domain. By using the isoprobabilistic transformation  $T$ , the previous integral is expressed in the standardized space, leading to recast the failure probability as:

$$P_f = \int_{D_f} \phi_n(\mathbf{u}) du_1 du_2 \dots du_n \quad (2.47)$$

where  $\phi_n$  is the joint standard Gaussian PDF. As detailed in the book of Lemaire [98], the introduction of the indicator function  $I_{D_f}(\mathbf{u}) = \{1 \text{ if } H(\mathbf{u}) \leq 0 \text{ and } 0 \text{ otherwise}\}$  enables to rewrite the previous integral as follows:

$$P_f = \int_{D_f} I_{D_f}(\mathbf{u}) \phi_n(\mathbf{u}) du_1 du_2 \dots du_n \quad (2.48)$$

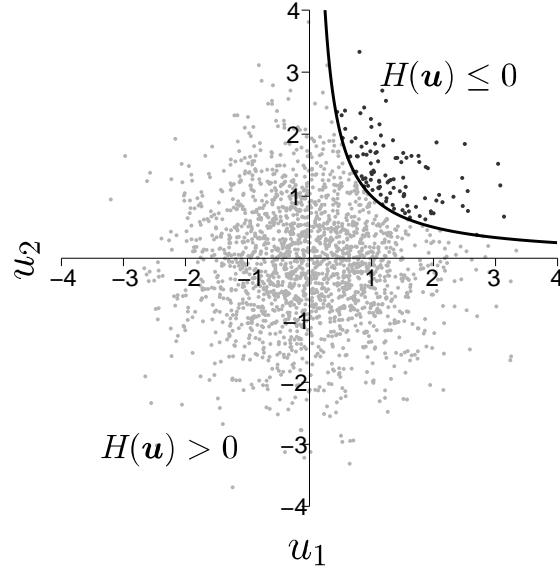


Figure 2.16 – Illustration of Monte Carlo simulations in the case of two standard Gaussian variables. Gray points mean that the realizations of  $U_1$  and  $U_2$  are located in the safe domain while the black points mean that they are located in the failure domain.

Thus, the failure probability defined in equation 2.48 can be approximated as:

$$P_f = \mathbb{E} [I_{D_f}(\mathbf{u})] \approx \tilde{P}_f = \frac{1}{N_{MC}} \sum_{i=1}^{N_{MC}} I_{D_f}(\mathbf{u}^{(i)}) \quad (2.49)$$

where  $\mathbb{E}[\cdot]$  is the mathematical expectation and  $N_{MC}$  is the number of Monte Carlo simulations. As depicted in figure 2.16 for the case of two standard Gaussian variables,  $P_f$  is assessed by dividing the number of points located in the failure domain (black dots) by the total number of sampled points. An estimation of the failure probability variance can be defined from the estimation of  $P_f$ :

$$\overline{\text{var}} [\tilde{P}_f] \approx \frac{\tilde{P}_f}{N_{MC}} (1 - \tilde{P}_f) \quad (2.50)$$

The estimation of  $\tilde{P}_f$  with unknown variance leads to the expression of a two-sided confidence interval:

$$\tilde{P}_f - t_{1-\frac{\alpha}{2}}(\nu) \sqrt{\overline{\text{var}} [\tilde{P}_f]} \leq P_f \leq \tilde{P}_f + t_{1-\frac{\alpha}{2}}(\nu) \sqrt{\overline{\text{var}} [\tilde{P}_f]} \quad (2.51)$$

where  $t_{1-\frac{\alpha}{2}}(\nu)$  is the Student variable of parameter  $\nu = N_{MC} - 1$  and  $\alpha$  is the percentage of confidence on the estimation. The reliability index  $\tilde{\beta}$  is then assessed by replacing  $(1 - \mathcal{R}(t))$  by the estimated failure probability  $\tilde{P}_f$  in equation (2.44).

Monte Carlo simulations constitute the most simple and general method to simulate

random situations because they do not require any simplification assumption enabling to solve the reliability problem. Nonetheless, the major drawback lies in the fact that this method is extremely time-consuming. For instance, the assessment of a  $10^{-n}$  probability with an acceptable confidence interval requires between  $10^{n+2}$  and  $10^{n+3}$  simulations. Hence, this numerical method cannot be used for complicated reliability studies involving heavy mechanical models. Despite this drawback, the results coming from Monte Carlo simulations are often used as reference case to judge of the efficiency and precision of alternative methods. The reader can refer to [12, 13] for more details about Monte Carlo simulations.

### 2.4.5 Stochastic sensitivity analysis

Sensitivity analyses enable the evaluation of the impact of random variables on a quantity of interest. Once integrated in the design process, they constitute efficient tools allowing to appreciate the significance of each random variable on the model response (*e.g.* the reliability index). This becomes particularly convenient when deciding what variables must be modified first in order to reach a reliability target. Furthermore, sensitivity analyses aim at avoiding the over-parametrization of a model by setting non-influential parameters to deterministic values. From this perspective, sensitivity analyses may be useful in the frame of this research work in order to evaluate the impact of input variables on the crane use model developed in chapter 4.

Sensitivity analyses can be divided into three main classes. First, *local analyses* focus on how a slight perturbation of input variables around a given value (*e.g.* the mean) influences the model output. Second, *screening methods* constitute a generalization of local analyses and enable the classification of input variables, while keeping a reasonable computational time. Third, *global procedures* aim at studying the influence of the whole variability of input parameters on model outputs. This section covers exclusively this class of method by presenting the variance-based Sobol's procedure because the variability of both stress and strength distributions influence the reliability results of the SSI method developed in chapter 4. Nonetheless, an overview of sensitivity analyses can be found in the book of Saltelli [99].

#### Variance decomposition

Let  $f$  be an integrable function on the  $p$ -dimensional interval  $I^p$ :

$$\begin{aligned} f : \mathbb{R}^p &\longrightarrow \mathbb{R} \\ \mathbf{X} &\longmapsto Y = f(\mathbf{X}) \end{aligned}$$

Assuming a model having independent inputs, Sobol' [100] introduced the decomposition of the variance of  $f$  into a sum of variance functions of increasing order:

$$V = \text{Var}(Y) = \sum_{i=1}^p V_i + \sum_{1 \leq i < j \leq p} V_{ij} + \dots + V_{1\dots p} \quad (2.52)$$

$$\text{with } \begin{cases} V_i &= \text{Var}(\mathbb{E}[Y|X_i]) \\ V_{ij} &= \text{Var}(\mathbb{E}[Y|X_i, X_j]) - V_i - V_j \\ V_{1\dots p} &= V - \sum_{i=1}^p V_i - \sum_{1 \leq i < j \leq p} V_{ij} - \dots - \sum_{1 \leq i_1 < \dots < i_{p-1} \leq p} V_{i_1 \dots i_{p-1}} \end{cases}$$

where  $V_i$  is the conditional variance of  $Y$  knowing  $X_i$ ,  $V_{ij}$  is the conditional variance of  $Y$  knowing  $X_i$  and  $X_j$  and so on. This decomposition of the variance of  $f$  enables to appreciate the impact of input random variables on the variance of  $Y$  by defining the following ratios:

$$S_i = \frac{V_i}{V} \quad (2.53)$$

$$S_{ij} = \frac{V_{ij}}{V} \quad (2.54)$$

$S_i$  and  $S_{ij}$  are named respectively first and second order Sobol' indices. When the number of input variables  $p$  is high, the number of sensitivity indices to assess increases rapidly, which may complicate their interpretation. Starting from this observation, Homma and Saltelli [101] introduced new global sensitivity indices, namely the total sensitivity indices  $S_{T_i}$ . They represent a measure of the total sensitivity of  $Y$  to  $X_i$ , *i.e.* this is the sum of all the Sobol' indices involving the variable  $X_i$ . For instance, in case of three input random variables,  $S_{T_1}$  is the sum of  $S_1$ ,  $S_{12}$ ,  $S_{13}$  and  $S_{123}$ . The total indices  $S_{T_i}$  can be assessed by using the following relation:

$$S_{T_i} = 1 - \frac{V_{\sim i}}{V} \quad (2.55)$$

where  $V_{\sim i}$  is the variance of the output resulting from the variation of all parameters excepted  $X_i$ .

### Sobol' indices estimation

A simple method to estimate Sobol' indices consists in using Monte Carlo simulations as presented in section 2.4.4. Let  $M_1$  and  $M_2$  be two independent  $N \times p$  matrices of  $N$  realizations of the  $p$  input variables. The estimation of first order and total Sobol' indices can be performed by estimating the total variance  $\hat{V}$  as follows:

$$\hat{V} = \frac{1}{N-1} \sum_{m=1}^N [f^2(x^{(1)(m)})] - \hat{f}_0^2 \quad (2.56)$$

with

$$\hat{f}_0^2 = \frac{1}{N} \sum_{m=1}^N [f(x^{(1)(m)})f(x^{(2)(m)})] \quad (2.57)$$

where  $x^{(1)(m)}$  and  $x^{(2)(m)}$  are respectively the sample sets coming from  $M_1$  and  $M_2$ , respectively. Then, the variances  $\hat{V}_i$  and  $\hat{V}_{\sim i}$  can be determined as follows:

$$\begin{aligned} \hat{V}_i &= \frac{1}{N-1} \sum_{m=1}^N [f(x^{(1)(m)})f(x_{\sim i}^{(2)(m)})] - \hat{f}_0^2 \\ \hat{V}_{\sim i} &= \frac{1}{N-1} \sum_{m=1}^N [f(x^{(1)(m)})f(x_{\sim i}^{(1)(m)})] - \hat{f}_0^2 \\ \hat{V}_{ij} &= \frac{1}{N-1} \sum_{m=1}^N [f(x^{(1)(m)})f(x_{\sim i,j}^{(2)(m)})] - \hat{f}_0^2 - \hat{V}_i - \hat{V}_j \end{aligned}$$

where  $x_{\sim i}^{(2)(m)}$  is the sample set coming from  $M_2$ , excepted for  $X_i$  taken from  $M_1$ . This means that all the input parameters vary, excepted  $X_i$ . Similarly,  $x_{\sim i}^{(1)(m)}$  is the sample set coming from  $M_1$ , excepted for  $X_i$  taken from  $M_2$ . In this case, only the input variable  $X_i$  varies. Lastly,  $x_{\sim i,j}^{(2)(m)}$  is the sample set coming from  $M_2$ , excepted for  $X_i$  and  $X_j$  which are picked from  $M_1$ . Subsequently, the first order, second order and total Sobol' indices are determined through equations (2.53), (2.55) and (2.54) by replacing  $V_i$ ,  $V_{\sim i}$ ,  $V_{ij}$  and  $V$  respectively by their estimates  $\hat{V}_i$ ,  $\hat{V}_{\sim i}$ ,  $\hat{V}_{ij}$  and  $\hat{V}$ .

Sobol' indices are fairly easy to interpret because they are all positives and their sum is equal to one. Hence, the greater the Sobol' index, the higher the impact of the variable on the variance of the result. By contrast, even though total Sobol' indices are also positives, their sum exceeds one. Nonetheless, these indices are useful to judge if a variable, apparently non-influential alone, turns to be important when combined with other variables.

The Sobol's method has grown in popularity thanks to the increase of computational capacities that occurred during the last decade. This global sensitivity analysis presents some advantages. First, no assumption is required concerning the linearity, additivity or monotonicity of the model. Second, this method accounts for the shape and the scale of input parameters as well as the possible interactions between them. Third, the Sobol's method provides the opportunity to manage grouped variables as if they were single parameters. Fourth, this method enables to identify the input variables that need to be well-characterized, which is very useful in the frame of this work. The main drawback of this method lies in the fact that the number of model evaluations needed to provide accurate sensitivity results is high. One possible alternative enabling to enhance convergence of Sobol' indices consists in performing Quasi-Monte Carlo simulations.



## 2.5 Conclusion

This chapter enabled us to define through three main topics (fatigue, loading and reliability) the basic principles used to fulfill the objectives of this research work. First, the fatigue phenomenon of welded connections has been introduced and the main influence factors on fatigue lifespan have been listed. Thereafter, the Dang Van fatigue criterion and S-N curves have been presented as a convenient tool to predict and analyze crack initiation of materials. Second, the concepts related to the assessment and modeling of fatigue loading have been outlined. Loading cycles can be counted by using the widely-used Rainflow procedure and cumulative damage can be quantified by means of the Palmgren-Miner's rule. Following these definitions, three methods enabling the modeling of fatigue loading have been detailed. The first model is based on random processes while the two others (elementary loads mix strategy and loading spectra mixture model) use the results coming from the Rainflow counting. Third, general notions concerning reliability have been illustrated through the definition of the time-dependent reliability, SSI methods and reliability index. Additionally, Monte Carlo simulations have been presented as the simplest method enabling the assessment of the reliability of a structural component. Finally, a global sensitivity analysis procedure, namely the Sobol's method, has been detailed. Most of the notions, concepts and methods presented in this chapter are used in chapter 3 and chapter 4.

**Chapter summary**

The fatigue phenomenon consists generally of two main steps: crack initiation and propagation. Furthermore, fatigue cracks of welded connections always appear either on the toe or the root of the welding depending on several factors (loading mode, surface roughness, ect.). In this thesis, crack initiation of weld toes is considered as the failure criterion for crane structural members. The Dang Van fatigue criterion, which considers crack initiation, aims at calculating an equivalent local stress at weld toe. Moreover, the results coming from constant amplitude tests are usually represented by means of S-N curves, the latter consisting in plotting the number of cycles to failure versus the stress range applied to the tested specimens. Standards dealing with fatigue usually provide probabilistic S-N curves guaranteeing a low failure risk for a great number of welded details. In addition, the fatigue damage of structures are usually quantified by using the Palmgren-Miner's rule to sum partial damages caused by fatigue cycles of different amplitudes.

The prediction of the fatigue behavior of components requires the assessment and modeling of the structural fatigue loading. Fatigue cycles of variable amplitude can be counted by using the Rainflow counting method. Furthermore, several modeling procedures exist to reproduce the fatigue loading reflecting the operating conditions. A first method consists in modeling the temporal evolutions of fatigue loads by means of random processes. Another method aims at performing on-site recording of multiple elementary loads and to pick them randomly in order to reconstruct several virtual lives for a structural component. The last method consists in quantifying the randomness of loading spectra from several measurements in order to simulate virtual loading spectra reflecting the real use of the structure.

As pointed out in chapter 1, the crane use depends on several uncertainties varying with time. The fatigue phenomenon being a non regenerative degradation process, the instantaneous and cumulative failure probability of structural members are equivalent. This probability, or its related reliability index, can be assessed by using a stress-strength interference method combined with Monte Carlo simulations. Stress-strength interference methods consist in calculating the failure probability of a structural member by studying separately uncertainties related to its use and to its resistance. Finally, the Sobol' sensitivity analysis method represents an efficient and interesting tool enabling to quantify the impact of input parameters on the outcomes (*e.g.* reliability index) of a model.



---

# Chapter 3

## Crane work data analysis

### Contents

---

|            |                                                                 |           |
|------------|-----------------------------------------------------------------|-----------|
| <b>3.1</b> | <b>Introduction</b>                                             | <b>64</b> |
| <b>3.2</b> | <b>Construction site data processing</b>                        | <b>64</b> |
| 3.2.1      | Construction site data recording                                | 64        |
| 3.2.2      | Crane cycle identification                                      | 66        |
| 3.2.3      | Crane cycle per type of work                                    | 67        |
| <b>3.3</b> | <b>Construction sites characteristics</b>                       | <b>71</b> |
| <b>3.4</b> | <b>Intra-construction site data post-processing</b>             | <b>72</b> |
| 3.4.1      | Data versus load chart                                          | 73        |
| 3.4.2      | Data versus construction site working area                      | 75        |
| 3.4.3      | Data depicted by using histograms                               | 75        |
| <b>3.5</b> | <b>Intra-construction site loading severity assessment</b>      | <b>80</b> |
| 3.5.1      | Severity calculation procedure                                  | 84        |
| 3.5.2      | Severity assessment of a jib top member connection              | 85        |
| <b>3.6</b> | <b>Inter-construction site variability quantification</b>       | <b>87</b> |
| 3.6.1      | Inter-construction site durations from crane rental agency data | 87        |
| 3.6.2      | Inter-construction site configuration parameters from drawings  | 89        |
| <b>3.7</b> | <b>Conclusion</b>                                               | <b>94</b> |
|            | <b>Chapter summary</b>                                          | <b>95</b> |

---

## 3.1 Introduction

As shown in section 1.4, the great variety of construction sites' topography and duration leads to crane use uncertainties that are classified into two groups (intra- and inter-construction site parameters). As seen in chapter 2, whatever the method that is chosen, the modeling of crane operating loads requires the understanding and the quantification of these uncertainties. This can be performed by collecting data by means of on-site recording, database collection, customer surveys, etc. In the frame of this research work, data coming from several sources have been collected. Recording was first performed on three similar tower cranes, working on different construction sites. Moreover, a database containing construction site durations was collected from a crane rental agency, and numerous construction site drawings were provided by a construction firm. Thus, this chapter gives the reader an overview of how these data were handled in order to develop the crane member use model in chapter 4. Section 3.2 presents the construction site data processing which consists in identifying and distinguishing crane cycles, while section 3.3 summarizes the global characteristics of the three studied construction sites. Then, section 3.4 focuses on various possible representations of the results reflecting the work performed by the crane on the sites, and section 3.5 discusses the quantification of the loading severity related to crane structural members. Section 3.6 finally deals with the handling of crane rental agency data and construction site drawings in order to quantify the variability of inter-construction site parameters.

## 3.2 Construction site data processing

This section details the crane cycle identification that is performed from records according to the definition given in section 1.3, and outlines the method used to distinguish crane cycles per type of work related to the possible hoisted loads presented in section 1.4.

### 3.2.1 Construction site data recording

An in-house recording device was developed during this PhD in order to record a large amount of temporal data. This device is able to record (each 250 ms) data such as time, radius (position of the trolley along the jib), height of the hook, hoisted load value, slewing angle, wind speed, drives speed (trolleying, slewing, hoisting), etc, which represents a file of almost 20 Mo for a 8-hours working day. Figure 3.1 depicts the useful data for the analysis of crane member loading over a time period of 280 min: load, radius, hook height and slewing angle. As seen in the figure, the periodical nature of these signals confirms that crane structural members are cyclically loaded and suggests that crane cycles identification is relevant.

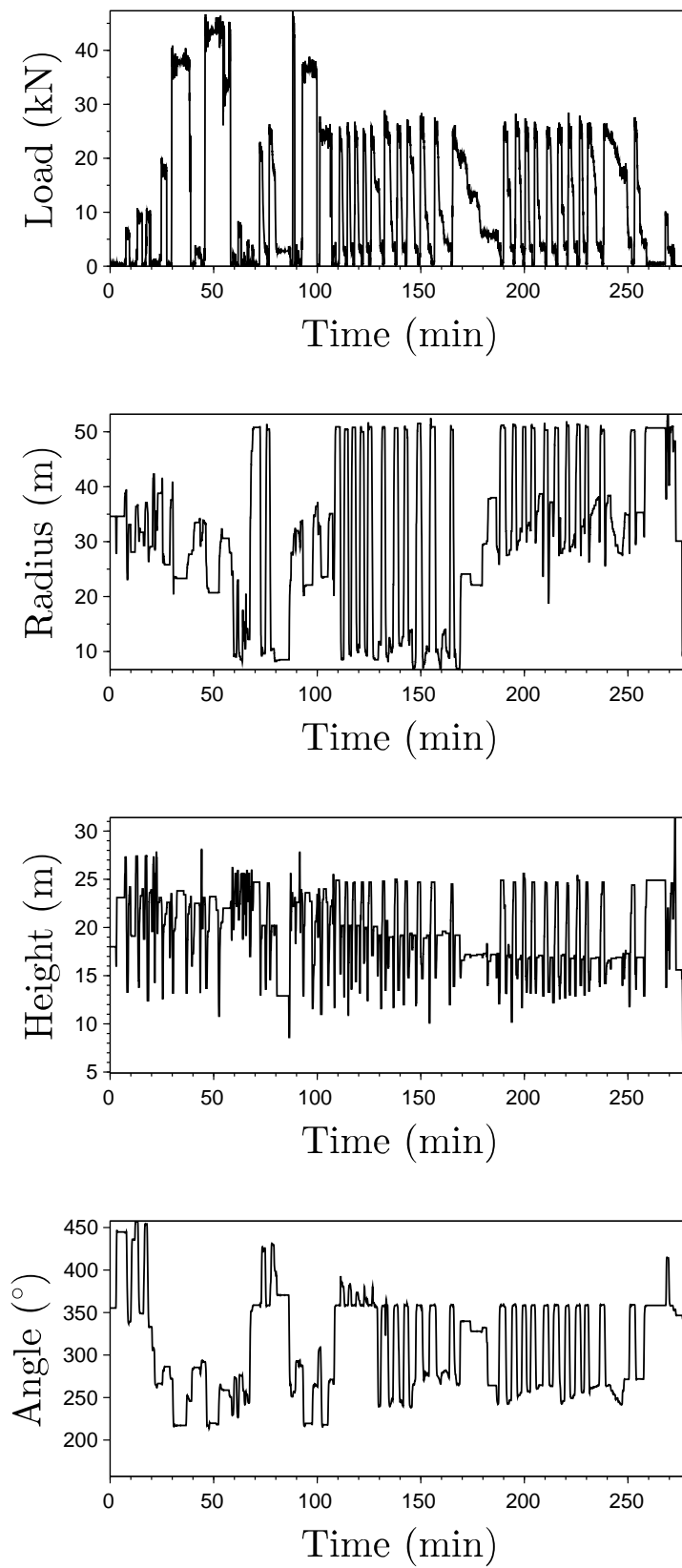


Figure 3.1 – 280 min in-site data: hoisted load, radius, hook height and slewing angle.

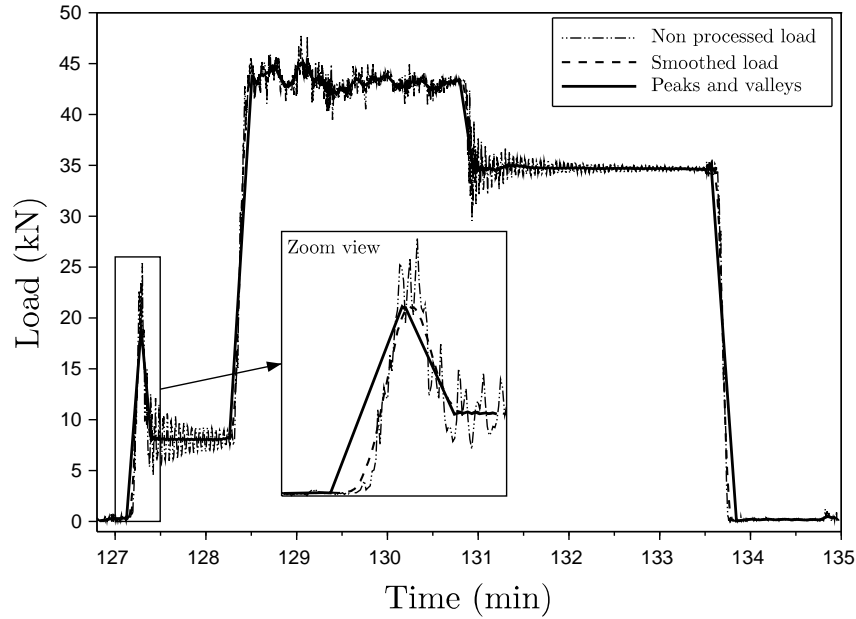


Figure 3.2 – Signal pre-processing considering a sample rate of four points per second.

### 3.2.2 Crane cycle identification

As defined in section 1.3, a crane cycle starts when the crane hoists a load and ends when the crane is ready to hoist another load. Thus, the first step of data analysis consists in identifying crane cycles by post-processing the load-time history recorded for each working day.

Crane cycle identification is performed in the following order. First, as depicted in figure 3.2, the raw signal (dot-dash line) is preprocessed. The load-time history is smoothed using a 5-seconds running average filter (dashed line) in order to reduce the number of dynamic oscillations which do not correspond to significant load changes. Then, a sequence of peaks and valleys (solid line) corresponding to local extrema is identified from the smoothed signal. Second, let  $L_i$  and  $L_{i+1}$  be two consecutive local extrema of the previous sequence of peaks and valleys. If the ratio  $(L_{i+1} - L_i) / \max(L_{i+1}, L_i)$  is higher than 0.5 (*i.e.* if a significative positive load change is identified), the point corresponding to the the load value  $L_i$  is stored as a possible crane cycle starting point. The previous value was found by successive iterations on various data sets.

As seen in figure 3.3, three possible starting points (black dots named 1, 2 and 3) verify the previous condition. Nonetheless, the point 2 is not an effective crane cycle starting point because during the first part of the signal, the crane hoists partially the load while workers help to control the load before moving it. Therefore, a new condition must be defined in order to delete points such as point 2. Let  $M$  be the maximum reached between two consecutive starting points (*e.g.* points 1 and 2 in figure 3.3).  $\Delta L_{1M}$  and  $\Delta L_{2M}$  represent

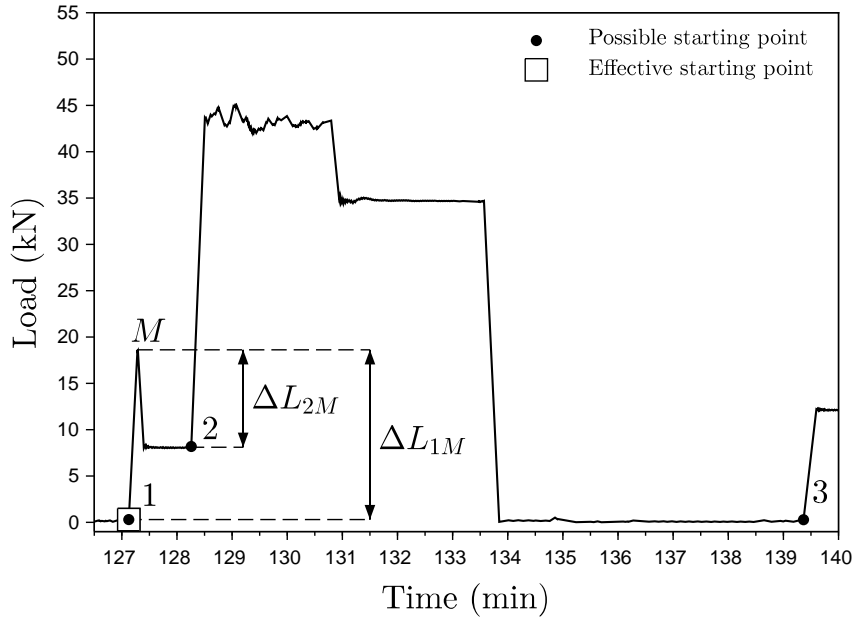


Figure 3.3 – First iteration of the identification of effective crane cycle starting points. The condition  $\Delta L_{1M}/\Delta L_{2M} \leq 1.2$  is not satisfied, leading to delete point 2.

respectively the load ranges between  $M$  and each of these possible starting points. If the ratio  $\Delta L_{1M}/\Delta L_{2M}$  is lower than 1.2, the point 2 is identified as an effective starting point. Otherwise, the point 2 is deleted and the procedure is repeated by starting from the remaining possible starting points. The value of 1.2 was found by successive iterations on various data sets. Concerning the illustrative example depicted in figure 3.3, given that the point 1 was already identified as an effective crane cycle starting point, the previous condition is not satisfied and point 2 is deleted during the first iteration. Then, points 1 and 3 are considered together in a second iteration (see figure 3.4), which leads to identify the point 3 as an effective crane cycle starting point.

The use of the two previous conditions enables the identification of the starting points of all crane cycles occurring during a given period of time. The following section shows how these cycles can be classified into three categories depending on the type of work performed by the crane on the site.

### 3.2.3 Crane cycle per type of work

As seen in section 1.4, various loads of different type are moved by the crane from one construction site location to another. Thus, the identification of different types of crane cycles may be relevant to detect which type of load has been hoisted by the crane during a cycle. Three main characteristic types of cycles were distinguished by analyzing the load-time history depicted in figure 3.5. The first cycle (in figure 3.5 (a)) corresponds to “concrete pouring cycles” where the concrete bucket is moved from the concrete mixing



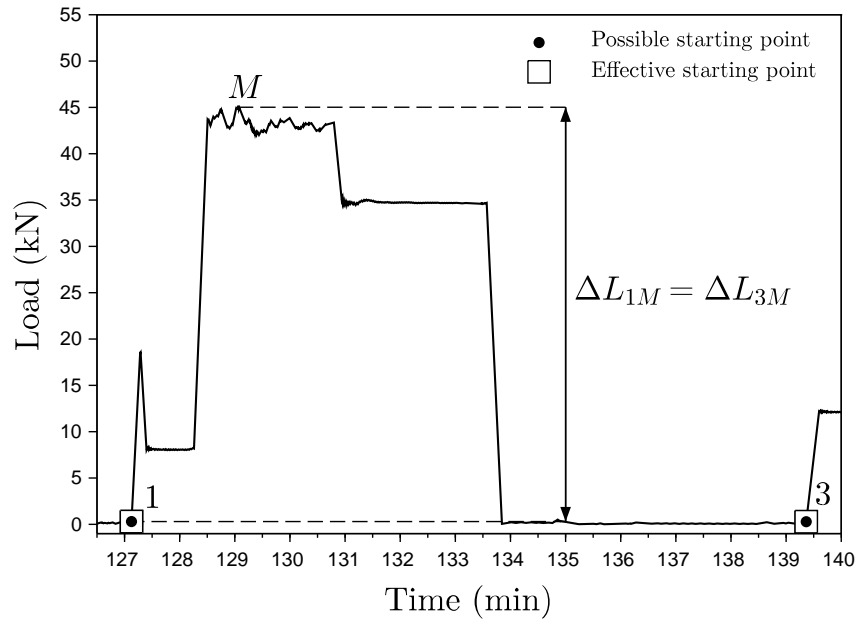


Figure 3.4 – Second iteration of the identification of effective crane cycle starting points. The condition  $\Delta L_{1M}/\Delta L_{3M} \leq 1.2$  is satisfied, leading to identify point 3 as an effective starting point.

plant or the truck mixer position to the wall or the floor to be cast. Such a cycle is formed by two load levels corresponding respectively to full (or partially full) and empty concrete bucket. Figure 3.5 (b) shows that the second type of cycle has various load levels, which means that the loads have to be hoisted in several steps. This is the case of forms, walkways or prefabs which are quite difficult to put in place and are partially set down while workers help to control them with caution. All these cycles belong to the “positioning cycles” category. By contrast, figure 3.5 (c) shows “transfer cycles” which represent the most simple type of crane cycle occurring on the construction site where a load (*e.g.* steel framework) is simply moved from one place to another.

Some assumptions are made from the previous observations in order to distinguish each type of cycles depending on the type of the work performed on the site. One important aspect to consider is that all the concrete pouring cycles start or end at the drop position of the concrete bucket (*i.e.* in the concrete loading area), which is helpful to differentiate concrete pouring cycles from all the identified crane cycles. This position is fixed if a concrete mixing plant is used on the construction site or slightly differs if the concrete is brought by means of mixer trucks. For instance, figure 3.6 depicts the crane working area on a construction site where a concrete mixing plant is used. As seen in the figure, the positions of crane cycle starting or ending points are depicted by means of gray circles. Note that all the crane cycles that are located at the position of the concrete mixing plant (see gray points in figure 3.6) are classified into the concrete pouring category.

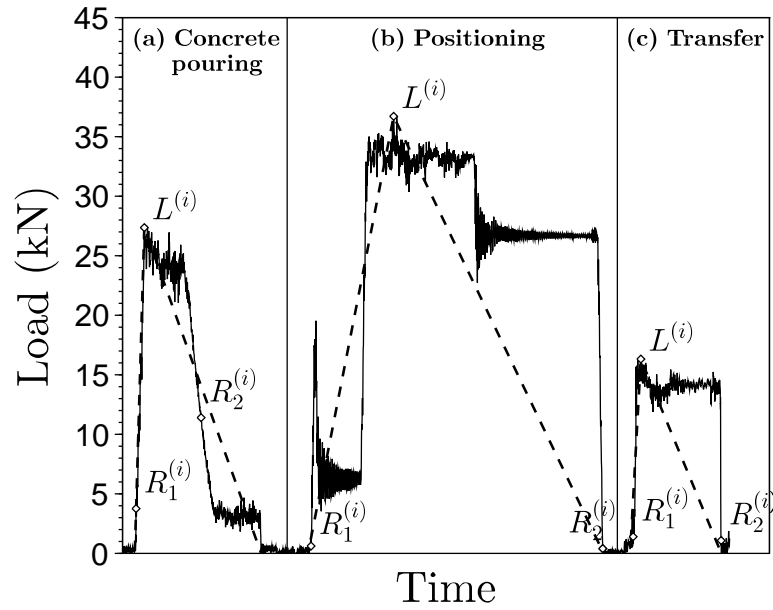


Figure 3.5 – Examples of cycle per type of work: (a) concrete pouring, (b) positioning and (c) transfer.

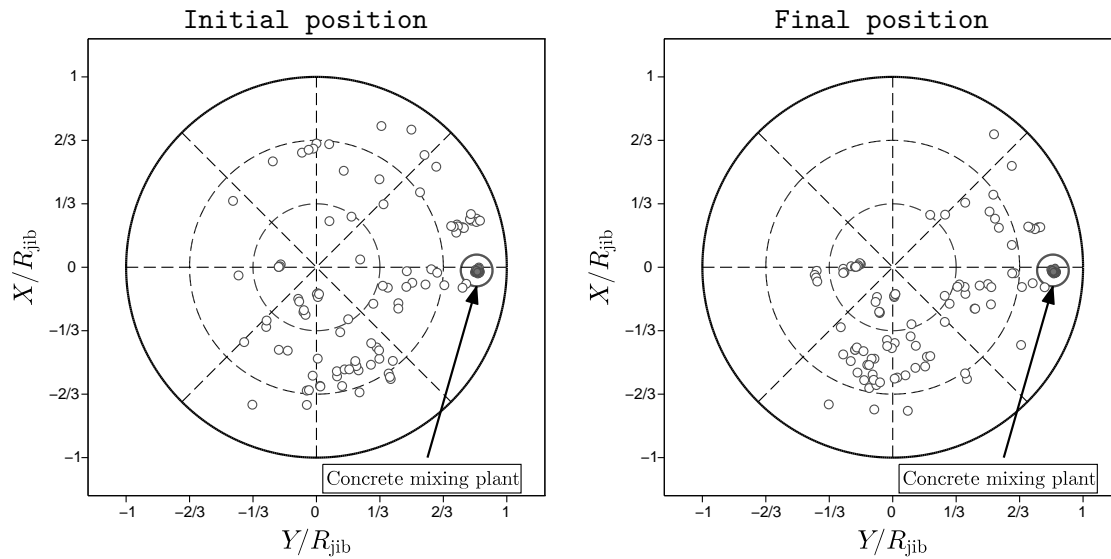


Figure 3.6 – Illustration of the distinction of concrete pouring cycles from all crane cycles for one day. The gray points indicate that crane cycles have started or ended at the drop position of the concrete bucket.

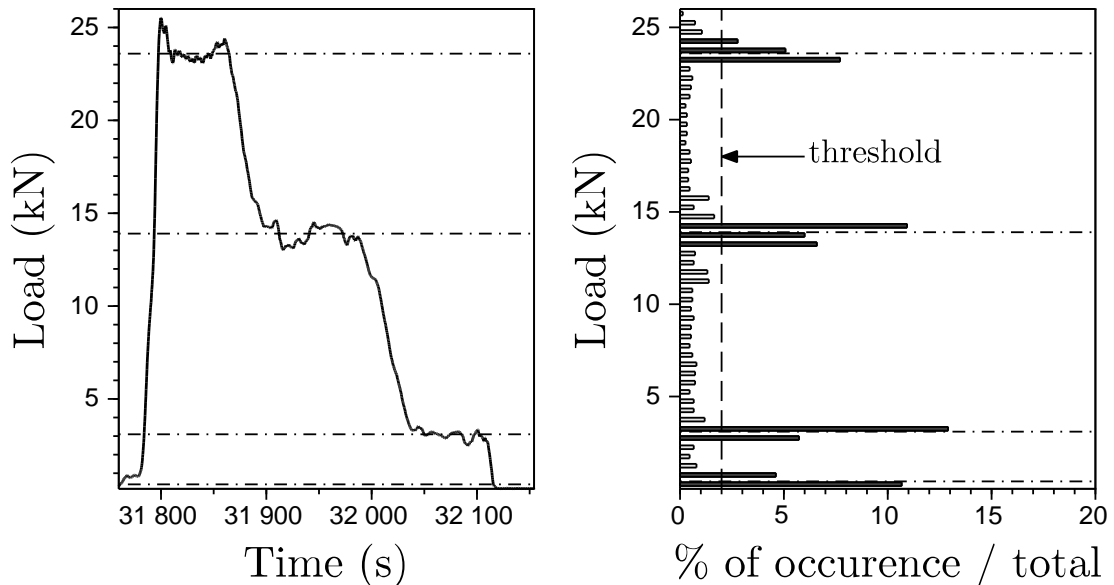


Figure 3.7 – Identification of load levels in a crane cycle. The black bars indicates that the load classes are considered as significant.

When concrete pouring cycles are well identified, other crane cycle characteristics are used to categorize the positioning and transfer cycles. Given that transfer cycles consist of a single non-zero load level, the main idea is to count the number of load levels related to each type of cycle in order to separate them. The identification of the number of load levels is performed by converting the load history into a histogram as given in figure 3.7. Each bar of the histogram represents the percentage of occurrence of a given load point relatively to the total number of points. For instance, given that the load history consists of 1519 time points, the first horizontal bar on the right side of the figure located between 0 and 0.5 kN equals almost 11% of total number of points of the crane cycle, *i.e.* it represents 167 time points.

When all the points of the load history are organized into classes, a threshold of 2% is defined in order to select only the most significant histogram classes (black horizontal bars figure 3.7). If consecutive significant classes are identified, they are considered together in the definition of a single load level. As seen in figure 3.7, the four identified load levels equal approximately 0.1 kN, 3 kN, 14 kN and 23.6 kN.

As seen before, transfer cycles consist theoretically of a single load level. Nonetheless, the definition of a threshold in the previous method leads sometimes to the identification of several very close load levels even if the crane cycle apparently belongs to the transfer cycle category. Therefore, without considering the lowest loading level whose value is close to zero, the following rules apply to classify each crane cycle in the right category:

- If the load levels don't deviate from their mean value by more than 20%, the crane cycle belongs to the transfer cycle category.

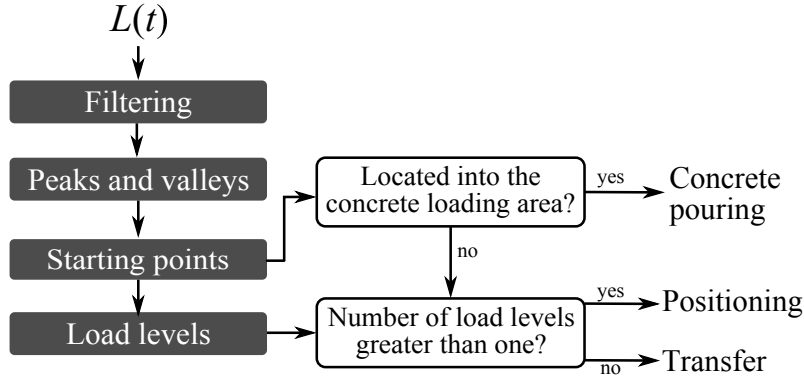


Figure 3.8 – Synoptic of the crane cycle identification procedure.

- If a single load level is identified, the crane cycle belongs to the transfer cycle category.
- Otherwise, the crane cycle belongs to the positioning category.

Figure 3.8 summarizes the different steps needed to identify and classify crane cycles according to the type of work performed in the construction site. As seen in the figure, the load-time history  $L(t)$  is first filtered by means of a 5-second running average. Then, peaks and valleys are extracted from the previous signal and crane cycle starting points are identified. If crane cycles start or end into the concrete loading area, they are classified into the concrete pouring cycle category. Otherwise, the different load levels constituting each crane cycle are obtained by means of the histogram method presented above, which enables us to classify the positioning and transfer cycles into two different categories. In the following sections, it is shown that the separation of crane cycles per type of work is helpful to analyze more accurately the crane use.

### 3.3 Construction sites characteristics

As seen in section 3.1, recording was performed on three top-slewing tower cranes working on different construction sites. Table 3.1 describes the characteristics of each construction site in terms of duration  $T_{\text{construction site}}$ , jib length ratio  $R_{\text{jib}}/R_{\text{jib}_{\text{max}}}$  (*i.e.* chosen jib length divided by the maximum possible jib length for the considered crane model), number of teams  $N_{\text{teams}}$  working on the construction site, median number of cycles per day  $N_{\text{cycles/day}}$  and concrete bucket capacity  $C_{\text{bucket}}$ . Moreover, schematic drawings representing the global topography of each construction site are given in figure 3.9. As seen in the figure, the topography of the three studied construction sites is very different.

Table 3.1 shows that the jib length ratio is somewhat different and is always lower than one, which means that, for the studied construction sites, the longest possible jib was not used. The jib configuration (*i.e.* jib length) constitutes an important aspect in

|        | $T_{\text{construction site}}$ |     |      | $N_{\text{cycles}}$ | $R_{\text{jib}}/R_{\text{jib}_{\text{max}}}$ | $N_{\text{teams}}$ | $N_{\text{cycles/day}}$ | $C_{\text{bucket}}$ |
|--------|--------------------------------|-----|------|---------------------|----------------------------------------------|--------------------|-------------------------|---------------------|
|        | month                          | day | hour |                     |                                              |                    |                         |                     |
| Site 1 | 5                              | 108 | 1232 | 15322               | 0.92                                         | 2                  | 142                     | 1                   |
| Site 2 | 8                              | 150 | 1154 | 10381               | 0.77                                         | 1                  | 69                      | 1.5                 |
| Site 3 | 6                              | 107 | 839  | 7314                | 0.85                                         | 1                  | 68                      | 2                   |

Table 3.1 – Studied construction sites characteristics.

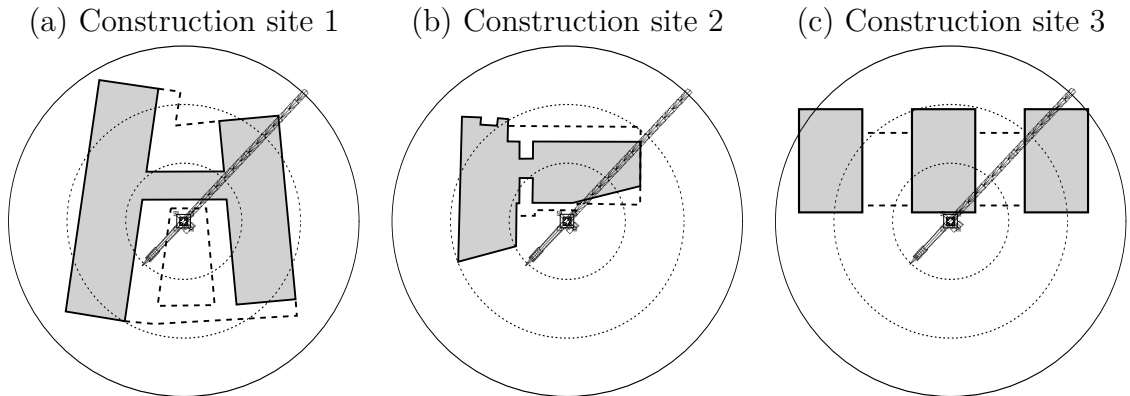


Figure 3.9 – Schematic view of the three studied construction sites. The gray areas represent the floors, while the dashed lines define the underground levels.

terms of crane use due to load chart limitations. As seen in table 3.1, the median number of cycles per day  $N_{\text{cycles/day}}$  and the number of teams  $N_{\text{teams}}$  working on the site seems to be correlated. The higher the number of workers on the site, the greater the number of crane cycles per day.

After classifying crane cycles by means of the method presented in section 3.2.3, table 3.2 gives the proportion of each type of work related to the total number of cycles and the total construction site duration. As seen in this table, the portion of positioning cycles remains small compared to the concrete pouring and transfer cycles both in terms of number of cycles or construction site duration. Furthermore, although transfer cycles represent between 53.9% and 66% of the total number of crane cycles, they always represent less than 50% of the construction site duration. The following section aims to describe three different representations of the results coming from crane cycles identification.

### 3.4 Intra-construction site data post-processing

As outlined in section 1.3, a crane cycle can be easily represented by the set of variables  $\{R_1^{(i)}, R_2^{(i)}, \alpha_1^{(i)}, \alpha_2^{(i)}, L^{(i)}, R_1^{(i+1)}, \alpha_1^{(i+1)}\}$ . Since crane cycles are identified by using the procedure introduced in section 3.2, the collected data can be presented differently. Thus,

|                     | Concrete pouring |        | Positioning |        | Transfer |        |
|---------------------|------------------|--------|-------------|--------|----------|--------|
|                     | %cycles          | %hours | %cycles     | %hours | %cycles  | %hours |
| Construction site 1 | 35.4             | 43     | 10.7        | 17.2   | 53.9     | 39.8   |
| Construction site 2 | 16.6             | 27.1   | 15.4        | 24.2   | 68       | 48.7   |
| Construction site 3 | 25.1             | 37.4   | 8.9         | 19.8   | 66       | 42.8   |

Table 3.2 – Proportion of each type of cycle in terms of crane cycles number and of total duration.

this section gives three possible illustrations of the results coming from crane cycle identification, each of them showing various advantages in terms of behavior understanding.

### 3.4.1 Data versus load chart

In this section, the recorded data are compared to the load chart of each monitored crane. Therefore, angle variations are not considered here, which leads to reduce the set of variables defined in section 1.3 to the triplet  $\{R_1^{(i)}, R_2^{(i)}, L^{(i)}, R_1^{(i+1)}\}$ . As depicted in figure 3.10, the initial and final radii and the hoisted load are retrieved for all identified crane cycles and the corresponding points are plotted versus the load chart. Note that since more than one load level can be identified for concrete pouring or positioning cycles,  $L^{(i)}$  is defined as the maximum load value reached during the cycle. Moreover, a particularity of concrete pouring cycles lies into the fact that these cycles start and end at the same position, namely the location of the concrete mixing plant or the truck mixer. Therefore, for these cycles, it is more relevant to retrieve and analyze  $R_2^{(i)}$  at the location where the concrete is poured rather than where the cycle ends (see figure 3.5).

Horizontal trends can be observed on figure 3.10 at different loading levels which corresponds to the different types of hoisted loads described previously. As seen in the figure for the three construction sites, although the maximum hoisted load equals 100 kN, heavy loads (more than 50 kN) are seldom hoisted.

Figure 3.10 is useful to understand the performed work according to the physical limits induced by the load chart. Nonetheless, if one is interested in the damage of structural members exclusively stressed by the hoisting and trolleying movements, a more relevant representation of the results is needed. In fact, the damage of this kind of crane members stems from the maximum moment range reached during the crane cycle, *i.e.* from the sequence of the minimum moment  $M_{\min}$  and maximum moment  $M_{\max}$ . These moments being obtained by the combination of a given load at a given radius, the pairs  $\{R_{M_{\min}}, L_{M_{\min}}\}$  and  $\{R_{M_{\max}}, L_{M_{\max}}\}$  are plotted versus the load chart in figure 3.11. As seen in the figure for the three construction sites, the minimum moment comes from the combination of a lifted load value close to zero and a small radius value while the maximum moment occurs at any radius for loads mainly ranging between 0 and 60 kN.

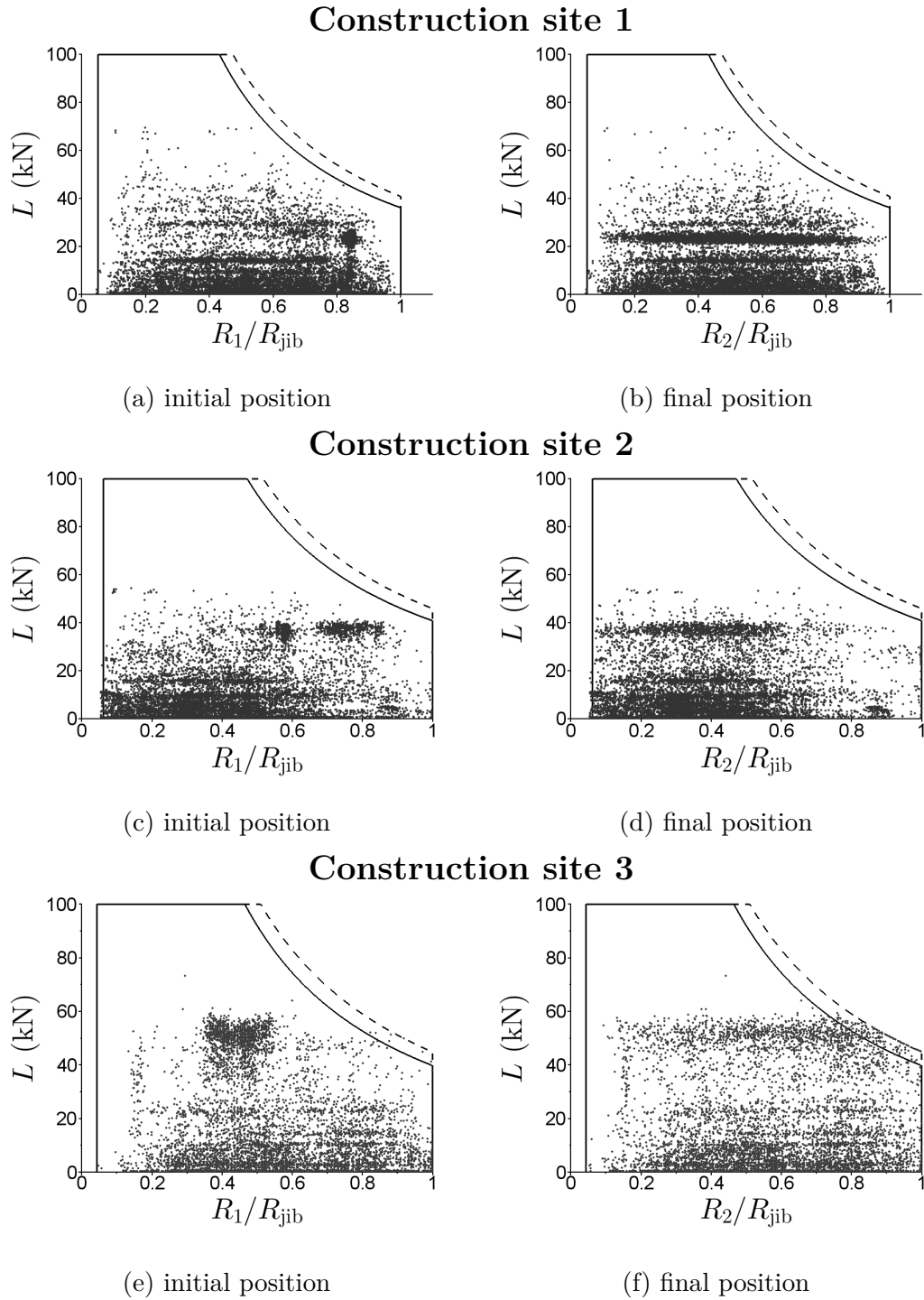


Figure 3.10 – Recorded data versus load chart for the pairs  $\{R_1, L\}$  and  $\{R_2, L\}$  for the three construction sites; the solid and dashed line correspond respectively to the 100% and 110% moment load charts.

Although plotting crane cycles versus the load chart is relevant, this does not give any information concerning the topography of the construction site. Thus, the following section shows how crane cycles can also be illustrated versus the crane working area to solve that issue.

### 3.4.2 Data versus construction site working area

As described before, the plotting of crane cycles versus the load chart reveals to be useful in some situations. Nonetheless, this does not give any information about angle variations or construction site's topography. A complementary representation of the data consists in calculating the Cartesian coordinates corresponding to the initial and final positions of the hook for each crane cycle. This is done respectively in figures 3.12, 3.13 and 3.14 for each construction site, where crane cycles are represented separately according to the type of work performed on the site.

These figures are helpful for several reasons. First, as seen in section 3.2.2 the position of the concrete mixing plant or truck mixers can be easily identified by using figures 3.12(a), 3.13(a) and 3.14(a). Second, the comparison of figure 3.9 with figures 3.12(b), 3.13(b) and 3.14(b) shows that the topography of the site can be assessed by viewing the final position of concrete pouring cycles. Note that this observation remains valid, even if the construction site drawing is not available. Third, in the same way, other relevant information such as the location of loading/unloading areas or prefabrication areas can be determined by using this type of figure.

Even though this kind of representation is useful to understand the topography of the construction site, one may want to depict separately each crane cycle feature (radius, angle or load), as described in the following section.

### 3.4.3 Data depicted by using histograms

As defined in the previous sections, the variables  $R_1^{(i)}$ ,  $R_2^{(i)}$ ,  $\alpha_1^{(i)}$ ,  $\alpha_2^{(i)}$ ,  $L^{(i)}$  are helpful to provide information about crane use in terms of both load chart limits and construction site topography. Those variables can also be studied separately by plotting the histograms of  $R_1$ ,  $R_2$ ,  $\alpha_1$ ,  $\alpha_2$  and  $L$ , as depicted in figures 3.15, 3.16 and 3.17 for the three construction sites and for each type of work.

As already observed in the previous section, concrete pouring cycles start at a given initial position, *i.e.* fixed radius and angle; this position corresponding to the position of the concrete mixing plant or truck mixer on the construction site. Therefore  $R_1$ - and  $\alpha_1$ -distributions are logically restricted to localized radius and angle values. Note that for construction sites 2 and 3, two different truck mixer positions were used. This explains the two modes of the  $R_1$ -distribution in figure 3.16(a) and the two modes of the  $\alpha_1$ -distribution in figure 3.17(a).  $R_2$ -distributions of concrete pouring cycles present triangular profiles,



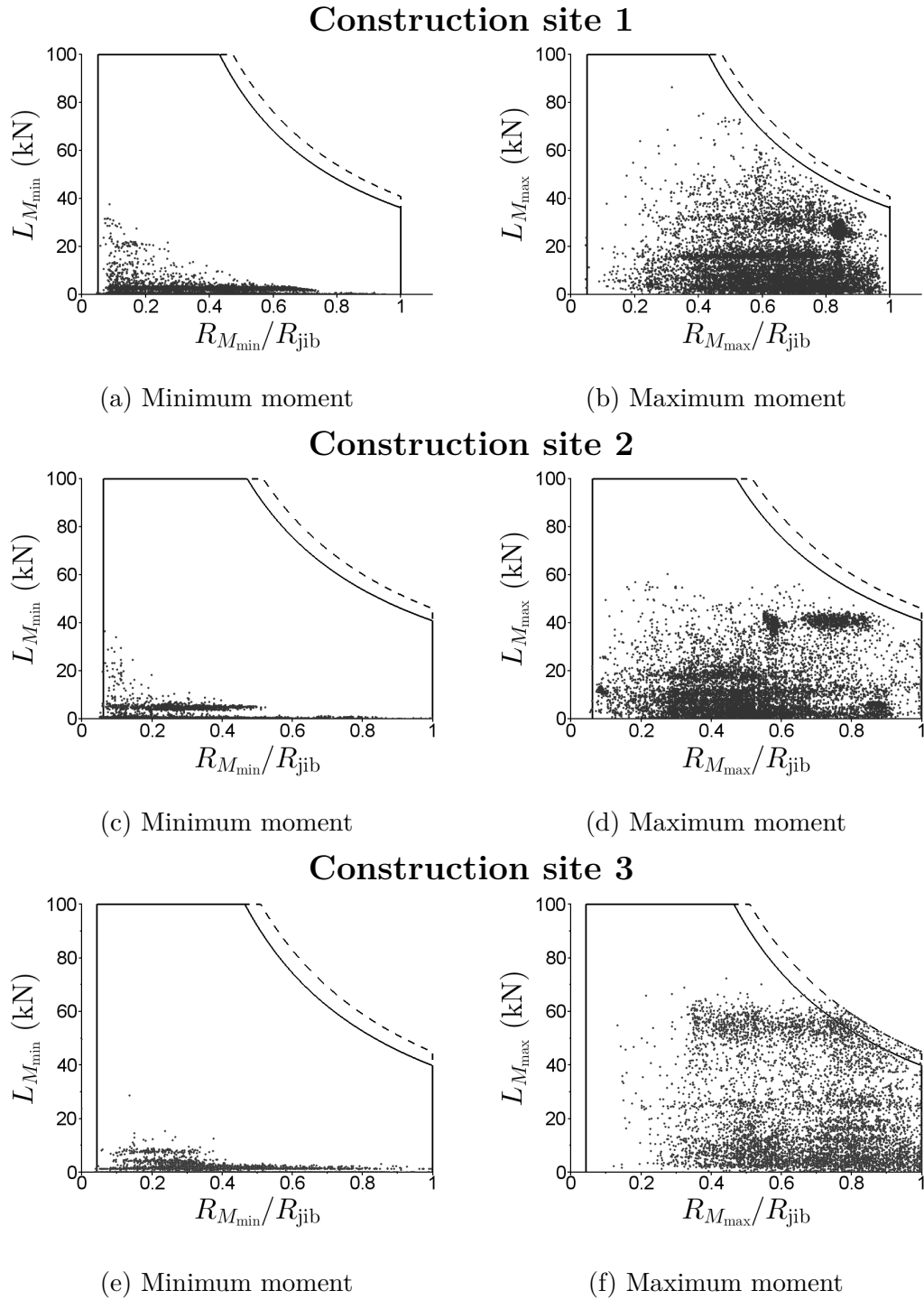
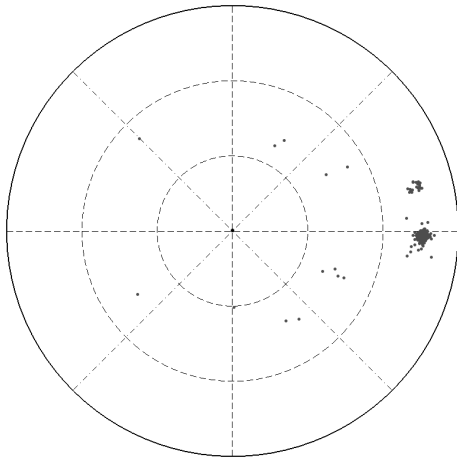
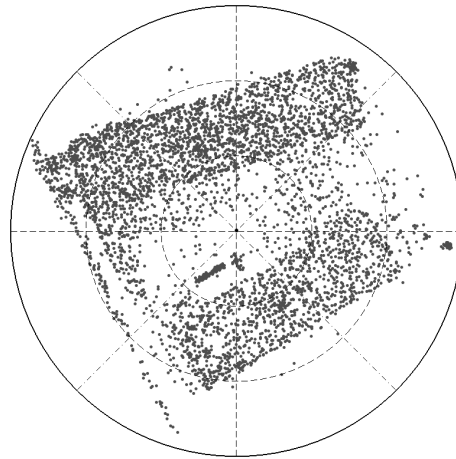


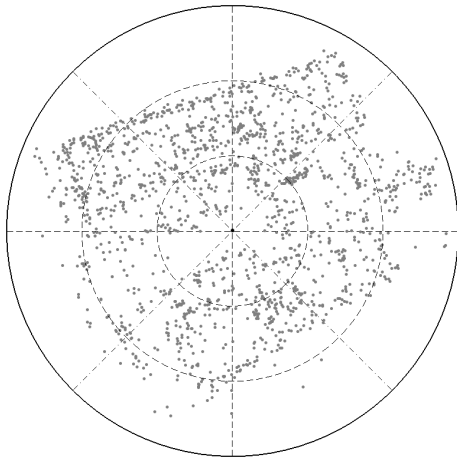
Figure 3.11 – Recorded data versus load chart for the pairs  $\{R_{M_{\min}}, L_{M_{\min}}\}$  and  $\{R_{M_{\max}}, L_{M_{\max}}\}$  for the three construction sites; the solid and dashed line charts correspond respectively to the 100% (solid line) and 110% (dashed line) moment load charts.

**Concrete pouring**

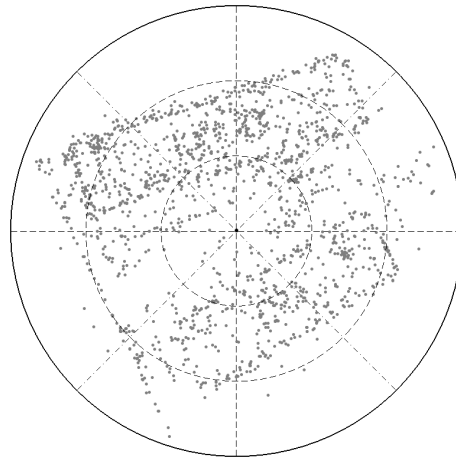
(a) initial position



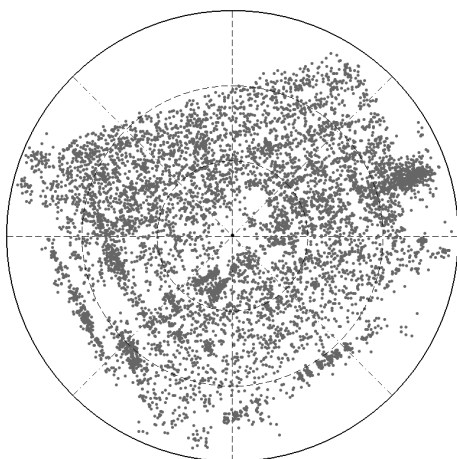
(b) final position

**Positioning**

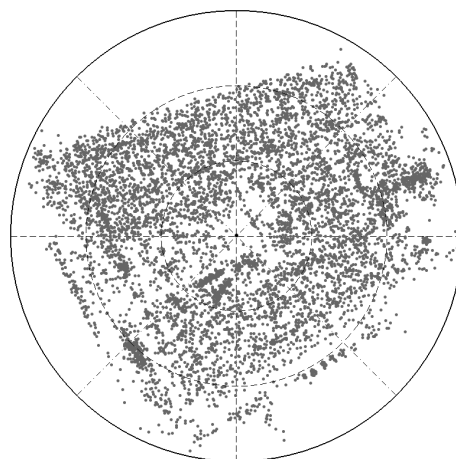
(c) initial position



(d) final position

**Transfer**

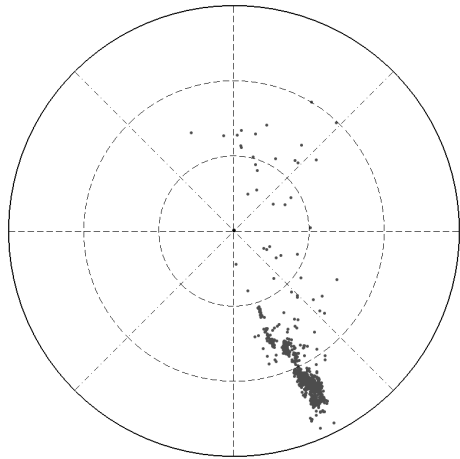
(e) initial position



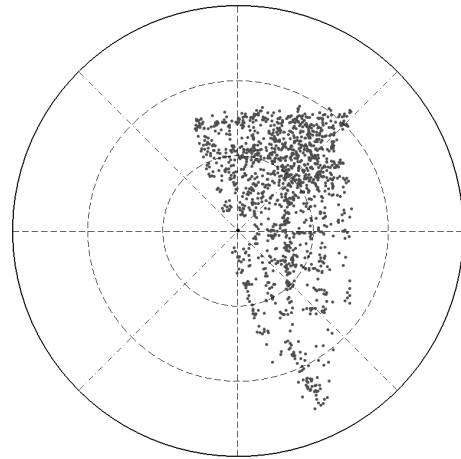
(f) final position

Figure 3.12 – Initial and final hook position for concrete pouring, positioning and transfer cycles for the construction site 1.

### Concrete pouring

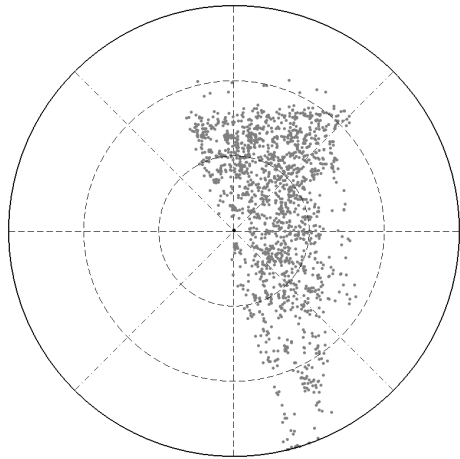


(a) initial position

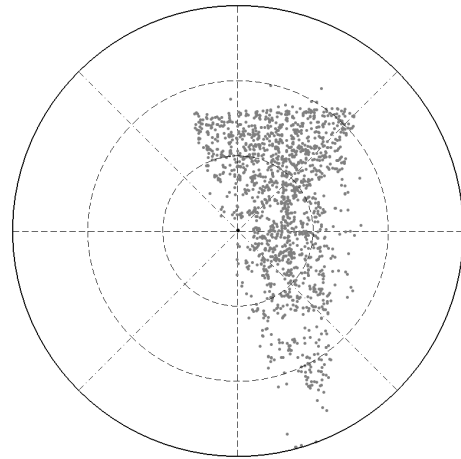


(b) final position

### Positioning

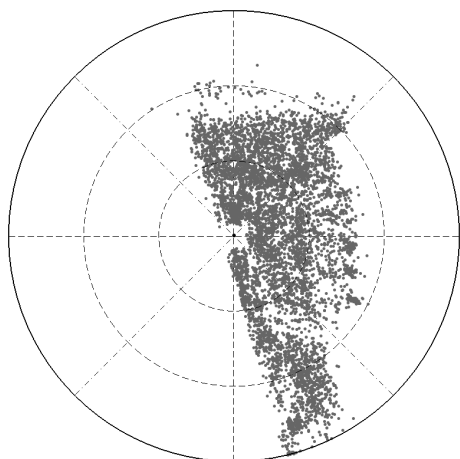


(c) initial position

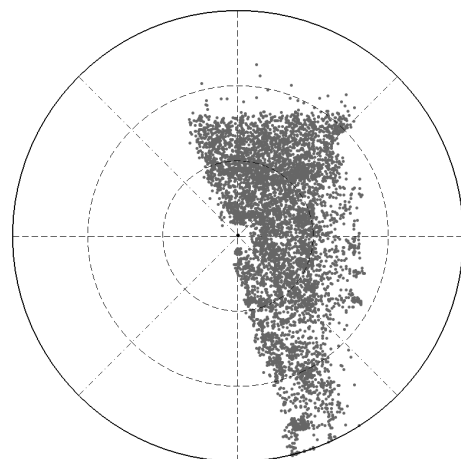


(d) final position

### Transfer

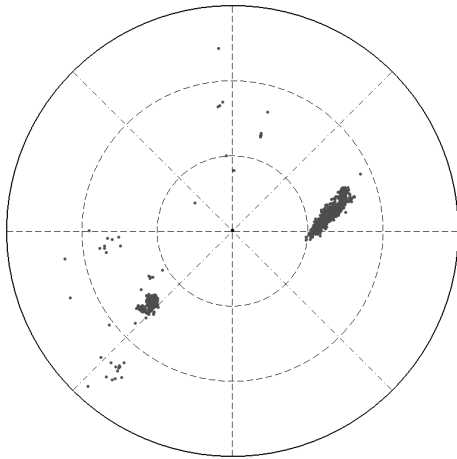


(e) initial position

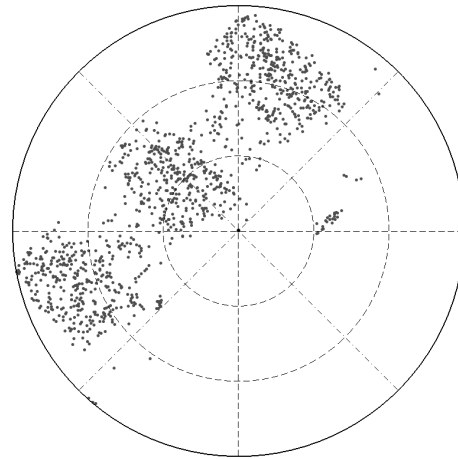


(f) final position

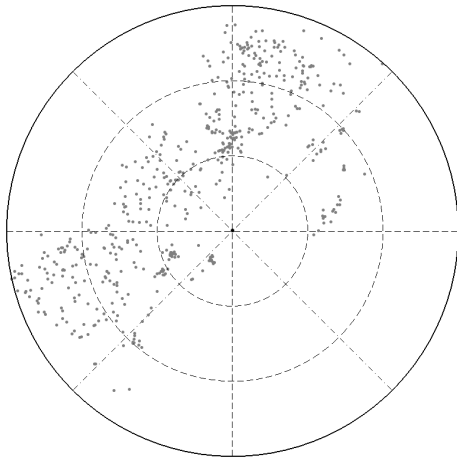
Figure 3.13 – Initial and final hook position for concrete pouring, positioning and transfer cycles for the construction site 2.

**Concrete pouring**

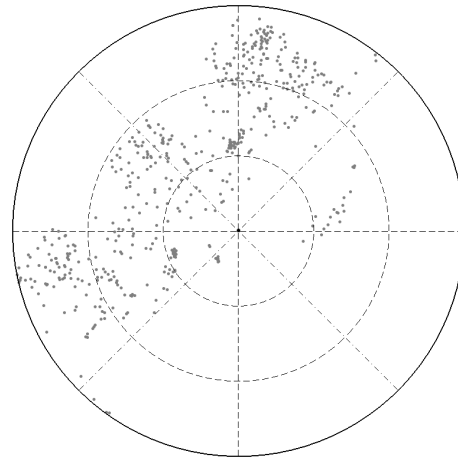
(a) initial position



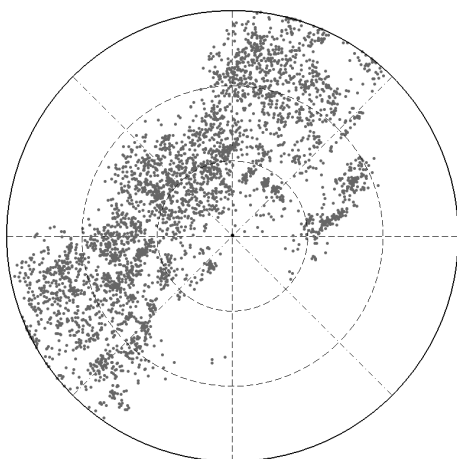
(b) final position

**Positioning**

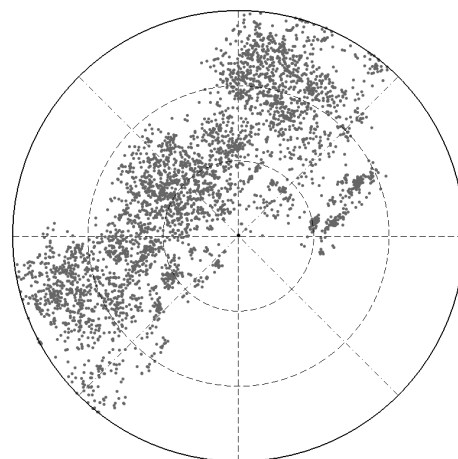
(c) initial position



(d) final position

**Transfer**

(e) initial position



(f) final position

Figure 3.14 – Initial and final hook position for concrete pouring, positioning and transfer cycles for the construction site 3.

the mode being located between the minimum and the maximum radius (*i.e.* the jib length  $R_{\text{jib}}$ ).  $\alpha_2$ -distributions of concrete pouring cycles are different depending on the considered construction site. Nonetheless, these distributions reflect the topography of the construction site, *i.e.* the proportion of building around the crane in terms of slewing angle. The uninterrupted  $\alpha_2$ -distribution of figure 3.15(a) shows for instance that there were buildings all around the crane. Furthermore,  $\alpha_2$ -distribution of figure 3.17(a) confirms that the crane worked mainly on a  $180^\circ$  area.

The other initial and final distributions of both radius and angle corresponding to positioning and transfer cycles are relatively close to the distributions of concrete pouring cycles. This seems to be logical since the casting of a wall or a floor requires the same material to be put in place successively: steel frameworks (transfer cycles), floor or wall forms (positioning cycles) and concrete (concrete pouring cycles).

$L$ -distributions on figures 3.15(a), 3.16(a) and 3.17(a) represent the maximum load histogram recorded during the concrete pouring cycles. The mean of the distribution equals respectively around 23, 37 and 51 kN. This corresponds to the concrete bucket weight, the latter increasing linearly with its capacity ( $1 \text{ m}^3$ ,  $1.5 \text{ m}^3$  and  $2 \text{ m}^3$ ). As seen in figures 3.15(b), 3.16(b) and 3.17(b), the maximum load histogram recorded during the positioning cycles is much more widespread. It can be explained by the fact that there is a lot of possible combinations of forms, walkways and prefabs. Most of the time, there are three standardized form sizes on European construction sites (2.5 m, 1.25 m and 0.625 m). A 2.5 m width equipped form weighs around 17 kN, dynamic overload included. It explains for instance the peaks approximately located at 34 kN, 17 kN and 8.5 kN in figure 3.15(b). The rest of the variability is due to the lifting of walkways or prefabs (balconies, stairs, etc.). Figures 3.15(c), 3.16(c) and 3.17(c) show that the hoisted load distribution corresponding to the transfer cycles present similar profiles. As seen in these figure, the weight of the material to hoist during this kind of cycles (steel frameworks, junk dumpsters, etc.) rarely exceeds 30 kN.

The histograms presented in this section are used in chapter 4 in order to develop a crane use model that accounts for the uncertainties related to intra-construction site parameters. The following section is concerned with a procedure enabling the assessment of the loading severity of crane structural members.

### 3.5 Intra-construction site loading severity assessment

As detailed before, the data collected from crane monitoring can be processed in order to understand the work performed by the crane on construction sites. This section aims to demonstrate how the previous data can also be used to assess the loading severity of crane structural members. A case study related to jib top member connections is then used to illustrate the procedure presented in this section.

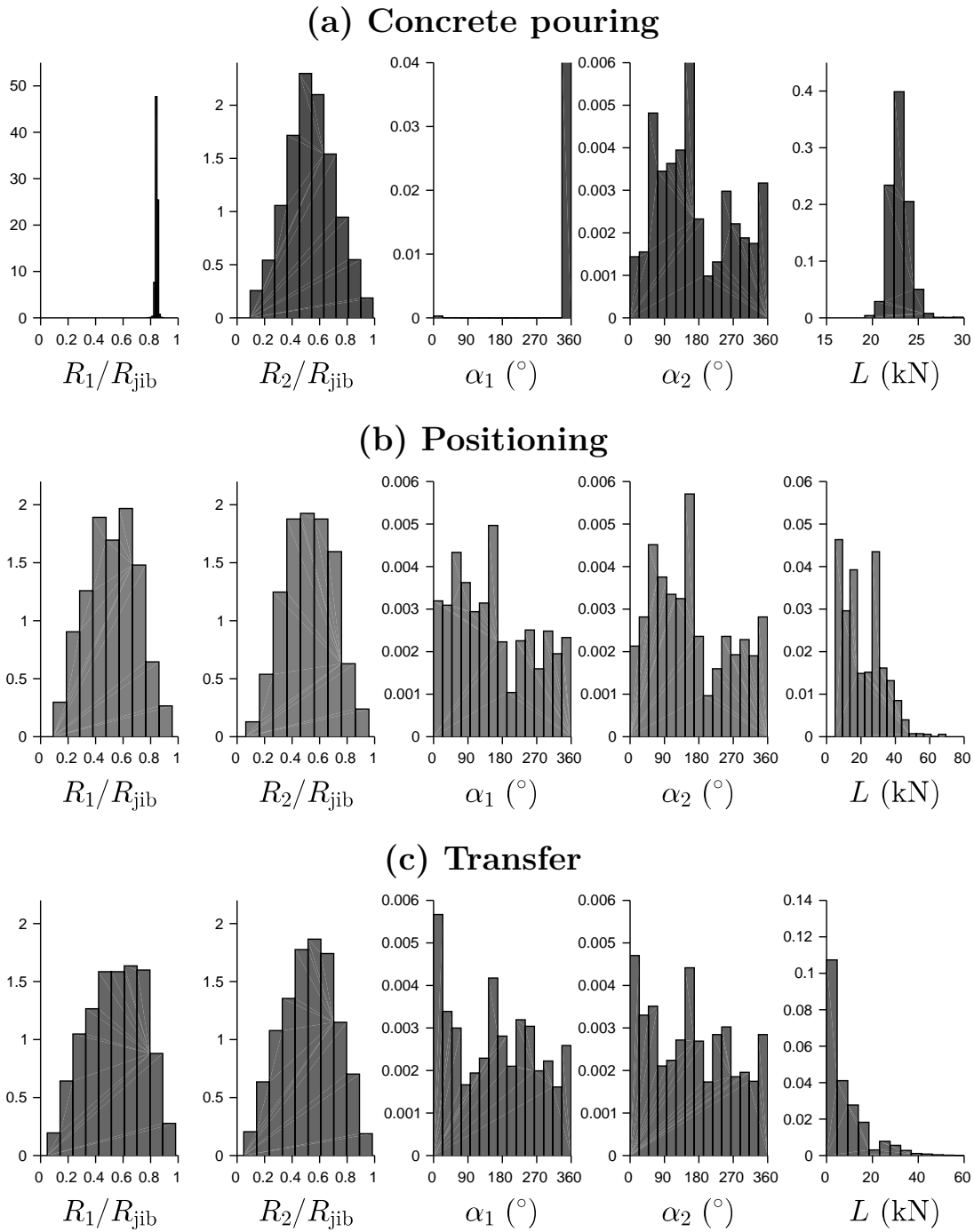


Figure 3.15 –  $R_1$ ,  $R_2$ ,  $\alpha_1$ ,  $\alpha_2$  and  $L$  histograms for the construction site 1.

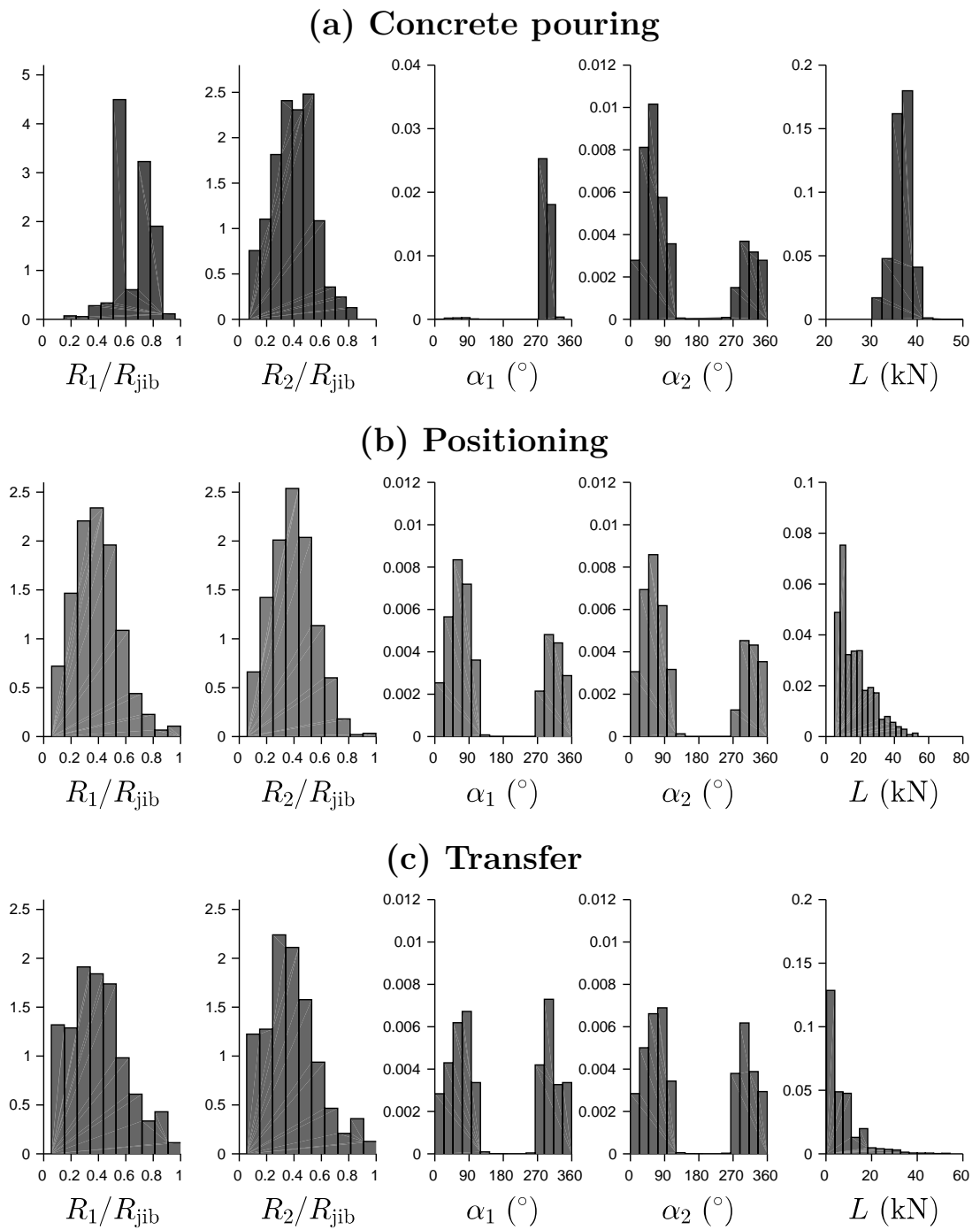
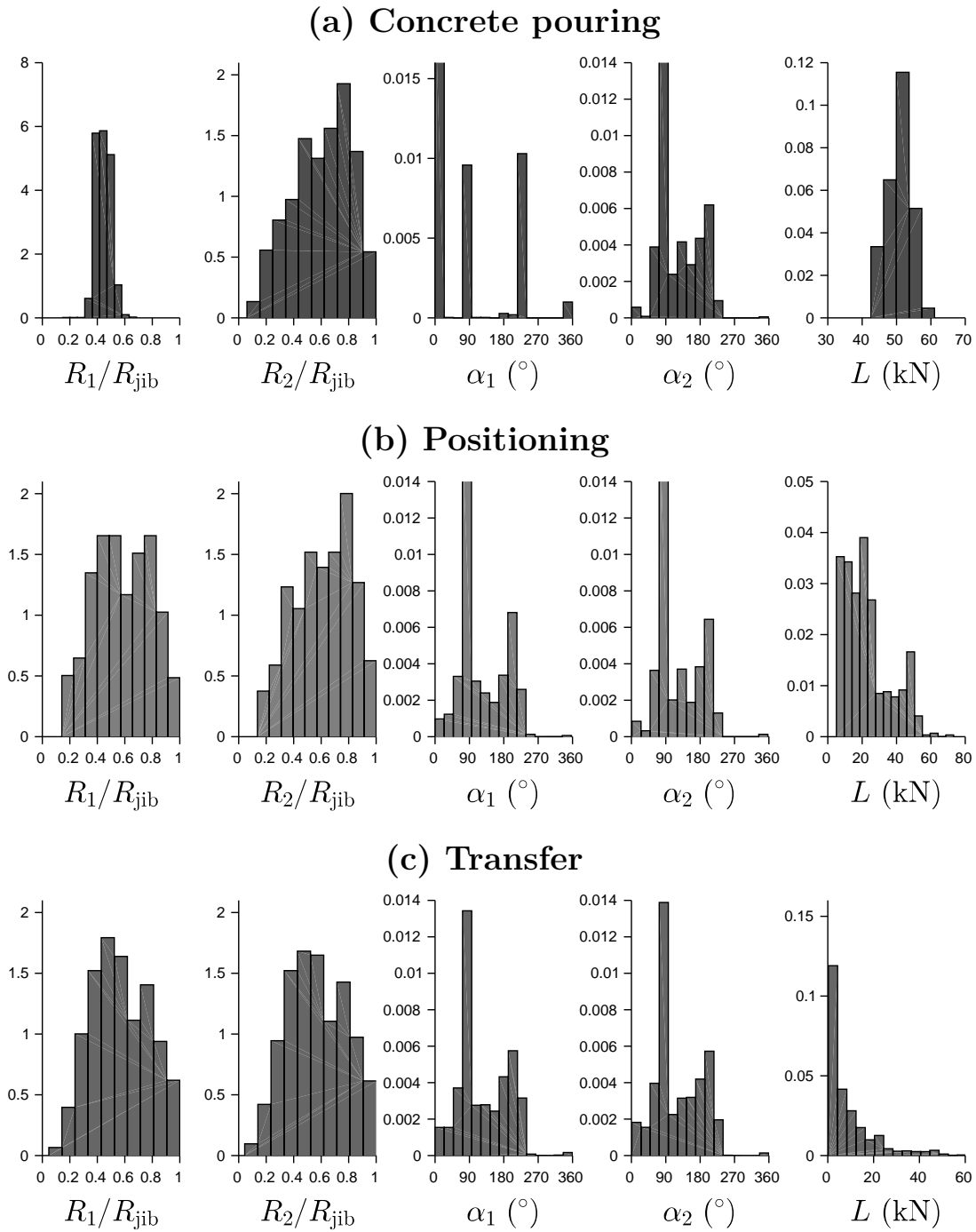


Figure 3.16 –  $R_1$ ,  $R_2$ ,  $\alpha_1$ ,  $\alpha_2$  and  $L$  histograms for the construction site 2.

Figure 3.17 –  $R_1$ ,  $R_2$ ,  $\alpha_1$ ,  $\alpha_2$  and  $L$  histograms for the construction site 3.



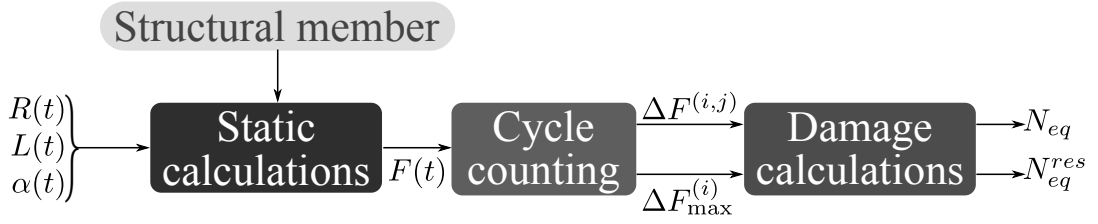


Figure 3.18 – Structural member damage calculation principle.

### 3.5.1 Severity calculation procedure

As depicted in figure 3.18, the severity assessment (*i.e.* damage calculations) of a crane structural member consists of three steps. First, the force-time history  $F(t)$  of the structural member is assessed by performing static calculations (using analytical functions) on the raw temporal data (*i.e.* not smoothed) coming from crane monitoring ( $R(t)$ ,  $L(t)$ ,  $\alpha(t)$ ). This means that all the dynamic oscillations are considered in the force-time history of the crane member. Note also that the number of variables involved in the force history assessment depends on the studied structural member. Second, fatigue cycles are counted from the force history by means of the widely-used rainflow counting method presented in section 2.3.1. Third, the Palmgren-Miner rule (see section 2.2.5) is used to determine the damage of the structural member; the latter being expressed in terms of equivalent number of cycles  $N_{eq}$ .

Note that instead of using the whole force-time history to assess  $N_{eq}$ , rainflow counting is performed for each type of identified crane cycle (concrete pouring, positioning, transfer), assuming that crane cycles are independent of each other:

$$N_{eq} = \sum_{i=1}^M \sum_{j=1}^N \left( \frac{\Delta F^{(i,j)}}{\Delta F_{\text{ref}}} \right)^c \quad (3.1)$$

where  $\Delta F^{(i,j)}$  is the force range of the  $j$ th stress cycle identified inside the  $i$ th crane cycle,  $c$  is the S-N curve slope given by standards ( $c = 3$  in EN 13001 [5] for welded details under consideration in this thesis) and  $\Delta F_{\text{ref}} (= |F^{(A)} - F^{(B)}|)$  is the crane member reference force. The counted cycles contain both the “dynamic” and “static” components of the loading. An interesting feature of the rainflow counting residual is that it contains the biggest force range encountered in the force-time history for each crane cycle. This force range can be seen as the maximum value reached during a crane cycle (*i.e.* it represents only the “static part” of the loading). Therefore, an equivalent number of cycles  $N_{eq}^{\text{res}}$  containing only the largest force ranges of all crane cycles can be defined as follows:

$$N_{eq}^{\text{res}} = \sum_{i=1}^M \left( \frac{\Delta F_{\text{max}}^{(i)}}{\Delta F_{\text{ref}}} \right)^c \quad (3.2)$$

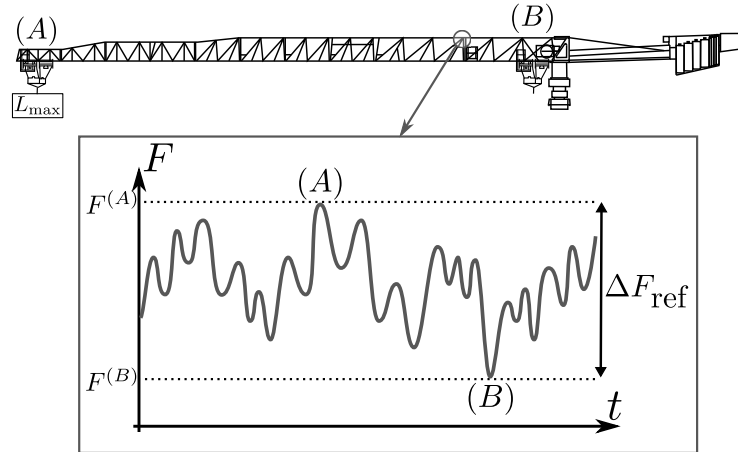


Figure 3.19 – Jib top member reference cycle from European standards: (A) maximum load at jib end and (B) unloaded jib.  $F$  is the force applied to the jib top member connection under consideration in this section.

where  $\Delta F_{\max}^{(i)}$  is the maximum residual force range identified by the rainflow algorithm inside the  $i$ th crane cycle. Note that performing rainflow counting for each crane cycle presents a collateral benefit because this enables to quantify the contribution of each type of crane cycle on the crane member equivalent number of cycles  $N_{eq}$ . This benefit is demonstrated in the following section, where the general procedure presented before is applied to jib top member connections.

### 3.5.2 Severity assessment of a jib top member connection

The procedure presented in the previous section is used to calculate the severity of jib top member connections whose loading depends exclusively on the hoisting and trolleying movements. This leads to consider only the radius and load histories ( $R(t)$ ,  $L(t)$ ) for the damage calculations. The most damaging loading cycle of this kind of crane structural member occurs when extreme loads (A) and (B) are reached successively (see figure 3.19). In this case, (A) refers to the hoisting of the maximum load at the jib end, while (B) indicates the unloaded jib with the trolley located at the minimum radius. Note that (A) and (B) load cases change if another crane member (stressed differently) is studied.

Figures 3.20 (a) and (b) depict the jib member loading and damage spectra for the three studied construction sites. In fatigue analyses, it is often admitted that stress cycles lower than a threshold do not contribute to the damage of the material. The endurance limit of the material is usually used as threshold when a stress spectrum is chosen to characterize the fatigue loading of a structure. The conversion of the endurance limit into a force applied to the jib top member leads to a normalized threshold value of approximately 0.1 (10 % of the reference force range  $\Delta F_{\text{ref}}$ ). Note that this choice is justified *a posteriori* because the damage induced by cycles whose force range is lower than 0.1 represent less

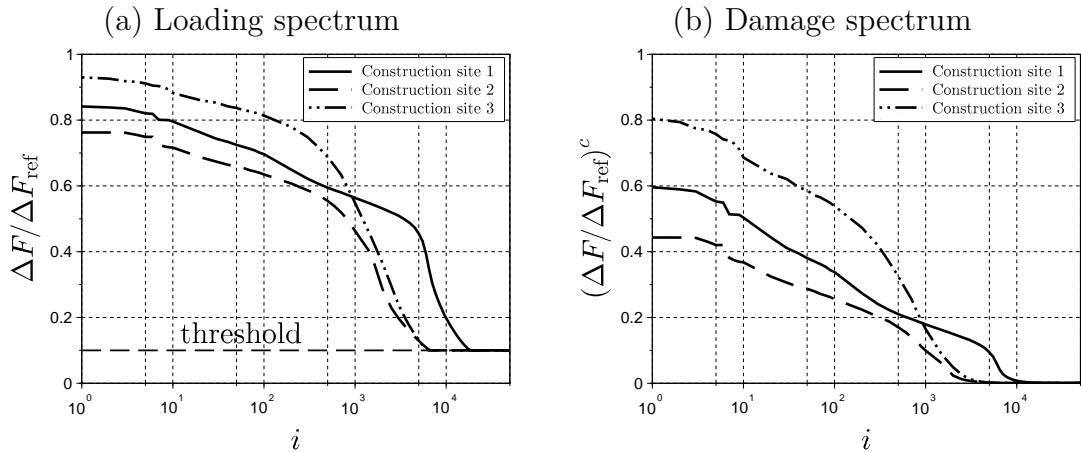


Figure 3.20 – Loading and damage spectra of the jib top member connection for the three construction sites.

than 1% of the total damage, regardless the considered construction site. As seen in figure 3.20 (a), the loading spectra corresponding to construction sites 2 and 3 have similar profiles; the main difference being the maximum force range which is much higher for the construction site 3. This difference becomes much more significant in terms of damage spectrum. In addition, figure 3.20 (b) shows that although the maximum damage ranges reached during construction site 1 are lower than those reached during construction site 3, the total number of damaging cycles (more than 5% damage in the range  $[10^3, 10^4]$  cycles) is higher for construction site 1. Finally, the ratio  $N_{eq}^{res}/N_{eq}$  found for the three studied construction sites equals respectively 95%, 97% and 98%. The small difference between  $N_{eq}$  and  $N_{eq}^{res}$  leads us to conclude that, for the studied construction sites, dynamic oscillations can be neglected in the crane use model of a jib top member connection.

As said before, performing Rainflow counting for each crane cycle enables to quantify the contribution of each type of crane cycle on the jib member equivalent number of cycles. As depicted in figure 3.21, concrete pouring cycles seem to be the most damaging compared to positioning and transfer cycles because the number of damaging cycles is greater than the one of the other categories. Table 3.3 enables to verify the previous observation by seeing that concrete pouring cycles represent almost 70% of  $N_{eq}$  for the three studied construction sites, while they represent less than 36% of the total number of crane cycles (see table 3.2). These construction sites being very different in terms of topography, it seems that, for usual constructions made principally of concrete, the jib top member damage is mainly governed by concrete pouring cycles. This result is easily understandable because directly related to the concrete bucket which is hoisted very often during construction site. Note that the use of a big concrete bucket can reduce the total number of damaging cycles which will increase the efficiency on the construction site. Nevertheless this also increases the cycle ranges leading to fatigue deterioration more

|                     | Concrete pouring | Positioning | Transfer |
|---------------------|------------------|-------------|----------|
| Construction site 1 | 71.1%            | 9.3%        | 19.6%    |
| Construction site 2 | 68.3%            | 12.8%       | 18.9%    |
| Construction site 3 | 69%              | 11.2%       | 19.8%    |

Table 3.3 – Jib member damage with respect to the type of work done on each construction site.

rapidly. Therefore, the concrete bucket choice have an impact on both the job efficiency and the crane fatigue loading severity.

The procedure presented before and applied in this section shows how the loading severity of crane structural members can be assessed. The following section describes the quantification of the uncertainties related to inter-construction site parameters by using data coming from a crane rental agency, on one hand, and drawings coming from a construction firm, on the other hand.

### 3.6 Inter-construction site variability quantification

As seen in section 3.4, data coming from crane monitoring reflect the variability of construction sites' topography (*i.e.* intra-construction site parameters). Nevertheless, the number of monitored cranes remaining small, no global information is available concerning the inter-construction site variability in terms of construction sites' durations, times between two construction sites, jib configurations, etc. This kind of data can be collected by performing customer surveys, by gathering data from crane rental agencies or by analyzing construction site drawings. This section covers the data processing of construction site durations from a crane rental agency and the analysis of multiple construction site drawings collected from a construction firm.

#### 3.6.1 Inter-construction site durations from crane rental agency data

The data processed in this section was provided by a crane rental agency containing information related to rental and non-rental periods from 1996 up to now for self-erecting and saddle jib tower cranes (see figure 1.1) exclusively used in France. This thesis being exclusively focused on saddle jib tower cranes, only the handling of data related to this range is discussed in the following. Most of the time, construction companies require rental agencies to provide a crane able to hoist a maximum load (full concrete bucket or prefab stairs) at a given radius, regardless of the crane model. This means that crane's choice is mainly governed by crane capacity  $C$  and/or maximum load  $L_{\max}$ . For this reason, crane rental data were classified into three groups according to these parameters in table 3.4.

A crane being used on various sites during its life and not used between two jobs, let  $T_{\text{on-site}}$  and  $T_{\text{stored}}$  be respectively the duration of a job and the time between two jobs.

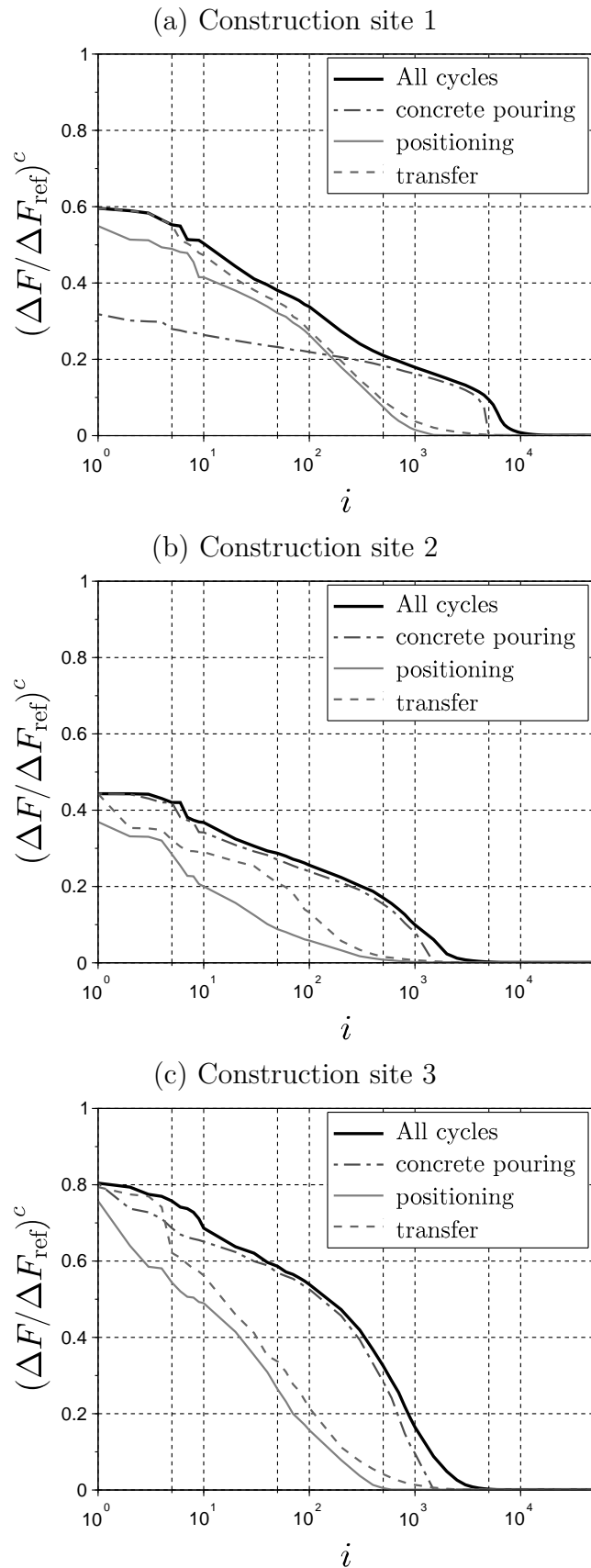


Figure 3.21 – Jib member damage spectra depending on the type of work.

|                   | Group 1            | Group 2                  | Group 3                   |
|-------------------|--------------------|--------------------------|---------------------------|
| Capacity (kN.m)   | $C \leq 900$       | $900 < C \leq 2200$      | $2200 < C \leq 4000$      |
| Maximum load (kN) | $L_{\max} \leq 60$ | $60 < L_{\max} \leq 100$ | $100 < L_{\max} \leq 160$ |

Table 3.4 – Classification of cranes by nominal capacity and maximum load.

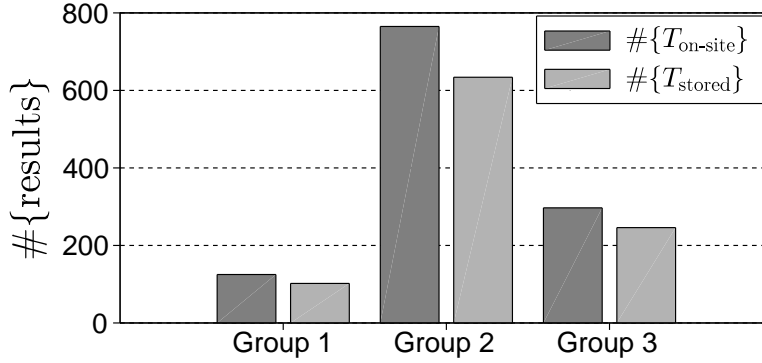


Figure 3.22 – Number of rental duration results according to each crane group.

Figure 3.22 shows the amount of data available for each crane group. As seen in the figure, more than 100 results are available for each crane group, thus constituting a significant statistical database for cranes whose capacity is lower than 4000 kN.m. Moreover, group 2 involves the greatest number of results due to the fact that it contains the most popular mid-range cranes.

Figure 3.23 depicts histograms of  $T_{\text{on-site}}$  and  $T_{\text{stored}}$  for each group. Overall, the distributions show similar profiles for  $T_{\text{on-site}}$  and  $T_{\text{stored}}$ . The main differences between groups arise from the estimated statistical parameters (mean and standard deviation) given in table 3.5. As seen in the table, groups 2 and 3 have close values of mean and standard deviation for both  $T_{\text{on-site}}$  and  $T_{\text{stored}}$ . This means that crane models belonging to groups 2 and 3 are rented approximately 7 months and remain unused during 2.5 months, on average. Group 1's results are slightly different because the mean and standard deviation of  $T_{\text{on-site}}$  are lower than for groups 2 and 3 while they are greater for  $T_{\text{stored}}$ . This implies that crane models belonging to group 1 may be more difficult to rent than those belonging to other groups because their non-use period mean and scatter are larger than those of groups 2 and 3.

### 3.6.2 Inter-construction site configuration parameters from drawings

In the frame of this thesis, a construction company has accepted to provide a great number of “typical” concrete construction drawings such as the one presented in figure 1.7 in chapter 1. In total, 63 construction drawings were collected which represents almost 82 cranes, due to the presence of several cranes on various construction sites. Note that

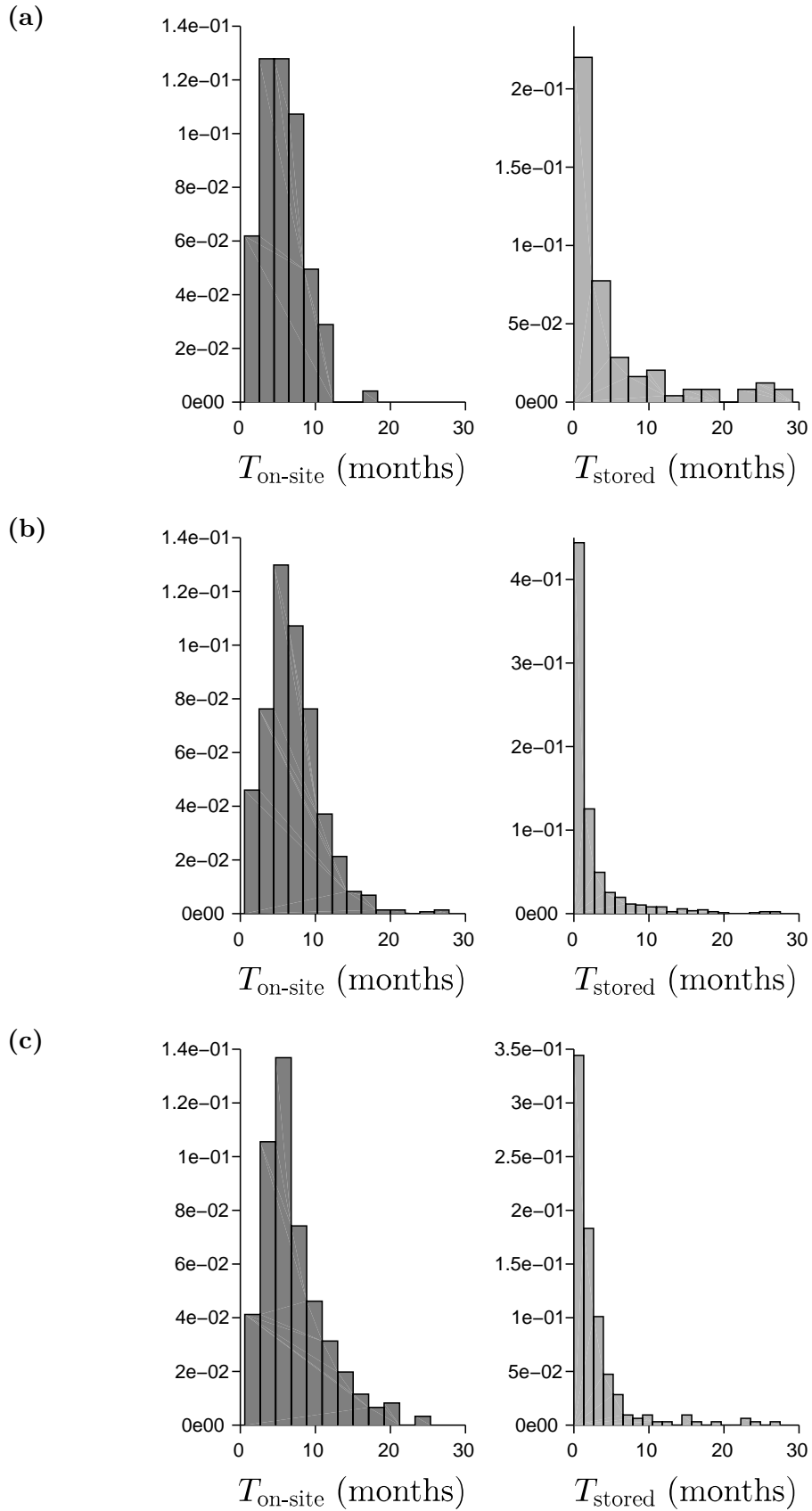


Figure 3.23 – Distributions of  $T_{\text{on-site}}$  and  $T_{\text{stored}}$  obtained from the crane rental agency database for (a) group 1, (b) group 2 and (c) group 3, respectively.

|                              | Group 1 |          | Group 2 |          | Group 3 |          |
|------------------------------|---------|----------|---------|----------|---------|----------|
|                              | Mean    | Std.Dev. | Mean    | Std.Dev. | Mean    | Std.Dev. |
| $T_{\text{on-site}}$ (month) | 5.7     | 2.9      | 6.8     | 3.6      | 7.0     | 4.2      |
| $T_{\text{stored}}$ (month)  | 5.0     | 7.1      | 2.4     | 3.9      | 2.7     | 4.0      |

Table 3.5 – Estimated mean and standard deviation for every crane group.

the studied cranes coming from this new database can be classified into the groups 2 and 3 presented in table 3.4. Construction drawings are helpful to retrieve statistical data reflecting the inter-construction site variability, such as jib configuration (jib length), loading/unloading area location, site's topography (building location), etc. This section aims at presenting the procedure developed for the assessment of these statistical data.

Numerical routines have been developed in this thesis in order to retrieve and analyze statistical data from construction drawings. First, a graphic user interface enables to retrieve data from drawings and store them in a text file with minimum effort. Second, the storage file is read and the data sets collected during the previous step are processed. For the sake of clarity, only the results obtained from the processing of the drawing database is presented in the following. Nonetheless, annex A provides the reader with further information concerning the routines developed during this PhD to process construction drawings.

### Jib configuration

As outlined in section 1.4, various crane configurations exist depending on the topography of each construction site. Thus, a unique crane model can be used with different jib lengths during its life. Therefore, assuming that all the studied cranes belong to the same population of cranes, the jib length ratio  $R_{\text{jib}}/R_{\text{jib}_{\text{max}}}$  (jib length divided by the maximum possible jib length for the considered crane model) distributions corresponding respectively to groups 2 and 3 are depicted in figure 3.24. The mean (standard deviation) inferred from these distributions equal respectively 0.73 (0.95) and 0.85 (0.97).

As seen in the figure, cranes belonging to group 2 are usually used with shorter jibs than those belonging to group 3. This can be explained by the fact that the longer the jib, the lower the tip load. Therefore, beyond a certain jib length, the tip load of cranes belonging to group 2 becomes too low in comparison with the weight of materials and tools used on the site (full concrete bucket, prefab beams, ect). Cranes belonging to group 3 can be used with longer jibs than those of group 2 due to bigger allowable tip loads. Finally, whatever the group to which cranes belong, cranes are seldom used in their maximum configuration, *i.e.* maximum jib length.

### Concrete loading area

Concrete mixing plants or truck mixers supply concrete throughout the duration of a



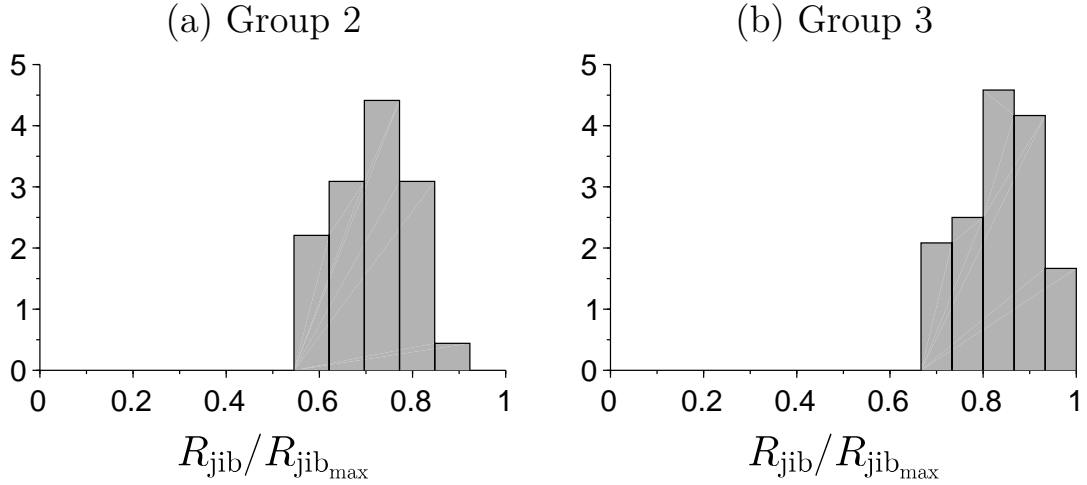


Figure 3.24 – Jib length ratio inferred from drawings for (a) group 2 and (b) group 3.

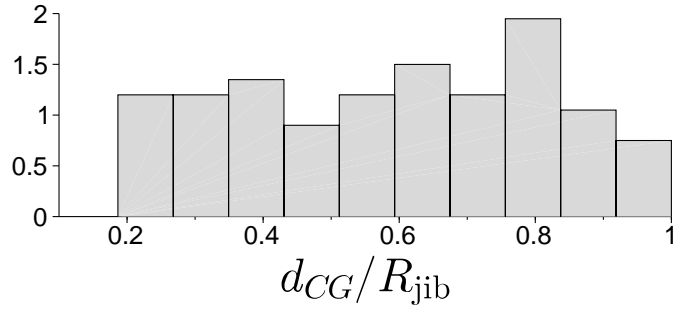


Figure 3.25 – Center of gravity of concrete loading areas assessed from 63 construction drawings.

construction site. Therefore, their location influences both the organization of the work performed on the site and the damage of crane structural members. As a result, studying concrete loading areas from construction site drawings becomes relevant. The location of these areas (*i.e.* coordinates) was assessed by using the simple graphic user interface presented in annex A. Starting from these coordinates, several relevant data can be plotted. Figure 3.25 depicts for instance the distribution of the normalized distance  $d_{CG}/R_{\text{jib}}$ . Note that the previous distance  $d_{CG}$  is measured for each construction site between the center of gravity of concrete loading areas and the location of the crane on the drawing (*i.e.* location of the slewing axis). As seen in the figure, the distribution is almost flat and is close to a uniform density function, indicating that the center of gravity of concrete loading areas is uniformly distributed between the minimum radius and maximum radius (*i.e.* jib length) for the studied drawings database. This observation conforms with the fact that the topography and accessibility of construction sites are random parameters from one site to another.

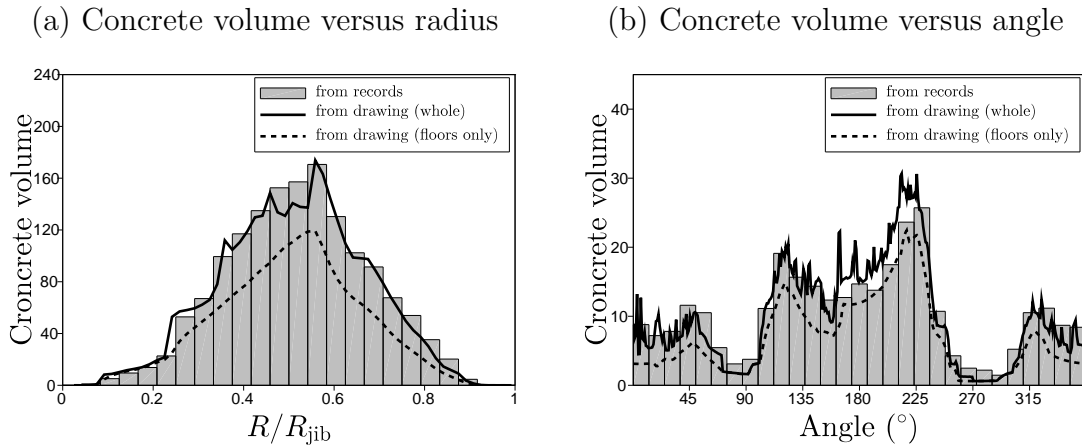


Figure 3.26 – Comparison of the concrete volume assessed from in-site data and determined theoretically from the drawing for the construction site 1.

### Correlation between construction site data and drawing

Concerning the construction sites 1 and 3 presented in section 3.4.2, on-site data and construction drawings are both available. This enables to compare the actual concrete volume cast during the construction with the expected volume inferred from the drawings. On one hand, the maximum load reached during the concrete pouring cycles identified in section 3.2.3 is combined with the concrete bucket capacity in order to infer the actual concrete volume. On the other hand, the graphic user interface detailed in annex A allows us to retrieve the expected cast areas (floors, walls, beams or columns).

As shown in figures 3.26 and 3.27, the results can be depicted either versus the normalized radius or versus the angle. In these figures, the actual concrete volume histogram is plotted in gray while the total and partial (floors only) concrete volumes inferred from drawings are respectively depicted by means of solid and dashed lines. Note that, although detailed layout drawings were available for construction site 1, only the overall layout plan was accessible concerning construction site 3. Thus, only the expected concrete volume related to floors can be assessed for construction site 3. As seen in figures 3.26 and 3.27, even though the expected concrete volume accounting for floors (dashed lines) underestimates the total concrete volume, the global shape of radius and angle distributions is conserved. This may be interesting in the sense that, even if a crane cannot be monitored for several reasons, the work performed on the site can be estimated by simply using general construction drawings.

Construction drawings represent a readily available means enabling the estimation of relevant information concerning cranes' work. Even though only three different illustrations of drawings processing have been presented before, other information can be assessed. For instance, this is the case of interference areas (area common to two close cranes), unloading/loading zones, concrete bucket cleaning areas, etc.

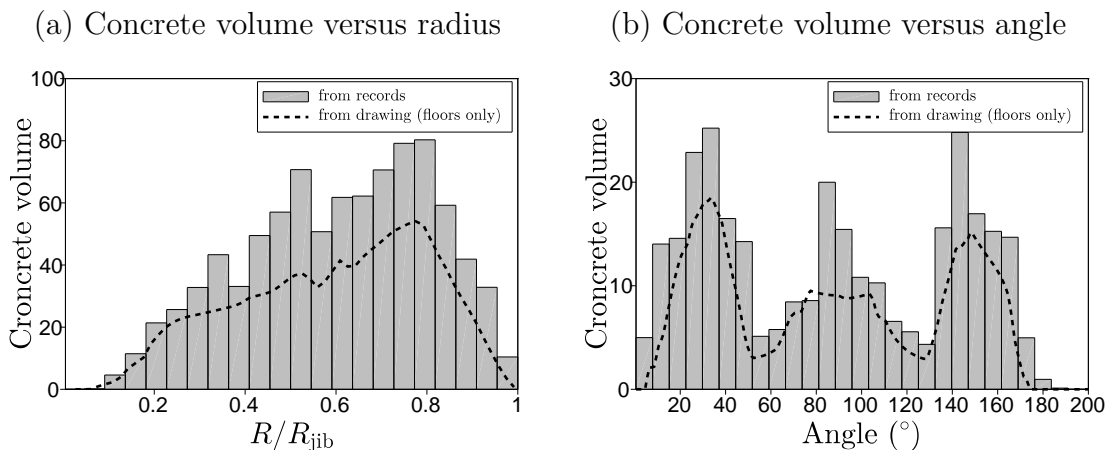


Figure 3.27 – Comparison of the concrete volume assessed from in-site data and determined theoretically from the drawing for the construction site 3.

### 3.7 Conclusion

In this chapter, a general overview of the nature of available data concerning tower cranes use has been provided. After presenting the crane monitoring device, the data processing method consisting of two main steps was described in detail. Subsequently, the main characteristics of the three studied construction sites have been listed and three different illustrations of the results of crane cycles identification have been presented, each of them having distinct advantages. Following the presentation of crane use data, the loading severity assessment procedure was explained and applied to a particular crane member (jib top member connection). Then, data coming from a crane rental agency were compiled and processed in order to assess the duration histograms of use and non-use depending on crane capacity ranges. Finally, relevant crane use information have been retrieved from construction site drawings collected from a construction firm. The intra- and inter-construction site data analyzed previously in order to define a probabilistic model of crane member use involved in the time-dependent reliability method presented in chapter 4.

**Chapter summary**

A recording device was developed during the PhD in order to monitor three tower cranes located on different construction sites. The objective was to record temporal data such as time, radius, hoisted load, slewing angle in order to characterize and model crane members loading. These data are handled in order to recognize and classify automatically crane cycles depending on the type of the work performed on the construction site (concrete pouring, positioning, transfer).

Once crane cycles are well-identified, various ways of illustrating the results exist. First, crane cycles can be depicted versus the load chart, which enables to compare crane use with the load chart limits. Second, the results can be presented versus the crane working area. This provides a good idea of the construction site's topography (built areas, loading/unloading areas, etc.). Third, the variables associated to a crane cycle (load, radius or angle) can be depicted separately by means of histograms.

The recorded data also provide engineers with the knowledge of the loading severity (*i.e.* fatigue damage) of crane structural members. Loading severity assessment is performed through rainflow cycle counting and Palmgren-Miner's rule applied to crane member force-time history. The application of this method on a jib top member connection shows that the loading severity of this kind of crane member is mainly governed by concrete pouring cycles. Moreover, it is shown that the contribution of dynamic oscillations represent a negligible part of the crane member fatigue damage.

Then, the processing of data coming from a crane rental agency enables the assessment of histograms of use and non-use durations depending on crane capacity ranges. Finally, relevant crane use information (jib configurations, concrete loading area location, etc) are assessed from construction site drawings collected from a construction firm.

The data presented above are used in chapter 4 in order to define a realistic model reflecting crane member operating loads. The previous stochastic model is then used to assess the reliability of crane members according to their operating time by means of the stress-strength interference procedure developed during this PhD.



---

## Chapter 4

# Reliability assessment of crane members using a time-dependent SSI method

### Contents

---

|            |                                                                     |            |
|------------|---------------------------------------------------------------------|------------|
| <b>4.1</b> | <b>Introduction</b>                                                 | <b>98</b>  |
| <b>4.2</b> | <b>Crane member strength stochastic modeling</b>                    | <b>98</b>  |
| 4.2.1      | Welded details FE modeling                                          | 98         |
| 4.2.2      | Fatigue lifespan prediction using shell elements with MPC equations | 101        |
| 4.2.3      | Strength distribution of crane welded details                       | 105        |
| <b>4.3</b> | <b>Crane use stochastic modeling</b>                                | <b>111</b> |
| 4.3.1      | Crane use distribution                                              | 111        |
| 4.3.2      | Application to a jib top member connection                          | 116        |
| <b>4.4</b> | <b>Sensitivity analysis of jib member use distribution</b>          | <b>125</b> |
| <b>4.5</b> | <b>Reliability assessment of crane welded details</b>               | <b>128</b> |
| 4.5.1      | General synoptic of the proposed SSI method in the design stage     | 128        |
| 4.5.2      | Application on jib top member connections                           | 130        |
| <b>4.6</b> | <b>Conclusion</b>                                                   | <b>131</b> |
|            | <b>Chapter summary</b>                                              | <b>133</b> |

---

## 4.1 Introduction

Standards dealing with fatigue design consider deterministic rules usually based on engineering practice. The use of these rules aims to ensure structural reliability by covering the uncertainties inherent to both the structural fatigue strength and the random fatigue loads. Although deterministic rules are convenient to use, they may lead to an unknown effective reliability level. Furthermore, the influence of each design parameter on the structural reliability remains unknown. As outlined in chapter 1, probabilistic approaches offer great opportunities enabling to better understand crane structural behavior. Thus, this chapter aims to present the time-dependent stress-strength interference method developed to assess the reliability of existing crane structural members over time. Moreover, the strength stochastic modeling is compared to the standards and a sensitivity analysis related to the crane use stochastic modeling is performed in order to ensure the relevance of the probabilistic method proposed in this chapter.

This chapter is organized as follows. Section 4.2 describes the stochastic modeling of the strength PDF of crane members. After describing the assessment of the average fatigue lifespan of crane welded details, this section shows how the dispersion of the strength PDF is determined and accounted for. Thereafter, section 4.3 presents the stochastic modeling of crane use. Based on the data collected in chapter 3, the method aims to define probability density functions related to intra- and inter-construction site parameters in order to assess the distribution of equivalent number of cycles of use according to operating time. Moreover, a global sensitivity analysis is performed in section 4.4 in order to quantify the impact of the variability of every input parameter on the developed crane use model. Lastly, section 4.5 covers the time-dependent reliability procedure developed in this thesis. A general synoptic describing the reliability assessment of any crane structural member is described and the proposed method is illustrated on a jib top member connection.

## 4.2 Crane member strength stochastic modeling

This section describes the assessment procedure of a fatigue strength distribution for crane welded details. After presenting the finite element model used in this thesis, an average fatigue lifespan expressed in number of cycles at nominal capacity is determined by using the Dang Van criterion. The strength distribution is then obtained by correlating numerical and experimental results.

### 4.2.1 Welded details FE modeling

As seen in section 2.2.1, the fatigue strength prediction of welded structural joints is of great importance in industrial context [102–104]. Sometimes, the fatigue strength of structural members can be assessed by performing endurance tests. Nonetheless, full-scale

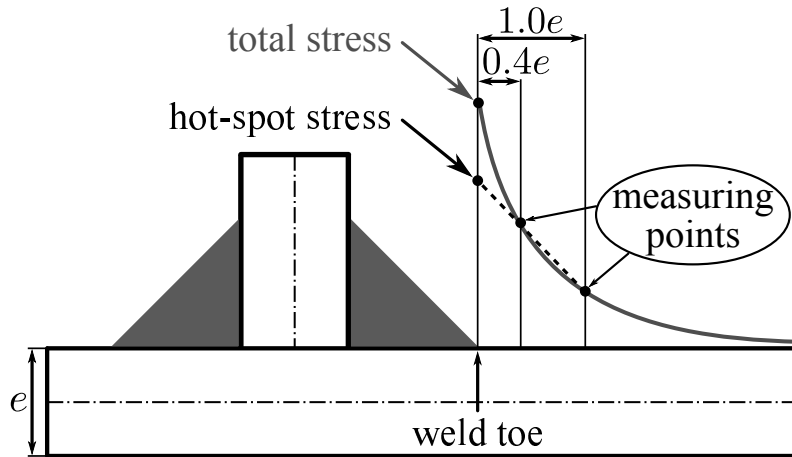


Figure 4.1 – Illustration of the hot-spot stress method.

tests of industrial structures may be infeasible due to welded details size exceeding the dimensions of classical testing benches or due to very expensive specimens. Therefore, engineers need efficient modeling tools with reasonable computational time that enable to predict crack initiation. Starting from this observation, a wide range of procedures using a FE software has been proposed during the last decade to model welded joints. Even though only a few methods are detailed in the following, the reader can refer to [105, 106] for detailed overviews of existing methods.

### Nominal stress approach

Standards generally specify that the fatigue strength validation of welded details can be made by using the nominal stress approach together with notch classes. This analytical method aims at calculating nominal stresses without considering any stress increase induced by local geometry changes close to the weld. Then, a reference stress is obtained by categorizing the studied welded detail into a notch class. The calculated nominal stresses are finally compared to the reference stress in order to validate or not the welded detail.

### Hot-spot stress approach

The hot-spot stress approach, also named structural stress approach, considers the stress increase due to the macro-geometry of the studied welded detail. As depicted in figure 4.1, the method aims at extrapolating stresses evaluated by finite element modeling at fixed distances from the weld toe without considering the stress concentration induced by the notch effect. These distances are always defined from weld toe location and generally depend on plate thickness  $e$  (e.g.  $0.4e$  and  $1.0e$ ). In a similar way as done for the nominal stress method, the hot-spot stress approach is based on various detail categories. The main difference between these methods lies in the fact that the number of detail classes is reduced for the hot-spot stress approach.



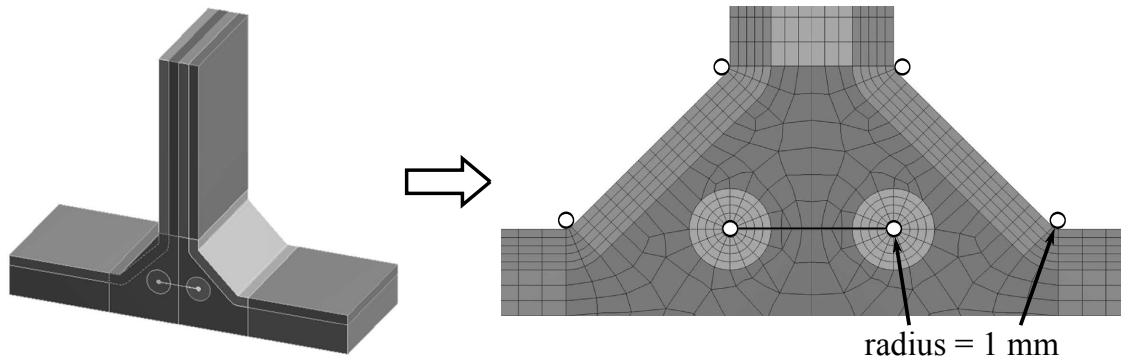


Figure 4.2 – Illustration of the effective notch stress approach.

### **Effective notch stress approach**

As depicted in figure 4.2, the effective notch stress approach consists in modeling the irregular geometry of weld toe or root by an effective notch of radius equal to 1 mm. Finite element or boundary element analyses may be used to determine the effective notch stress. This method presents several advantages such as the possibility to predict either weld toe or weld root cracks and the ability to account for the effects of weld toe angle or leg lengths, which is not the case for the previous methods. However, the main limit of this method derives from the high computational effort required in some situations where solid elements and/or local remeshing are necessary to obtain accurate stress results.

### **Modeling method based on MPC equations**

The nominal stress approach becomes unsuitable when nominal stresses cannot be determined with ease in complex structures. Moreover, in such cases, welded assemblies usually differ greatly from the notch classes provided by standards, which complicates the validation process. As seen previously, the hot-spot stress and effective notch stress methods use finite element analysis. Nonetheless, both methods are very sensitive to the meshing (element type, size and arrangement), leading to high computational efforts required in the modeling or processing steps. As a result, these methods may be difficult to use for the prediction of the fatigue strength of crane structural members, which implies the use of another modeling method in this thesis.

Crane structures are principally made of metal plates connected by welding. Furthermore, shell theory represents a good balance between prediction quality and computational time for modeling structural members. Therefore, as shown in figure 4.3, steel plates are modeled by their mid-surface and Multi-Point Constraint (MPC) equations [107] of type RBE3 are used to reflect the mechanical behavior of welds. RBE3, which are typically used to model the connection between dissimilar meshes, distribute linearly loads and mass from one node (master) to a set of nodes (slaves), the displacement of the master

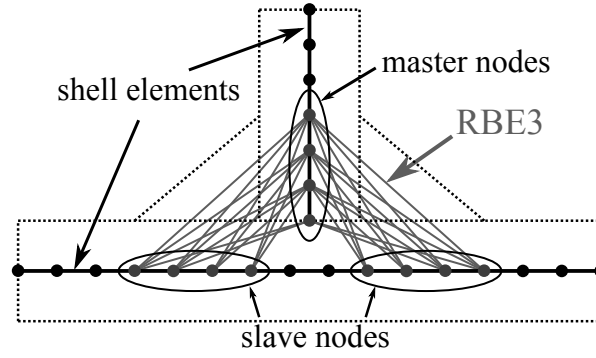


Figure 4.3 – Illustration of the modeling method that is used in this PhD. The method is based on MPC equations.

node being constrained by the average displacement of the slave nodes. The following section shows that the use of this modeling method with the Dang Van criterion enables the prediction of crack initiation at weld toe of structural joints.

#### 4.2.2 Fatigue lifespan prediction using shell elements with MPC equations

As seen in section 2.2.3, a local equivalent stress  $\tau_0$ , deriving from the Dang Van criterion [44], may be used in practical applications. The local shear stress amplitude and hydrostatic pressure involved in the evaluation of  $\tau_0$  at weld toe is detailed in the following for welded structural members modeled with the modeling method discussed in the previous section. Concerning tower cranes, the relevant reference loads are those which result in the maximum fatigue damage for a given crane member. For instance, as illustrated in figure 3.19 for jib top member connections, those loads correspond to the maximum load at the end of the jib (*A*) and the unloaded jib (*B*). Hence, linear FE analysis enables the assessment of the corresponding reference stress tensors at weld toe:

$$\bar{\sigma}^A = \begin{pmatrix} \sigma_{1,1}^A & \sigma_{1,2}^A & \sigma_{1,3}^A \\ \sigma_{2,1}^A & \sigma_{2,2}^A & \sigma_{2,3}^A \\ \sigma_{3,1}^A & \sigma_{3,2}^A & \sigma_{3,3}^A \end{pmatrix} \text{ and } \bar{\sigma}^B = \begin{pmatrix} \sigma_{1,1}^B & \sigma_{1,2}^B & \sigma_{1,3}^B \\ \sigma_{2,1}^B & \sigma_{2,2}^B & \sigma_{2,3}^B \\ \sigma_{3,1}^B & \sigma_{3,2}^B & \sigma_{3,3}^B \end{pmatrix} \quad (4.1)$$

Assuming a proportional stress state, the *amplitude* tensor between the (*A*) and (*B*) loads can be constructed by the linear combination of the tensors given in equation (4.1):

$$\bar{\sigma}^{\frac{A-B}{2}} = \frac{\bar{\sigma}^A - \bar{\sigma}^B}{2} = \begin{pmatrix} \frac{A-B}{2} & \frac{A-B}{2} & \frac{A-B}{2} \\ \sigma_{1,1}^{\frac{A-B}{2}} & \sigma_{1,2}^{\frac{A-B}{2}} & \sigma_{1,3}^{\frac{A-B}{2}} \\ \frac{A-B}{2} & \frac{A-B}{2} & \frac{A-B}{2} \\ \sigma_{2,1}^{\frac{A-B}{2}} & \sigma_{2,2}^{\frac{A-B}{2}} & \sigma_{2,3}^{\frac{A-B}{2}} \\ \frac{A-B}{2} & \frac{A-B}{2} & \frac{A-B}{2} \\ \sigma_{3,1}^{\frac{A-B}{2}} & \sigma_{3,2}^{\frac{A-B}{2}} & \sigma_{3,3}^{\frac{A-B}{2}} \end{pmatrix} \quad (4.2)$$

The maximum shear stress amplitude in the critical plane is assessed by considering the greatest and smallest principal stresses  $\sigma_I^{\frac{A-B}{2}}$  and  $\sigma_{III}^{\frac{A-B}{2}}$  derived from the previous tensor:

$$\tau_{\max}^{\frac{A-B}{2}} = \frac{\sigma_I^{\frac{A-B}{2}} - \sigma_{III}^{\frac{A-B}{2}}}{2} \quad (4.3)$$

Note that although  $\tau_{\max}^{\frac{A-B}{2}}$  is evaluated for every node of the finite element model, its maximum value is usually found close to the weld toe. Then, considering the tensors expressed in equation (4.1), the maximum hydrostatic pressure between the (A) and (B) loads reads:

$$P_{\max}^{(A,B)} = \max_{A,B} \left( \frac{\sigma_{1,1}^A + \sigma_{2,2}^A + \sigma_{3,3}^A}{3}, \frac{\sigma_{1,1}^B + \sigma_{2,2}^B + \sigma_{3,3}^B}{3} \right) \quad (4.4)$$

Finally, the equivalent local stress  $\tau_0$  given in equation (2.3) becomes:

$$\tau_0 = \tau_{\max}^{\frac{A-B}{2}} + a_0 P_{\max}^{(A,B)} \quad (4.5)$$

Dang Van *et al.* [44] determined a value of  $a_0$  close to 1/3 for thin metal sheet specimens (approximately 2 to 5 mm thick) commonly used in the automotive industry. The thickness of crane members being always larger than 6 mm, the previous value is considered to be unknown in this work and has to be calibrated from test results.

A median number of cycles to fatigue damage  $N_{\text{cal}}$  is determined from  $\tau_0$  by using the Basquin relation presented in section 2.2.4:

$$N_{\text{cal}} = b (\tau_0)^{-c} \quad (4.6)$$

By introducing the reference number of cycles  $N_{\text{ref}}$  and the reference stress  $\tau_{\text{ref}}$  such as  $b = N_{\text{ref}} / \tau_{\text{ref}}^{-c}$ , the previous relation reads:

$$N_{\text{cal}} = N_{\text{ref}} \left( \frac{\tau_0}{\tau_{\text{ref}}} \right)^{-c} \quad (4.7)$$

FEM 1.001 [22] and EN 13001 [5] give respectively  $c = 3.322$  and  $c = 3$  for most of welded details. In this study, the value of  $c$  is considered to be unknown and has to be calibrated from test results.

As listed in section 2.2.2, other secondary factors (base material, plate thickness, etc) influence fatigue lifespan of welded structures. These factors are implicitly taken into account in European standards (FEM 1.001 or EN 13001) through the ranking of every welded details in various notch classes. In this research work, two influence factors are considered explicitly, namely the plate thickness and the loading mode. As detailed in section 2.2.2, the classical approach enabling to account for plate thickness effect consists in defining a correction factor on  $\tau_0$  of the form  $(e/e_{\text{ref}})^\gamma$ . Hence, the calculated fatigue

lifespan expressed in equation (4.7) becomes:

$$\begin{aligned} N_{\text{cal}} &= N_{\text{ref}} \left( \frac{\tau_0}{\tau_{\text{ref}}} \left( \frac{e}{e_{\text{ref}}} \right)^\gamma \right)^{-c} \\ &= N_{\text{ref}} \left( \frac{\tau_0}{\tau_{\text{ref}}} \right)^{-c} \left( \frac{e}{e_{\text{ref}}} \right)^{-a_1} \end{aligned} \quad (4.8)$$

with  $a_1$  (equals to  $c\gamma$ ) a real coefficient;  $e$  and  $e_{\text{ref}}$  are respectively the actual and reference thicknesses. In this work,  $e_{\text{ref}}$  is set to 6 mm and  $a_1$  has to be calibrated. As outlined in section 2.2.2, the loading mode also influences fatigue lifespan of welded members. To our best knowledge, very few authors have taken this effect into account to correct the predicted fatigue lifespan. Dong [42], whose approach to welded component fatigue is founded on fracture mechanics issues, defined a dimensionless correction factor  $I(r_0)$  for the calculated local stress.  $I(r_0)$  is a function of the crack length and the bending index  $r_0$ , with:

$$r_0 = \frac{\Delta\sigma_s - \Delta\sigma_m}{\Delta\sigma_s} \quad (4.9)$$

where  $\Delta\sigma_s$  is the structural (weld toe) stress and  $\Delta\sigma_m$  is the membrane stress. Since fracture mechanics theory is not used in this thesis,  $I(r_0)$  cannot be used as it is. However, in the same manner as Dong [42], a bending index can be defined from the maximum shear stress amplitude  $\tau_{\text{max}}^{\frac{A-B}{2}}$ :

$$r = \frac{\left( \tau_{\text{max}}^{\frac{A-B}{2}} \right)_s - \left( \tau_{\text{max}}^{\frac{A-B}{2}} \right)_m}{\left( \tau_{\text{max}}^{\frac{A-B}{2}} \right)_s} \quad (4.10)$$

The use of the finite element modeling described previously leads to the assessment of  $(\tau_{\text{max}}^{(A-B)/2})_s$  and  $(\tau_{\text{max}}^{(A-B)/2})_m$  respectively on the top and middle surfaces of shell elements. Note that  $r$  ranges between 0 and 1 and equals 0 in pure tension, implying that pure tension is the reference case. The correction factor relative to the bending index is assumed to vary in accordance to a power function. Hence the calculated fatigue lifespan  $N_{\text{cal}}$  is multiplied by  $10^{a_2 r}$  ( $a_2$  being a constant parameter), leading to:

$$N_{\text{cal}} = N_{\text{ref}} \left( \frac{\tau_0}{\tau_{\text{ref}}} \right)^{-c} \left( \frac{e}{e_{\text{ref}}} \right)^{-a_1} 10^{a_2 r} \quad (4.11)$$

In summary, four influence factors are explicitly accounted for in the assessment of  $N_{\text{cal}}$ . First, the linear FE analysis presented in section 4.2.1 enables the assessment of the maximum shear stress amplitude and the hydrostatic pressure (reflecting the mean stress). Second, the plate thickness and loading mode effects are considered through correction factors on calculated fatigue lifespan. Moreover, as pointed out in section 2.2.2, material yield strength does not influence significantly crack initiation of welded assemblies made of usual structural steels, which explains why this parameter is not considered

| Reference                     | Type                      | $e$ (mm)   | Loading ratio | Loading mode       | Number of results |
|-------------------------------|---------------------------|------------|---------------|--------------------|-------------------|
| Lieurade <i>et al.</i> [108]  | X-joint                   | 10         | 0.1           | Tension            | 17                |
| Kihl <i>et al.</i> [36]       | X-joint                   | 6/11/19/25 | -1            | Tension            | 24                |
| Huther [109]                  | X-joint                   | 8/15       | 0.2/0.5       | Tension            | 144               |
| Maddox [110]                  | X-joint                   | 13         | 0             | Tension            | 10                |
| Lindqvist [37]                | X-joint                   | 6/12       | 0             | Tension<br>Bending | 17                |
| Gustafsson [38]               | X-joint                   | 6/12       | 0/0.75        | Tension<br>Bending | 73                |
| Janosch [111]                 | T-joint                   | 10         | 0.1           | Bending            | 24                |
| Huther <i>et al.</i> [112]    | Longitudinal<br>Stiffener | 20         | 0.1           | Bending            | 24                |
| Trufiakov <i>et al.</i> [113] | T-joint                   | 20         | 0.1           | Bending            | 12                |
| Galtier <i>et al.</i> [114]   | T-joint                   | 6          | 0.1           | Bending            | 13                |
| Pedersen <i>et al.</i> [115]  | T-joint                   | 6          | 0.1           | Bending            | 17                |

Table 4.1 – Summary of fatigue test results used for the calibration of constant parameters involved in equation 4.11.

in the following. Lastly, other influence factors such as residual stresses or weld shape are generally unknown and contribute intrinsically to the scatter observed in fatigue strength.

A fatigue test database has been established during this PhD in order to calibrate the constant parameters involved in the assessment of  $N_{\text{cal}}$  in equation 4.11. The studies collected from literature are listed in table 4.1 and concern constant amplitude tests on simple welded details (X-joints, T-joints, longitudinal stiffeners) whose geometry is comparable to the shape of welded details commonly used in crane structural design. Specimens are tested either in tension or bending, stress ratio is mainly greater than zero, plate thickness ranges between 6 mm and 25 mm and cracks initiate at weld toe. The calibration process consists in minimizing the squared logarithmic difference between the experimental and predicted lifespans:

$$\min_{p_g} f(p_g) = \sum_{h=1}^n \left( \log N_{\text{exp}}^{(h)} - \log N_{\text{cal}}^{(h)}(p_g) \right)^2 \quad (4.12)$$

where  $p_g$  is the  $g$ th parameter to calibrate, and  $N_{\text{exp}}^{(h)}$  and  $N_{\text{cal}}^{(h)}$  are the  $h$ th fatigue lives obtained respectively by testing and modeling. The parameters to calibrate in equation (4.12) are  $p = \{\tau_{\text{ref}}, c, a_0, a_1, a_2\}$  considering that  $e_{\text{ref}}$  and  $N_{\text{ref}}$  are fixed respectively at 6 mm and 250000 stress cycles.

|                    | Eq.    | Slope         | $\tau_{ref}$ | $c$  | $a_0$  | $a_1$ | $a_2$ |
|--------------------|--------|---------------|--------------|------|--------|-------|-------|
| Before calibration | (4.7)  | Constrained   | 44*          | 3*   | 0.33*  | -     | -     |
| After calibration  | (4.11) | Unconstrained | 71           | 3.37 | 0.005  | 1.07  | 0.61  |
|                    | (4.11) | Constrained   | 70           | 3*   | -0.014 | 0.97  | 0.54  |

\* fixed values

Table 4.2 – Parameters sets respectively before and after calibration.

The scatter plot of calculated lives versus experimental results for literature specimens respectively before and after factor calibration are depicted in figure 4.4 (a) and (b), and the corresponding parameters sets are listed in table 4.2. The parameters used before calibration by using equation (4.7) are given in the first line of the table. The two other sets are the parameters calibrated by means of equation (4.11), with respectively unconstrained and constrained S-N curve slopes (*i.e.* parameter  $c$ ). The obtained value of  $c$  is close to 3 in the first case, which is the usual value given by European standards dealing with fatigue of welded details. The second case consists in fixing the value of  $c$  as 3 and performing the calibration on the parameter set  $p = \{\tau_{ref}, a_0, a_1, a_2\}$ . Note that in this case the evaluated parameters are almost identical to those found with a unconstrained S-N curve slope. Moreover, in both cases the small value of  $a_0$  shows that the coefficient related to hydrostatic pressure has a very small influence for the studied specimens.

### 4.2.3 Strength distribution of crane welded details

The assessment of a strength model for the welded joints in the literature is reduced to the modeling of the scatter plot depicted in figure 4.4 (b). For each point ( $h$ ) of the scatter plot, the difference between the logarithms of the experimental and predicted lives is expressed as follows:

$$\epsilon^{(h)} = \log [N_{exp}^{(h)}] - \log [N_{cal}^{(h)}] \quad (4.13)$$

Thus, the problem consists of characterizing the scatter of the predictive model error  $\epsilon$  illustrated in figure 4.5. Assuming that the predictive model error  $\epsilon$  follows a normal probability law, the mean  $\mu_\epsilon$  and standard deviation  $\sigma_\epsilon$  of the fitted PDF respectively equal 0.0 and 0.528 for  $c = 3.37$  (unconstrained slope) and 0.0 and 0.54 for  $c = 3$  (constrained slope).  $\epsilon$  being normally distributed,  $\eta = N_{exp}/N_{cal}$  is log-normally distributed, with mean  $\mu_\eta$  and standard deviation  $\sigma_\eta$  given by:

$$\mu_\eta = e^{\mu_\epsilon + \sigma_\epsilon^2/2} \quad (4.14)$$

$$\sigma_\eta = \mu_\eta \sqrt{e^{\sigma_\epsilon^2} - 1} \quad (4.15)$$

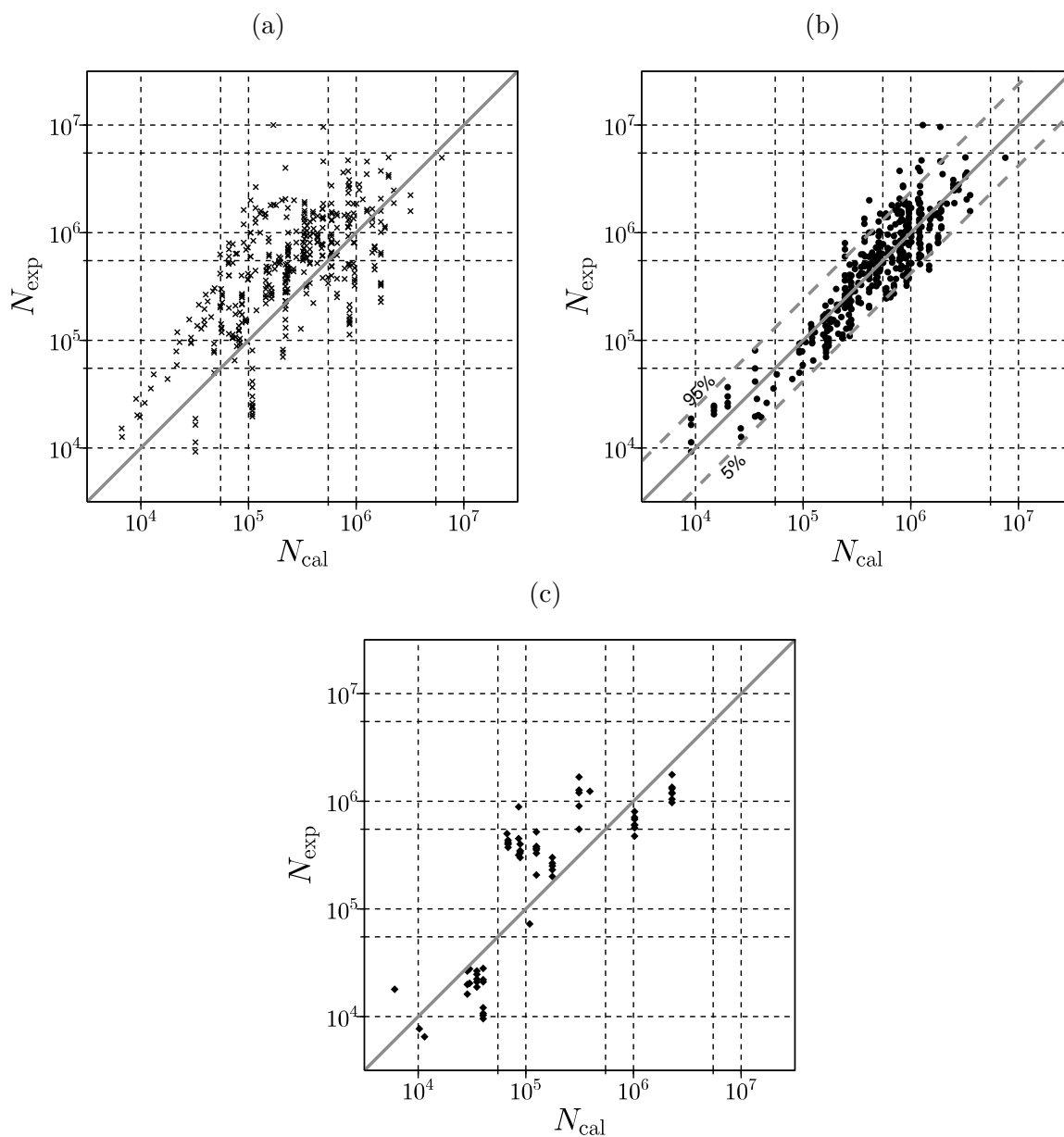


Figure 4.4 – Scatter plots obtained for literature specimens respectively (a) before and (b) after factor calibration and (c) scatter plot related to industrial structures (not used in the factor calibration). The dashed lines in (b) represent the 5% and 95% quantiles of the scatter plot.

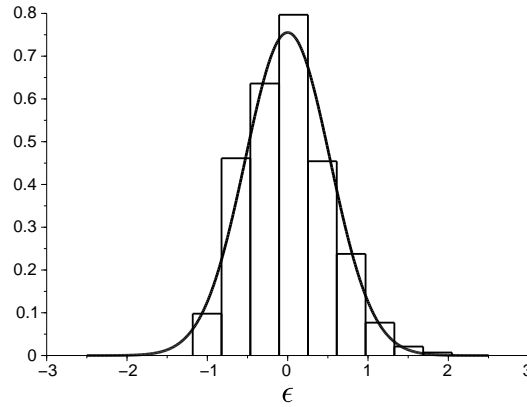


Figure 4.5 – Distribution of predictive model error.

The coefficient of variation ( $\delta_\eta = \sigma_\eta/\mu_\eta$ ) of the strength distribution (in number of cycles) of the literature specimens equals respectively 57% for  $c = 3.37$  and 58% for  $c = 3$ . These values are higher than those usually found in studies that focus on single types of joints studied separately. This high scatter is the logical consequence of gathering multiple welded joint test results, thus accounting for a variety of geometries, materials, welders and models. The difference between the values for  $\delta_\eta$  of unconstrained and constrained S-N curve slopes remaining small, the value of  $c$  is fixed as 3 in the following.

Literature specimens were used before to calibrate the parameters involved in equation (4.11). The next step aims at assessing  $N_{\text{cal}}$  for Manitowoc structures in order to validate the prediction model and to quantify the strength randomness of crane welded details. Some results are available for industrial structures [116, 117] in the literature and a few others come from Manitowoc testing fields. Therefore,  $N_{\text{cal}}$  is calculated for these structures by using equation (4.11) with the set of optimal parameters found for the literature specimens in case of constrained S-N curve slope (see third line of table 4.2). Points  $\{N_{\text{exp}}^{(h)}, N_{\text{cal}}^{(h)}\}$ , corresponding to industrial structures, are thus depicted in figure 4.4 (c). As seen in the figure, the fatigue test database for industrial structures is too small to allow the accurate definition of a crane member strength model, as done previously for literature specimens. At this stage of knowledge, the authors make the assumption that the strength of the literature specimens is representative of the population of industrial welded structures, including welded details used in tower cranes.

As seen before, the random distribution  $\epsilon$  is modeled by a normal PDF. Assuming that the scatter in the log-log plot is constant, a generic strength distribution is obtained for all crane members, regardless their geometry, materials and loading modes. Note that this corresponds to the case of a strength number of cycles log-normally distributed with a constant coefficient of variation at any stress level, as presented in figure 2.4 (b). Thus, this coefficient of variation being known ( $\delta_\eta = 58\%$ ), any crane member strength distribution can be assessed by finding a median strength number of cycles by FE modeling. For



|                            | EN 13001                              | Proposed approach               |
|----------------------------|---------------------------------------|---------------------------------|
| Probability of survival    | 97.7%                                 | 50%                             |
| Prediction stress          | Nominal stress range $\Delta\sigma_c$ | Shear stress amplitude $\tau_0$ |
| Reference plate thickness  | $\leq 12$ mm                          | 6 mm                            |
| Reference number of cycles | $2 \cdot 10^6$                        | 250000                          |

Table 4.3 – Comparison of the reference assumptions respectively used in EN 13001 [5] and in the proposed approach.

instance, if the median number of cycles of strength  $\mu_\eta$  equals  $10^5$  cycles, the scatter of the strength distribution  $N_R \sim \mathcal{LN}(\mu_\eta, \sigma_\eta)$  is given by  $\sigma_\eta = \delta_\eta \mu_\eta = 0.58 \cdot 10^5 = 58000$  cycles.

### Comparison of the proposed approach with EN13001

The following procedure aims at showing how the fatigue strength assessment approach proposed in this work can be compared with European standards such as EN 13001 [5]. The main differences between EN 13001 and the proposed approach are listed in table 4.3. On one hand, the procedure provided by EN 13001 considers a characteristic fatigue strength  $\Delta\sigma_c$  corresponding to a given notch class.  $\Delta\sigma_c$  is a stress range given at  $2 \cdot 10^6$  cycles under constant amplitude uniaxial loading with a 97.7% probability of survival. On the other hand, the fatigue strength distribution assessed in the proposed approach was calibrated by considering a shear stress amplitude  $\tau_0$  at 250000 cycles with a 50% probability of survival:

$$N_{50\%} = N_{\text{cal}} = N_{\text{ref-50\%}} \left( \frac{\tau_0}{\tau_{\text{ref}}} \right)^{-c} \left( \frac{e}{e_{\text{ref}}} \right)^{-a_1} 10^{a_2 r} \quad (4.16)$$

where  $N_{\text{ref-50\%}}$  is the reference number of cycles corresponding to a 50% probability of survival. Thus, for the sake of comparison, EN 13001 is considered as reference and the previous formula is adapted in order to account for the same assumptions. This is done by performing the following steps:

1. Assessment of the formula corresponding to  $N_{97.7\%}$  instead of  $N_{50\%}$  at a given  $\tau_0$ . This consists in finding the reference number of cycles  $N_{\text{ref-97.7\%}}$  by means of the isoprobabilistic curve equation given in section 2.2.4.
2. Conversion of the reference shear stress amplitude  $\tau_0$  into a reference stress range  $\Delta\sigma$  in the formula assessed in step 1 and eventual simplification depending on the considered assumptions (plate thickness, bending index).
3. Evaluation of the reference stress range  $\Delta\sigma$  corresponding to  $2 \cdot 10^6$  cycles with a 97.7% probability of survival by inverting the formula found in step 2.

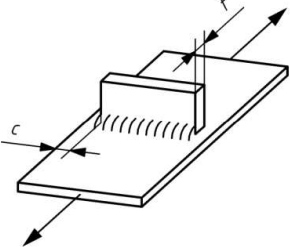
|      |                                                                     |                                                                                   |                                                                                                                                                                                                                                                                                                                                   |                                                                  |
|------|---------------------------------------------------------------------|-----------------------------------------------------------------------------------|-----------------------------------------------------------------------------------------------------------------------------------------------------------------------------------------------------------------------------------------------------------------------------------------------------------------------------------|------------------------------------------------------------------|
| 3.28 | S-N curve slope<br>$m = 3$                                          |  | Basic conditions:<br>— plate thickness $t \leq 12$ mm<br>— $c \geq 10$ mm<br>— quality level D not allowed for K-weld<br><br>Special conditions:<br>— plate thickness $t > 12$ mm (Double fillet welds only) -1 NC<br>— $c < 10$ mm -1 NC<br>— K-weld instead of double fillet weld +1 NC<br>— quality level D instead of C -1 NC |                                                                  |
|      |                                                                     |                                                                                   |                                                                                                                                                                                                                                                                                                                                   | Continuous component to which parts are welded transversally     |
|      | 112                                                                 |                                                                                   |                                                                                                                                                                                                                                                                                                                                   | Double fillet weld, quality level B*                             |
|      | 100                                                                 |                                                                                   |                                                                                                                                                                                                                                                                                                                                   | Double fillet weld, quality level B $\rightarrow \Delta\sigma_c$ |
|      | 90                                                                  |                                                                                   |                                                                                                                                                                                                                                                                                                                                   | Double fillet weld, quality level C                              |
|      | 71                                                                  |                                                                                   |                                                                                                                                                                                                                                                                                                                                   | Single fillet weld, quality level B, C                           |
| 71   | Partial penetration V-weld on remaining backing, quality level B, C |                                                                                   |                                                                                                                                                                                                                                                                                                                                   |                                                                  |

Figure 4.6 – Reference welded detail taken from EN 13001 [5].

### Illustration of the comparison of the proposed approach with EN13001

The notch class 3.28 of EN 13001 is selected to illustrate the comparison of these approaches on a practical example. As depicted in figure 4.6, the reference detail is a T-joint subjected to uniaxial tensile stress (*i.e.* pure tension) and the S-N curve slope equals 3. The specimen is assumed to conform with the specified basic conditions, *i.e.* the plate thickness is lower or equal to 12 mm. In addition, the welding quality level is supposed to be at least B. Hence, considering all the previous assumptions, the characteristic fatigue strength  $\Delta\sigma_c$  equals 100 MPa.

**Step 1.** Equation (4.16) is thus adapted in the case of the detail belonging to notch class 3.28. As detailed before, the first step consists in using the isoprobabilistic curve equation given in section 2.2.4 in order to find the reference number of cycles  $N_{\text{ref}-97.7\%}$  related to a 97.7% probability of survival:

$$N_{\text{ref}-97.7\%} = \exp \left[ \Phi^{-1}(0.023) \sqrt{\ln(1 + \delta_N^2)} + \ln \left( \frac{N_{\text{ref}-50\%}}{\sqrt{1 + \delta_N^2}} \right) \right] \quad (4.17)$$

Considering from section 4.2.3 that  $\delta_N$  equal to 0.58, the previous formula enables to find that the reference number of cycles  $N_{\text{ref}-97.7\%}$  is equal to 73844 cycles. Hence, equation (4.16) can be written as follows:

$$N_{97.7\%} = N_{\text{ref}-97.7\%} \left( \frac{\tau_0}{\tau_{\text{ref}}} \right)^{-c} \left( \frac{e}{e_{\text{ref}}} \right)^{-a_1} 10^{a_2 r} \quad (4.18)$$

**Step 2.** Remembering that the hydrostatic pressure is negligible in the assessment of  $\tau_0$  (*i.e.*  $a_0 \sim 0$ ), and considering an uniaxial loading regardless the value of stress ratio  $\kappa$ ,

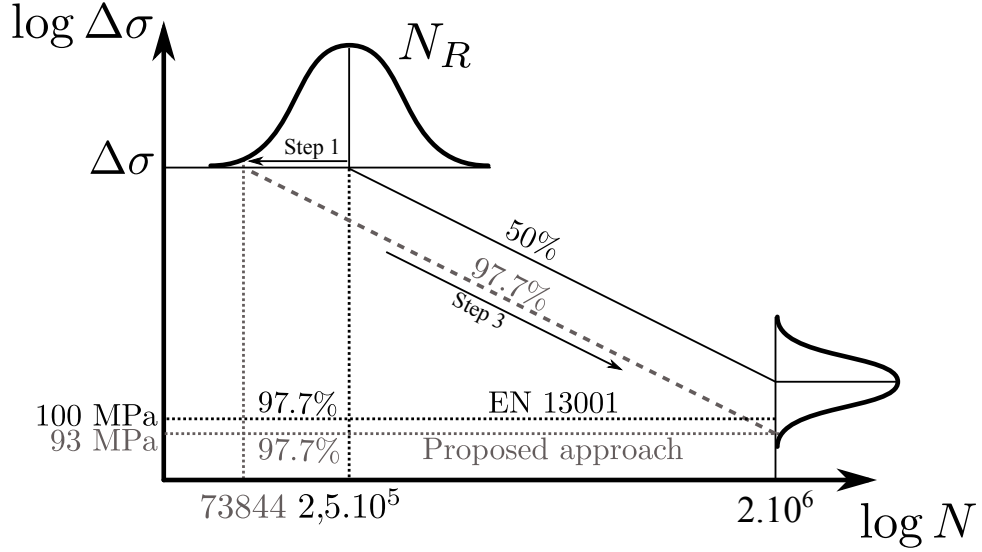


Figure 4.7 – Illustration of the comparison of safety margins induced respectively by the proposed approach and the standards.

equation (4.5) becomes:

$$\tau_0 = \tau_{\max}^{\frac{A-B}{2}} = \frac{\Delta\sigma}{4} \quad (4.19)$$

where  $\Delta\sigma$  is the nominal stress range in the welded joint. Then, considering that the T-joint has a plate thickness  $e$  equal to 6 mm and is subjected to pure tension (*i.e.*  $r = 0$ ), the predicted number of cycles  $N_{97.7\%}$  at 97% probability of survival can be simplified as follows:

$$N_{97.7\%} = N_{\text{ref}-97\%} \left( \frac{\Delta\sigma}{4\tau_{\text{ref}}} \right)^{-c} \quad (4.20)$$

**Step 3.** The final step consists in inverting equation (4.20) in order to assess the nominal stress range  $\Delta\sigma$  corresponding to  $N_{97.7\%} = 2.10^6$  cycles:

$$\Delta\sigma = 4\tau_{\text{ref}} \left( \frac{N_{97.7\%}}{N_{\text{ref}-97\%}} \right)^{-1/c} \quad (4.21)$$

Given that  $\tau_{\text{ref}} = 70$  MPa and  $N_{\text{ref}-97\%} = 73844$  cycles, the previous equation leads to  $\Delta\sigma = 93$  MPa. This value is lower than the value of 100 MPa specified by EN 13001, meaning that in this particular case, the proposed approach is conservative in comparison with EN 13001. Note that figure 4.7 provides an illustration of the proposed comparison approach in order to facilitate understanding.

As the previous example shows, the proposed procedure for the assessment of crane member strength leads to a safety level comparable to the one specified by standards, whilst avoiding the step required to classify a welded detail into a notch class. This proves to be particularly convenient when welded structural members cannot be classified with

ease due to their complex geometry. Furthermore, influence parameters such as plate thickness or loading mode are considered by means of continuous correction factors on fatigue lifespan, while standards consider these factors through discrete notch class changes. Additionally, FE analysis enables to deal with other influence parameters on crack initiation and contributes to improve fatigue lifespan prediction of welded joints.

### 4.3 Crane use stochastic modeling

This section describes the general procedure enabling the stochastic modeling of crane use, and highlights an application example related a jib top member connection.

#### 4.3.1 Crane use distribution

Three fatigue load modeling methods were detailed in chapter 2 and the collected data obtained by crane monitoring were presented in chapter 3. This section discusses the choice of an appropriate method for the crane use modeling considering the available data.

##### **Choice of appropriate fatigue loading model**

As seen in section 2.3.2, random processes such as ARMA models or Markov chains are convenient when the value of a random variable observed at time  $t$  is supposed to be affected by the observed past values. This feature may be particularly helpful in crack propagation analyses in order to see the impact of fatigue loading on crack opening. Nonetheless, the failure criterion considered in this PhD concerns exclusively the initiation of macroscopic cracks at weld toe. From another perspective, random processes might also be used to model the dynamic oscillations occurring during each crane cycle, because these oscillations are known to be highly correlated over time. Nevertheless, as seen in section 3.5, almost all the fatigue damage of crane structural members comes from the ‘static part’ of crane cycles, *i.e.* dynamic oscillations are negligible. Furthermore, although random processes may be used to model the temporal correlation between crane cycles (*e.g.* sequence of cycles), those are supposed to be independent from each other because the fatigue damage accumulation rule used in this work (the Palmgren-Miner linear rule) does not account for the crane cycles sequence. For all these reasons, random processes don’t seem to be suitable to model fatigue operating loads in the frame of this PhD.

As shown in section 2.3.4, the variability of fatigue loading can be assessed by performing several short time-period field recording in similar operating conditions in order to model fatigue loading spectra by means of multi-modal mixture PDFs. The efficiency of this method was demonstrated on various examples where a sufficient number of experimental data sets was available. As seen in chapter 3, three cranes were monitored on different construction sites. Therefore, three experimental data sets are theoretically available, which remains small to estimate accurately the model parameters. Moreover, as seen

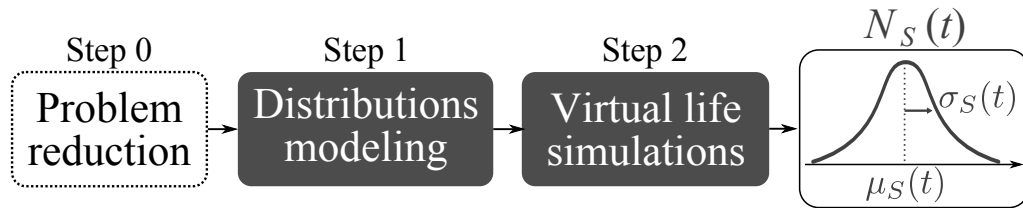


Figure 4.8 – Synoptic of the crane member use modeling procedure.

in section 3.5.2 for the jib member connection, the shape of loading spectra differs significantly, meaning that operating conditions vary from one construction site to another. As a result, the mismatch between required and available data shows that the mixture models of loading spectra are not suitable for the modeling of crane members fatigue loading.

As seen in section 2.3.3, the elementary load mix strategy enables to reconstruct virtual lives of structural members by mixing elementary loads assessed by measurements and/or simulations. An important aspect to consider in this approach is the ability to account for main events leading to fatigue damage in order to model accurately the operating load scatter. The classification of crane cycles per type of work (concrete pouring, positioning, transfer) performed in chapter 3 may look like a possible starting point which could justify the use of the elementary load mix strategy. However, as seen in section 3.3, the percentage of occurrence of each type of crane cycle is substantially different from one construction site to another, which may complicate the use of this method. In addition, as highlighted in section 1.4, crane use is also greatly influenced by the change of construction site (duration, topography, etc.). The measurements performed on few cranes during this PhD are thus not sufficient to reflect all the possible elementary life situations supposed to occur during the crane lifespan.

As seen previously, none of the models presented in chapter 2 is suitable for the modeling of crane members operating loads. Nonetheless, as presented in chapter 3, data coming from several sources (crane monitoring, crane rental agency, construction drawings) are available concerning crane use. The proposed method consists in using these data to reconstruct artificial construction sites by considering that the work performed by the crane on a unique construction site is almost deterministic. Thus, the crane use randomness is assumed to originate exclusively from the construction sites' changes. Figure 4.8 depicts the general synoptic describing the assessment method of crane member use, the latter being expressed in terms of number of cycles according to the time in service  $N_S(t)$ . The procedure consists of three steps, the first step being optional: the problem reduction, the modeling of distributions related to both intra and inter-construction site parameters (*i.e.* two-level modeling) and the simulation of crane member lives.

#### Step 0. Reduction of the problem dimension

Although the proposed procedure remains suitable in the general case, the reduction of

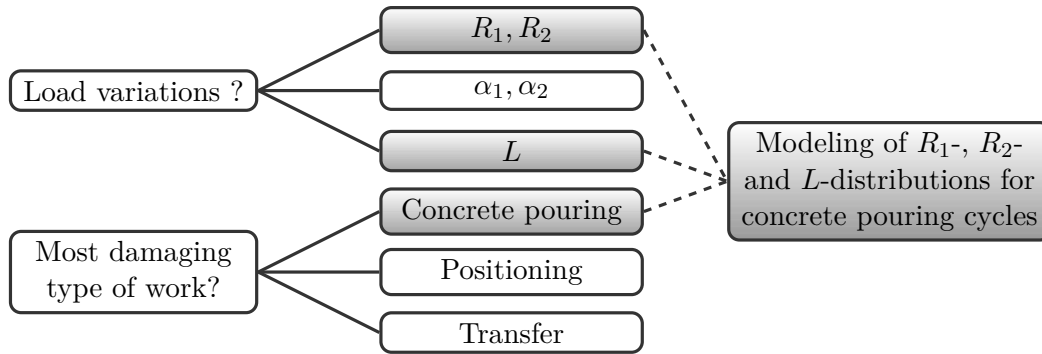


Figure 4.9 – Illustration of the problem reduction in the case of jib top member connections.

the modeling procedure to the case of a specific crane member may be convenient because this enables to manage a reduced number of random variables. Considering a specific crane member, this step is performed by addressing two questions :

- Where do load variations in the crane member originate from? Variations of hoisted load, trolley radius or jib angle?
- What is the most damaging crane cycle type (concrete pouring, positioning, transfer)?

The first question can be answered by studying the variables involved in the analytical transfer function used to assess the force applied to the crane member from load, radius and angle temporal data. For instance, given that the loading of jib top member connections is not influenced by angle variations, the modeling of  $\alpha_1$ - and  $\alpha_2$ -distributions can be avoided for this type of crane member. The second question can be clarified by using the fatigue damage assessment method described in section 3.5 in order to determine if one of the three types of work is susceptible to govern the structural member damage. Considering for instance the results presented in section 3.5.2, the fatigue damage of jib top member connections is mainly governed by concrete pouring cycles. Thus, as illustrated in figure 4.9 for this type of crane member, the proposed procedure can be reduced to the modeling of radius and load distributions for concrete pouring cycles exclusively.

Note that even though the number of distributions to be modeled is significantly reduced concerning jib top member connections, this is not necessarily the case for other crane structural members. For instance, if none of the cycle type predominates and if the loading of the considered crane member depends on load, radius and angle variations, the number of distributions to be modeled is equal to 15 ( $3 \times 5$ ). Moreover, as seen in chapter 3, the shape of  $\alpha_1$ - and  $\alpha_2$ - distributions is significantly different from one construction site to another, which may complicate the modeling of angle distributions.

**Step 1. Two-level modeling of construction site parameters**

Following the optional preliminary step, the proposed method consists in choosing the probability density functions in order to model intra- and inter-construction site parameters in accordance with the data presented in chapter 3. Two types of distribution related to each modeling level are thus required:

- **Intra-construction site parameters:** artificial crane cycles reflecting the work performed within one construction site are replicated by selecting randomly values of load, radius and angle in distributions of  $R_1$ ,  $R_2$ ,  $\alpha_1$ ,  $\alpha_2$  and  $L$  for each type of work (concrete pouring, positioning, transfer).
- **Inter-construction site parameters:** the parameters characterizing the previous distributions and other variables such as construction site duration or crane configuration are assumed to vary from one construction site to another. Therefore, distributions are defined to account for the variability reflecting the change of construction site, *i.e.* the randomness of inter-construction site parameters.

Considering a given construction site (*i.e.* inter-construction site parameters fixed), figure 4.10 illustrates how a crane cycle is artificially reproduced by selecting randomly a set of realizations of load, radius and angle in the corresponding distributions. As seen in the figure, the loading sequence consists of four steps. Assuming that the initial values of radius and angle are known from the previous cycle, step (1) aims to choose a realization of load in the  $L$ -distribution. Then, realizations of  $R_2^{(i)}$  and  $\alpha_2^{(i)}$  are simultaneously selected in  $R_2$ - and  $\alpha_2$ -distributions during step (2), and the hoisted load is dropped off in step (3) meaning that  $L = 0$ . Finally, step (4) consists in selecting  $R_1^{(i+1)}$  and  $\alpha_1^{(i+1)}$  in  $R_1$ - and  $\alpha_1$ -distributions. Note that these realizations constitute either the end of  $i$  or the beginning of  $i + 1$ . Finally, assuming that the crane performs  $N_k$  cycles on the site  $k$ , one possible realization of the work done on this construction site is determined by reiterating the previous four steps until  $N_k$  is reached.

Once the work on one construction site is characterized, all the variabilities resulting from the change of site must be accounted for, including changes of materials and tools, crane configuration, construction site duration, time between two construction sites, location of loading/unloading areas or buildings location. Figure 4.11 depicts examples of distributions related respectively to intra and inter-construction site parameters. As seen in the figure, a generic parametric PDF denoted  $X$  represents one of the intra-construction site parameters ( $L$ ,  $R_1$ ,  $R_2$ ,  $\alpha_1$ ,  $\alpha_2$ ), involving theoretically  $m$  ( $\in \mathbb{N}$ ) parameters denoted  $\theta_{X,m}$ . Therefore, a change of construction site leads to a change of  $\theta_{X,m}$ , these parameters being randomly selected in inter-construction site parameters distributions denoted  $\Theta_{X,m}$ . Furthermore, other inter-construction site parameters such as the construction site duration  $T_{\text{on-site}}$ , the time between two jobs  $T_{\text{stored}}$  or the jib length  $R_{\text{jib}}$  are also modeled by means of parametric distributions. Note that a few of these inter-construction site

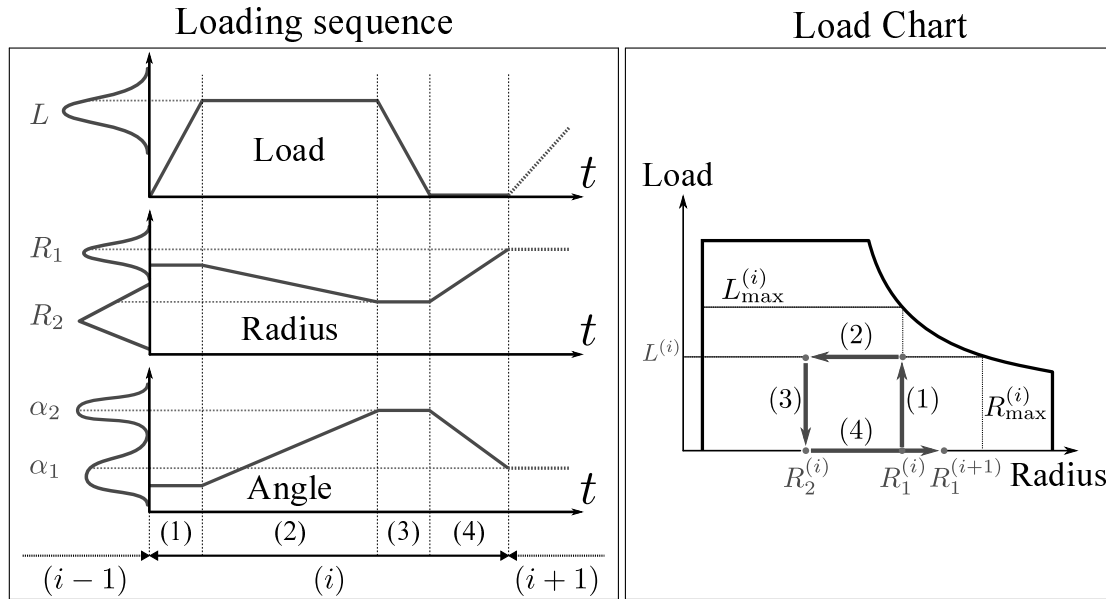


Figure 4.10 – Illustration of the generation of crane cycles for a given construction site and a given type of work.

parameter distributions are modeled regardless the studied crane member.

At this point, parametric distributions related respectively to intra and inter-construction site parameters were defined. As explained in the next step, these distributions enable the generation of artificial crane cycles for various cranes performing multiple construction sites.

## Step 2. Virtual life simulations

As described in figure 4.12, this step aims at reconstituting virtual lives of a crane member by using the distributions modeled in the previous step. First, one realization of inter-construction site parameters is randomly selected in their corresponding distributions, which leads to characterize one construction site. Therefore, the intra-construction site variables ( $L$ ,  $R_1$ ,  $R_2$ ,  $\alpha_1$ ,  $\alpha_2$ ) are fully defined. Second, the work performed by the crane on the site is simulated by generating crane cycles from the previous distributions. Third, the sequence of load, radius and angle variations describing crane cycles are transformed into force or stress variations in the crane member by means of structural analyses. These force or stress variations are usually determined analytically. Nonetheless, when the member geometry is excessively complex, a linear FE analysis must be performed in order to link the applied force with the local stress in the crane member. Fourth, a cycle counting method, such as the Rainflow procedure presented in section 2.3.1, is used to extract force ranges from the generated force-time history. Finally, the assessed force ranges are converted into a number of cycles of stress  $N_S(t)$  according to operating time by means of a damage accumulation rule such as the Palmgren-Miner method illustrated in section



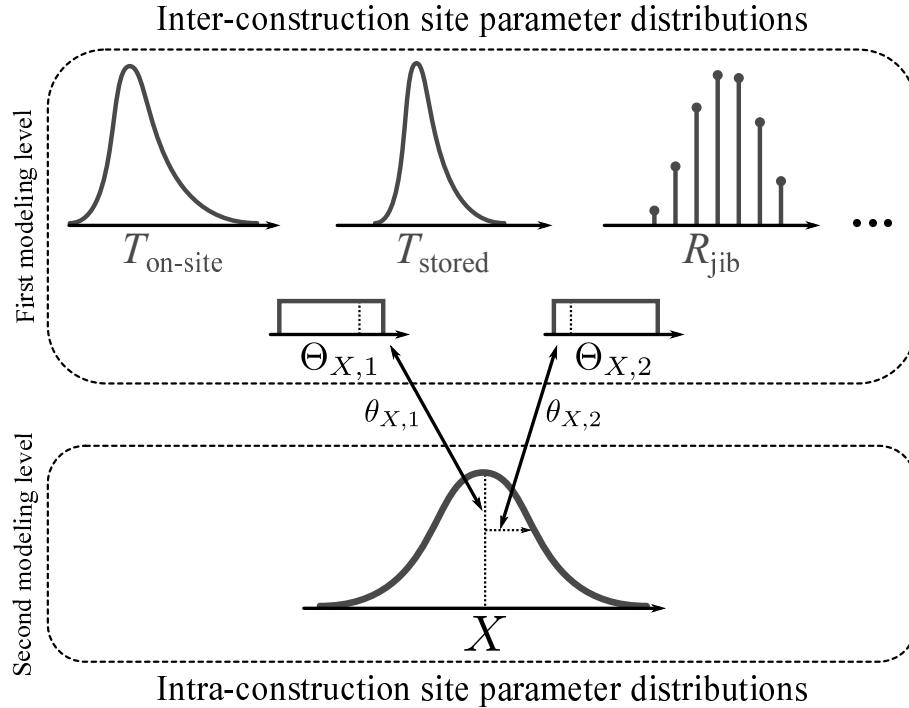


Figure 4.11 – Illustration of the definition of distributions related to each modeling level (*i.e.* intra- and inter-construction site parameters).

2.2.5. Note that  $N_S(t)$  corresponds to an equivalent number of cycles performed at the nominal capacity of the crane member.

Thereafter, the Monte Carlo (MC) simulation method described in section 2.4.4 is used to assess the stress (*i.e.* use) distribution  $N_S(t)$  for a given crane element group (E2, E3 and E4 or S1, S2 and S3). This consists in reiterating the procedure previously described for a large number of cranes knowing that, for each crane, various construction sites are randomly selected until a given number of years of use is reached (*e.g.* 40 years). Thus, as illustrated in figure 4.12, the procedure presented in this work includes two loops related respectively to crane cycles and construction sites. Note that the number of MC simulations  $N_{MC}$  must be adequate to assess the parameters (mean and standard deviation) of the number of cycles distribution  $N_S(t)$  with sufficient confidence.

In the following section, the proposed procedure is illustrated for the case of a specific crane member belonging to the S1-class according to EN 13001 [5], namely a jib top member connection.

### 4.3.2 Application to a jib top member connection

As illustrated in Step 0 of the previous section, the use of jib top member connections can be modeled by means of radius and load distributions for concrete pouring cycles exclusively. Starting from this observation, a use model is presented in this section in the

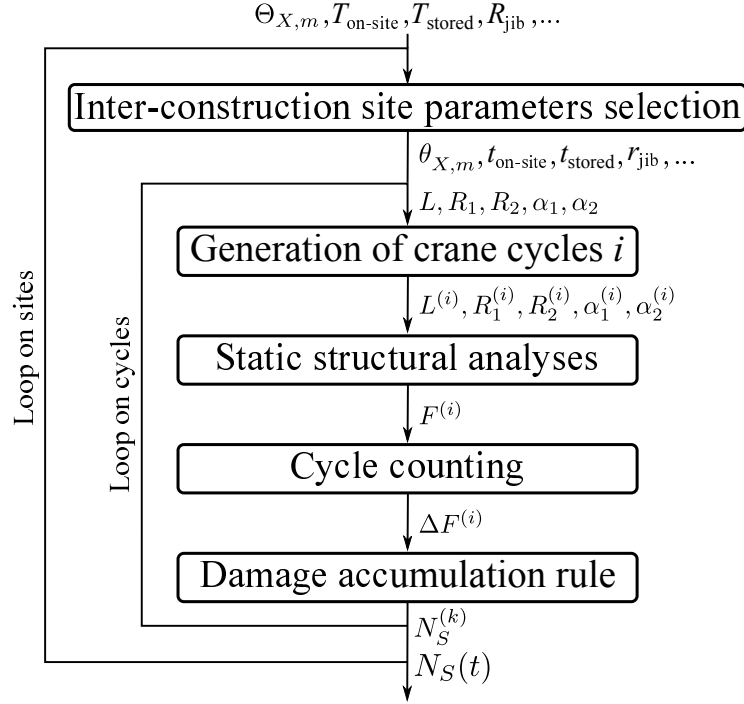


Figure 4.12 – Illustration of crane member virtual life simulation procedure. The inner loop consists in generating crane cycles for a given construction site while the outer loop aims at randomly selecting construction site parameters.

case of jib top member connections used in cranes belonging to group 3, *i.e.*  $2200 \text{ kN.m} \leq C \leq 4000 \text{ kN.m}$  (see section 3.6.1).

### Modeling of intra-construction site parameters

The distributions of initial radius, final radius and maximum hoisted load related to concrete pouring cycles presented in chapter 3 are remembered in figures 4.13, 4.14 and 4.15. As shown in these figures,  $R_1$ -,  $R_2$ - and  $L$ -histograms present similar profiles for the three studied construction sites. Therefore, assuming that these sites are representative of usual concrete constructions built in European cities, parametric PDFs are chosen to fit the empirical distributions.  $R_1/R_{jib}$  and  $L$  are modeled by means of Gaussian PDFs parametrized by their mean ( $\mu_{R_1}/R_{jib}$  and  $\mu_L$ ) and standard deviation ( $\sigma_{R_1}$  and  $\sigma_L$ ) while  $R_2/R_{jib}$  is modeled by means of a triangular distribution accounting for three parameters (lower bound  $a_{R_2}/R_{jib}$ , upper bound  $b_{R_2}/R_{jib}$  and mode  $c_{R_2}/R_{jib}$ ). Note that these parameters depend on the location of the crane on the construction site. The chosen PDF models are depicted on the right-hand side of figures 4.13, 4.14 and 4.15 and their corresponding parameters inferred from the studied construction sites are listed in table 4.4. At this point, the intra-construction site variables  $R_1$ ,  $R_2$  and  $L$  are entirely parameterized by 7 variables, namely  $\mu_{R_1}/R_{jib}$ ,  $\sigma_{R_1}/R_{jib}$ ,  $a_{R_2}/R_{jib}$ ,  $b_{R_2}/R_{jib}$ ,  $c_{R_2}/R_{jib}$ ,  $\mu_L$  and  $\sigma_L$ . Note that the previous distributions remain valid for the modeling of the use of any other crane

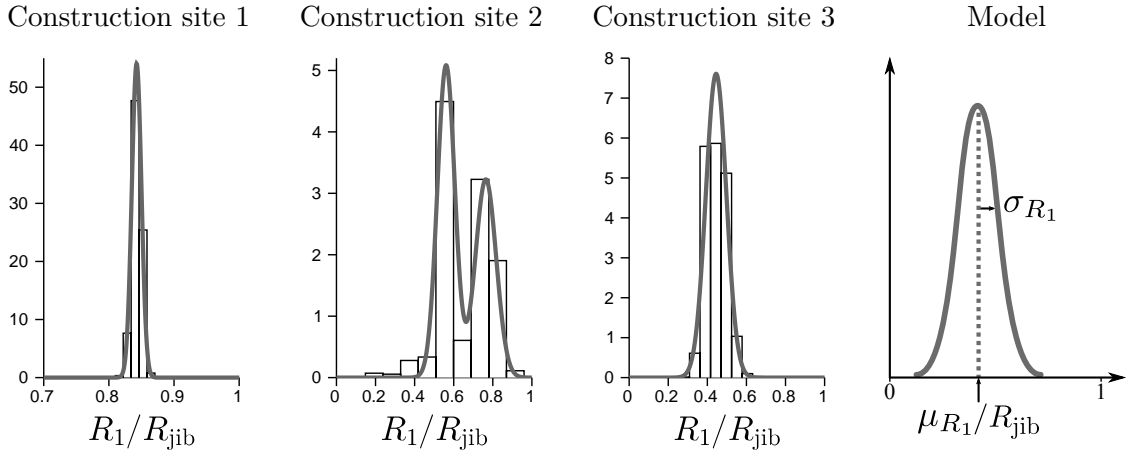


Figure 4.13 –  $R_1$ -distributions for concrete pouring cycles for the construction sites 1, 2 and 3 and chosen PDF model.

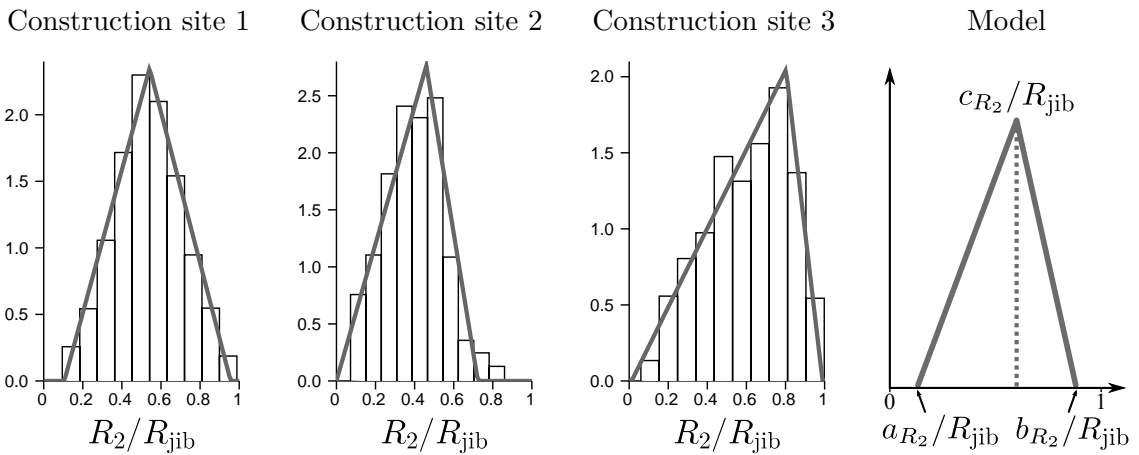


Figure 4.14 –  $R_2$ -distributions for concrete pouring cycles for the construction sites 1, 2 and 3 and chosen PDF model.

structural member.

### Modeling of inter-construction site parameters

Considering that the order in which crane cycles appear has no influence on fatigue lifespan, load and radius time-histories can be reconstructed for each construction site by random sampling in the distributions modeled before. Therefore, the change of construction site consists in varying their parameters. As depicted in figure 4.16,  $\mu_{R_1}/R_{jib}$  is uniformly selected between 0.05 (minimum normalized radius) and 1 (maximum normalized radius). Note that this conforms with the histogram of location of the center of gravity of loading/unloading areas obtained from construction drawings in section 3.6.2. Moreover,  $\sigma_{R_1}$  is fixed to 2.5 by expert opinion, and the normalized parameters  $a_{R_2}/R_{jib}$ ,  $b_{R_2}/R_{jib}$

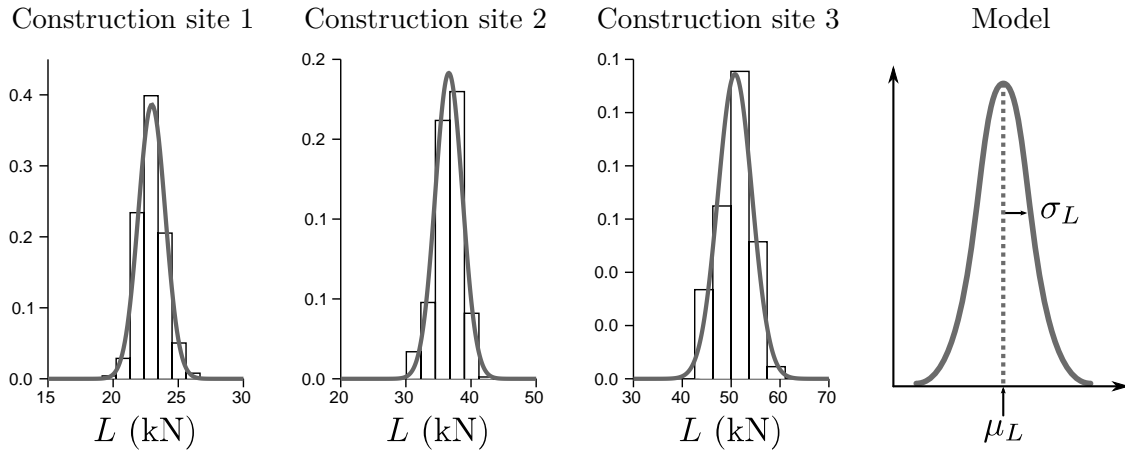


Figure 4.15 –  $L$ -distributions for concrete pouring cycles for the construction sites 1, 2 and 3 and chosen PDF model.

| Law   | Construction site   | Estimation          |                    |      |
|-------|---------------------|---------------------|--------------------|------|
|       |                     | $\mu_{R_1}/R_{jib}$ | $\sigma_{R_1}$ (m) | -    |
| $R_1$ | Construction site 1 | 0.84                | 0.50               | -    |
|       | Construction site 2 | 0.56 ; 0.76         | 2.25 ; 2.65        | -    |
|       | Construction site 3 | 0.45                | 2.97               | -    |
| $R_2$ | Construction site 1 | 0.11                | 0.96               | 0.54 |
|       | Construction site 2 | 0.00                | 0.72               | 0.46 |
|       | Construction site 3 | 0.01                | 1.00               | 0.78 |
| $L$   |                     | $\mu_L$             | $\sigma_L/\mu_L$   | -    |
|       | Construction site 1 | 23                  | 0.05               | -    |
|       | Construction site 2 | 37                  | 0.06               | -    |
|       | Construction site 3 | 51                  | 0.07               | -    |

Table 4.4 – Parameters for the fitted distributions of  $R_1/R_{jib}$ ,  $R_2/R_{jib}$  and  $L$  for each construction site.

| Capacity (m <sup>3</sup> ) | 1    | 1.5  | 2    |
|----------------------------|------|------|------|
| $\mu_L$ (kN)               | 23   | 37   | 51   |
| $\sigma_L/\mu_L$           | 0.05 | 0.06 | 0.07 |

Table 4.5 – Standardized concrete bucket characteristics.

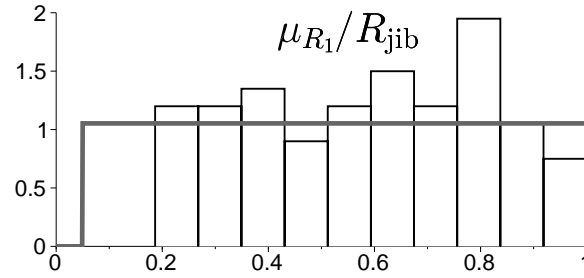


Figure 4.16 – Modeling of  $\mu_{R_1}/R_{jib}$  by fitting a continuous uniform PDF on the distribution of  $d_{CG}/R_{jib}$  assessed from 63 construction drawings (82 cranes).

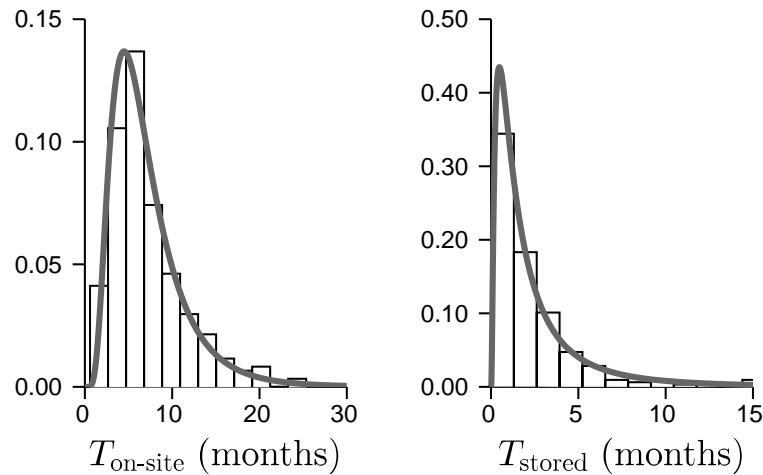


Figure 4.17 – Modeling of  $T_{on-site}$  and  $T_{stored}$  by means of lognormal PDFs for group 3 (see section 3.6.1).

and  $c_{R_2}/R_{jib}$  are randomly selected in uniform probability laws, respectively  $\mathcal{U}(0.04, 0.15)$ ,  $\mathcal{U}(0.85, 1)$ ,  $\mathcal{U}(0.4, 0.8)$ . Finally,  $\mu_L$  and  $\sigma_L/\mu_L$  are chosen by uniformly selecting a standard concrete bucket (1, 1.5 or 2 m<sup>3</sup> capacity) in table 4.5.

As seen in section 3.6, other inter-construction site parameters contributing to the variability of crane use (*i.e.* of jib top member connections) must be accounted for. Due to the studied crane capacity ( $2200 \text{ kN.m} \leq C \leq 4000 \text{ kN.m}$ ), the histograms of  $T_{on-site}$  and  $T_{stored}$  presented in section 3.6.1 for group 3 are remembered in figure 4.17. As seen in the figure,  $T_{on-site}$ - and  $T_{stored}$ -distributions present lognormal profiles, which justifies the use of two lognormal PDFs to model them. The inferred mean equal respectively 7.1 and 2.7 months and their standard deviation respectively equal 4.2 and 4.0.

The construction site duration  $T_{on-site}$  needs to be converted into a number of cycles in order to generate  $N_{concrete}$  concrete pouring cycles in the simulation process. Nonetheless, as seen in table 3.1 (chapter 3), the number of crane cycles per day can vary significantly depending on the construction site. Therefore, the relationship between  $T_{on-site}$  and  $N_{concrete}$  is not straightforward. Actually, the number of concrete pouring cycles performed

on one construction site depends on three main parameters which are:

- the number of shifts  $N_{\text{shifts}}$  per day on the site (1, 2 or 3 teams per day). The work performed by two or three teams in one day is logically greater than the work done by only one team.
- the “efficiency” of these teams measured in volume of concrete poured per month and per shift  $V_{\text{concrete}}$  ( $\text{m}^3/\text{month}/\text{shift}$ ).
- the concrete bucket capacity  $C_{\text{bucket}}$ . The higher the concrete bucket capacity, the lower the number of concrete pouring cycles to be performed.

This leads to express the relationship between the construction site duration and the number of concrete pouring cycles as follows:

$$N_{\text{concrete}} = \frac{T_{\text{on-site}} N_{\text{shifts}} V_{\text{concrete}}}{C_{\text{bucket}}} \quad (4.22)$$

Thus,  $N_{\text{shifts}}$ ,  $V_{\text{concrete}}$  and  $C_{\text{bucket}}$  must be modeled by random variables in order to reflect the variability of crane use in terms of number of concrete pouring cycles. Therefore, for each construction site,  $N_{\text{shifts}}$  is randomly selected between 1, 2 and 3 shifts by considering a discrete probability law ( $p = \{3/7; 3/7; 1/7\}$ ). Note that the probability to work with three shifts in one day on the construction site is lower than the others. This is due to the underlying assumption which considers that most of the time, the work is organized in 1 or 2 shifts but rarely in 3 shifts. Moreover,  $V_{\text{concrete}}$  is chosen in a uniform distribution of bounds respectively equal to 150 and 650  $\text{m}^3/\text{month}/\text{shift}$  according to expert opinion. Lastly, the concrete bucket capacity  $C_{\text{bucket}}$  is picked for each construction site from table 4.5 by means of a discrete uniform probability law. This means that each concrete bucket has the same odds to be randomly selected ( $p = \{1/3; 1/3; 1/3\}$ ).

Finally, as outlined in section 1.4, a unique crane model can be used with different configurations in terms of jib length or tower height. The latter does not influence the use of jib top members. Thus, the last inter-construction site parameter to be accounted for is the jib length  $R_{\text{jib}}$ , or equivalently the jib length ratio  $R_{\text{jib}}/R_{\text{jib}_{\text{max}}}$ . Figure 4.18 remembers the jib length ratio histogram related to group 3 which was obtained from construction drawings in section 3.6.2. As seen in the figure, a truncated Gaussian distribution (dashed line) fits quite well the empirical histogram. Its mean and standard deviation equal respectively 0.85 and 0.1 and the lower and upper bounds are respectively defined as 0.3 and 1. The jib length of a tower crane being a discrete variable, the jib length ratio  $R_{\text{jib}}/R_{\text{jib}_{\text{max}}}$  is randomly selected in a discrete probability law defined by the quantiles of the fitted truncated Gaussian PDF (gray lines ended by points). This means that long jibs have more probability to be chosen than short ones. This reflects the underlying assumption which considers that a crane is generally chosen to be suitable for a given construction site

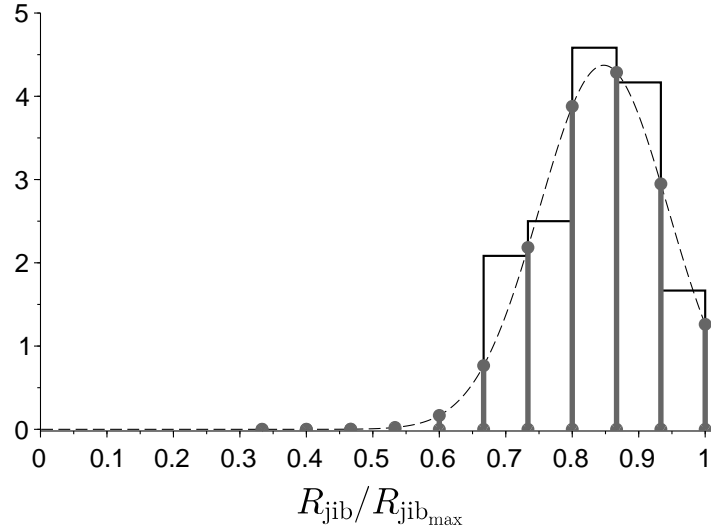


Figure 4.18 – Modeling of  $R_{jib}/R_{jib_{max}}$  by means of discrete quantiles of a normal PDF truncated between 0.3 and 1.  $R_{jib_{max}}$  is the maximum jib length that can be used for a given crane model.

in terms of loading capacity and radius variations, *i.e.* extended construction sites require large cranes and vice-versa.

Table 4.6 summarizes the assumptions described before concerning inter-construction site parameters. At this point, all the assumptions required to artificially reconstruct virtual lives of a jib top members have been detailed. The following section highlights the simulation procedure illustrated in figure 4.12 in the case of jib top member connections.

### Virtual life simulations - Distribution of $N_S(t)$

In this section, the jib top member use distribution expressed in terms of equivalent number of cycles is assessed assuming that the order in which crane cycles occur has no influence on fatigue lifespan. The general simulation procedure presented in the previous section is detailed in figure 4.19 for the case of jib top member connections. Considering a given crane, the inter-construction site parameters are randomly selected in the distributions presented before. Then, equation 4.22 is used to convert  $T_{on-site}$ ,  $N_{shifts}$ ,  $V_{concrete}$  and  $C_{bucket}$  into a number of concrete pouring cycles performed during the construction site. Moreover, the realizations of  $\mu_{R_1}/R_{jib}$ ,  $a_{R_2}/R_{jib}$ ,  $b_{R_2}/R_{jib}$ ,  $c_{R_2}/R_{jib}$ ,  $R_{jib}/R_{jib_{max}}$  and  $C_{bucket}$  characterize the three distributions related to  $L$ ,  $R_1$  and  $R_2$ . After that, crane cycles are generated considering the sampled construction site and the force applied to the jib top member connection is assessed by structural analyses. Then, cycle counting is performed in order to find the force variations  $\Delta F^{(i)}$  in the structural member and the linear Palmgren-Miner damage accumulation rule enables the assessment of an equivalent

| Variable                                     | Type       | Law                             | Parameters                |
|----------------------------------------------|------------|---------------------------------|---------------------------|
| $\mu_{R_1}/R_{\text{jib}}$                   | Continuous | Uniform                         | $\mathcal{U}(0.05, 1)$    |
| $a_{R_2}/R_{\text{jib}}$                     | Continuous | Uniform                         | $\mathcal{U}(0.04, 0.15)$ |
| $b_{R_2}/R_{\text{jib}}$                     | Continuous | Uniform                         | $\mathcal{U}(0.85, 1)$    |
| $c_{R_2}/R_{\text{jib}}$                     | Continuous | Uniform                         | $\mathcal{U}(0.4, 0.8)$   |
| $T_{\text{on-site}}$                         | Continuous | Lognormal                       | $\mathcal{LN}(7.1, 4.2)$  |
| $T_{\text{stored}}$                          | Continuous | Lognormal                       | $\mathcal{LN}(2.7, 4.0)$  |
| $N_{\text{shifts}}$                          | Discrete   | -                               | $p = \{3/7; 3/7; 1/7\}$   |
| $V_{\text{concrete}}$                        | Continuous | Uniform                         | $\mathcal{U}(150, 650)$   |
| $C_{\text{bucket}}$                          | Discrete   | Uniform                         | $p = \{1/3; 1/3; 1/3\}$   |
| $R_{\text{jib}}/R_{\text{jib}_{\text{max}}}$ | Discrete   | Quantiles of truncated Gaussian | $\mathcal{N}(0.85, 0.1)$  |

Table 4.6 – Summary of the assumptions made concerning inter-construction site parameters.

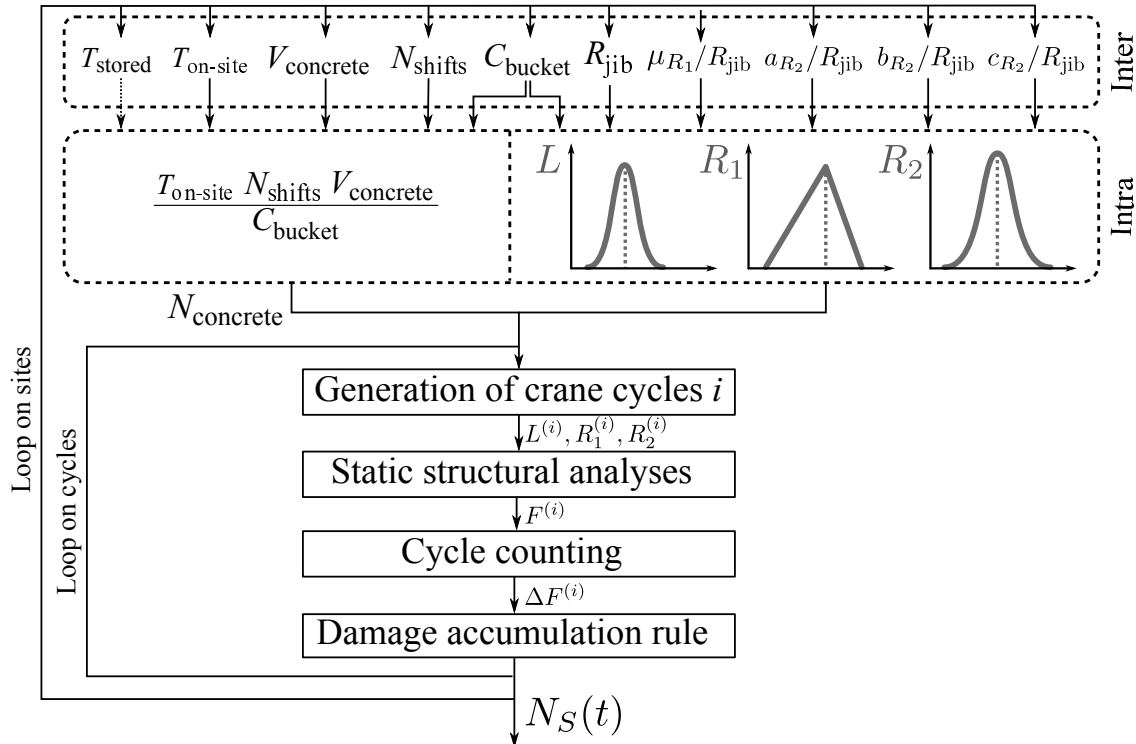


Figure 4.19 – Crane cycles generation procedure in the case of a jib top member connection.



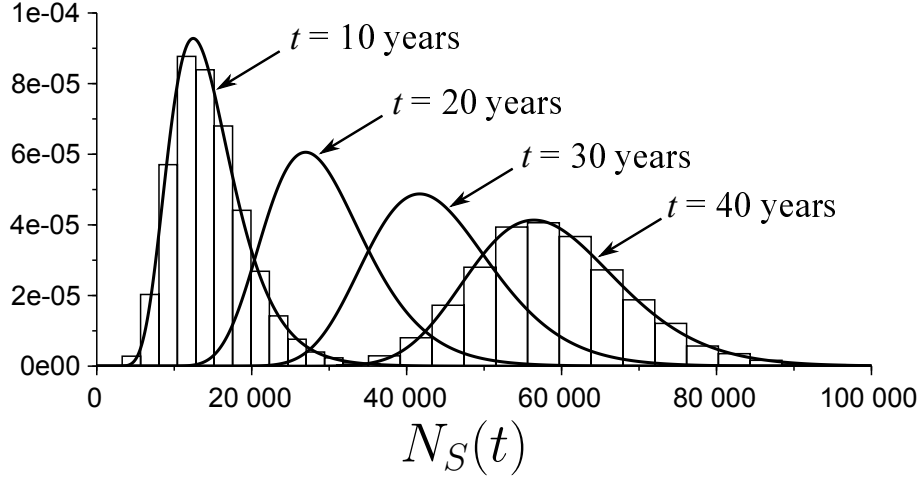


Figure 4.20 – Jib member equivalent number of cycles after 10, 20, 30 and 40 years of work.

number of cycles  $N_S^{(k)}$  for the construction site  $k$ :

$$N_S^{(k)} = \frac{1}{w} \sum_{i=1}^{N_{\text{concrete}}} \left( \frac{\Delta F^{(i)}}{\Delta F_{\text{ref}}} \right)^c \quad (4.23)$$

with  $c = 3$  (EN 13001 [5]) and  $w = 0.7$ . The latter value which was defined in section 3.5.2 corresponds to the contribution of concrete pouring cycles on the total damage of the jib top member connections.

Afterward,  $N_S(t)$  is obtained for a given crane by reiterating the previous procedure for various construction sites until a given number of years of work is reached (*e.g.* 40 years). This can be expressed by the following relationship:

$$N_S(t) = \sum_{k=1}^K N_S^{(k)} \quad \text{with } t = \sum_{k=1}^K t_{\text{on-site}}^{(k)} \geq 40 \quad (4.24)$$

Lastly, the distribution of  $N_S(t)$  is assessed by repeating the whole procedure for 10 000 cranes ( $N_{MC} = 10000$ ). Figure 4.20 depicts the use distributions assessed after 10, 20, 30 and 40 years of work for the jib top member connection. As seen in the figure, lognormal PDFs can be used to fit the empirical distributions, for which the mean  $\mu_S(t)$  and standard deviation  $\sigma_S(t)$  are listed in table 4.7.

As seen previously, data coming from crane monitoring, construction drawings or a crane rental agency have been used to model parametric distributions of intra and inter-construction site parameters. Afterward, these distributions enabled to reconstruct virtual lives for jib top member connections and to assess the distribution of equivalent number of cycles  $N_S(t)$  according to the time by performing Monte Carlo simulations. In the next section, a sensitivity analysis is conducted in order to evaluate the significance of the

| $t$           | 10    | 20    | 30    | 40    |
|---------------|-------|-------|-------|-------|
| $\mu_S(t)$    | 14620 | 29343 | 44066 | 58876 |
| $\sigma_S(t)$ | 4916  | 7069  | 8570  | 9997  |

Table 4.7 – Mean and standard deviation of the distribution of  $N_S(t)$  according to the operating time.

variability of each input variable on the scatter of the distribution of  $N_S(t)$ .

## 4.4 Sensitivity analysis of jib member use distribution

A crane use model has been created in the previous section by making assumptions concerning intra and inter-construction site parametric distributions. However, it remains important to evaluate the significance of these assumptions on the dispersion of the distribution of equivalent number of cycles  $N_S(t)$  according to the operating time. As seen in section 2.4.5, sensitivity analyses constitute efficient tools allowing to perform this task. In this section, Sobol's indices are calculated in order to judge of the impact of the variability of each input variable involved in the crane use model on the dispersion of the distribution of  $N_S(t)$ .

The method presented in section 2.4.5 is applied to the crane use modeling procedure presented before. The aim is to avoid over-parametrization of the model by fixing non-influential variables to deterministic values, on one hand and, to identify those which need to be studied more carefully due to their great influence on the final result, on the other hand. As seen in figure 4.19, the input variables involved in the jib chord member use model have different influences. First,  $T_{\text{stored}}$ ,  $T_{\text{on-site}}$ ,  $V_{\text{concrete}}$  and  $N_{\text{shifts}}$  influence directly the number of crane cycles performed on a construction site. Therefore, these variables have an impact on the distribution of equivalent number of cycles  $N_S$  over the operating time  $t$ . Second,  $R_{\text{jib}}/R_{\text{jib}_{\text{max}}}$ ,  $\mu_{R_1}/R_{\text{jib}}$ ,  $a_{R_2}/R_{\text{jib}}$ ,  $b_{R_2}/R_{\text{jib}}$ ,  $c_{R_2}/R_{\text{jib}}$  reflect the topography of each construction site, *i.e.* the distribution of crane use over the working area. Third, the concrete bucket capacity  $C_{\text{bucket}}$  influences both the equivalent number of cycles  $N_S(t)$  and the distribution of hoisted loads on each construction site. The higher the concrete bucket capacity, the heavier the loads to be hoisted but the lower the number of crane cycles. Therefore, the sensitivity analysis presented in this thesis consists in evaluating the impact of the scatter of each of these input variables on the scatter of  $N_S(t)$ .

The first-order and total Sobol' indices are assessed by means of Monte Carlo simulations. As depicted in figure 4.21, the convergence of the estimator of the first-order Sobol' indices is checked by plotting their sum versus several values of Monte Carlo iterations  $N$ . As seen in the figure, the sum of these indices converges after 20 000 iterations to 0.75, which means that the variance of input variables taken separately explain 75% of

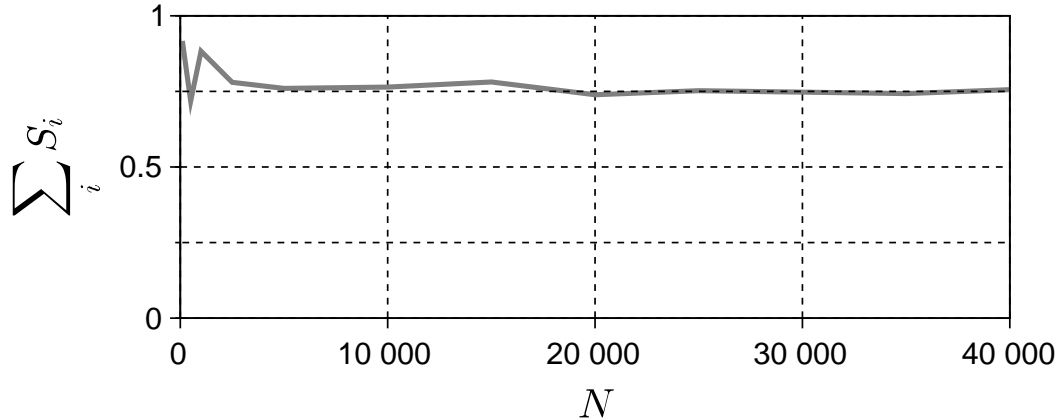


Figure 4.21 – Convergence of the sum of first-order Sobol' indices versus  $N$ .

the scatter of the distributions of  $N_S(t)$ .

Figure 4.22 depicts the results of the sensitivity analysis in terms of first order and total Sobol' indices. The remaining 25% of the variance of  $N_S(t)$  comes from the interactions between variables. Therefore, as a second step, second order Sobol' indices  $S_{ij}$  are assessed by means of the formulas given in section 2.4.5. This leads to determine 45 second order Sobol' indices whose estimates are listed in table 4.8 for 20 000 iterations. The indices whose value is greater than 1% are written with bold font in the table. This enables us to highlight the most influential pairs of variables on the scatter of  $N_S(t)$ . Although some pairs slightly influence the scatter of the distribution of number of cycles of use, there is no predominant pair of variables. Moreover, the sum of all second order indices equals 20% meaning that almost 95% of the variance of  $N_S(t)$  is explained by first and second order Sobol' indices exclusively.

#### **Influence of the scatter of inter-construction site parameters**

As seen in figure 4.22, the first order Sobol' indices related to the distributions of  $T_{\text{on-site}}$ ,  $T_{\text{stored}}$  and  $R_{\text{jib}}/R_{\text{jib}_{\text{max}}}$  remain below 6%, meaning that the influence of the scatter of these three variables taken separately is limited. Nonetheless, note that their impact becomes greater when associated with other variables because their corresponding total Sobol' indices are greater than the first order indices. In addition, the influence of  $V_{\text{concrete}}$ ,  $N_{\text{shifts}}$  and  $C_{\text{bucket}}$  equal respectively 13%, 17% and 15%, meaning that the impact of the dispersion of these variables is much more significant than the impact of the others on the scatter of  $N_S(t)$ . Remembering the calculation of the number of concrete pouring cycles in equation (4.22), the previous observation becomes readily understandable since a change of number of shifts (1, 2 or 3 teams per day) and/or concrete bucket capacity (1, 1.5 or 2 m<sup>3</sup>) leads to a significant change of number of concrete pouring cycles. As noticed in figure 4.22, the total Sobol' indices related to  $V_{\text{concrete}}$ ,  $N_{\text{shifts}}$  and  $C_{\text{bucket}}$  are

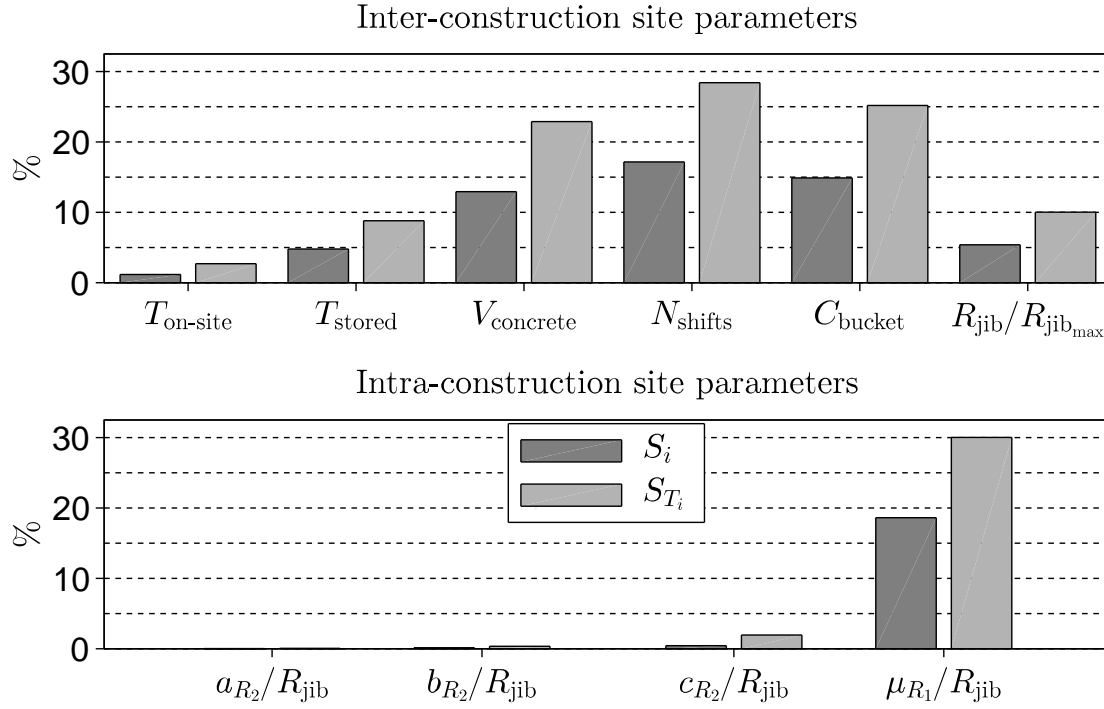


Figure 4.22 – Results coming from the Sobol' sensitivity analysis after 20 000 iterations.

| $S_{ij}$ (%)                                 | $T_{\text{stored}}$ | $V_{\text{concrete}}$ | $N_{\text{shifts}}$ | $C_{\text{bucket}}$ | $R_{\text{jib}}/R_{\text{jib}_{\text{max}}}$ | $a_{R_2}/R_{\text{jib}}$ | $b_{R_2}/R_{\text{jib}}$ | $c_{R_2}/R_{\text{jib}}$ | $\mu_{R_1}/R_{\text{jib}}$ |
|----------------------------------------------|---------------------|-----------------------|---------------------|---------------------|----------------------------------------------|--------------------------|--------------------------|--------------------------|----------------------------|
| $T_{\text{on-site}}$                         | 0.4                 | 0                     | 0                   | 0                   | 0                                            | 0                        | 0                        | 0                        | 0.2                        |
| $T_{\text{stored}}$                          | -                   | 0.6                   | 0.8                 | <b>1.0</b>          | 0.4                                          | 0                        | 0                        | 0                        | 0.4                        |
| $V_{\text{concrete}}$                        | -                   | -                     | <b>1.9</b>          | <b>1.4</b>          | <b>1.0</b>                                   | 0                        | 0.1                      | 0                        | <b>2.4</b>                 |
| $N_{\text{shifts}}$                          | -                   | -                     | -                   | <b>2.8</b>          | 0.8                                          | 0                        | 0                        | 0                        | <b>3.3</b>                 |
| $C_{\text{bucket}}$                          | -                   | -                     | -                   | -                   | 0                                            | 0                        | 0                        | 0.2                      | <b>1.6</b>                 |
| $R_{\text{jib}}/R_{\text{jib}_{\text{max}}}$ | -                   | -                     | -                   | -                   | -                                            | 0                        | 0                        | 0.1                      | 0.1                        |
| $a_{R_2}/R_{\text{jib}}$                     | -                   | -                     | -                   | -                   | -                                            | -                        | 0                        | 0                        | 0                          |
| $b_{R_2}/R_{\text{jib}}$                     | -                   | -                     | -                   | -                   | -                                            | -                        | -                        | 0                        | 0.2                        |
| $c_{R_2}/R_{\text{jib}}$                     | -                   | -                     | -                   | -                   | -                                            | -                        | -                        | -                        | 0.3                        |

Table 4.8 – Estimates of second-order Sobol' indices (in %) assessed for 20 000 iterations.

also important which means that the scatter of these three random variables becomes more significant when mixed in equation (4.22). The results given in table 4.8 confirm this observation given that the second-order indices related to the pairs involving these variables are higher than 1%.

#### **Influence of the scatter of intra-construction site parameters**

As seen in figure 4.22 and table 4.8, the variability of  $a_{R_2}/R_{\text{jib}}$ ,  $b_{R_2}/R_{\text{jib}}$  and  $c_{R_2}/R_{\text{jib}}$  have clearly no influence on the scatter of  $N_S(t)$ . This means that the variance of the distribution of final radius  $R_2$ , which is directly related the buildings location on the site, have no influence on the scatter of the jib chord member equivalent number of cycles distribution. Nevertheless, the unique intra-construction site parameter whose scatter greatly influences the dispersion of  $N_S(t)$  is the truck mixer location  $\mu_{R_1}/R_{\text{jib}}$  (see figure 4.22). Moreover, the impact of the scatter of this variable becomes more significant when paired with other input variables such as  $V_{\text{concrete}}$ ,  $N_{\text{shifts}}$  or  $C_{\text{bucket}}$  (see table 4.8).

As seen previously, the sensitivity analysis performed in this work reveals that the scatter of the distribution of  $R_2$  have no impact on the dispersion of the damage of jib top member connections. Moreover, further efforts may be concentrated on variables such as the volume of concrete poured per month and per team, the number of shifts per day, the concrete bucket capacity, the jib length and the location of truck mixers. The assumptions related to the latter may be verified by studying more construction drawings. In addition, customer surveys may be conducted in order to get significant statistical data enabling to corroborate the assumptions made concerning other influential variables ( $V_{\text{concrete}}$ ,  $N_{\text{shifts}}$ ,  $C_{\text{bucket}}$  and  $R_{\text{jib}}$ ).

Given that, at this stage, the strength and stress distributions are determined, the following section aims to describe the procedure developed in this work to assess the reliability index of crane welded details.

## **4.5 Reliability assessment of crane welded details**

The assessment of strength and stress distributions have been detailed before. In this section, the stress-strength Interference method proposed in this thesis is applied. After describing the general synoptic summarizing the reliability procedure, the proposed method is applied to jib chord member connections.

### **4.5.1 General synoptic of the proposed SSI method in the design stage**

As detailed in sections 4.2 and 4.3, the distributions of strength  $N_R$  and stress  $N_S(t)$  can be determined for any crane structural member. Since both distributions are assessed by considering the same reference cycle (see figure 3.19), the stress-strength Interference method described in section 2.4.2 can be used in order to assess the reliability of a given

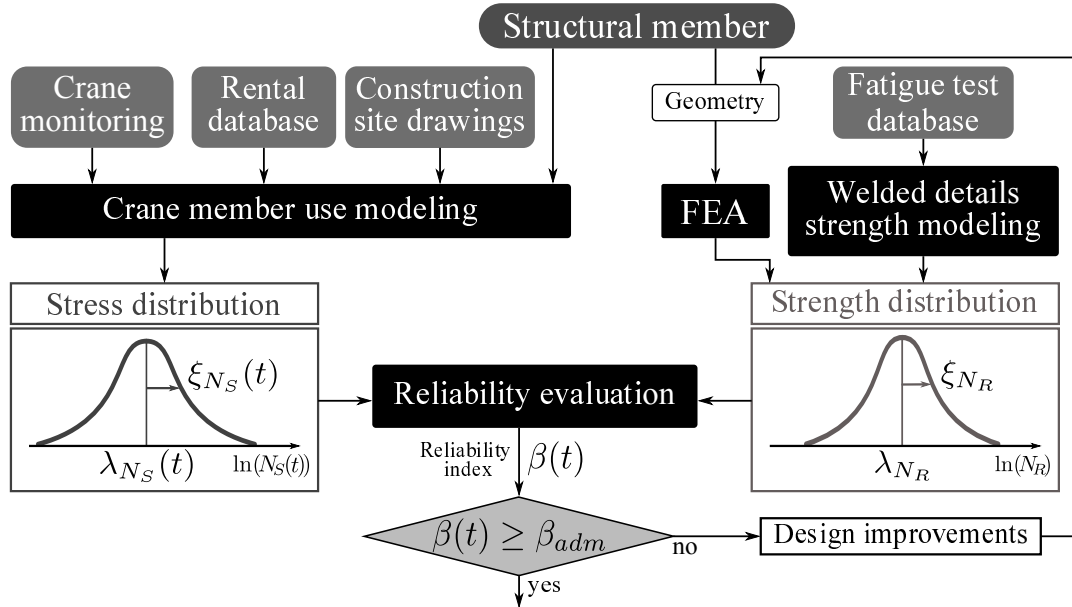


Figure 4.23 – Crane structural member reliability assessment procedure in the design stage.

structural member. This section aims at describing the proposed SSI method in the general case.

The reliability procedure proposed in this thesis for fatigue design of crane welded members can be summarized through the general synoptic depicted in figure 4.23. On one hand all available data are analyzed in chapter 3 in order to define a representative crane member use model. These data, which may be obtained from crane monitoring, from rental agency databases and from construction site drawings, are used to characterize intra and inter-construction site parameters. Then, random sampling is performed to generate crane cycles which are finally converted into an equivalent number of cycles of use at nominal capacity  $N_S(t)$  according to the crane operating period (see section 4.3.2). On the other hand the study of a fatigue test database enables to calibrate fatigue lifespan parameters leading to define a unique strength model for all crane structural members. Thus, the geometry of the studied crane welded detail is used in the Finite Element Analysis (FEA) in order to determine a median number of cycles related to the strength distribution  $N_R$  (see section 4.2). Since  $N_R$  and  $N_S(t)$  distributions are fully determined, the reliability  $\mathcal{R}(t)$  or its corresponding index  $\beta(t)$  are evaluated as described in section 2.4.2. Finally, the last step of the method consists in using the previous results during the design stage by comparing the obtained reliability index with an admissible value, *i.e.* with a target reliability index. If the condition  $\beta(t) \geq \beta_{adm}$  is satisfied, the design of the crane structural member is validated according to the probabilistic criterion. Otherwise, design improvements must be performed (*e.g.* changes of geometry) until the probabilistic condition is satisfied. The next section focuses on the application of the proposed SSI

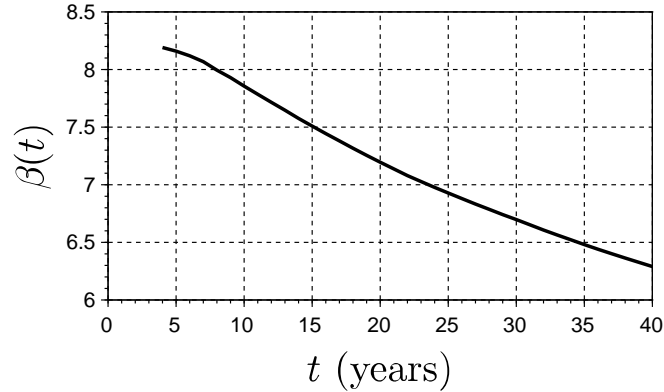


Figure 4.24 – Calculated reliability index of the jib member over time.

method to the case of jib chord member connections.

#### 4.5.2 Application on jib top member connections

An application of the reliability method presented previously is outlined in this section. The case study focuses on jib top member connections which are classified S1 in EN 13001 [5] (or E2 in FEM 1.001 [22]).

As seen in section 2.4.2, fatigue strength of crane welded joints is supposed to be time-independent while crane structural members loading evolves according to operating time. Therefore, the performance function expressed in equation 2.38 can be written in terms of equivalent number of cycles at nominal capacity:

$$G(t) = N_R - N_S(t) \quad (4.25)$$

As detailed respectively in sections 4.2.3 and 4.3.2, the distributions of strength  $N_R$  and stress  $N_S(t)$  considered in the previous equation are lognormal. Considering that  $G(t)$  is linear, the reliability index  $\beta(t)$  can be expressed by means of the analytical relation, as detailed in section 2.4.3:

$$\beta(t) = \frac{\lambda_{N_R} - \lambda_{N_S}(t)}{\sqrt{\xi_{N_R}^2 + \xi_{N_S}^2(t)}} \quad (4.26)$$

where  $\lambda_X$  and  $\xi_X$  are respectively the mean and standard deviation of the random variable  $\ln(X)$ . Figure 4.24 depicts the jib top member reliability index versus the time  $t$  in years and the corresponding values are listed in table 4.9. Bearing in mind all the assumptions made before concerning the strength and stress distributions, note that the calculated reliability index of the jib top member connections is high, regardless of the number of years of crane service (greater than 6 even after 40 years).

The case study presented in this section showed that the reliability of crane structural members can be assessed by using the SSI method proposed in this thesis. Thus, the whole

---

| $t$ (years) | 5    | 10   | 15   | 20   | 25   | 30   | 35   | 40   |
|-------------|------|------|------|------|------|------|------|------|
| $\beta(t)$  | 8.16 | 7.86 | 7.51 | 7.20 | 6.93 | 6.70 | 6.48 | 6.29 |

---

Table 4.9 – Reliability index according to operating time.

procedure presented in figure 4.23 for jib chord member connections can be reiterated for other crane structural members which are classified differently according to standards, *e.g.* S2 or S3 in EN 13001 [5]. The loading of these crane members can also depend on the slewing movement (*e.g.* mast chord member) in addition to the hoisting and trolleying movements. Therefore, angle variations must be considered in the same way as done in section 4.3.2 for load and radius variations, and the procedure presented in figure 4.19 is repeated in order to assess the stress distribution depending on time in service. Since the strength model is valid for all crane welded details, a unique FE analysis of the crane member is performed in order to estimate the median number of cycles of the strength distribution. Lastly, the reliability index of the considered crane member can be assessed in the same manner as defined in this section.

## 4.6 Conclusion

A probabilistic approach was developed in this chapter to determine the reliability of tower crane members. The stress-strength interference method applied in this thesis requires the precise definition of strength (resistance) and stress (use) models. First, influential parameters on fatigue lifespan (bending index, plate thickness, etc) were calibrated by using fatigue test results combined with finite element analyses. Then, a strength distribution was assessed by making the assumption that the fatigue resistance of literature specimens was representative of the strength of crane welded details. Second, recording made over several months on three different cranes enabled an understanding of the work performed by a crane on a construction site. In addition, rental data and construction drawings were analyzed in order to understand the crane use variability induced by the change of construction site. Then, assuming that the monitored construction sites were representative of concrete construction sites, a procedure was elaborated to assess the distribution of equivalent number of cycles of use at nominal capacity according to time in service. Furthermore, a sensitivity analysis was performed in order to identify the most influential variables on the scatter of the stress distribution  $N_S(t)$ . Finally, the stress-strength interference method enabling the assessment of the reliability index of any crane structural member was detailed and jib top member connections was used as a case study.

Assumptions have been made concerning the assessment of the strength and stress distributions involved in the reliability procedure. The consolidation of these assumptions constitutes a perspective of this work. The bias introduced by the assumption related



to the representativeness of literature specimens fatigue strength will be updated in the future when a sufficient amount of data will be available for crane welded details, *i.e.* when FE results coming from industrial welded details will be included in the  $N_{exp} - N_{cal}$  scatter plot. Moreover, the assumptions related to crane members use modeling will be confirmed (or not) by studying more data from all possible sources. Additional cranes will be monitored and other data from crane rental companies or construction firms will be analyzed in order to refine the assumptions related to the stress distribution. Note that the sensitivity analysis conducted in the studied crane structural member will help to concentrate the efforts on the most relevant and significant data in the future. In addition, another perspective of this work aims at defining admissible reliability indices  $\beta_{adm}$  related to each crane structural member. The final step of the probabilistic procedure proposed in this thesis consists in comparing the assessed reliability index with a target in order to judge if the studied crane member is sufficiently reliable. If not, the crane member design must be changed until the admissible index is reached. Note, for instance, that  $\beta_{adm}$  may be defined by considering the capacity to detect a crack, the ability of the part to resist fatigue crack, the consequences of the failure of the member and the number of identical parts in the impacted zone. Lastly, the correlation between theoretical reliability results and experience feedback related to cranes in operations for several decades constitutes another task which may be done in the future. For instance, this task could be performed by analyzing various data such as the claims or long term warranty databases.

**Chapter summary**

The reliability analysis developed in this chapter aims at assessing the reliability of crane structural members. The procedure consists in determining two probability density functions related to the strength (resistance) of crane members on one hand and their stress (loading) on the other hand.

Fatigue test results from literature enable the calibration of parameters (plate thickness, loading mode, etc) involved in the fatigue lifespan prediction model of welded details. Then, the scatter of the strength distribution related to crane welded details is assessed by assuming that the resistance of literature specimens is representative of the fatigue lifespan of industrial welded details. After that, a median number of cycles of strength is determined by performing a finite element analysis in order to fully define the strength distribution related to a given crane member.

Following this, a general procedure is developed to assess the stress distribution of crane structural members according to the time in service. The procedure consists in using the data processed in chapter 3 in order to define parametric distributions reflecting the work done within a construction site on one hand and the variability induced by the change of construction site on the other hand. After that, artificial crane cycles are iteratively generated by randomly selecting realizations from these distributions. Then, the force applied to the studied crane member is assessed through a linear analysis and the Rainflow procedure is used to count stress cycles which are converted into an equivalent number of cycles at nominal capacity by means of the Palmgren-Miner damage accumulation rule.

A sensitivity analysis using Sobol' indices is performed in order to quantify the impact of the scatter of each input variable on the scatter of the assessed stress distribution. Once both strength and stress distributions are entirely characterized, the stress-strength interference method is applied in order to assess the reliability of a given crane structural member. Lastly, the illustration of the whole reliability procedure on a specific crane member (jib top member connection) shows the relevance and the efficiency of the reliability approach proposed in this work.



---

# Conclusion and future works

## Conclusion

The fatigue design of crane structures is usually considered in standards by means of deterministic rules supposed to ensure structural integrity. Although these approaches give a satisfactory design in most cases, they do not enable to evaluate the reliability level of structural members. Furthermore, they give no information concerning the impact of design parameter uncertainties on structural safety. From that perspective, probabilistic approaches represent efficient tools allowing designers to acquire this additional knowledge. The research presented in this thesis represents a promising probabilistic approach enabling to assess the reliability of crane structural members depending on their operating time, and to quantify the importance of the uncertainties inherent to crane use. The proposed procedure is based on the development of a time-dependent stress-strength interference method. This probabilistic approach considers separately the stochastic modeling of the uncertainties inherent to the strength of crane members, on one hand, and the stochastic modeling of the uncertainties related to their use, on the other hand.

The first contribution of this research work is the development of a procedure enabling the capitalization of fatigue test results in order to predict the fatigue strength of crane members. Welded details are usually classified by standards into notch classes, which aims at providing the fatigue strength of simple welded joints with known characteristics, and tested under specific loading conditions (*e.g.* uniaxial loading). Knowing that real operating conditions are generally more complex than a simple uniaxial loading and, that the geometry of crane details does not always correspond to the usual simple geometries given by notch classes, the fatigue design of crane welded details may become extremely complicated in various cases. As a result, the capitalization procedure proposed in this thesis overcomes the previous limits by defining a unique scatter plot accounting for the strength variability of all crane welded details. The main advantage is to avoid the notch classification while satisfying the required structural safety level.

The second contribution of this work concerns the stochastic modeling of crane operating loads. Standards generally specify the loading of crane members in accordance with two main parameters, namely the loading severity level and the theoretical fatigue lifespan expressed in number of cycles. However, they do not link this number of cycles to the crane

operating time, which makes the structural reliability unpredictable after a given period of time. Moreover, various uncertainties that affect the evolution of crane use with time are not considered in standards. For these reasons, the present thesis proposes a general method enabling to assess the distribution of crane member use according to operating time. The method is based on the analysis of several data sets coming from various sources (*e.g.* crane monitoring, rental agency and construction drawings) enabling the characterization of the uncertainties related to crane member operating loads. A two-level iterative procedure consisting in performing random sampling in parametric distributions is suggested to reconstruct numerically the work performed by a crane on various construction sites. The main advantage of this modeling procedure lies in the fact that both construction sites topography and crane operating time are considered in the crane member use distribution assessment.

In the proposed approach, the scatter of the distributions of strength and stress may influence the reliability results according to the crane operating time. Assuming that a sufficient amount of experimental results can be correlated with the corresponding finite element models, the strength dispersion is established once and for all, and is not supposed to evolve with time. However, more attention needs to be paid concerning the various assumptions which were made for the parameters involved in the crane use predictive model. This research work thus proposes the use of a global sensitivity analysis enabling to identify the parameters whose scatter has a significant effect on the dispersion of crane member use distribution. The method aims to evaluate the so-called Sobol' indices by means of Monte Carlo simulations in order to quantify the impact of the scatter of input parameters on the variance of the model output. The main benefit of this sensitivity analysis lies in the ability to guide further investigations, because it provides designers with a decision-making tool enabling to focus only on the most influential parameters.

Finally, the last contribution of this research work is the development of a time-dependent stress-strength interference method enabling to assess the crane structural member reliability according to their operating time. The procedure is applied to an illustrative example dealing with jib chord member connections. Given that the uncertainties related to the strength and stress distributions are accounted for by means of two lognormal probability density functions, the reliability index of crane structural members is evaluated according to the crane operating period. The proposed method represents a significant step forward in comparison with standards, because it provides engineers with the possibility to link structural reliability to crane operating time. This may be helpful for instance to improve the maintenance plan of crane structures.

**Future works**

Following the conclusion on the benefits arising from the time-dependent reliability procedure developed in this research work, further investigations should be conducted in the stochastic modeling of the strength and stress distributions. On one hand, the bias introduced by the assumption concerning the representativeness of literature specimen fatigue strength should be first corrected. This long-term task consists in modeling a large number of crane structural details whose experimental lifespan is known from fatigue tests in order to enrich the  $N_{\text{exp}}-N_{\text{cal}}$  scatter plot related to industrial structures. On the other hand, the assumptions made about the crane member use stochastic modeling should be confirmed by monitoring more cranes on real construction sites and by collecting more duration and drawing databases. This data collection should be guided by the conclusions of the sensitivity analysis performed in this thesis by focusing on the most significant parameters involved in the crane use model.

The research work presented in this document is concerned with the application of a time-dependent probabilistic method to jib top member connections. The application of this procedure to other crane details should be performed in order to map the reliability level of every existing crane structural members. The loading of other crane members such as mast chord members depends also on the slewing movement in addition to the hoisting and trolleying. Although the developed crane use model enables us to account for angle variations, further investigations should be conducted concerning the modeling angle distributions since they are significantly different from one construction site to another.

The results assessed by means of the proposed reliability approach are helpful to map the reliability level of existing crane structures. Reliability-based design constitutes a step forward for a better management of the design of crane structural members in terms of cost and safety. This may be performed by defining during the design stage reliability targets related to each crane member according to several criteria. These reliability targets may for instance consider the capacity of the structural member to resist a crack (*e.g.* redundancy), the gravity of the consequences in case of total failure, the ability to detect a crack (*e.g.* accessibility of the member when inspected) and the number of identical crane members in operation. The reliability objectives to be defined during the design stage should also conform with the experience feedback coming from claims or long-term warranty databases.

In this research work, sensitivities are calculated using the Sobol's method. This method aims at evaluating the contribution of the variance of input parameters on the dispersion of a mathematical model or the mechanical response of a structure. Nevertheless, Sobol' indices do not provide any information concerning the influence of the mean value of random variables on the mean value of the random structural response. Other sensitivity measures such as Borgonovo indices [18] should thus be assessed in order to enhance the global sensitivity analysis conducted in this work.



---

# Bibliography

- [1] M. Ferlin, A. Pyre, and F. Lefebvre. DEFFI project for a new concept of fatigue design in the aerospace domain. In *50th AIAA/ASME/ASCE/AHS/ASC Structures, Structural Dynamics, and Materials Conference*, Palm Springs, California, May 2009. American Institute of Aeronautics and Astronautics.
- [2] F. Lefebvre, M. Ferlin, Pyre A., A. Ghouali, S. Oriol, J. El Maghnouji, and A. Bignonnet. Reliability approach in fatigue design for aerospace industry. In *Fatigue Design 2009*, Senlis, France, November 2009. CETIM.
- [3] A. Bignonnet, H.P. Lieurade, I. Huther, F. Lefebvre, A. Carcan, E. Babaud, J.C. Escoffier, and D. Marquand. The reliability approach in fatigue design : DEFFI project. In *Fatigue Design 2009*, Senlis, France, November 2009. CETIM.
- [4] N. Gayton, M. Afzali, and P.A. Boucard. APPRoFi project - probabilistic methods for the reliability assessment of structures subjected to fatigue. In *Fatigue Design 2011*, Senlis, France, November 2011. CETIM.
- [5] *EN 13001-3-1: Cranes - General Design - Part 3-1: Limit States and proof competence of steel structure*. European Committee for Standardization, 2011.
- [6] J.J. Thomas, G. Perroud, A. Bignonnet, and D. Monnet. Fatigue design and reliability in the automotive industry. In G. Marquis and J. Solin, editors, *Fatigue Design and Reliability*, volume 23 of *European Structural Integrity Society*, pages 1 – 11. Elsevier, 1999.
- [7] T. Endo, K. Mitsunaga, H. Nakagawa, and K. Ikeda. Fatigue of metals subjected to varying stress - low cycle, middle cycle fatigue. In *Preliminary Proceedings of The Chugoku-Shikoku District Meeting*, pages 45–48. The Japanese Society of Mechanical Engineers, November 1967.
- [8] M. Matsuisaki and T. Endo. Fatigue of metals subjected to varying stress. In *Proceedings*, Fukuoka, Japan, 1969. The Japanese Society of Mechanical Engineers.



- [9] C. Amzallag, J.P. Gerey, J.L. Robert, and J. Bahuaud. Standardization of the rainflow counting method for fatigue analysis. *International journal of fatigue*, 16 (4):287–293, 1994.
- [10] A. Palmgren. On life duration of ball bearings (transl.). *VDI-Z*, 68:339–341, 1924.
- [11] M.A. Miner. Cumulative damage in fatigue. *Journal of applied mechanics*, 12(3): 159–164, 1945.
- [12] M. Lemaire, A. Chateaufneuf, and J.C. Mitteau. *Fiabilité des structures: Couplage mécano-fiabiliste statique*. Hermès Science Publications, 2005.
- [13] A.H.S. Ang and W.H. Tang. *Probability concepts in engineering planning and design*. Wiley, 2006.
- [14] R.L. Disney, N.J. Sheth, and C. Lipson. The determination of the probability of failure by stress/strength interference theory. In *Proceedings of annual symposium on reliability*, pages 417–422, New York, 1968. American Society of Mechanical Engineers.
- [15] F.J. Witt. Stress–strength interference methods. *Pressure Vessel and Piping Technology*, pages 761–769, 1985.
- [16] J.D. Booker, M. Raines, and K.G. Swift. *Designing capable and reliable products*. Butterworth-Heinemann, 2001.
- [17] P. Basso, S. Casciati, and L. Faravelli. Estimating the remaining service life of a historical railway bridge. In Biondini and Frangopol, editors, *Bridge Maintenance, Safety, Management, Resilience and Sustainability*, pages 608–616, London, 2012. Taylor & Francis group.
- [18] E. Borgonovo. A new uncertainty importance measure. *Reliability Engineering & System Safety*, 92(6):771 – 784, 2007.
- [19] *EN 1933-1-9: Eurocode 3: Design of steel structures - Part 1-9: Fatigue*. European Committee for Standardization, 2005.
- [20] *DNV-RP-C203: Fatigue design of offshore steel structures*. Det Norske Veritas AS, 2011.
- [21] *NF E 52-081: Tower cranes - Calculating rules*. AFNOR: French national organization for standardization, 1975.
- [22] *Heavy Lifting Appliances - Rules for the design of hoisting appliances - FEM1.001*. European Federation of Materials Handling, 1998.

- [23] X. Lorang, T.M.I. Nguyen, A. Ouradi, and C. Roux. A new reliability approach for the fatigue design of railway wheels. In *Fatigue Design 2011, CETIM*, Senlis, France, November 2011.
- [24] M.M. Szerszen, A.S. Nowak, and J.A. Laman. Fatigue reliability of steel bridges. *Journal of Constructional Steel Research*, 52(1):83–92, 1999.
- [25] J.J. Thomas. Fatigue modeling for automotive applications. Technical Report 2002-01-0655, SAE International, 2002.
- [26] F. Szmytka and A. Oudin. A reliability analysis method in thermomechanical fatigue design. *International Journal of Fatigue*, 53(0):82 – 91, 2013.
- [27] B. Echard, N. Gayton, M. Lemaire, and N. Relun. A combined importance sampling and kriging reliability method for small failure probabilities with time-demanding numerical models. *Reliability Engineering & System Safety*, 111(0):232 – 240, 2013.
- [28] C. Weicheng. A state-of-the-art review on fatigue life prediction methods for metal structures. *Journal of Marine Science and Technology*, 7(1):43–56, 2002.
- [29] S.J. Maddox. *Fatigue Strength of Welded Structures*. Series in Welding and Other Joining Technologies. Abington Pub., 1991.
- [30] J. Rörup and H. Petershagen. Effets des contraintes moyennes de compression sur la résistance en fatigue des constructions soudées. *Soudage et techniques connexes*, 54(11-12):11–17, 2000.
- [31] J. Rörup and W. Fricke. Mean compressive stresses - experimental and theoretical investigations into the influence on the fatigue strength of welded structures. Technical Report IIW Document XIII-2007-04, International Institute of Welding, 2004.
- [32] T.R. Gurney. *Cumulative Damage of Welded Joints*. Woodhead Publishing Series in Welding and Other Joining Technologies. Elsevier Science, 2006.
- [33] J. Krebs and M. Kassner. Influence of welding residual stresses on fatigue design of welded joints and components. *Welding in the World*, 51(7-8):54–68, 2007.
- [34] A. Hobbacher. Recommendations for fatigue design of welded joints and components. Technical Report IIW-1823-07 ex XIII-2151r4-07/XV-1254r4-07, International Institute of Welding, 2008.
- [35] S. J. Maddox. Influence of tensile residual stresses on the fatigue behavior of welded joints in steel. *ASTM STP*, 776:63–96, 1982.

- [36] D.P. Kihl and S. Sarkani. Thickness effects on the fatigue strength of welded steel cruciforms. *International Journal of Fatigue*, 19(93):311 – 316, 1997.
- [37] J. Lindqvist. Fatigue strength thickness dependence in welded constructions. Master's thesis, SSAB Tunnlåt's Borlänge, Borlänge, Sweden, 2002.
- [38] M. Gustafsson. A study of thickness effect on fatigue in thin welded high strength steel joints. *Steel research international*, 77(12):873–881, 2006.
- [39] I. V. Papadopoulos and V. P. Panoskaltis. Invariant formulation of a gradient dependent multiaxial high-cycle fatigue criterion. *Engineering Fracture Mechanics*, 55(4):513–528, 1996.
- [40] B. Weber. *Fatigue multiaxiale des structures industrielles sous chargement quelconque*. PhD thesis, Institut National des Sciences Appliquées de Lyon, 1999.
- [41] T.R. Gurney and T.R. Gurney. *Fatigue of thin walled joints under complex loading*. Woodhead Publishing, 1997.
- [42] P. Dong. Verity™weld fatigue method in Fe-Safe™using ansys. In *International ANSYS Conference: A world of simulation*, David L. Lawrence Convention Center, Pittsburgh, Pennsylvania, May 2006.
- [43] K.J. Kirkhope, R. Bell, L. Caron, R.I. Basu, and K.T. Ma. Weld detail fatigue life improvement techniques. part 1: review. *Marine Structures*, 12(6):447–474, 1999.
- [44] K. Dang Van, A. Bignonnet, and J.L. Fayard. Assessment of welded structures by a structural multiaxial fatigue approach. In Manuel de Freitas Andrea Carpinteri and Andrea Spagnoli, editors, *Biaxial/Multiaxial Fatigue and Fracture 6th International Conference on Biaxial/Multiaxial Fatigue and Fracture*, volume 31 of *European Structural Integrity Society*, pages 3–21. Elsevier, 2003.
- [45] A. Wöhler. *Ueber die Festigkeits-versuche mit Eisen und Stahl*. Ernst & Korn, 1870.
- [46] O.H. Basquin. The exponential law of endurance tests. In *Proceedings*, volume 10. American Society for Testing and Materials, ASTEA, 1910.
- [47] C.E. Stromeyer. The determination of fatigue limits under alternating stress conditions. *Proceedings of the Royal Society of London A*, 90(320):411–425, 1914.
- [48] F. Bastenaire. New method for the statistical evaluation of constant stress amplitude fatigue-test results. Technical Report 511, ASTM international, 1971.
- [49] C. Lalanne. *Mechanical Vibration and Shock Analysis, Fatigue Damage*. Mechanical Vibration and Shock Analysis. Wiley, 2014.

- [50] Frédéric Perrin. *Prise en compte des données expérimentales dans les modèles probabilistes pour la prévision de la durée de vie des structures*. PhD thesis, PhD thesis, Université Blaise Pascal, Clermont-Ferrand, 2008.
- [51] A. Fatemi and L. Yang. Cumulative fatigue damage and life prediction theories : a survey of the state of the art for homogeneous materials. *International Journal of Fatigue*, 20(1):9–34, 1998.
- [52] N.E. Dowling. Fatigue failure predictions for complicated stress-strain histories. T.& A.M. Report 337, University of Illinois, 1971.
- [53] A. Burns. Fatigue loadings in flight: loads in the tailplane and fin of a varsity. technical report C.P. 256, Aeronautical research council, London, 1956.
- [54] S.D. Downing and D.F. Socie. Simple rainflow counting algorithms. *International Journal of Fatigue*, 4(1):31–40, 1982.
- [55] R.J. Anthes. Modified rainflow counting keeping the load sequence. *International Journal of Fatigue*, 19(7):529–535, 1997.
- [56] N. Hong. A modified rainflow counting method. *International Journal of Fatigue*, 13(6):465 – 469, 1991.
- [57] I. Rychlik. A new definition of the rainflow cycle counting method. *International Journal of Fatigue*, 9(2):119 – 121, 1987.
- [58] M.B. Priestley. *Spectral analysis and time series*. Academic press, 1981.
- [59] J.D. Hamilton. *Time series analysis*, volume 2. Princeton university press, Princeton, 1994.
- [60] G.E.P. Box, G.M. Jenkins, and G.C. Reinsel. *Time series analysis: forecasting and control*. John Wiley & Sons, 2013.
- [61] G.U. Yule. On a method of investigating periodicities in disturbed series, with special reference to wolfer’s sunspot numbers. *Philosophical Transactions of the Royal Society of London. Series A, Containing Papers of a Mathematical or Physical Character*, 226(636-646):267–298, 1927.
- [62] E. Slutsky. The summation of random causes as the source of cyclic processes. *Econometrica: Journal of the Econometric Society*, pages 105–146, 1937.
- [63] Theodore W Anderson and Leo A Goodman. Statistical inference about markov chains. *The Annals of Mathematical Statistics*, pages 89–110, 1957.

- [64] J.D. Hamilton. Regime-switching models. *The new palgrave dictionary of economics*, 2, 2008.
- [65] A.A. Mobarakeh, F.R. Rofooei, and G. Ahmadi. Simulation of earthquake records using time-varying arma (2,1) model. *Probabilistic Engineering Mechanics*, 17(1):15 – 34, 2002.
- [66] R.V. Field Jr. and M. Grigoriu. Level cut gaussian random field models for transitions from laminar to turbulent flow. *Probabilistic Engineering Mechanics*, 28(0):91 – 102, 2012.
- [67] I. Rychlik, P. Johannesson, and M.R. Leadbetter. Modelling and statistical analysis of ocean-wave data using transformed gaussian processes. *Marine Structures*, 10(1): 13 – 47, 1997.
- [68] A. Naess and O. Batsevych. Space-time extreme value statistics of non-gaussian random fields. *Probabilistic Engineering Mechanics*, 28(0):169 – 175, 2012.
- [69] C. Castillo, E. Castillo, A. Fernández-Canteli, R. Gómez, and R. Molina. Rainflow analysis in coastal engineering using switching second order markov models. *Applied Mathematical Modelling*, 36(9):4286 – 4303, 2012.
- [70] M. Guida and G. Pulcini. A continuous-state markov model for age- and state-dependent degradation processes. *Structural Safety*, 33(6):354 – 366, 2011.
- [71] I. Rychlik, G. Lindgren, and Y.K. Lin. Markov based correlations of damage cycles in gaussian and non-gaussian loads. *Probabilistic Engineering Mechanics*, 10(2):103 – 115, 1995.
- [72] I. Rychlik. Simulation of load sequences from rainflow matrices: Markov method. *International Journal of Fatigue*, 18(7):429 – 438, 1996.
- [73] P. Johannesson. Rainflow cycles for switching processes with markov structure, 1998.
- [74] D. Benasciutti and R. Tovo. On fatigue cycle distribution in non-stationary switching loadings with markov chain structure. *Probabilistic Engineering Mechanics*, 25(4): 406 – 418, 2010.
- [75] C. Mattrand and J.M. Bourinet. Random load sequences and stochastic crack growth based on measured load data. *Engineering Fracture Mechanics*, 78(17):3030 – 3048, 2011.
- [76] Y. Ling, C. Shantz, S. Mahadevan, and S. Sankararaman. Stochastic prediction of fatigue loading using real-time monitoring data. *International Journal of Fatigue*, 33(7):868 – 879, 2011.

- [77] X. Pitoiset. *Méthodes spectrales pour une analyse en fatigue des structures métalliques sous chargements aléatoires multiaxiaux*. PhD thesis, Université libre de Bruxelles, Mars 2001.
- [78] D. Benasciutti. *Fatigue analysis of random loadings*. PhD thesis, University of Ferrara, Italy, December 2004.
- [79] M. Nagode and M. Fajdiga. On a new method for prediction of the scatter of loading spectra. *International Journal of Fatigue*, 20(4):271 – 277, 1998.
- [80] M. Nagode and M. Fajdiga. A general multi-modal probability density function suitable for the rainflow ranges of stationary random processes. *International Journal of Fatigue*, 20(3):211 – 223, 1998.
- [81] M. Nagode and M. Fajdiga. The influence of variable operating conditions upon the general multi-modal weibull distribution. *Reliability Engineering & System Safety*, 64(3):383 – 389, 1999.
- [82] R. Tovo. On the fatigue reliability evaluation of structural components under service loading. *International journal of fatigue*, 23(7):587–598, 2001.
- [83] J. Klemenc and M. Fajdiga. Description of statistical dependencies of parameters of random load states (dependency of random load parameters). *International Journal of Fatigue*, 22(5):357 – 367, 2000.
- [84] J. Klemenc and M. Fajdiga. Prediction of loading spectra under diverse operating conditions by a localised basis function neural network. *International Journal of Fatigue*, 27(5):555–568, 2005.
- [85] J. Klemenc and M. Fajdiga. Predicting smoothed loading spectra using a combined multilayer perceptron neural network. *International Journal of Fatigue*, 28(7):777–791, 2006.
- [86] Marko Nagode and Matija Fajdiga. The rebmix algorithm for the univariate finite mixture estimation. *Communications in Statistics - Theory and Methods*, 40(5): 876–892, 2011.
- [87] T. Bučar, M. Nagode, and M. Fajdiga. Reliability approximation using finite weibull mixture distributions. *Reliability Engineering & System Safety*, 84(3):241 – 251, 2004.
- [88] R. Tovo. A damage-based evaluation of probability density distribution for rain-flow ranges from random processes. *International Journal of Fatigue*, 22(5):425 – 429, 2000.

- [89] M. Nagode and M. Fajdiga. An improved algorithm for parameter estimation suitable for mixed weibull distributions. *International Journal of Fatigue*, 22(1):75–80, 2000.
- [90] M. Nagode, J. Klemenc, and M. Fajdiga. Parametric modelling and scatter prediction of rainflow matrices. *International Journal of Fatigue*, 23(6):525 – 532, 2001.
- [91] J. Klemenc and M. Fajdiga. An improvement to the methods for estimating the statistical dependencies of the parameters of random load states. *International Journal of Fatigue*, 26(2):141–154, 2004. ISSN 0142-1123.
- [92] J. Klemenc and M. Fajdiga. Improved modelling of the loading spectra using a mixture model approach. *International Journal of Fatigue*, 30(7):1298 – 1313, 2008.
- [93] M. Nagode and M. Fajdiga. An alternative perspective on the mixture estimation problem. *Reliability Engineering & System Safety*, 91(4):388 – 397, 2006.
- [94] Céline Andrieu-Renaud. *Fiabilité mécanique des structures soumises à des phénomènes physiques dépendant du temps*. PhD thesis, PhD thesis, Université Blaise Pascal, Clermont-Ferrand, 2002.
- [95] B. Echard, N. Gayton, and A. Bignonnet. A reliability analysis method for fatigue design. *International Journal of Fatigue*, 59:292–300, 2014.
- [96] JR Benjamin and CA Cornell. *Probability, statistics and decision for civil engineers.*, 1970.
- [97] A.M. Hasofer and N.C. Lind. Exact and invariant second-moment code format. *Journal of the Engineering Mechanics Division*, 100(1):111–121, 1974.
- [98] M. Lemaire. *Structural reliability*, volume 84. John Wiley & Sons, 2010.
- [99] A. Saltelli, K. Chan, and E.M. Scott. *Sensitivity Analysis*. Wiley paperback series. Wiley, 2009.
- [100] I. Sobol. Sensitivity estimates for nonlinear mathematical models. *Mathematical Modeling & Computational Experiment*, 1:407–414, 1993.
- [101] T. Homma and A. Saltelli. Importance measures in global sensitivity analysis of nonlinear models. *Reliability Engineering & System Safety*, 52(1):1 – 17, 1996. doi: [http://dx.doi.org/10.1016/0951-8320\(96\)00002-6](http://dx.doi.org/10.1016/0951-8320(96)00002-6).
- [102] G. Savaidis and M. Vormwald. Hot-spot stress evaluation of fatigue in welded structural connections supported by finite element analysis. *International journal of fatigue*, 22(2):85–91, 2000.

- [103] A. Callens and A. Bignonnet. Fatigue assesement of welded bicycle frames. In *Fatigue Design 2011*, Senlis, France, Novembre 2011.
- [104] J. Baumgartner, T. Bruder, and H. Hanselka. Fatigue strength of laser beam welded automotive components made of thin steel sheets considering size effects. *International Journal of Fatigue*, 34(1):65 – 75, 2012.
- [105] W. Fricke. Fatigue analysis of welded joints: state of development. *Marine Structures*, 16(3):185 – 200, 2003.
- [106] A.F. Hobbacher. The new {IIW} recommendations for fatigue assessment of welded joints and components - a comprehensive code recently updated. *International Journal of Fatigue*, 31(1):50 – 58, 2009.
- [107] U. Sellgren. *Simulation-driven design: motives, means, and opportunities*. PhD thesis, The Royal Institute of Technology, Stockholm, Sweden, 1999.
- [108] H.P. Lieurade, P. Castellucci, G. Bel, J. Lu, and J.F. Flavenot. Tenue en fatigue d’assemblages soudés en acier hle avec ou sans traitement de parachèvement. Technical Report 107900, CETIM, 1992.
- [109] I. Huther. Recueil de résultats de fatigue sur assemblages soudés. Technical Report 1O8260, CETIM, 2005.
- [110] S.J. Maddox. Fatigue life improvement of steel fillet welds by hammer, needle or shot peening. Technical Report XIII-2327-10, International Institute of Welding, 2010.
- [111] J.J. Janosch. Evaluation de la tenue en fatigue des assemblages en angle en fonction de la pénétration des soudures dans le cas d’une sollicitation en traction et flexion. Technical Report 26068, Institut de soudure, Décembre 1990.
- [112] I. Huther, H.P. Lieurade, N. Sayhi, and R. Buisson. Tenue en fatigue des assemblages soudés comportant des raidisseurs longitudinaux (synthèse). Technical Report 184483, CETIM, 1996.
- [113] V.I. Trufiakov, E.S. Statnikov, P.P. Mikheev, and A.Z. Kuzmenko. The efficiency of ultrasonic impact treatment for improving the fatigue strength of welded joints. *IIW Document*, 13:1745–98, 1998.
- [114] A. Galtier and E. Statnikov. The influence of ultrasonic impact treatment on fatigue behavious of welded joints in high-strength steel. Technical Report XIII-03, International Institute of Welding, 2003.



- [115] M.M. Pedersen, O.O. Mouritsen, M.R. Hansen, J.G. Andersen, and J. Wenderby. Comparison of post weld treatment of high strength steel welded joints in medium cycle fatigue. Technical Report XIII-2272-09, International Institute of Welding, 2009.
- [116] Y. Kudryavtsev, J. Kleinman, A. Lugovskoy, and G. Prokopenko. Fatigue life improvement of tubular welded joints by ultrasonic peening. Technical Report IIW Document XIII-2117-06, International Institute of Welding, 2006.
- [117] D. Thévenet, M.F. Ghanameh, and A. Zeghloul. Fatigue strength assessment of tubular welded joints by an alternative structural stress approach. *International Journal of Fatigue*, 51(0):74 – 82, 2013.

---

# Appendix A

## Construction site drawing processing

In this research work, we have developed numerical routines enabling to retrieve and process data from construction site drawings. As detailed in this appendix, this includes a Graphic User Interface (GUI) enabling to acquire relevant data from drawings and numerical functions allowing to handle these data automatically.

### A.1 Data collection from construction site drawings

The first step of the procedure consists in creating a GUI enabling to retrieve relevant data from a construction site drawing with minimum effort. The developed GUI enables us to:

- Open a construction site drawing (in PNG or JPEG format).
- Specify a crane coordinate system.
- Define surfaces (poured floors, loading/unloading areas, etc.).
- Register automatically the coordinate system parameters (origin, orientation, scale) and the surface features (coordinates of edge vertices, thickness, etc.).

As seen in Figure A.1, the three first points listed above can be easily performed by the user by clicking the buttons named respectively “Open drawing”, “Specify coordinate system” and “Define surfaces”.

#### Drawing opening

Construction drawings are usually provided in DWG or PDF format. However, the developed GUI only support PNG or JPEG format. Therefore, the DWG drawing must be converted into a PDF file. Then, an image file can be obtained from a PDF file by pressing

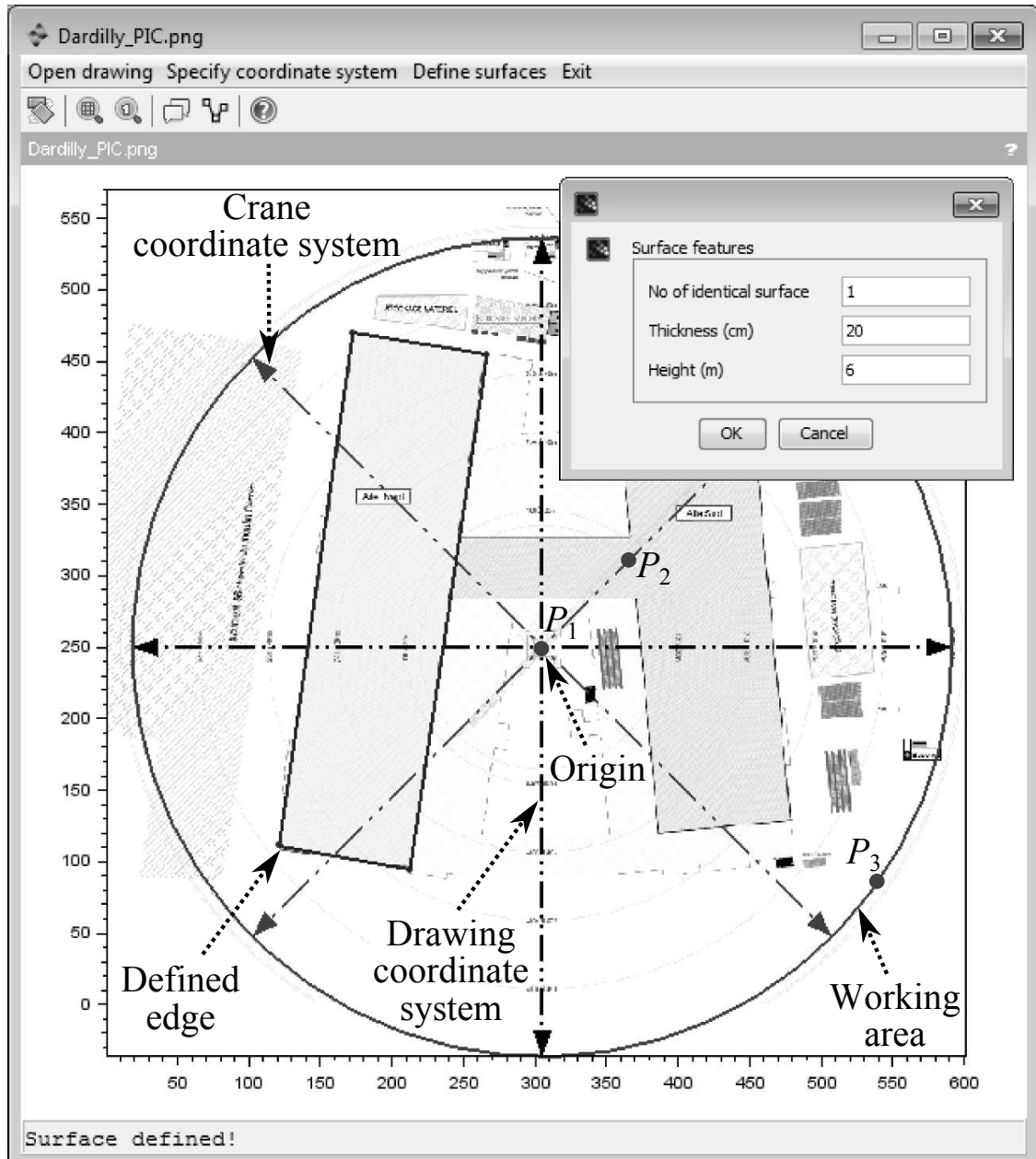


Figure A.1 – Illustration of the data collection performed from construction site drawings.

the button “printscreen” on the keyboard and registering the created image in the right format (PNG or JPEG).

### **Coordinate system specification**

When the construction drawing is loaded in the GUI window, the user must specify the characteristics (origin, orientation, scale) of the crane coordinate system (see Figure A.1):

1. The **origin** of both coordinate systems is obtained by clicking on crane location on the drawing (see point  $P_1$ ).
2. The **orientation** of one coordinate system relative to the other is assessed by clicking on one point defining the direction of the positive X-axis of the crane coordinate system (see point  $P_2$ ).
3. The **scale** of the construction site drawing is calculated by:
  - retrieving the coordinates of one point defining the crane working area (see point  $P_3$ ),
  - writing the jib length in an editor box.

The three steps mentioned before enable the full definition of the crane coordinate system relative to the drawing coordinate system (see Figure A.1). Note that, in order to facilitate further processing, the data retrieved during the following step are expressed in the crane coordinate system, the latter being considered as the reference. At the end of this step, the origin coordinates, the orientation angle and the scale of the construction drawing are stored automatically in a text file.

### **Surface definition**

After specifying entirely the crane coordinate system, various surfaces (loading/unloading areas, building locations, etc.) can be defined with minimum effort. To achieve this, the user must click on the button named “Define surfaces” and click on the successive vertices that define the edge of the surface. When he validates, an editor box appears with various surface features that must be specified. For instance, the user can set the number of identical surfaces if several floors are defined from the same edge, the thickness of the surface, if any, and the height of the surface calculated from the reference floor. An illustration of the result obtained after performing this step is given in Figure A.1. When the user has finished to define a surface, the coordinates of the vertices and the surface features are automatically stored in the text file created before. The following section explains how the data collected from construction drawings can be processed.

## A.2 Processing of the collected data

This section describes how the data collected from drawings and stored in a text file can be processed to estimate surfaces and volumes of concrete according to the working radius or working angle. The basic principle of the processing method is to discretize the crane working area into numerous four-sided polygons, and to detect if these polygons are located inside the surface edges retrieved during the data collection step. This leads to verify if the corners and the center of gravity of the four-sided polygons are located inside the surface edge. A simple way to achieve this consists in using the following geometry property:

*A point is located inside a **convex** polygon if the sum of the angles calculated from it and each vertex of the polygon equals  $360^\circ$ .*

Therefore, given a surface edge identified in the previous section, the method consists of several steps:

1. Discretize the crane working area into four-sided polygons having the same area.
2. Detect the elements which are entirely located inside the surface edge and those located at the limit of the edge (see Figure A.2(a)):
  - If the four corners **and** the center of gravity of the polygon are all located inside the surface edge, the polygon is entirely inside the surface edge.
  - If at least one corner **or** the center of gravity of the polygon is located inside the surface edge, the polygon is considered as a borderline element.
  - Otherwise, the polygon is located outside the surface edge.
3. Refine the borderline elements into smaller four-sided polygons and detect if these polygons are also located inside the surface edge (see Figure A.2(b)).
4. Calculate the proportion of borderline element area that is inside the surface edge by summing all the small polygon areas located inside the surface edge.

Once the four steps listed before are completed, various results can be plotted. As depicted in Figure A.3, the estimated volume of concrete that must be poured theoretically can be plotted in accordance with the crane working area, *i.e.* in three dimensions. The results can also be presented by plotting separately the estimated concrete volume versus the working radius or versus the working angle, as shown in Figure A.4.

As seen in this annex, useful data can be extracted from construction drawings by using a simple graphic user interface, and processed by means of numerical routines enabling to estimate for instance the volume of concrete that must be theoretically poured on the construction site.

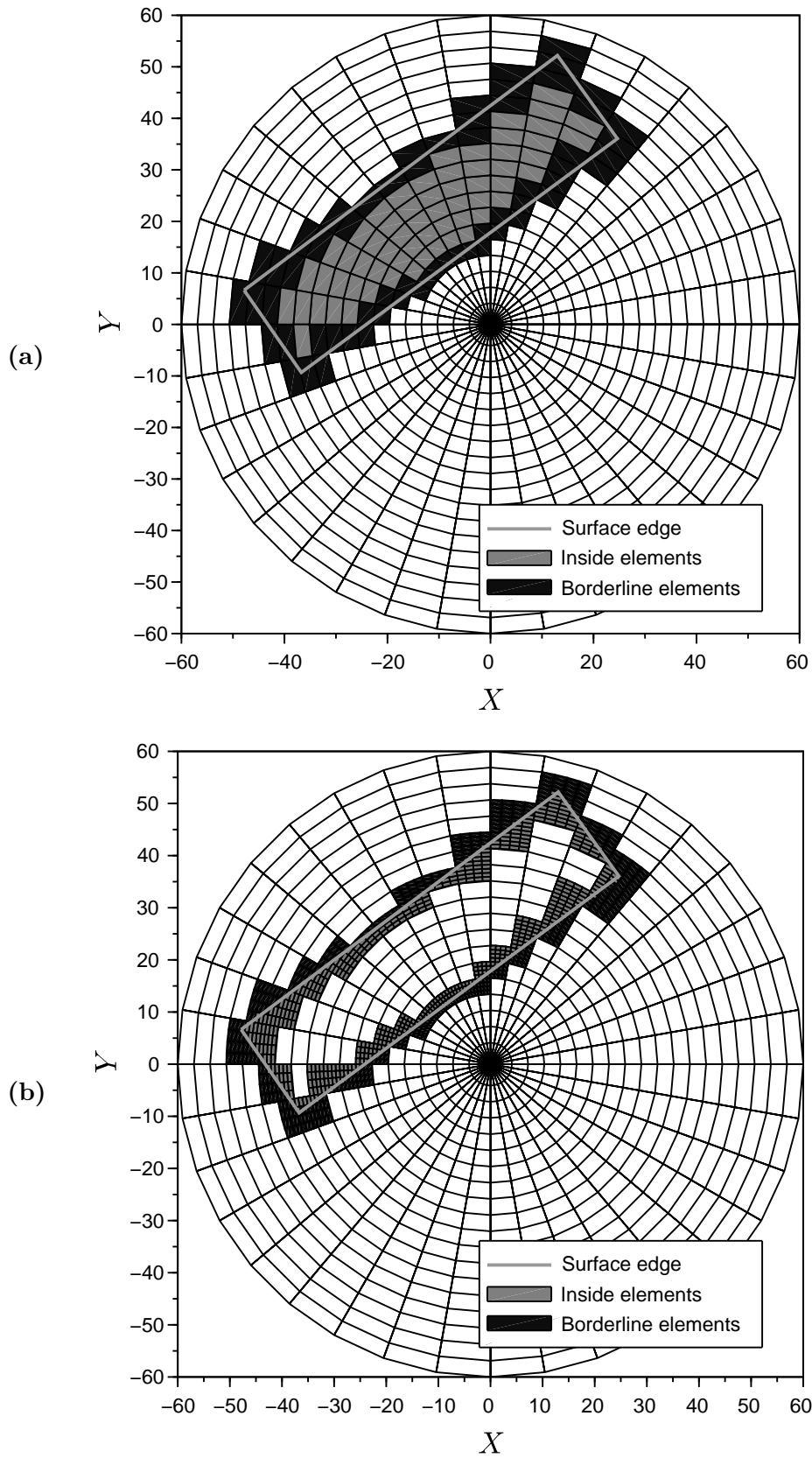


Figure A.2 – Identification of elements that are entirely within the surface or those which are located at the limit of the edge respectively during (a) step 2 and (b) step 3.

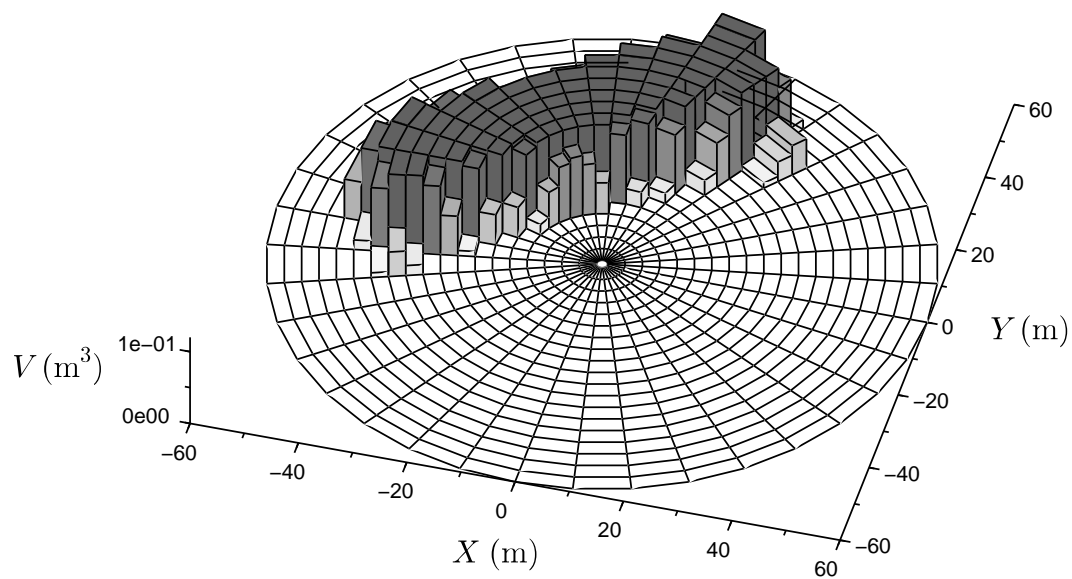


Figure A.3 – Illustration of the 3D results obtained after the data processing according to the crane working area.

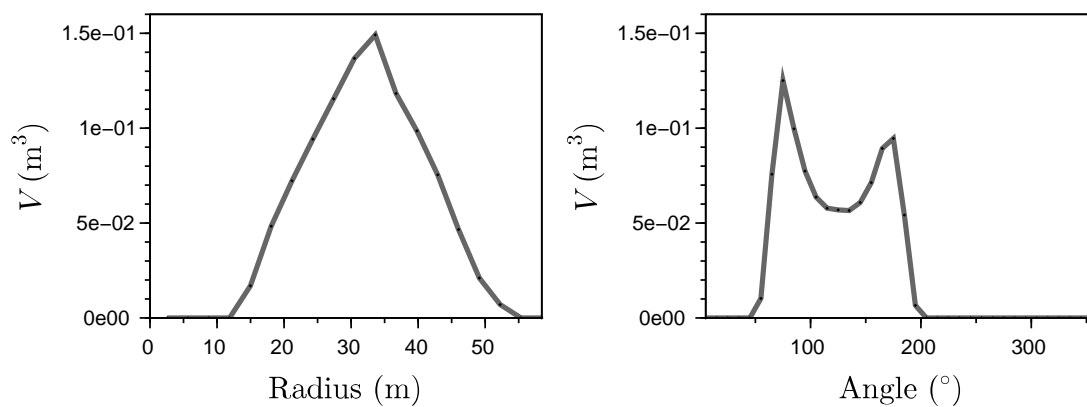


Figure A.4 – Illustration of the results obtained after the data processing according to working radius and angle, respectively.

